INFORMATION TO USERS

This manuscript has been reproduced from the microfilm master. UMI films the text directly from the original or copy submitted. Thus, some thesis and dissertation copies are in typewriter face, while others may be from any type of computer printer.

The quality of this reproduction is dependent upon the quality of the copy submitted. Broken or indistinct print, colored or poor quality illustrations and photographs, print bleedthrough, substandard margins, and improper alignment can adversely affect reproduction.

In the unlikely event that the author did not send UMI a complete manuscript and there are missing pages, these will be noted. Also, if unauthorized copyright material had to be removed, a note will indicate the deletion.

Oversize materials (e.g., maps, drawings, charts) are reproduced by sectioning the original, beginning at the upper left-hand corner and continuing from left to right in equal sections with small overlaps.

Photographs included in the original manuscript have been reproduced xerographically in this copy. Higher quality 6" x 9" black and white photographic prints are available for any photographs or illustrations appearing in this copy for an additional charge. Contact UMI directly to order.

ProQuest Information and Learning
300 North Zeeb Road, Ann Arbor, MI 48106-1346 USA
800-521-0600

Université d'Ottawa • University of Ottawa

The Triaxial Vane Apparatus with Stress Control

Thomas Walsh, B.A.Sc.

A Dissertation
Submitted to the Faculty of Graduate and Postdoctoral Studies

Under the supervision of

Dr. Vinod Garga, P.Eng, F.EIC.

In partial fulfillment of the requirements for the degree of

M.A.Sc. in Civil Engineering

Department of Civil Engineering
University of Ottawa
Ottawa, Ontario
Canada, K1N 6N5

May 2001

The M.A.Sc. in Civil Engineering Degree is a joint program between the University of Ottawa and Carleton University, and is administered by the Ottawa-Carleton Joint Institute in Civil Engineering

Acknowledgements

The author would like to express his appreciation to his research advisor, Dr. Vinod Garga for his support, advice and guidance throughout this research program.

The author would also like to thank all the support staff in the department of Civil Engineering, and in particular Mr. Richard Moore, without his assistance and technical support this research would not have been possible.

Finally, it is to the author's family, whose encouragement, patience and support made this research successful.

Summary

The scope of this research has been two fold. The first stage was to develop a Tri Vane Apparatus. The Tri Vane Apparatus uses a miniature vane incorporated into a triaxial cell in order to study the use of the vane in different soils as well as allowing the effects of different vane parameters, such as rotation rate and vane geometry, to be studied in controlled conditions. Initial research was conducted into the history of this device with special emphasis on any previous designs. Three previous designs of this device were found in the literature, by Kenney and Landva (1965), Law (1979) and Pamukcu and Suhayda (1988). The design used in the current research has incorporated many design aspects used in these previous devices but has also made several improvements. One of the most significant improvements is the incorporation of a full data acquisition system. All measurements made during the tests are now measured by electronic transducers, which are monitored and recorded by computer. Another important improvement over the previous designs is that the current device has been developed to allow for the testing of both clays and sands.

This leads into the second stage of this research. Since the development of the vane test in 1948 by Cadling and Odenstad (1948), the test has almost exclusively been used for the study of the undrained shear strength of clays. This research has investigated the use of the vane test in sands. While there has been some investigation into this before (Wilson, 1963), the available information is less than complete. Through the use of the Tri Vane Apparatus constructed in the first stage of this research, extensive testing has been conducted on sand, in both isotropic and anisotropic stress conditions. The sand used in the investigation, Unimin 2010 crushed quartz, has been studied extensively by past researchers at the University of Ottawa (Zhang , 1997 and Sedano, 1998). Through the comparison of the Tri Vane results to the previous research and to theoretical models, the applicability of the Tri Vane as a test for sand has been investigated. Additionally, this research studies the effects of various parameters associated with the vane tests, such as rotation speed and soil density.

Table of Contents

Acknowledgements 2
Summary 3
Table of Contents 4
Table of Figures and Tables 7
Chapter 1: Introduction 9
1.1 General 9
1.2 Objectives of the Research 10
1.3 Scope of the Research 10
1.4 Outline of Thesis 11
Chapter 2: Literature Review 12
2.1 The Vane Test 12
2.1.1 Historical and Theoretical Developments 12
2.1.2 Current Practice 14
2.2 The Triaxial Vane Apparatus 16
2.2.1 NGI Triaxial Vane 17
2.2.2 NRC Triaxial Vane 18
2.3 Theoretical Behavior of Vane Test 19
2.4 Use of the Vane Shear Test in Cohesionless Soils 22
2.4.1 Vane Stress Distribution in Sands 22
2.4.2 Effect of Pore Pressure 23
2.4.3 The Piezovane 24
2.5 Steady State and the Steady State Line 25
2.5.1 Liquefaction and Post Liquefaction Shear Strength 25
2.5.2 Critical Void Ratio 26
2.5.3 Steady State of Deformation 26
2.5.4 Steady State Line 27
2.6 Factors Affecting the Steady State Strength 28
2.6.1 Void Ratio 28
2.6.2 Consolidation Stress 28
2.6.3 Sampling 28
2.6.4 Localization of Shear Failure 29
Chapter 3: Apparatus 56
3.1 The Triaxial Vane 56
3.2 The Triaxial Vane Apparatus 56
3.2.1 Vane 56
3.2.2 Drive Shaft and Power Unit 57
3.2.3 Pressurization System 58
3.2.4 Triaxial Cell 58
3.2.5 Sample Base and Cap 59
3.2.5 Volume Gauge 60
3.3 Transducers 61
3.4 Transducer Calibration 62
3.4.1 Pressure Transducers 62
3.5 Cyclical Response in Torque Transducer 62

3.6 Additional Test Equipment 63
Chapter 4: Sample Preparation 83
4.1 Clay Samples 83
4.1.1 Apparatus Set Up 83
4.1.2 Sample Set Up 83
4.1.3 Testing Set Up 84
4.2 Sand Samples 84
4.2.1 Apparatus Set Up 84
4.2.2 Sample Set Up 85
4.2.3 Testing Set Up 85
Chapter 5: Material Tested and Density Verification Tests 91
5.1 Material Tested 91
5.2 Density Verification Tests 92
5.2.1 Gelatin Concentration 92
5.2.2 Gelatin Sample Preparation 92
5.2.3 Sample Recovery and Filtration 93
5.2.4 Results of Density Verifcation 93
5.3 Factors Affecting Density Distibution 94
5.3.1 Presence on Turbulence 94
5.3.2 Effect of Flow Disturbance and the Presence of the Vane During Sample Preparation 95
Chapter 6: Test Program and Experimental Results 103
6.1 Test Program 103
6.2 Experimental Results 104
6.2.1 Conventional Testing 104
6.2.2 Triaxial Vane Test Procedures and Analysis Method 104
6.2.3 Variation in Vane Shaft Friction 106
6.2.4 Effects of Initial Void Ratio 106
6.2.5 Influence of Shear Rate 107
6.2.6 Isotropically Consolidated Drained Tests (IC-D) 108
6.2.7 Isotropically Consolidated Undrained Tests (IC-U) 108
6.2.8 Anisotropically Consolidated Drained Tests (AC-D) 109
6.2.9 Anisotropically Consolidated Undrained Tests (AC-U) 110
6.3 Comparison and Discussion of Test Results 110
6.3.1 Drained Peak Strength 110
6.3.2 Undrained Peak Strength 111
6.3.3 Residual Shear Strength 111
6.3.4 Steady State Line 111
6.3.5 Effect of Initial Void Ratio 112
6.3.6 Effect of Vertical Stress 112
6.3.7 Apparent Cohesion 113
Chapter 7: Conclusions and Recommendations 134
7.1 Conclusions 134
7.2 Recommendations for Further Research 135
References 136
Appendix 1: Calibration 141

Appendix 2: Conventional Tests 147
Appendix 3: Effects of Shaft Friction, Density and Rotation Rate 159
Appendix 4: IC-D Triaxial Vane Tests 188
Appendix 5: IC-U Triaxial Vane Tests 213
Appendix 6: AC-D Triaxial Vane Tests 236

Table of Figures and Tables

Figure 2.1: The Vane Test (Chandler, 1988) 30
Figure 2.2: μ_R Correction Factor (Bjerrum 1973) 31
Figure 2.3: μ_A Correction Factors (Bjerrum, 1973) 32
Figure 2.4: Stress Distribution Along Vane Blades (after Wroth, 1984) 33
Figure 2.5: State of Stress during the Vane Test (after Wroth, 1984) 34
Figure 2.6: Effect of Rotation Rate on Swedish Clay (taken from Chandler, 1988) 35
Figure 2.7: Effect of Rate on Canadian Clay (taken from Chandler, 1988) 36
Figure 2.8: Effects of Rate on Pierre Shale and Kaolinite (Sharifounnasab and Ullrich, 1984) 37
Figure 2.9: ASTM Field Vane Geometry (ASTM D-2573) 38
Figure 2.10: ASTM Miniature Vane Geometry (ASTM D-4648) 39
Figure 2.12: Photo of the NGI Triaxial Vane (Kenny and Landva, 1965) 41
Figure 2.13: Details of the NGI Triaxial Vane (Kenny and Landva, 1965) 42
Figure 2.14: Photo of NRC Triaxial Vane (Law, 1978) 43
Figure 2.15: Details of NRC Triaxial Vane (Law, 1978) 44
Figure 2.16: Slip Pin Used in NRC Triaxial Vane (Law, 1978) 45
Figure 2.17: NRC Results of Increase in All Around Stress (Law, 1978) 46
Figure 2.18: NRC Results of Increase in Horizontal Stress (Law, 1978) 46
Figure 2.19: NRC Results of Increase in Vertical Stress (Law, 1978) 46
Figure 2.20: Mohr's Circle as Defined by Hansen and Gibson (Hansen and Gibson, 1954) 47
Figure 2.21: Inclination of Failure Surface to the Horizontal (Hansen and Gibson, 1954) 48
Figure 2.22: Instrumented Vane from Menzies and Merrifield (Menzies and Merrifield, 1980) 49
Figure 2.23: Stress Distribution along the a) vertical blade edge, b) horizontal blade edge (Menzies and Merrifield, 1980) 50
Figure 2.24: Results of Vane Tests in Sand (Wilson, 1963) 51
Figure 2.25: Photo of CSU Piezovane (Charlie et al, 1995) 52
Figure 2.26: CSU Piezovane (Charlie et al, 1994) 53
Figure 2.27: Piezovane Results showing Contractive Behaviour (Charlie et al, 1994) 54
Figure 2.28: Piezivane Results showing Dilative Behaviour (Charlie et al, 1994) 54
Figure 2.29: Liquefaction Potential Based on steady State (Casagrande, 1976) 55
Figure 3.1: Triaxial Vane Schematic 64
Figure 3.3: Vane Configuration 66
Figure 3.5: Drive Shaft 68
Figure 3.6: A/C Motor and Variable Speed Control Unit 69
Figure 3.7: Worm Gear 70
Figure 3.8: Rotation Transducer 71
Figure 3.9: Mercury Pressure System Schematic 72
Figure 3.10: Valve Configuration 73
Figure 3.11: Location of Anti Rotation Rods 74
Figure 3.12: Clay Base 75
Figure 3.13: Sand Base 76

Figure 3.14: a) Compression Cap, b) Extension Cap 77
Figure 3.15: Volume Gauge 78
Figure 3.16: Test results a) with a cyclical response due to shaft damage and b) without a cyclical response after repair 79
Figure 3.17: Triaxial Equipment used during conventional testing 80
Figure 3.18: Direct Shear equipment used during conventional testing 81
Figure 3.19: Odeometer used during conventional testing 82
Figure 4.1: Vane in position for sand sample 86
Figure 4.2: Boiling sand in a pycnometer to ensure saturation 87
Figure 4.3: Pluvated sample 88
Figure 4.4: Completed sand sample 89
Figure 4.5: fully assembled cell with sand sample 90
Figure 5.1: Grain size distribution of Unimin 2010 sand 98
Figure 5.2: Gelatin sample mold 99
Figure 5.3: Suction filtration device 100
Figure 5.4: Density verification results 101
Figure 5.5: Character of the drag coefficient as a function of Reynolds number for objects with various degrees of streamlining (from Munson, Young and Okiishi, 1994) .. 102
Table 6.1: Conventional Test Program 115
Table 6.2: Triaxial Vane Apparatus Test Program 117
Table 6.3: Comparison of Triaxial Vane Results to Previous Results 118
Figure 6.1: Drained Triaxial Tests Results 119
Figure 6.2: Undrained Triaxial Test Results 120
Figure 6.3: Drained Direct Shear Test Results 121
Figure 6.5: Effects of Initial Void Ratio on Drained Shear Strength Measured by the Triaxial Vane 123
Figure 6.6: Influence of Shear Rate 124
Figure 6.7: Typical IC-D Triaxial Vane test results 125
Figure 6.8: IC-D Triaxial Vane Results 126
Figure 6.10: Typical IC-U Triaxial Vane test results 128
Figure 6.11: IC-U Triaxial Vane Results 129
Figure 6.13: AC-D Triaxial Vane Results 131
Figure 6.14: Steady State Line for Unimin 2010 Sand 132
Figure 6.15: Effect of Relative Density on Shear Strength (Deschenes, 1978) 133

Chapter 1: Introduction

1.1 General

Since the development of the vane shear in the first half of the twentieth century, it has become one of the most widely used field tests in the world. Initially developed by Cadling in 1948, the vane test has been used to provide rapid in-situ measurements of both peak and residual shear strengths of clays. Although perceived as a relatively simple test, the vane test is in fact a theoretically complex test with complex stress paths that are even to this day not fully understood.

To help provide a better understanding of the vane test, in 1965 Kenney and Landva developed the first Triaxial Vane Apparatus at the Norwegian Geotechnical Institute. The purpose of this device was to allow for the study of the vane under controlled conditions to better understand all the factors that affect vane test results. Subsequent development was undertaken by Law (1978) and Pamukcu and Suhayda (1988).

However, previous investigation into the vane test has been almost exclusively limited to the study of this test in clays. Whether this limitation was caused by the perception that the vane test was valid for clay only or by technical limitation when the test was first developed is not understood. In either case the effect has been the same; the vane test has been all but excluded as a viable test for cohesionless materials.

This research has focused on the development of a new Triaxial Vane Apparatus as part of on going research on strength-deformation behaviour of soils at the University of Ottawa. Additionally, this device has then been used to study the applicability of using the vane test to determine the shear strength of sands. It was also of interest to compare the results from this research to previous investigations conducted on the same material with more conventional testing methods.

1.2 Objectives of the Research

The objectives of this research were:

1) To develop a Triaxial Vane Apparatus that:
    a. had the ability to reproduce any stress history;
    b. had the ability to accommodate and soil type;
    c. incorporated full data acquisition systems.
2) Use the Triaxial Vane Apparatus to study the use of the vane in determining the shear strength of cohesionless materials including the effects of:
    a. shaft friction;
    b. initial void ratio;
    c. rate of shearing;
    d. influence of initial stress conditions.

1.3 Scope of the Research

In order to accomplish the research objectives, experimental work was undertaken on the following:

1) Develop a working device capable of meeting all requirements;
2) Investigate the ability to produce uniform samples;
3) Investigate the friction developed along the vane shaft;
4) Investigate the influence of initial relative density on measured shear strength;
5) Investigate the effect of different shear rates on measured peak and residual strength;
6) Investigate the use of the vane in a sand under the following test conditions
    a. Isotropically consolidated drained
    b. Isotropically consolidated undrained
    c. Anisotropically consolidated drained
    d. Anisotropically consolidated undrained

1.4 Outline of Thesis

Chapter 2 presents a literature review on the history of the vane shear test, the Triaxial Vane Apparatus and previous investigations into the use of the vane test in sands.

Chapter 3 describes the Triaxial Vane Apparatus developed during this research.

Chapter 4 describes the sample preparation method.

Chapter 5 describes the material selected for this research and density verification tests.

Chapter 6 describes the results of the experimental program.

Chapter 7 presents the conclusions of this study and additional recommendations for further research.

Appendix 1 presents the results of the calibration of the Triaxial Vane Apparatus.

Appendix 2 presents the results of conventional testing on the material used.

Appendix 3 presents the results of the testing to determine the effects of density, vane shaft friction and rotation rate.

Appendix 4 presents the results of the isotropically consolidated drained testing.

Appendix 5 presents the results of the isotropically consolidated undrained testing.

Appendix 6 presents the results of the anisotropically consolidated drained testing.

Chapter 2: Literature Review

2.1 The Vane Test

This section will discuss some of the key points in the historical development of the vane shear test, focusing on the theoretical interpretation of the vane test results and some of the current conflicts in the understanding of the vane test. Additionally, the current standards for interpreting the vane test will be discussed.

2.1.1 Historical and Theoretical Developments

The vane test has become one of the most common in-situ tests used today for any site that has clay soils. Originally conceived in the early 1900's, the vane test as it is known today was proposed by Cadling in the late 1940's (Cadling and Odenstad, 1948). Essentially, the vane test is composed of inserting a vane (as shown in **Figure 2.1**) and rotating the vane to shear the soil. The maximum torque required to turn the vane then provides an estimate of the shear strength of the soil. Since the vane is commonly used in clays, with lower permeability, the vane test is believed to be rapid enough to be considered an undrained test. Although the vane test appears to be a simple test, in reality it is very complicated and even to this day is not fully understood.

From the beginning of the vane test, it was realized that the strengths measured by the vane were not similar when compared to values obtained from other test methods or strengths back calculated from failures. In order to relieve this apparent contradiction, Bjerrum (1973) proposed two empirical correction factors in the form:

$$(s_u)_{field} = (s_u)_{vane} \cdot \mu_R \cdot \mu_A \quad \text{..... (Eq 1)}$$

In this equation, μ_R is a correction factor that corrects for the effects of time required to shear the soil to failure and μ_A is a correction factor for the anisotropic strength of clay.

Figure 2.2 shows the proposed values for μ_R and **Figure 2.3** shows the values of μ_A for three different soil plasticity levels.

A major difficulty that many researchers had with the initial investigations into the vane tests was the assumptions concerning the stress distribution around the vane blades. Initially, the assumption was that the stresses were uniformly distributed along the horizontal and vertical edges of the vane. Consequentially, recent investigations have focused on determining the actual stress distribution on the vane (Donald et al, 1977; Menzies and Merrifield, 1980; Wroth, 1984). Resulting from these investigations was the proposed stress distributions shown in **Figure 2.4**. The stresses along the vertical surfaces do conform to the assumption of uniform stress distribution, however along the horizontal surfaces, the stresses are far from uniform. Wroth proposed that the stresses along these horizontal segments follow the polynomial form:

$$\frac{\tau}{\tau_m} = \left(\frac{r}{d/2}\right)^n \quad \text{..... (Eq 2)}$$

Where τ_m is the maximum value of shear stress, assumed to occur simultaneously along the entire vertical failure surface and r is the radial distance from the vane centerline to the failure surface. From this, the torque contributions from the horizontal surfaces, T_h, and the vertical surfaces, T_v, have been determined.

$$T_h = 2\int_0^{d/2} 2\pi r^2 \tau dr$$

$$T_h = \frac{\pi d^3 \tau_m}{2(n+3)} \quad \text{..... (Eq's 3,4,5)}$$

$$T_v = \frac{\pi d^2 h \tau_m}{2}$$

Additionally, Wroth proposed a possible state of stress that occurs during the vane test as shown in **Figure 2.5**. The overall result from these investigations was the suggestion that the vane test actually underestimates the undrained strength by approximately 9%.

An additional conflict concerning the vane test arises over the effect of vane rotation rate. Several researchers have conducted experiments to determine the effect of vane rotation rate on measured shear strength, but these results appear to contradict each other. Torstensson (1977) and Wiesel (1973) both conducted tests on plastic Swedish clays, the results of which are shown in **Figure 2.6**. Both of these data sets shown similar results. However, when compared to the results of Roy and Leblanc (1988) shown in **Figure 2.7**, the results are contradictory. Torstensson and Wiesel show that the measured shear strength continuously and significantly decreases as rotation rate decreases, while Roy and Leblanc show only a minor decrease in strength as rotation rate decreases until a rate of approximately 10^{o} per min, when strength starts increasing. This contradiction is further increased by the results of Sharifounnasab and Ullrich (1984) as shown in **Figure 2.8**. Sharifounnasab and Ullrich studied the effects of rotation rate on both Pierre Shale and Kaolinite and determined that for the shale, the strength increased with increased shear rate while strength decreased with increased shear rate for the kaolinite. As such, it is not believed that the effects of rotation rate can be generalized; the effect must be determined for each soil independently.

2.1.2 Current Practice

The current North American standard practice concerning performance and interpretation on the vane test is outlined in ASTM D-2573. For simplicity, the performance of the vane test will not be covered here; only the interpretation will be discussed. ASTM requirements do not specify dimensions for the vane blades, however a specific geometry is required, as shown in **Figure 2.9**. For the calculation of shear strength, s (in kPa), ASTM gives the following formula:

$$s = T \cdot \frac{1}{K} \quad \text{..... (Eq 6)}$$

Where T is the maximum measured torque (in N•m) and K is a vane constant given by:

$$K = \left(\frac{\pi}{10^6}\right)\left(\frac{D^2 H}{2}\right)\left(1 + \frac{D}{3H}\right) \quad \text{..... (Eq 7)}$$

For rectangular vanes; and,

$$K = \frac{1}{10^6}\left[\pi D^3 + 0.37\left(2D^3 - d^3\right)\right] \quad \text{..... (Eq 8)}$$

For tapered vanes.

Where D is the vane diameter (in cm), H is the vane height (in cm) and d is the rod diameter (in cm).

Additionally, a miniature vane shear device is used for testing of soils in the laboratory and is described in ASTM D-4648. The miniature vane uses either rectangular or square blade configurations (as shown in **Figure 2.10**). The vane is attached to a device capable of measuring the torque (**Figure 2.11**), either by mechanical springs (A) or by electronic transducers (B). Rotation of the vane is provided by a motor capable of rotating the vane at a constant rotation rate of between 60° to 90° per minute. The vane blade is pushed directly into the open end of an undisturbed tube sample and rotated to test the sample. This is one limitation of the miniature vane device; since the sample has undergone stress relief after sampling, the strength measured in the lab by the miniature vane is not indicative of the in-situ strength.

After the maximum torque has been measured, the strength is calculated similarly to the field vane such that:

$$s = T \cdot \frac{1}{K}$$

However, the calculation of the vane constant is given by:

$$K = \frac{\pi D^2 H}{2 \cdot 10^{-6}} \left[1 + \frac{D}{3H} \right] \quad \text{..... (Eq 9)}$$

Where D is the vane diameter (in cm), H is the vane height (in cm).

2.2 The Triaxial Vane Apparatus

The concept of the triaxial vane is quite simple; combine the triaxial test and the miniature laboratory vane into one device. This device uses a miniature vane incorporated into a triaxial cell in order to study the use of the vane in different soils as well as allowing the effects of different vane parameters, such as rotation rate and vane geometry, to be studied in controlled stress conditions. Although this device appears to be the ideal equipment to study the vane shear test, it has remained relatively unused and obscure. Only three reference to this device were found in the literature: Kenny and Landva (1965), Law (1978) and Pamukcu and Suhayda (1988).

This section will describe the development of two of these devices; the original device, developed by Kenny and Landva for the Norwegian Geotechnical Institue (and will hence be referred to as the NGI Triaxial Vane), followed by that developed by Law for the National Research Council of Canada (and hence will be referred to as the NRC Triaxial Vane). The third device, by Pamukcu and Suhayda, was essential identical to the device designed by Law and such will not be described here.

2.2.1 NGI Triaxial Vane

The NGI Triaxial Vane is shown in **Figures 2.12 and 2.13**. The device was designed as part of an investigation into the undrained shear strength of soils to study the benefits and limitations of the vane shear test.

The vane (labeled 1 on Figure 2.13) was constructed from 0.33 mm spring bronze with a 2.0 mm silver steel shaft. Since the friction on the shaft can drastically affect the measured shear strength in the vane test, an inventive solution was devised in this design to eliminate the effect. The vane shaft was encased in an oil filled, stainless steel tube (2). The vane shaft rotated inside this fixed tube and as such, the friction on the shaft always remained constant, regardless of the soil type or confining stress.

The triaxial cell used was a standard Geonor cell with a $20cm^2$ sample area (i.e. a standard 50mm diameter sample). The only major modification required to the cell was the addition of a slotted opening in the base (as shown in section A-A) to house the vane when in a recess position and a removable metal plug (4) to allow the vane to be inserted from the bottom.

Power was provided to the device by a small electric motor (18) coupled to a gear box (19). By using various combinations of different motors and different gearing ratios, any combination of required torque and rotation speed could be achieved.

The torque provided by the motor was then transferred to the vane by a chain drive attached to jewel bearing rollers (14). Connected to the rollers are three pairs of blade springs (20) which are then connected to the vane shaft by additional bearing (12) (as shown in section B-B). By measuring the deflection between the blade springs and the shaft bearing, using the pointer and scale (15 and 16), the torque can be determined.

2.2.2 NRC Triaxial Vane

The NRC Triaxial Vane is shown in **Figures 2.14 and 2.15**. The device was developed to investigate the effect of different stress ratios on the measured vane shear strength on Leda clays found in the Ottawa, Ontario, Canada area. This device was designed by essentially mounting a standard commercial miniature laboratory vane onto a triaxial cell.

The vane, labeled 10 on figure 15, was constructed with 0.28 mm nichrome, with a height of 20mm and a diameter of 10mm. In order to determine the shaft friction, the vane was designed with a slip pin arrangement shown in Figure 16. When the vane is rotated to shear the soil, the pin locks the vane blade into position, measuring the total torque required. Once maximum torque has been achieved, the rotation is reversed and the shaft can turn independently of the vane, allowing the shaft friction to be measured. This value is then subtracted from the total torque to determine the torque required to fail the soil.

As with the NGI Triaxial Vane, the triaxial cell used in the NRC device remains essentially unchanged from its originally configuration with the capability of handling a sample of 36mm diameter and 80mm height. The vertical load piston (3) has been hollowed out, allowing the vane shaft (1) to pass through the piston, eliminating the need for major modifications to be done to the triaxial cell itself. The only modifications required are the inclusion of posts (14) on either side of the sample to prevent rotation of the sample and a recess (12) cut into the sample cap (6) to allow the vane to be retracted during consolidation.

Once the vane shaft has passed through the load piston it is then directly attached to a standard miniature laboratory vane device, which controls rotation and torque measurements.

As mentioned earlier, the NRC triaxial device was used to investigate the effects of different stress ratios on the measured vane strength of Leda clays. Law conducted several series of triaxial vane tests changing; a) the all around consolidation stress, b) the

horizontal consolidation stress and c) the vertical consolidation stress. The results of these tests are shown in Figures **2.17, 2.18 and 2.19** respectively. As can be seen from the results, the vane measured strength of the Leda clay increases approximately 50% for both increases in overall and horizontal stress but only 5% for a similar increase in vertical stress.

2.3 Theoretical Behavior of Vane Test

In order to better determine the applicability of the Triaxial Vane test, a model is needed with which to evaluate the test results. However, with the complexity of the Triaxial Vane test, the model needs very specific requirements. It needs to be able to predict the results from the vane test, including accounting for the difference between the stresses acting on the horizontal and vertical surfaces, and it must be able to account for both isotropic and anisotropic stress conditions. Fortunately, a model was available that, with some modifications, handled all requirements.

Hansen and Gibson (1954) developed a model to predict the undrained shear strength of clays. Starting with the Hvorslev (1937) equation for the shear strength of soil:

$$s = c_e + (\sigma_n - u)\cdot \tan\phi = c_e + \sigma_n' \tan\phi \quad \text{..... (Eq 10)}$$

which can be rewritten as:

$$s = \kappa p + \sigma_n' \tan\phi \quad \text{..... (Eq 11)}$$

Where p is the greatest effective pressure to which the soil has been subjected and κ is a soil constant. This can also be represented by a Mohr's failure surface as shown in **Figure 2.20** where:

$$\sigma_1' = \frac{c - \kappa p \cdot \cos\phi}{\sin\phi} + c \quad \text{..... (Eq 11)}$$

$$\sigma_3' = \frac{c - \kappa p \cdot \cos\phi}{\sin\phi} - c \quad \text{..... (Eq 12)}$$

$$s = c \cdot \cos\phi \quad \text{..... (Eq 13)}$$

$$\Delta V = C_1 \Delta\sigma_1' + C_2 \Delta\sigma_2' + C_3 \Delta\sigma_3' \quad \text{..... (Eq 12)}$$

Where C is equal to C_s, C_c or C_{cr} (the expansibility, compressibility or recompressibility defined by volume change per unit volume per unit change in effective stress) and corresponds to $\Delta\sigma'$. Additionally:

$$\lambda = \frac{C_s}{C_c} \quad \text{..... (Eq 13)}$$

$$\lambda_r = \frac{C_s}{C_{cr}} \quad \text{..... (Eq 14)}$$

The initial state of stress for any point in the soil can be represented by

$$c_o = \tfrac{1}{2} \cdot p(1 - K) \quad \text{..... (Eq 15)}$$

$$K = \frac{\sigma_h'}{\sigma_v'} \quad \text{..... (Eq 16)}$$

From these equations, the strength, c, along any surface at angle β to the horizontal (see **Figure 2.21**) can be determined:

$$\frac{c}{p} = \kappa \cdot \cos\phi + \frac{1}{2}(1 + K)\sin\phi - \sin\phi\left(\frac{1-\lambda}{1+\lambda}\right)\left[\left(\frac{c}{p}\right)^2 - 2\frac{c}{p}\frac{c_o}{p}\cos 2(\alpha - \beta) + \left(\frac{c_o}{p}\right)^2\right]^{\frac{1}{2}}$$

..... (Eq 17)

$$\alpha = 45^o + \frac{\phi}{2} \quad \text{... (Eq 18)}$$

Hansen and Gibson showed that for the vane test:

$$c_v = c_c \left[\frac{1 + \frac{D}{3H}\frac{c_r}{c_c}}{1 + \frac{D}{3H}} \right] \quad \text{..... (Eq 19)}$$

Where c_v is the strength measured by the vane test, c_c is the strength along the horizontal surfaces and c_r is the strength along the vertical surface. For the horizontal plane, at failure:

$$\sigma_1' = \frac{c_o - \kappa p \cos\phi}{\sin\phi} + c_c \quad \text{..... (Eq 20)}$$

$$\sigma_3' = \frac{c_o - \kappa p \cos\phi}{\sin\phi} - c_c \quad \text{..... (Eq 21)}$$

For the condition of no volume change:

$$(\sigma_1' - Kp) + \lambda(\sigma_3' - Kp) = 0 \quad \text{..... (Eq 22)}$$

From equations 20,21 and 22:

$$\frac{c_c}{p} = \frac{\kappa \cos\phi + K \sin\phi}{1 + \left(\frac{1-\lambda}{1+\lambda}\right)\sin\phi} \quad \text{..... (Eq 23)}$$

c_r can then be determined from equation 17 by setting $\beta = 90^\circ$ and c_v can be calculated from equation 19.

However, in equation 22, the assumption is made the undrained conditions apply. What happens if this is not the case? By modifying the Hansen and Gibson model:

$$(\sigma_1' - Kp) + \lambda(\sigma_3' - Kp) = \Delta V \quad \text{..... (Eq 24)}$$

Leads to:

$$c_c = \frac{\frac{\Delta V \sin\phi}{1+\lambda} + p(\kappa\cos\phi + K\sin\phi)}{1+\left(\frac{1-\lambda}{1+\lambda}\right)\sin\phi} \quad \text{..... (Eq 25)}$$

2.4 Use of the Vane Shear Test in Cohesionless Soils

Since its advent, the vane test has been used primarily to determine the undrained shear strength of clays. The use of the test in cohesionless materials has been all but ignored. The cause of this lack of research is unknown; whether due to the traditional thinking that the vane was only to be used in clay or physical limitations of the vane devices themselves at the tests inception (since the higher shear stresses in cohesionless materials require stronger materials). However, though the research is limited compared to the vast amount of research conducted on the vane test in clays, several researchers have studied this area. The results of these research efforts are discussed here.

2.4.1 Vane Stress Distribution in Sands

One of the commonly debated aspects of the vane test is the exact nature of the stress distribution along the edges of the vane during the vane shear test. This distribution has important consequences; the exact distribution will drastically alter the horizontal to vertical strength ratio, s_h/s_v (Wroth, 1984). In order to help establish the exact distribution of stresses along the edge, Menzies and Merrifield (1980) developed an instrumented vane shown in **Figure 2.22**. The vane was 240mm high and 120mm in diameter and two of the blades had cantilevered "fingers" with foil strain gauges, which allowed the shear stress to be measured independently on each section. Tests were then conducted on both sand and clay to determine the stress distribution along the vane edges. The results of these tests are shown in **Figure 2.23**. These results shown that the stress distribution along the vertical blade edge is the same for both clays and sands, and can be reasonably

approximated with a rectangular stress distribution. However, the stress distribution along the horizontal blade edge is quite different between the two materials. For the clay, the distribution is a polynomial distribution while the sand has a definite triangular distribution. This difference is best shown in equation 2, given earlier, where for clays, n=5, but for sands, n=1. With these values, the s_h/s_v ratios can be determined from equations 4 and 5, which are 1/16 for clays and 1/8 for sands. This indicates that the change in shear strength due to a change in stress conditions will be different for clays and sands. As such, care must be taken when directly comparing the effectiveness of the vane in sands and clays.

2.4.2 Effect of Pore Pressure

Wilson (1963) investigated the effects of pore water stresses on the strength of soils measured using the vane in clays, sands and silts. The investigation was undertaken to show that, for dilatant soils, the negative pore pressures induced during shear would increase effective stress and thereby create an artificially high measurement of shear strength. For the research, Wilson used a standard Wykeham-Farrance laboratory vane apparatus with a special vane blade, having a small boring in one blade to allow for the attachment of a pore pressure measuring device to measure excess pore pressures induced at the failure surface. Medium fine-grained Zircon sand was used in a dense state for all testing done in sand. **Figure 2.24 a)** shows the results of testing to compare the maximum vane torque to the vane rate and pore pressure. Wilson claims that this plot shows that the measured torque is completely independent of vane rotation rate. However, two variables, rotation rate and pore pressure, are being changed in these plots, and this may provide a false conclusion. Close inspection of the data points shows that, at similar values of pore pressure, the slower vane rotation rates appear to plot higher than the high rotation rates, indicating that there is a rotation rate effect. Since only three rotation rates were used, the data set is not large enough to make any definitive relationships. **Figure 2.24 b)** shows the results of testing to compare the maximum torque to pore pressure. These results show that, as negative pore pressure increases, maximum torque also increases, validated

Wilson's hypothesis that the negative pore pressure induced during shear will artificially increase the measured shear strength in dilative soils.

2.4.3 The Piezovane

One of the most extensive investigations into the use of the vane in sand came with the development of the piezovane. The piezovane was developed independently by both Charlie et al (1994,1995), and Atkinson and Jesset (1990). However, this section will concentrate on the Chalie Piezovane, also called the CSU (Colorado State University) Piezovane, shown in **Figures 2.25 and 2.26.**

The CSU Piezovane is essentially a field vane that allows for pore pressure measurements directly at the failure surface. The vane itself is the same as outlined in ASTM D2573, with a height of 127mm, a diameter of 63.5mm and a blade thickness of 3.2mm, but the vane shaft is slightly larger (19mm diameter as opposed to 12.7mm) to accommodate the pressure transducer. The vane blades themselves have four small ports (as shown in Figure 2.26), which allow the pore pressure to be transferred to the pressure transducer. Testing procedures are also as outlined in ASTM D2573, with the exception that vane rotation rate is increased to 90° per min.

The Piezovane was developed as a method to test in-situ liquefaction potential of saturated sand. Unlike the piezocone, the piezovane does not suffer from the difficulties of volumetric strain strains caused by the testing itself or the variation in pore pressure measurement caused by measurement location. Typically results from the piezovane are shown in **Figures 2.27 and 2.28**. These figures show a definitive difference between the behavior of contractive and dilative soils. Since only contractive soils will liquefy, layers that may have liquefaction potential can be quickly identified for additional study. It should be noted that the piezovane cannot determine if a soil will liquefy, only whether the potential for liquefaction exists.

The applicability of the CSU Piezovane was tested during the Loma Prieta earthquake in 1989 (Charlie et al, 1994). During the earthquake, a farm in Monterey County, California experienced liquefaction induced lateral spreading. SPT, CPT and Piezovane tests were conducted at the site and showed that the Piezovane was able to identify the layers that had actually liquefied during the earthquake with 92% accuracy.

It should also be noted that, although the piezovane has been shown to be able to identify potentially liquefiable soils, Charlie et al have not investigated whether the actual shear strength of the sand determined during the piezovane test is representative of the pear or steady state shear strength of the soil.

2.5 Steady State and the Steady State Line

The development of the steady state concept has had a long and extensive history. A brief description of its importance and development will be presented in this section.

2.5.1 Liquefaction and Post Liquefaction Shear Strength

Liquefaction is the phenomenon where the behaviour of loose, saturated sand changes to a fluid state from a solid state. When this type of material is subjected to a sudden shock, such as an earthquake, the pore pressures will rise to a value very near the overburden stress, thereby reducing the effective stress to very close to zero. At this point the sand can begin to flow like a viscous fluid. Over the years, many researchers have proposed various definitions of liquefaction, including Poulos (1997):

> Liquefaction is the undrained shear failure of a loose sand or a soft clay that results when 1) the in-situ driving shear stresses on the soil mass prior to failure exceed the undrained steady state shear strength of the mass, 2) additional shear stresses are applied fast enough to cause undrained shear, and 3) the latter stresses are large enough to cause strains that exceed the strain at peak in the mass such that steady state deformation can be approached.

Once liquefaction has occurred, the available shear strength in the soil is reduced to the post liquefaction shear strength. As is apparent in the preceding definition, the post liquefaction shear strength is reached once steady state deformation has been achieved and is thus equal to the steady state strength.

2.5.2 Critical Void Ratio

The steady state concept began with Casagrande (1936) with the critical void ratio. During drained testing, the critical void ratio is the point at which a cohesionless soil can undergo any amount of deformation with a change in volume. For undrained testing, where volume changes are prevented, dense sands will tend to increase in strength, while looses sands will tend to decrease in strength during shearing. However, there must be a point between these two zones where the strength will not change; this is also the critical void ratio (Taylor, 1948).

2.5.3 Steady State of Deformation

Poulos (1971, 1981) expanded the critical void ratio concept as follows:

> The steady state of deformation for any mass of particles is that state in which the mass is continually deforming at constant volume, constant normal effective stress, constant shear stress and constant velocity. The steady state of deformation is achieved only after all particle orientation has reached a statistically steady state condition and after all particle breakage, if any, is complete, so that the shear stress needed to continue deformations and the velocity of deformation remains constant.

Steady state can only occur during continuous deformation of a soil at a constant velocity and can occur for any condition, either loading or drainage, that can completely break down the original structure of the soil mass into a flow structure.

2.5.4 Steady State Line

The steady state line (SSL) is defined as:

> A locus of points at which the soil can deform continuously at the steady state. It is not a line connecting static states of a soil. (Poulos, 1981)

It is conventionally shown as a two dimensional plot; either e vs. log p' or e vs. log τ, and the postion of the steady state line is a unique property of a soil (Castro and Poulos, 1977).

Casagrande (1975) proposed a liquefaction potential based on steady state:

$$L_p = \frac{\sigma'_{3i} - \sigma'_{3f}}{\sigma'_{3f}} \quad \text{..... (Eq 25)}$$

Where σ_{3i}' is the consolidation effective minor principle stress and σ_{3f}' is the effective minor principle stress at steady state (see **Figure 2.29**). If L_p is negative, the soil is in a dilative state where liquefaction is not possible. However, if L_p is <6, the soil is contractive with a high liquefaction potential. Casro and Poulos (1977) modified Equation 25 based on the pore pressure parameter A and the angle of friction

$$L_p = A\frac{2\sin\phi}{1+\sin\phi} \quad \text{..... (Eq 26)}$$

2.6 Factors Affecting the Steady State Strength

The steady state strength of a soil can be altered by many factors. This section gives a brief discussion of some of these factors and their influence on the steady state strength.

2.6.1 Void Ratio

Probably the single most important factor affecting the steady state strength of a soil is the void ratio. Previous research (Casagrande, 1938; Roscoe et al, 1958; Bishop et al, 1965; Castro, 1969) has shown that both the shear and effective normal stresses at steady state increase as void ratio decreases. Additionally, the effect of the initial void ratio is based on its position relative to the steady state line. If the void ratio is below the steady state line, the soil will exhibit a dilative behavior; if it is above the steady state line, the soil will exhibit a contractive behavior. Additionally, as the void ratio deceases, the steady state stresses (shear and effective normal) will increase (Casagrande, 1975; Castro et al, 1982).

2.6.2 Consolidation Stress

The consolidation stress in the soil also plays an important role in the steady state strength of a soil. For a given void ratio, a soil may be dilative at a lower stress, but become contractive at a higher stress (Casagrande, 1975) Additionally, while the steady state line is conventionally shown as a straight line, at very high and very low stresses, the steady state line tends to become curved (Tatsuoka et al, 1986).

2.6.3 Sampling

Potentially liquefiable soils, for which the steady state strength is most important to determine, are notoriously difficult to sample completely undisturbed. Any disturbance during sampling, transportation, handling or test preparation can densify the sample, which as mentioned earlier, will then increase the steady state strength measured during a

laboratory test. This value will then not be indicative of the in-situ steady state strength of the material.

2.6.4 Localization of Shear Failure

In steady state shear tests, shear failure occurs along a distinct, localized shear zone. Within this shear zone, as failure progresses, the void ratio will change from that of the overall sample void ratio. In a contractive sample, the void ratio within this shear zone will be lower than in the rest of the sample. However, during testing, only the overall void ratio can be determined and, as a result of this difference in void ratio, the steady state line will be shifted, resulting in a non-conservative positioning of the steady state line.

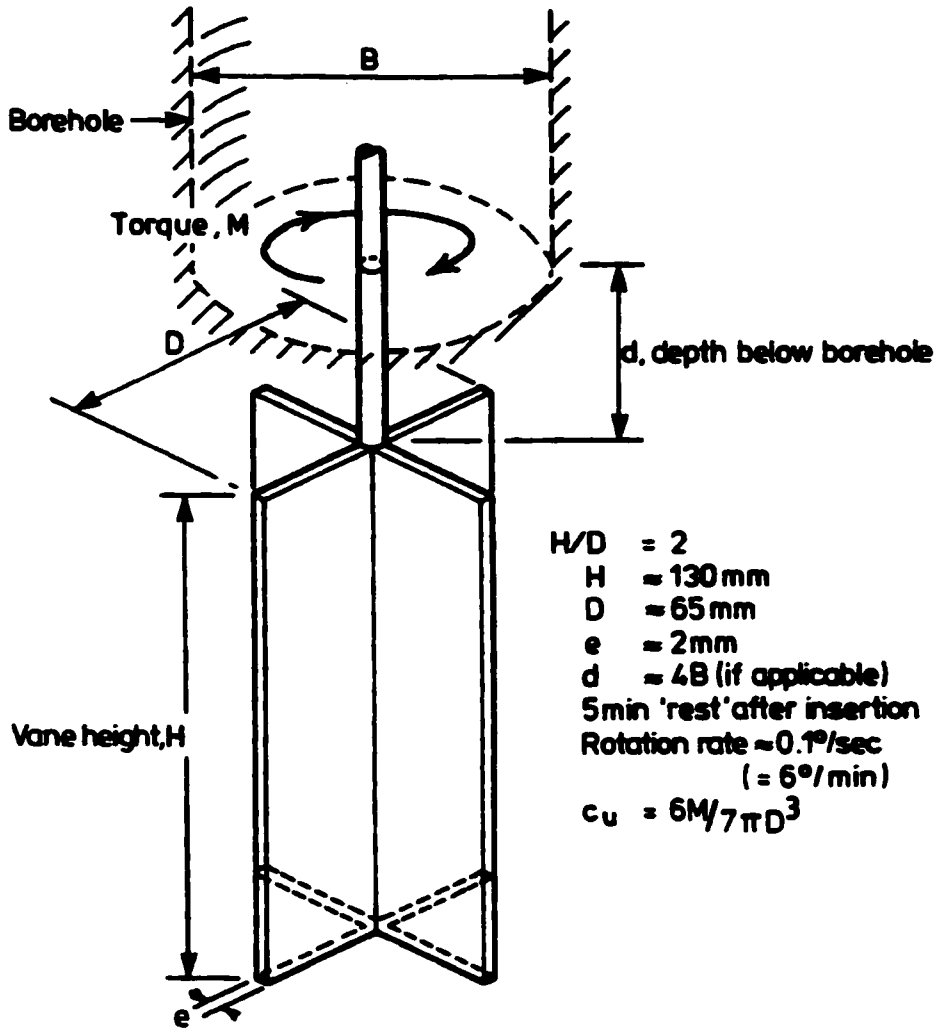

Figure 2.1: The Vane Test (Chandler, 1988)

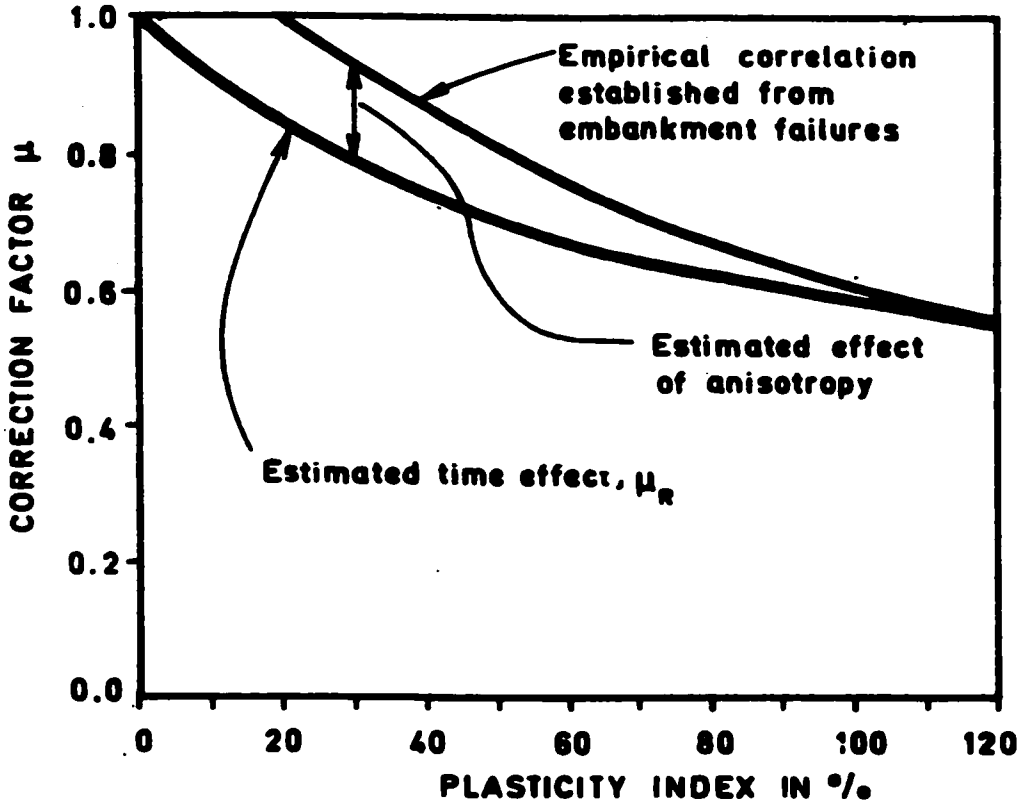

Figure 2.2: μ_R Correction Factor (Bjerrum 1973)

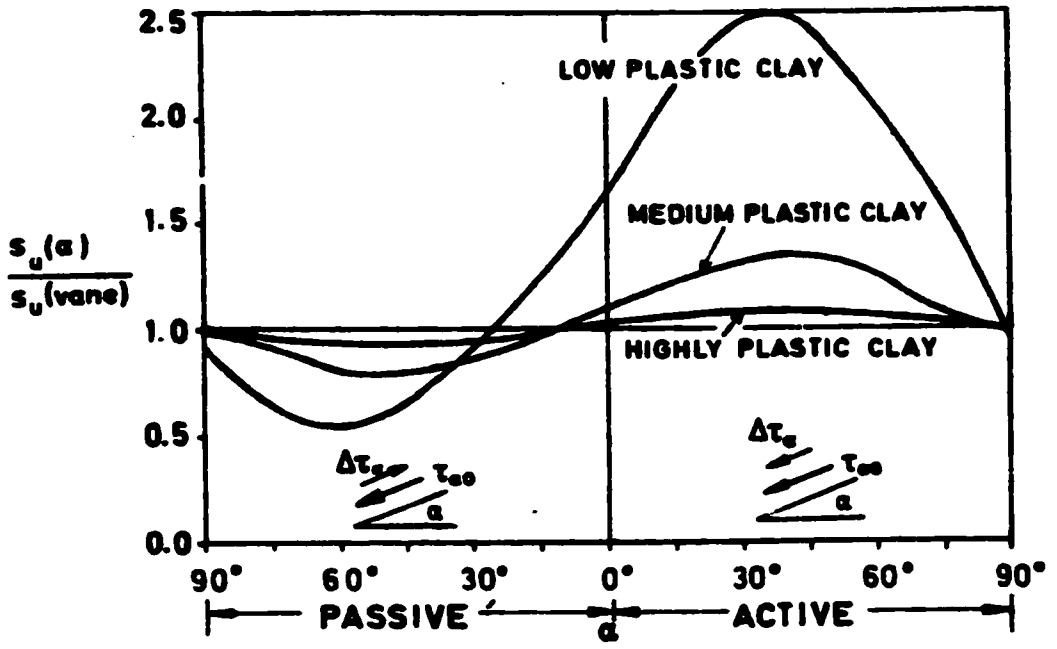

TYP. OF CLAY	I_p (%)	K_0	α'	ϕ'_c	$\frac{p_c}{p_0}$	Dm
LOW PLASTIC	10	0.50	0.03	30°	1.2	0.30
MEDIUM PLASTIC	50	0.65	0.15	15°	1.6	0.45
HIGHLY PLASTIC	100	0.80	0.30	10°	2.0	0.60

Figure 2.3: μ_A Correction Factors (Bjerrum, 1973)

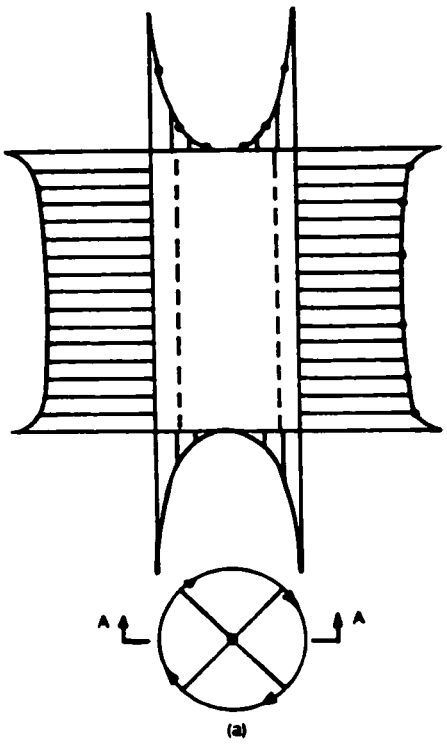

Figure 2.4: Stress Distribution Along Vane Blades (after Wroth, 1984)

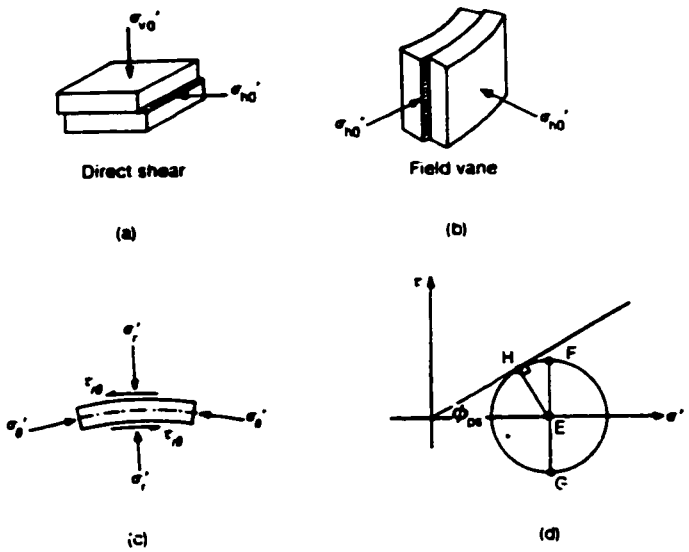

Figure 2.5: State of Stress during the Vane Test (after Wroth, 1984)

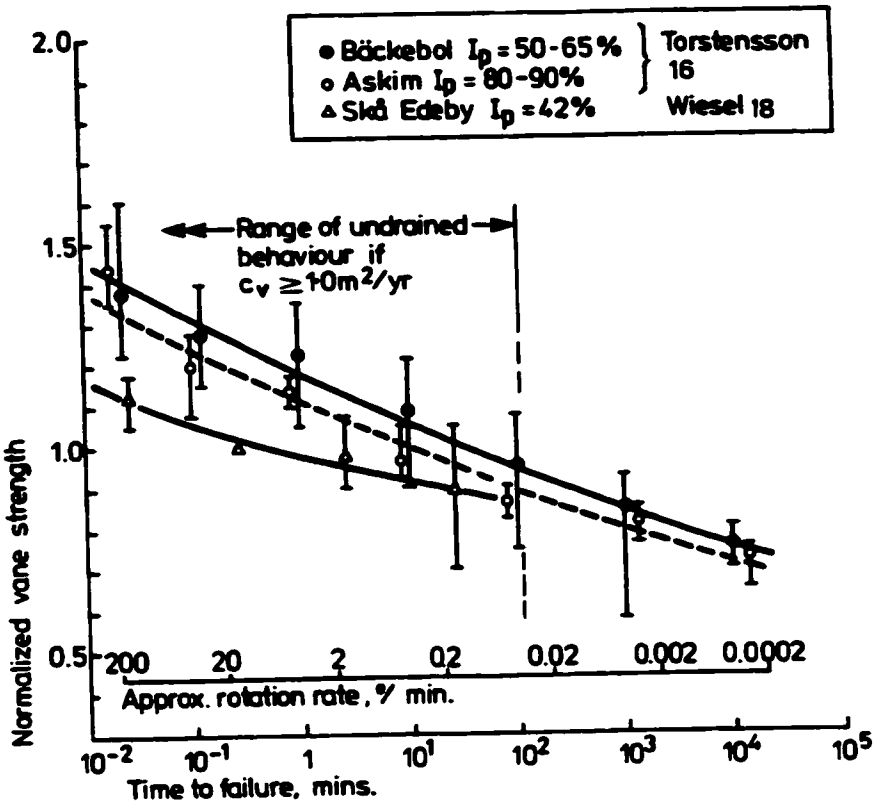

Figure 2.6: Effect of Rotation Rate on Swedish Clay (taken from Chandler, 1988)

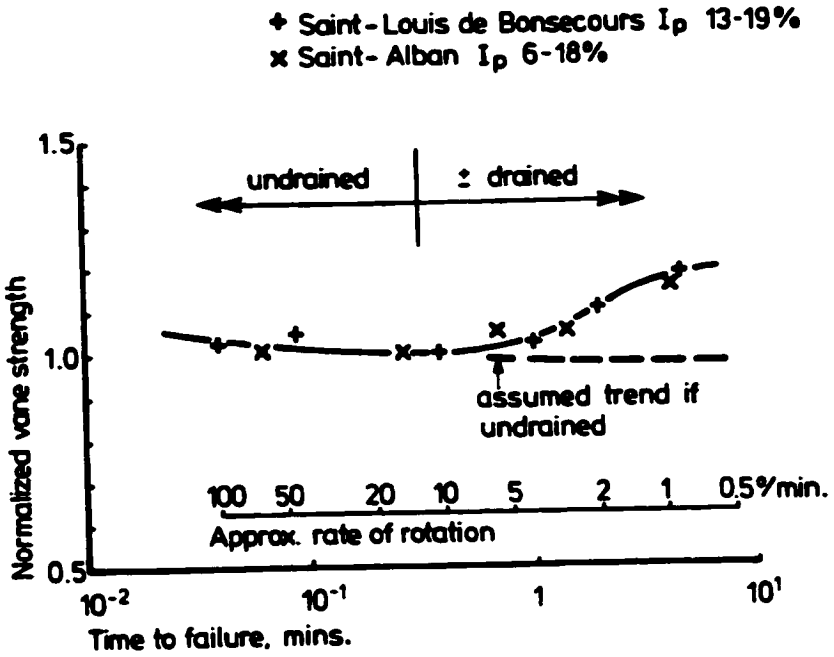

Figure 2.7: Effect of Rate on Canadian Clay (taken from Chandler, 1988)

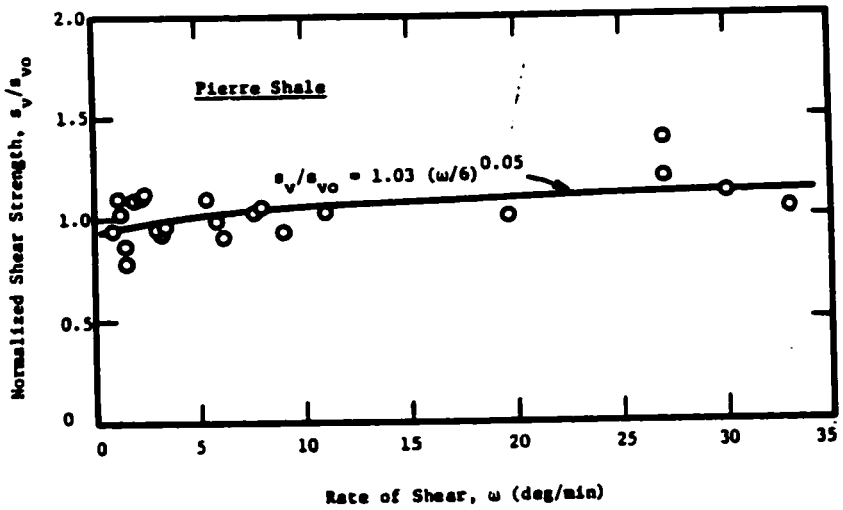

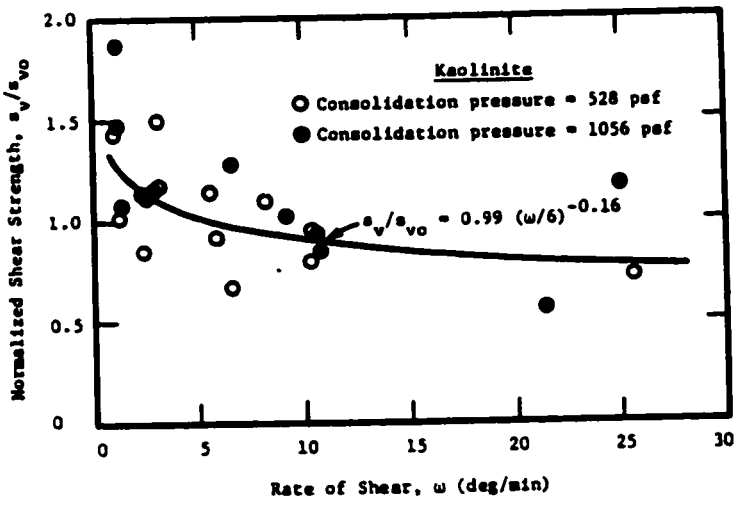

Figure 2.8: Effects of Rate on Pierre Shale and Kaolinite (Sharifounnasab and Ullrich, 1984)

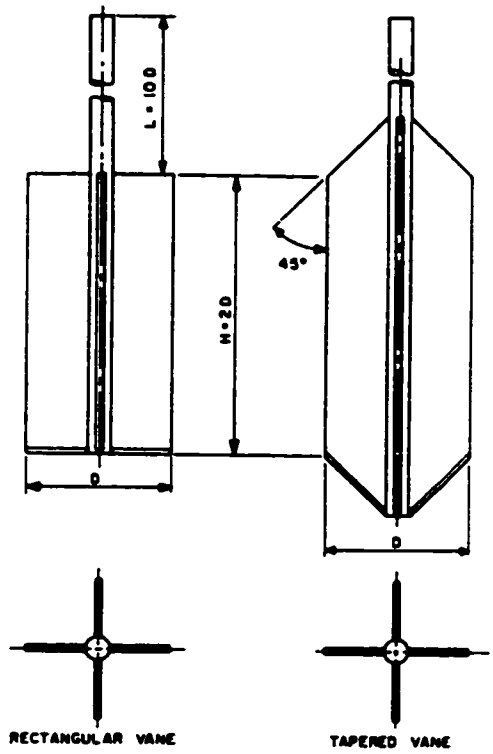

Figure 2.9: ASTM Field Vane Geometry (ASTM D-2573)

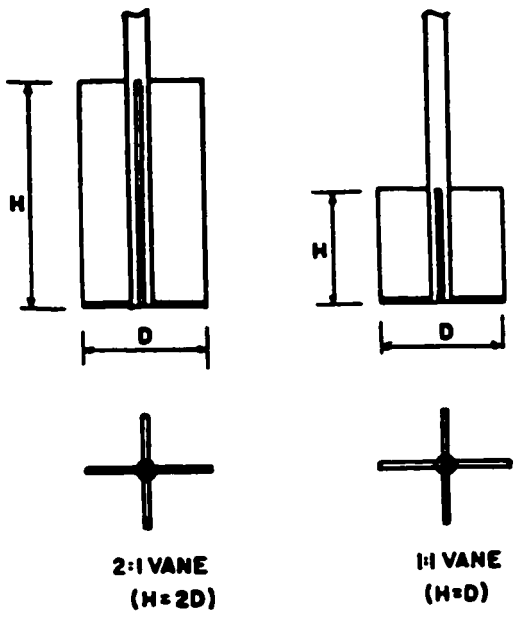

Figure 2.10: ASTM Miniature Vane Geometry (ASTM D-4648)

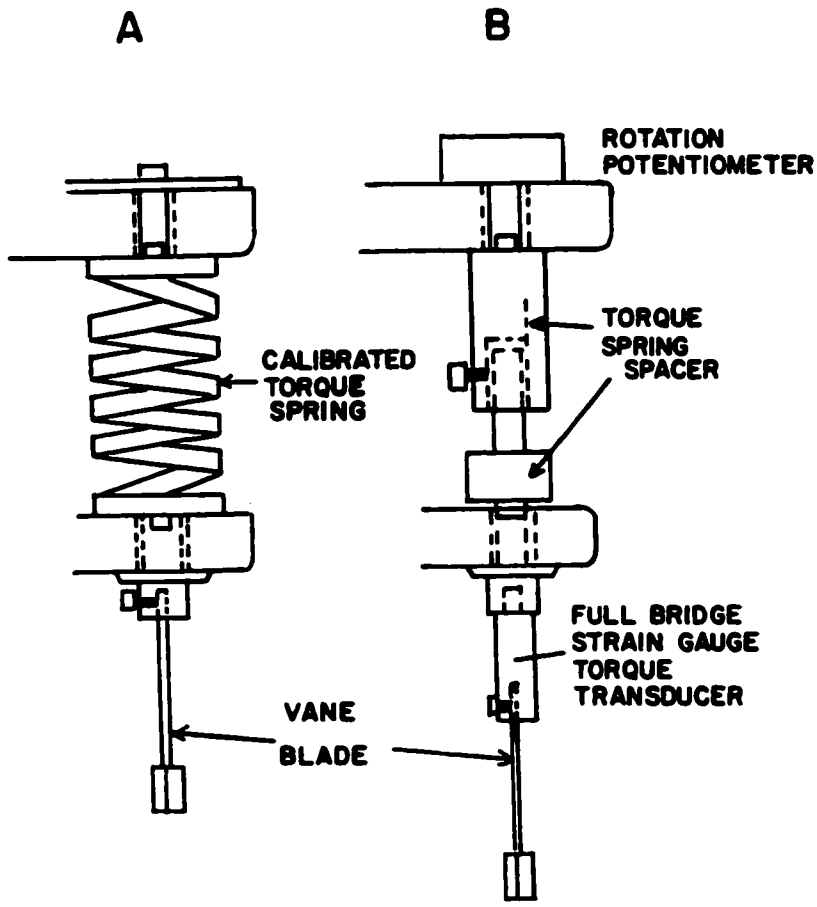

Figure 2.11: ASTM Miniature Vane Torque Configuration (ASTM D-4648)

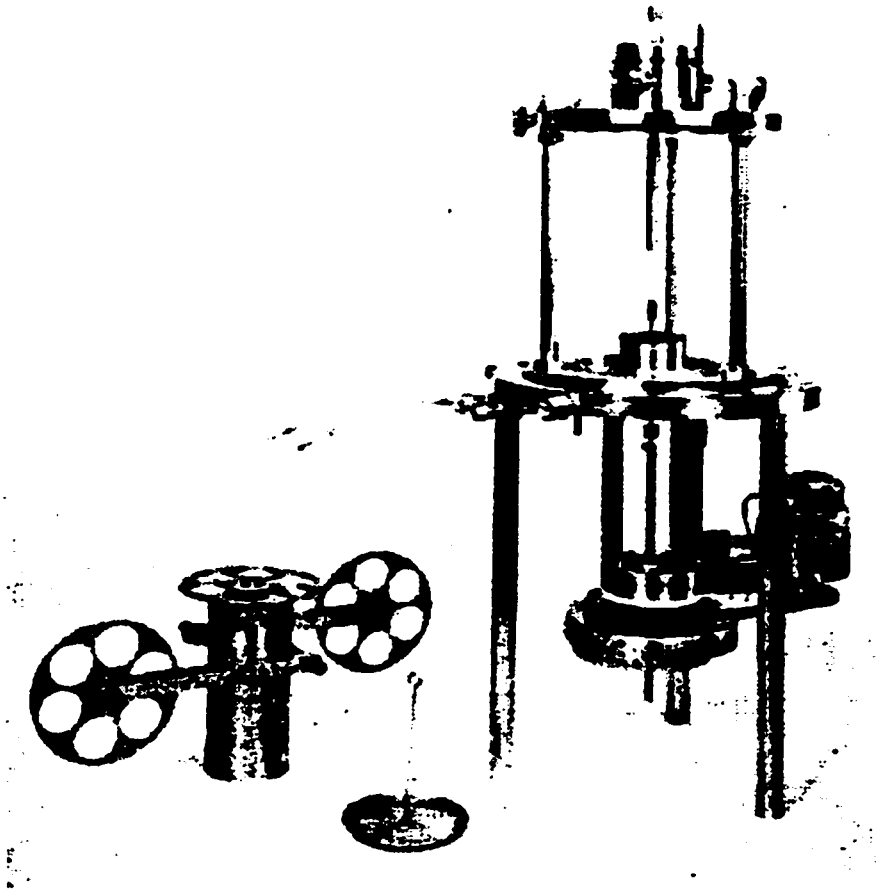

Figure 2.12: Photo of the NGI Triaxial Vane (Kenny and Landva, 1965)

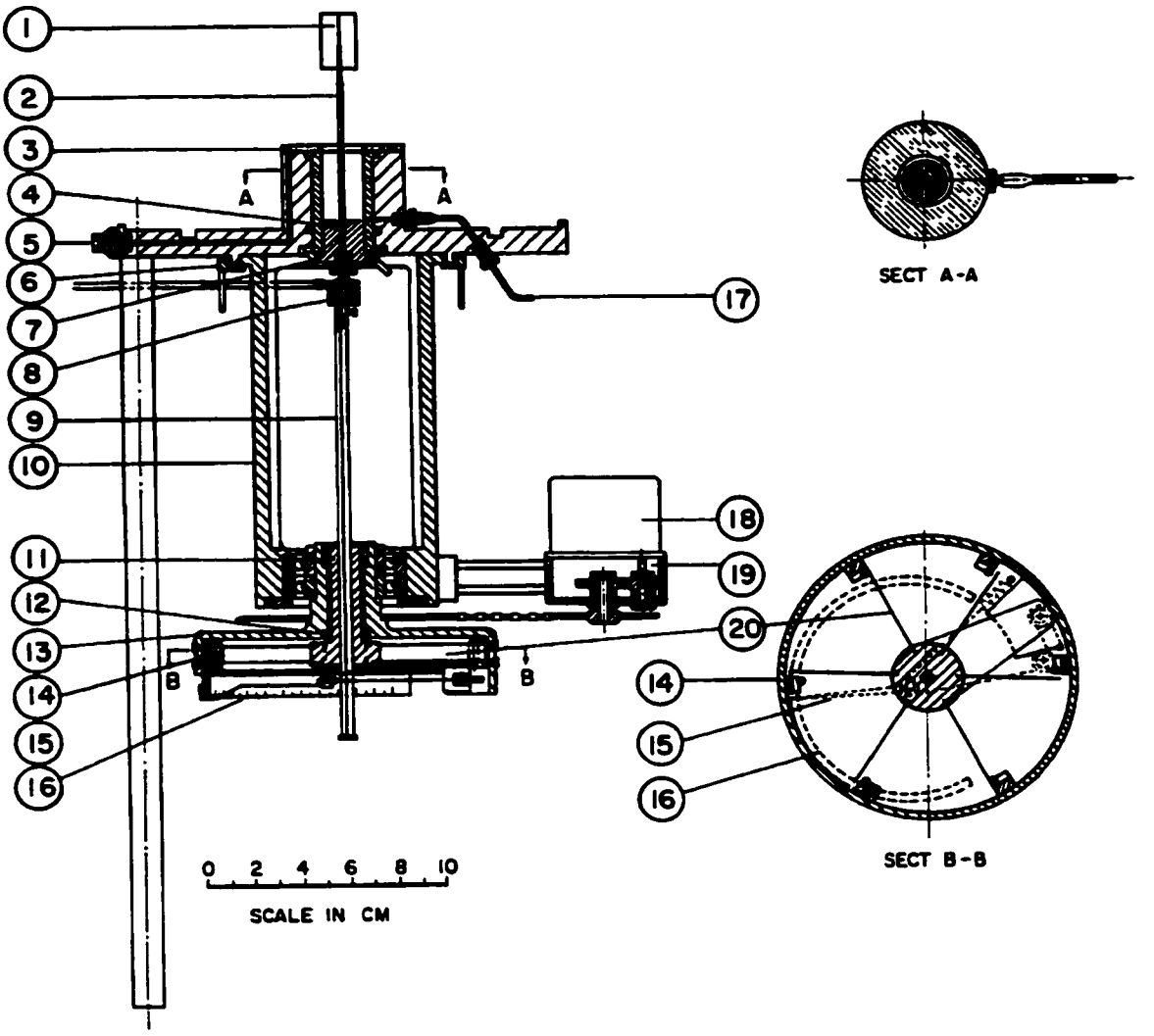

Figure 2.13: Details of the NGI Triaxial Vane (Kenny and Landva, 1965)

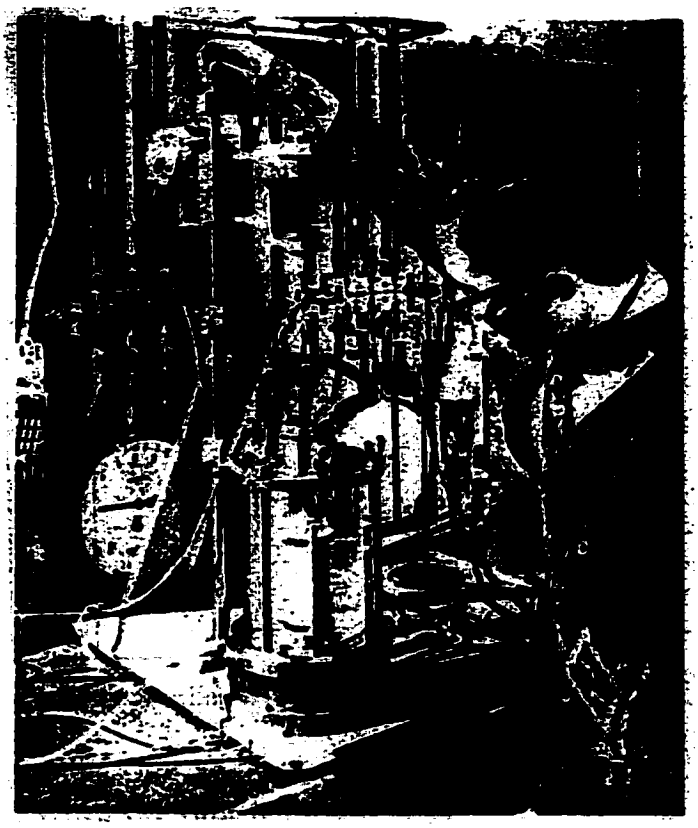

Figure 2.14: Photo of NRC Triaxial Vane (Law, 1978)

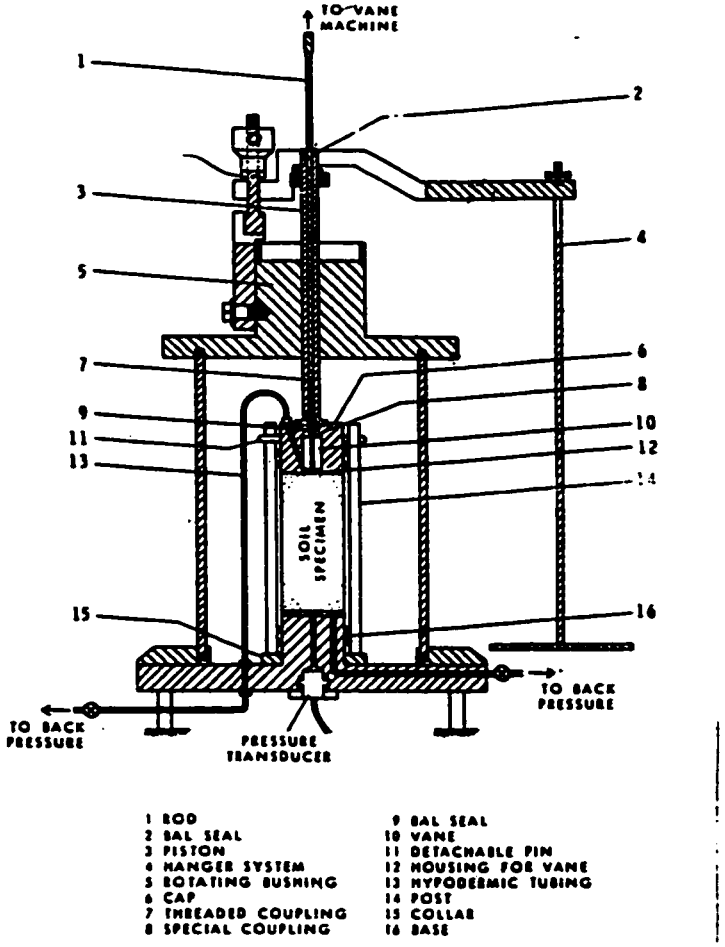

Figure 2.15: Details of NRC Triaxial Vane (Law, 1978)

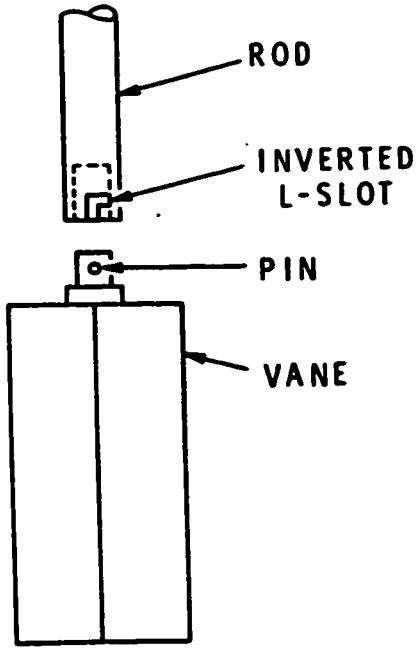

Figure 2.16: Slip Pin Used in NRC Triaxial Vane (Law, 1978)

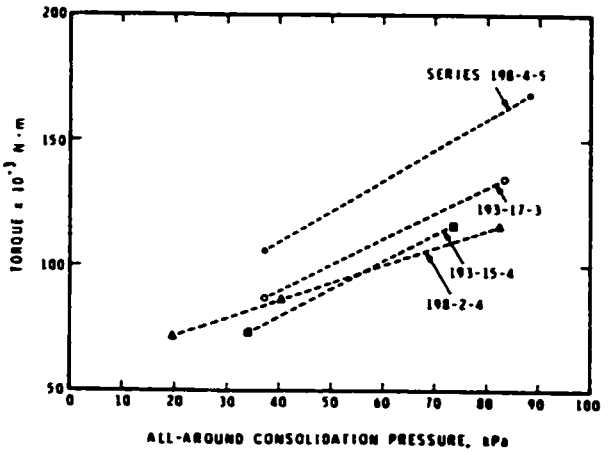

Figure 2.17: NRC Results of Increase in All Around Stress (Law, 1978)

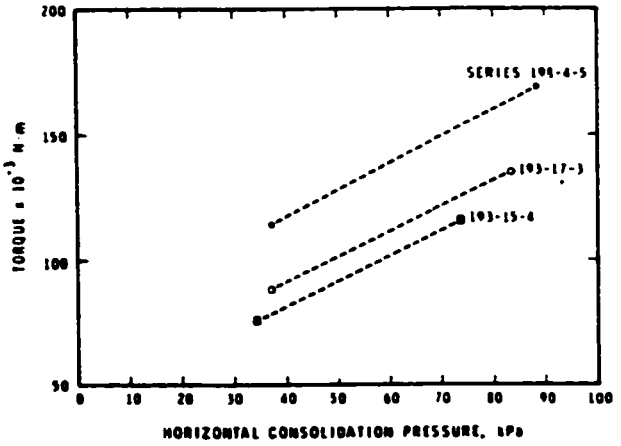

Figure 2.18: NRC Results of Increase in Horizontal Stress (Law, 1978)

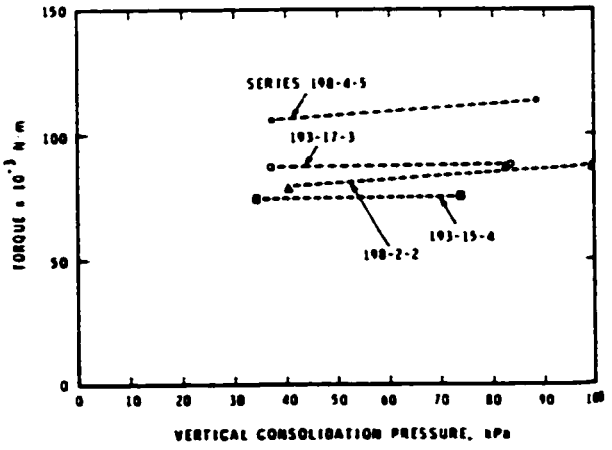

Figure 2.19: NRC Results of Increase in Vertical Stress (Law, 1978)

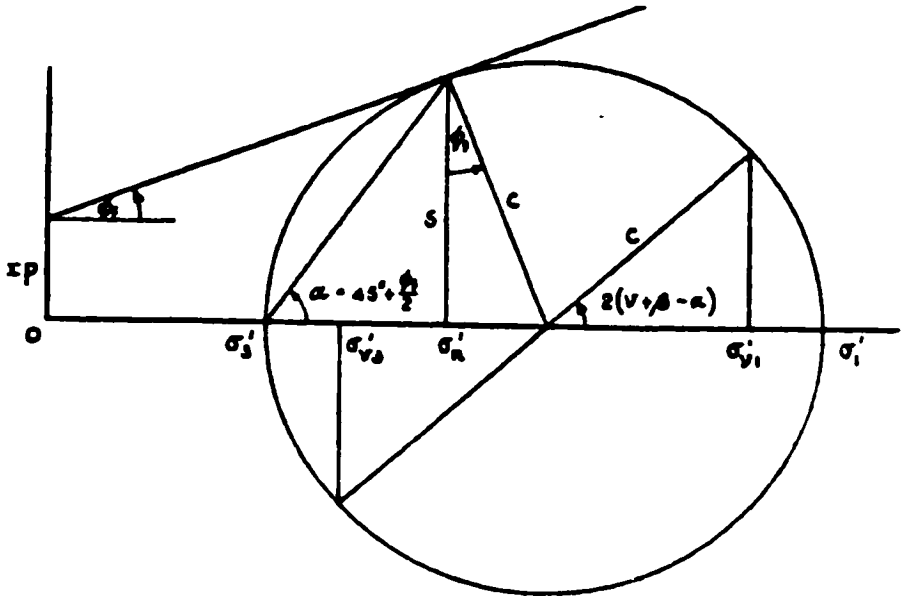

Figure 2.20: Mohr's Circle as Defined by Hansen and Gibson (Hansen and Gibson, 1954)

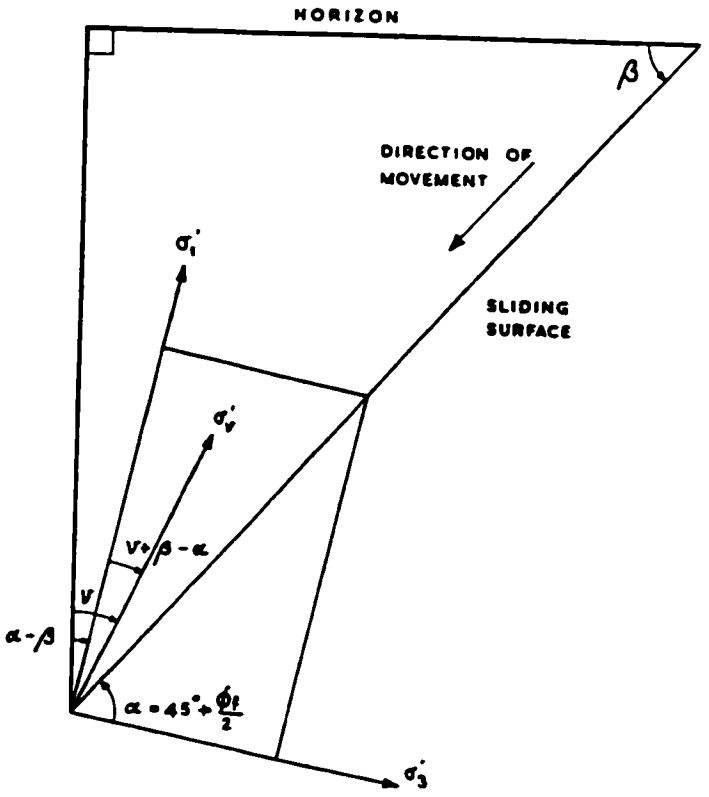

Figure 2.21: Inclination of Failure Surface to the Horizontal (Hansen and Gibson, 1954)

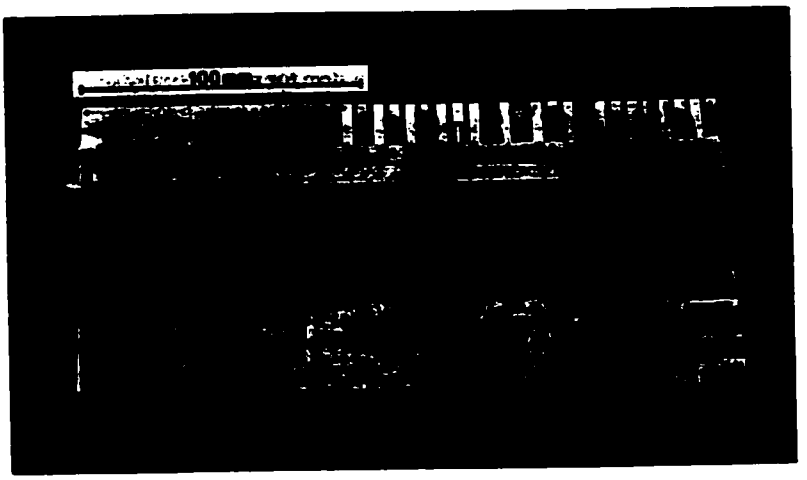

Figure 2.22: Instrumented Vane from Menzies and Merrifield (Menzies and Merrifield, 1980)

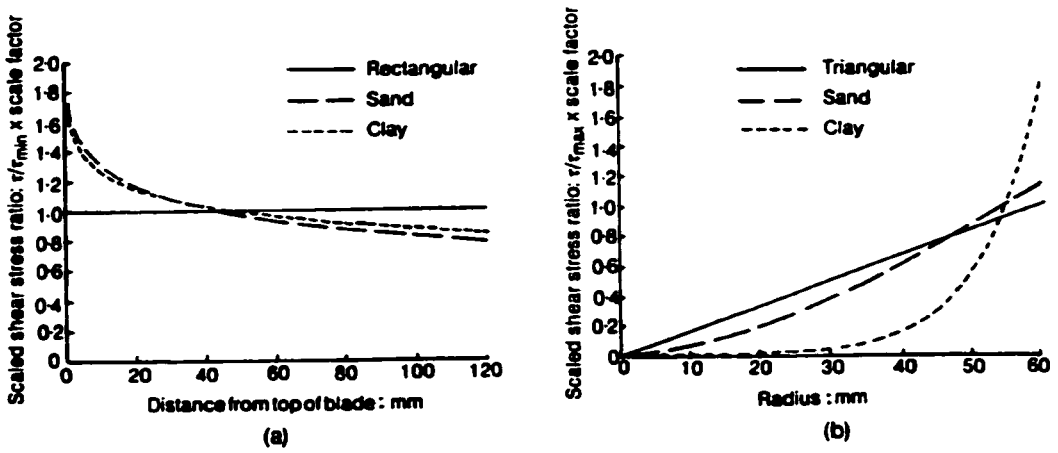

Figure 2.23: Stress Distribution along the a) vertical blade edge, b) horizontal blade edge (Menzies and Merrifield, 1980)

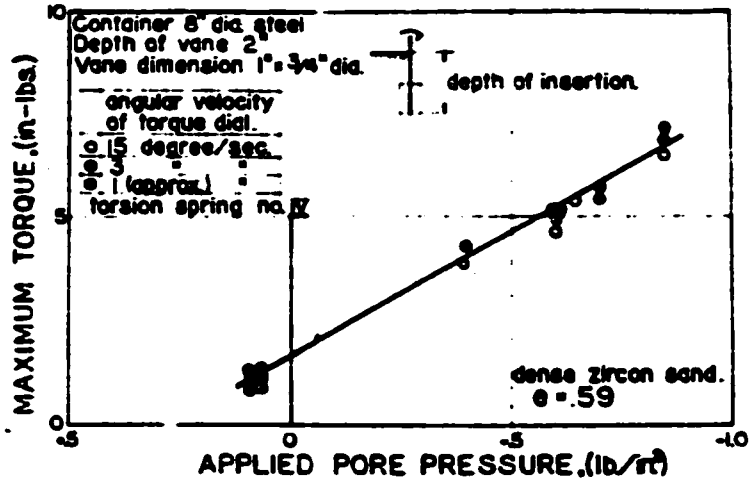

(a) MAXIMUM TORQUE vs. PORE PRESSURE, AT VARYING TESTING SPEEDS.

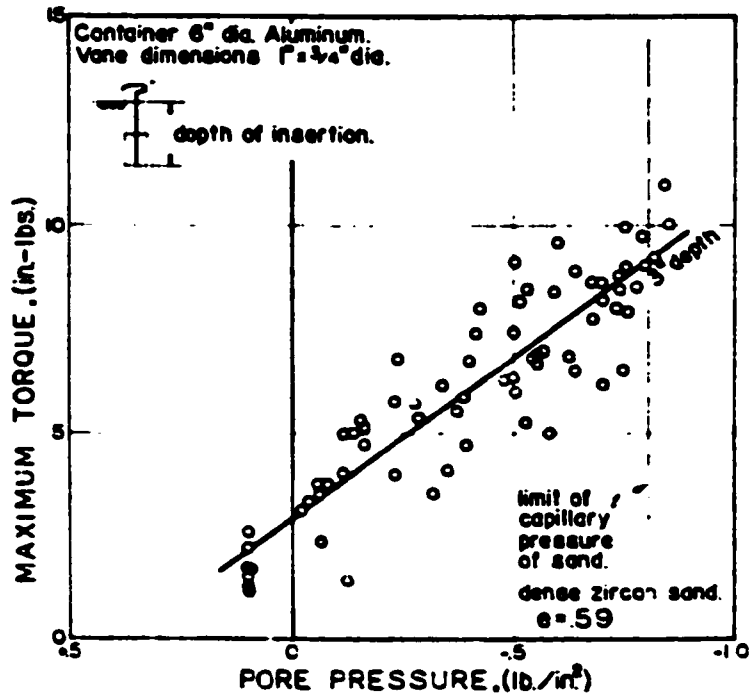

(b) MAXIMUM TORQUE vs. PORE PRESSURE, AT CONSTANT DEPTH.

Figure 2.24: Results of Vane Tests in Sand (Wilson, 1963)

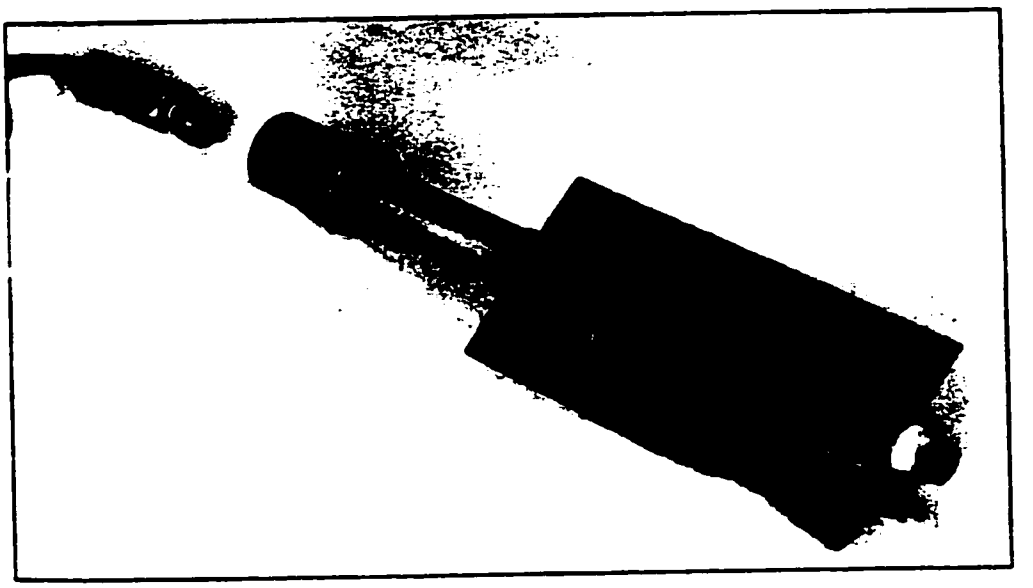

Figure 2.25: Photo of CSU Piezovane (Charlie et al, 1995)

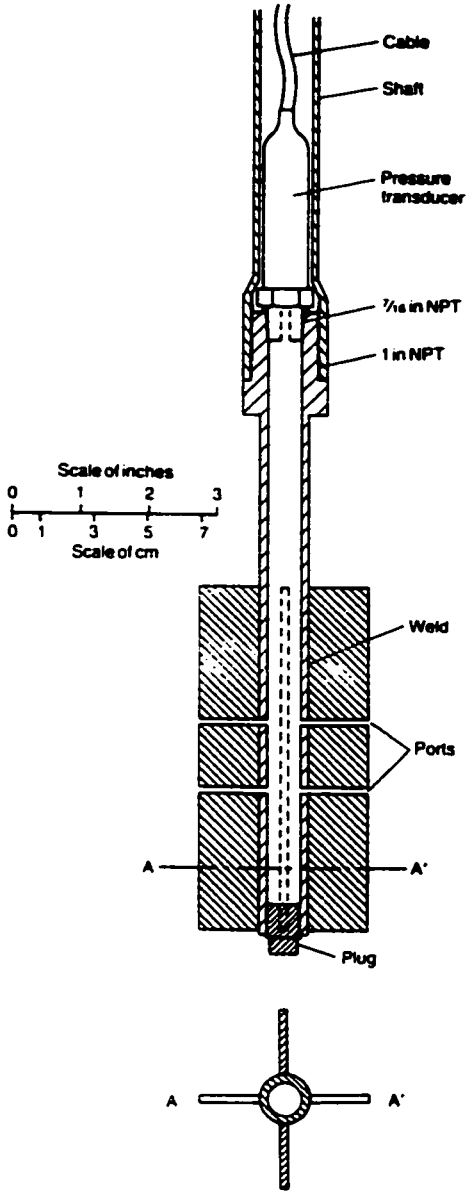

Figure 2.26: CSU Piezovane (Charlie et al, 1994)

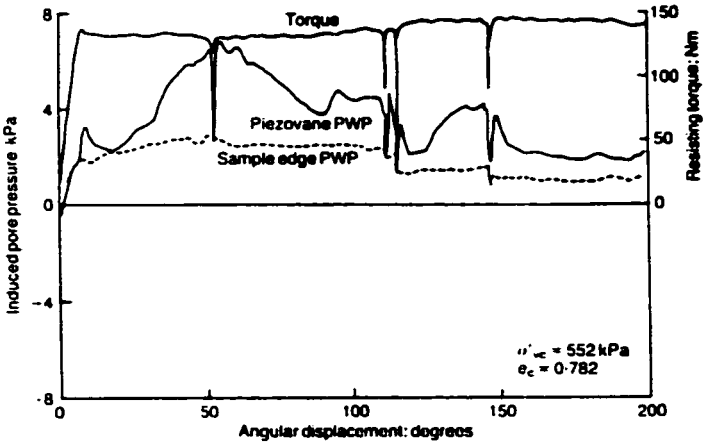

Figure 2.27: Piezovane Results showing Contractive Behaviour (Charlie et al, 1994)

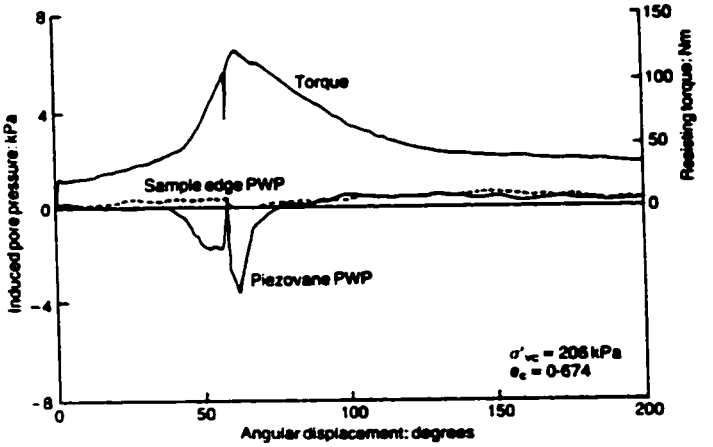

Figure 2.28: Piezivane Results showing Dilative Behaviour (Charlie et al, 1994)

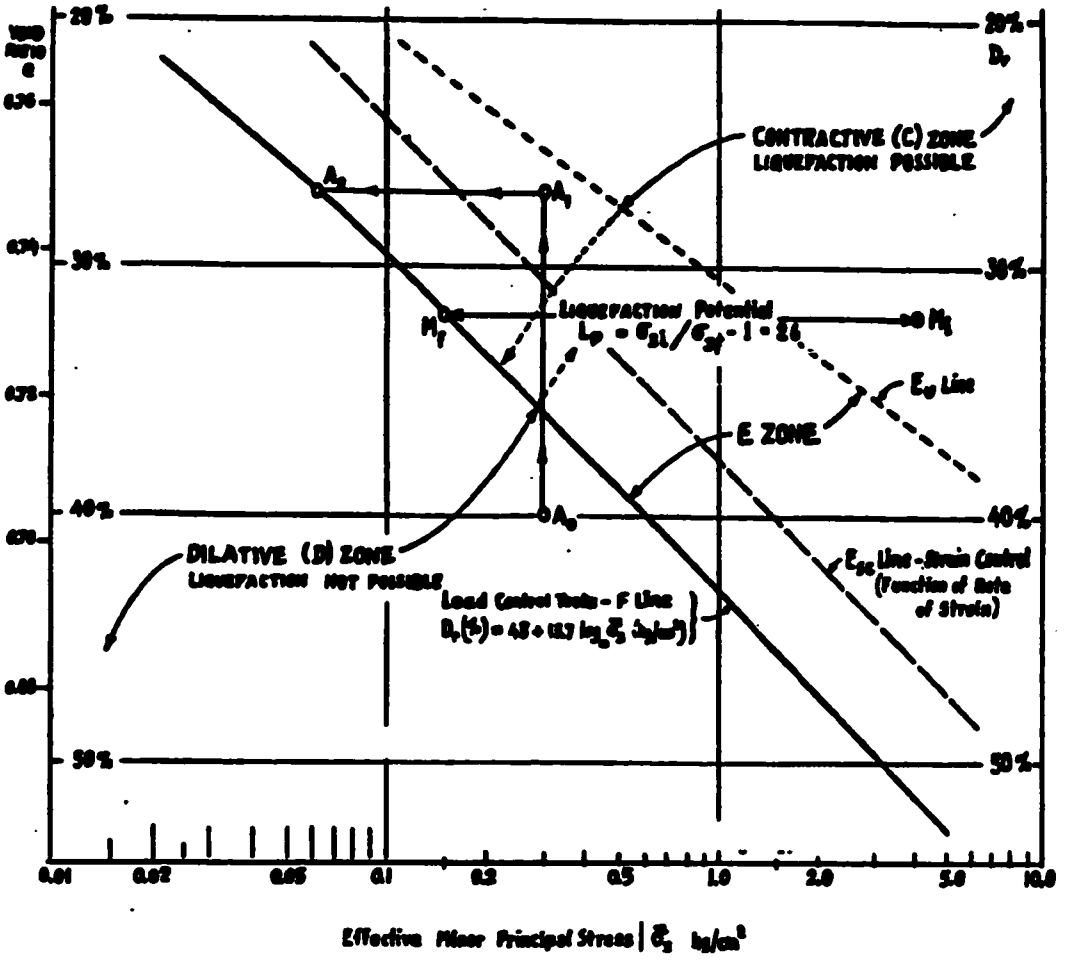

Figure 2.29: Liquefaction Potential Based on steady State (Casagrande, 1976)

Chapter 3: Apparatus

3.1 The Triaxial Vane

The concept behind the Triaxial Vane Apparatus (herein referred to as the Triaxial Vane) is quite simple; combine the triaxial test and the vane test into one device. The Tri Vane Apparatus uses a miniature vane incorporated into a triaxial cell in order to study the use of the vane in different soils as well as allowing the effects of different vane parameters, such as rotation rate and vane geometry, to be studied in controlled conditions. The design of the triaxial vane used in the current research is based on the original triaxial vane device designed by the Norwegian Geotechnical Institute (NGI) in the early 1960's, as well as the design used at the National Research Council of Canada (NRC), Division of Building Research in the 1970s, as discussed in Chapter 2.

3.2 The Triaxial Vane Apparatus

A schematic of the Triaxial Vane device used in the current research is shown in **Figure 3.1** and a photo is shown in **Figure 3.2**. The current design uses an essentially unmodified triaxial cell with a miniature vane introduced into a sample through the bottom of the cell. The vane can then rotated by a chain drive connecting the vane shaft to a drive shaft located to the side of the triaxial cell. Transducers located on the drive shaft measure rotation and shaft torque.

3.2.1 Vane

The vane blades are constructed using 0.46mm stainless steel and the vane assembly has a diameter of 12.7mm and a height of 25.4mm (0.5" x 1"), as shown in **Figure 3.3**. The blades are attached to a 6mm stainless steel shaft by the reverse thread. This reverse thread allows for the measurement of the shaft friction resistance. The vane mounting

thread is initially loosened by approximately half a turn. As the test starts, the shaft is allowed to turn without engaging the vane, during which time the frictional component can be measured. Over tightening of the vane onto the shaft was prevented by a small steel plug placed into the bottom of the threaded opening. A moveable retaining plate (**Figure 3.4**) was located below the base of the triaxial cell to hold the lower end of the vane shaft. A circular bearing was located at the point of contact between the vane and the retaining plate to reduce friction. The purpose of this plate was threefold; to allow for easier positioning of the vane (the vane is raised until the bottom of the vane shaft is flush with the bottom of the plate); to provide assistance in locating the proper position of the sprocket for the chain connecting the vane to the drive shaft; and to prevent any bending of the vane shaft. Adjusting nuts are located above and below the retaining plate to adjust the height of the plate and ensure that the vane is positioned such that the midpoint of the vane is located at the midpoint of the sample.

3.2.2 Drive Shaft and Power Unit

The original design of the Triaxial Vane Apparatus (NGI design described earlier) had the drive shaft directly connected to the vane shaft in a vertical arrangement. The current design was modified to place the drive shaft separately from the vane and cell assembly due to space limitations and to allow for easier inclusion of the torque transducer into the assembly. A photo of the drive shaft is shown in **Figure 3.5**.

Power is provided by a small AC electric motor (**Figure 3.6**) coupled to a variable speed control unit. The control unit allows the rotation to be controlled from a minimum of 60 degrees per minutes to a maximum of 1100 degrees per minute. The torque is then transferred from the motor to the drive shaft through a worm and worm gear assembly located at the top of the drive shaft (as shown in **Figure 3.7**).

The drive shaft itself if composed of two steel shafts, with the reaction torque gauge transducer connected between the two halves (as shown in Figure 3.5). To help reduce friction and maintain alignment, four circular roller bearings were initially placed along

the shaft. However these bearing were found to create problems, as will be subsequently discussed, and were reduced to two bearings, located only at the top and the bottom of the shaft.

Torque is transferred from the drive shaft to the vane through a second chain and sprocket assembly located below to torque transducer. A circular plate is attached to the shaft below the second sprocket and was used for calibration of the torque gauge and to provide a visual rotation reference (as shown in Figure 3.5).

Rotation of the shaft was monitored by a rotation pot transducer (**Figure 3.8**). Initially, the transducer was mounted directly to the top of the shaft. Problems arose with the wire to the torque transducer becoming tangled in the drive shaft, and the decision was made to feed this wire directly through the drive shaft. To accommodate this change, the rotation pot was mounted beside the drive shaft and connected via a chain and sprocket assembly located at the top of the drive shaft.

3.2.3 Pressurization System

Cell pressure and back pressure for the Triaxial Vane Apparatus were provided by two mercury constant pressure systems. A schematic of the mercury pressure system is shown in **Figure 3.9**. With this system, pressures ranging from –30 to 1500 kPa can be achieved. A major benefit with this system was that, since suctions could be made by the mercury system, a supplemental suction system did not need to be introduced to the apparatus to provide suction to the sample, guaranteeing that the pressure lines will remain saturated. The back pressure line was uniquely valved (**Figure 3.10**), such that pressure can be applied to either the top or bottom of the sample or both ends simultaneously.

3.2.4 Triaxial Cell

The triaxial cell was a standard design cell capable of holding a 50mm x 100mm sample with a few minor modifications, including:

1) A hole in the base for the vane shaft to pass through. Three rubber seals have been placed inside the hole to prevent water leaking out of the sample or loss of pressure
2) The vertical load application system has been changed from a constant strain system found on most triaxial cells to a constant load system. This change was necessary to maintain a constant stress ratio during anisotropic testing. The constant load system consists of a two-chamber bellofram cylinder. Both chambers of the cylinder are saturated and connected to independent mercury constant pressure systems to allow for separate control of the pressure in each chamber. By controlling the difference in pressure between the two chambers, a constant load can be maintained.
3) Anti rotation rods are inserted vertically into the triaxial cell base on either side of the sample, which connect with retaining pins inserted in the sample cap, to prevent rotation of the sample during testing (**Figure 3.11**)

3.2.5 Sample Base and Cap

Since the Triaxial Vane apparatus has been designed for the testing of both clay and sand, different lower sample platens (referred to as the clay base and sand base) had to be designed for each sample type.

The clay base is made with a slotted recess to allow the vane to be retracted during the consolidation of the clay samples. After consolidation has finished, the vane is then pushed up into the sample and testing can commence. The back pressure line also feeds an additional water line that leads into the vane recess in order to maintain saturation an constant back pressure during vane insertion. **Figure 3.12** shows the details of the clay base.

The sand base, in contrast, does not have the vane recess. The sand base has only a single hole through which the vane shaft passes. This hole has a rubber seal to prevent water from leaking out. When testing sand, the vane is placed at an elevation, equivalent to the

middle of the sample, inside the sample space and the sample is then formed around the vane. Since the vane is already inside the sample, the vane recess was not required for the sand base. **Figure 3.13** shows the details of the sand base.

In addition to being able to test both sand and clay, the Triaxial Vane Apparatus has also been designed to test samples in both axial compression and axial extension. To accommodate these tests, two different top caps have been designed. For axial compression, a cap similar to that used for triaxial compression test is used. This cap has a small depression on the top to allow the loading ram to lock into the cap to prevent movement between the cap and the sample. For axial extension, a cap has been designed with a threaded rod inserted into the top, which fits into a threaded hole in the loading ram. By joining the cap to the rod, the sample can then be loaded in tension. Both caps are shown **Figure 3.14**.

3.2.5 Volume Gauge

In order to measure the volume change in the sample during both consolidation and drained testing, an improved simple volume gauge was included in the design (**Figure 3.15**). This device, which was developed at the University of Ottawa by Khan and Garga (1994), is capable of measuring volume changes up to 110cc and the data can be read directly by the data acquisition unit. The volume gauge is placed between the mercury pressure system and the triaxial cell so that any water displaced, either from the top or the bottom of the sample will be measured. The volume gauge is based on a double bellofram design, similar to the load ram used in the Triaxial Vane design. However, this design did create a problem during sample preparation. When making a sand sample, suction pressure needs to be applied in order to maintain the sample while the mold is removed. This suction, as mentioned earlier, is applied directly by the mercury pressure system, without the need for an additional suction system. As a result, the suction is transferred to the sample through the volume gauge. This has the result of partially collapsing the rubber belloframs in the gauge. As the back pressure is increased from suction to positive pressure, the belloframs reinflate with water, resulting in a sharp change in the reading

from the gauge. This change is *not* a change in the sample volume, only in the amount of water in the belloframs. As a result, the back pressure must be held constant at a pressure just above zero until this change stabilizes at a constant value. This value is now the zero reference for measurement of the change in sample volume that occurs during consolidation.

3.3 Transducers

To allow for full data acquisition during the testing, several transducers were incorporated into the design as follows:

1) A linear displacement transducer, attached to the vertical loading ram to measure vertical displacement. (Transducer resolution: 0.01 mm)
2) Three pressure transducers to monitor cell pressure and back pressure at both the top and bottom of the sample. (Transducer resolution: 0.2 kPa)
3) A reaction torque transducer mounted in the drive shaft to measure the applied torque on the vane. (Transducer resolution: 0.00075 Nm corresponding to 0.1 kPa shear strength resolution)
4) A rotation pot transducer mounted to the drive shaft to measure the angular rotation of the vane. (Transducer resolution: 0.2 degrees)
5) A linear displacement transducer mounted to the volumetric gauge to monitor the volume change of the sample. (Transducer resolution: 0.17 cm^3)
6) A load transducer mounted on the vertical load ram to measure the applied vertical load. (Transducer resolution: 0.002 N)

These eight transducers are then connected to a Scimetrics Model 7000 data acquisition unit and monitored by a PC computer. A computer program was then created in Quick Basic to monitor and record the transducer readings.

3.4 Transducer Calibration

The transducers were individually calibrated and the calibration curve can be found in Appendix 1. However, a special circumstance came about during the calibration of the pressure transducers, which will be discussed.

3.4.1 Pressure Transducers

The pressure transducers used in the Triaxial Vane Apparatus were calibrated several times and an interesting trend was noted. Although the calibration of the transducers remained linear, the slope of the calibration curve changed with each test. After several tests it was determined that the calibration of the transducers changed each time the power to the transducer was turned off. As a result, a calibration routine was added into the test program, which calibrates the pressure transducers before every test.

3.5 Cyclical Response in Torque Transducer

During the initial testing stages, it was discovered that there was a large cyclical response in the torque transducer. **Figure 3.16 a)** shows the results of one of the early tests in which this cyclical response is apparent. After much investigation, it was determined that the cause of this response was that the drive shaft had become bent. When the drive shaft support had been constructed, the supports for the circular bearings in which the drive shaft turns were not perfectly aligned. After the drive shaft was installed, it became bent due to this misalignment. As the shaft then turned, it would bind as it rotated through the high side of the bend.

In order to solve the problem, the two central bearings were removed, leaving only the bearings on the ends of the shaft. The drive shaft was then slowly bent back into proper alignment. **Figure 3.16 b)** shows the results of a test performed after the cyclical response was removed. Although the cyclical response could not be fully removed, it was

reduced to an acceptable level; the response was reduced from approximately 50 kPa to less than 5 kPa.

3.6 Additional Test Equipment

In addition to the Triaxial Vane Apparatus, testing was also conducted using conventional equipment. The shear strength of the material was tested using both triaxial tests (**Figure 3.17**) and direct shear tests (**Figure 3.18**). Additionally, the consolidation characteristics of the material were measured using a odeometer (**Figure 3.19**). All these tests were conducted according to ASTM guidelines.

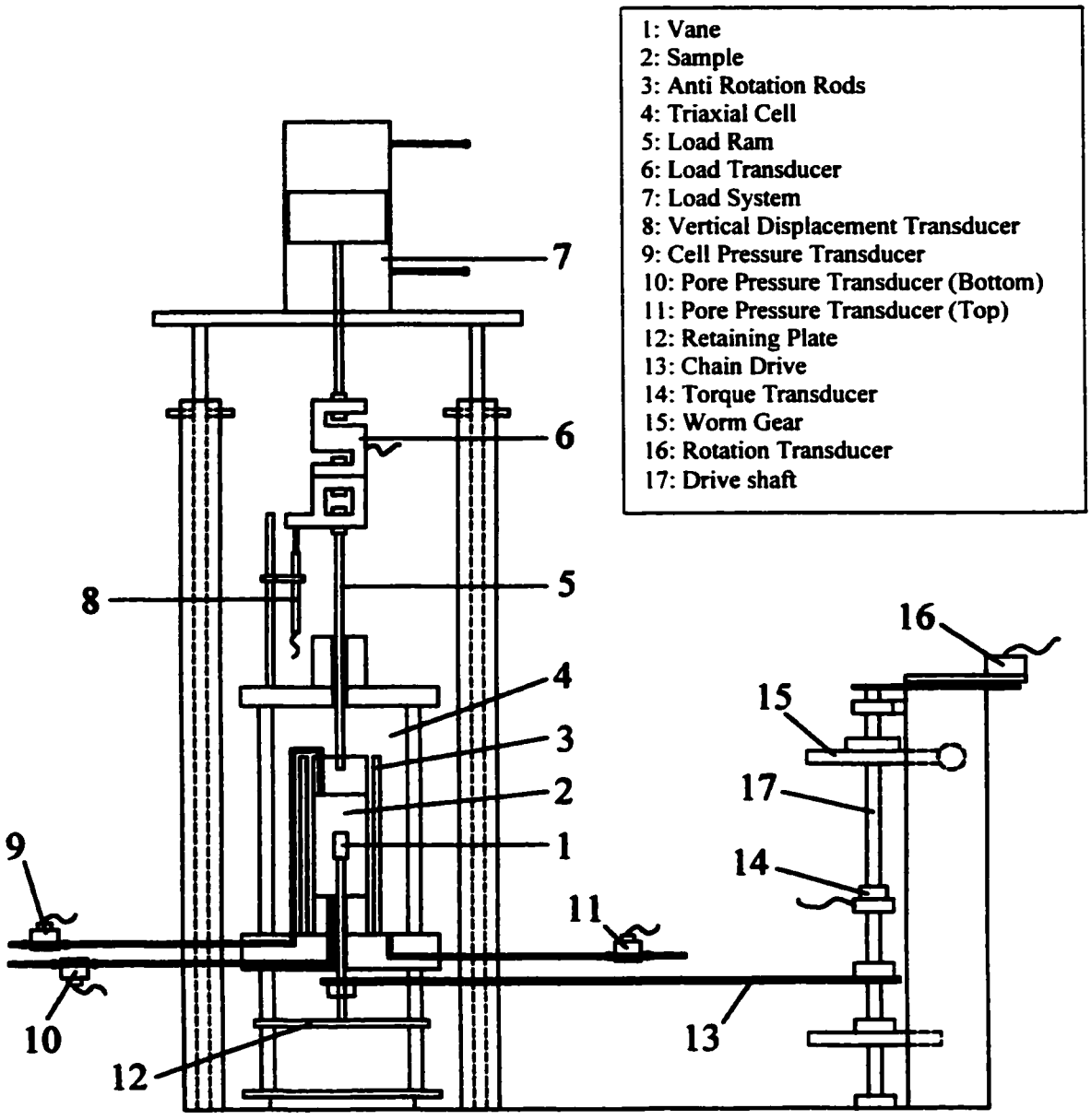

Figure 3.1: Triaxial Vane Schematic

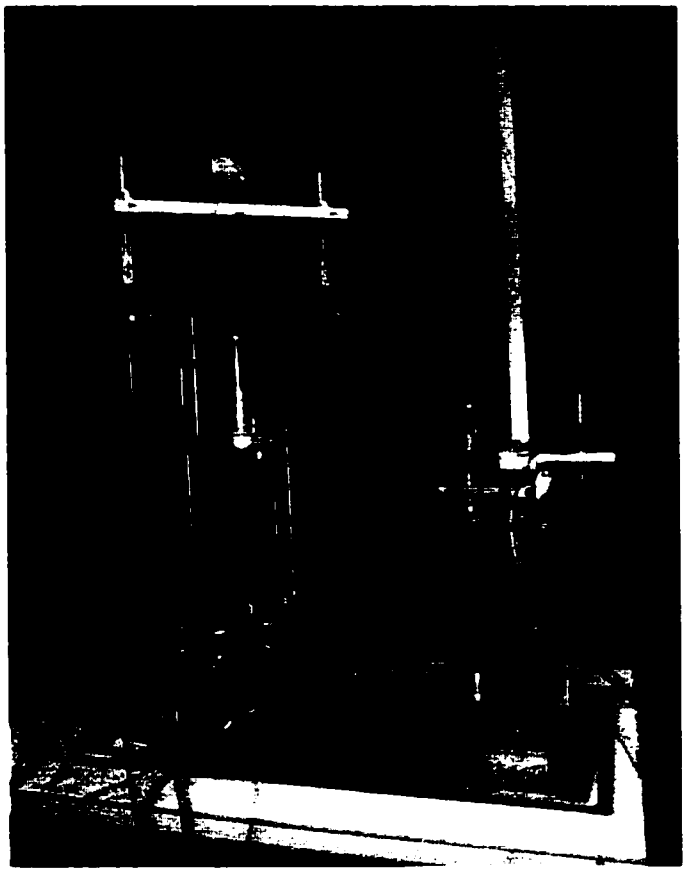

Figure 3.2: Triaxial Vane Apparatus

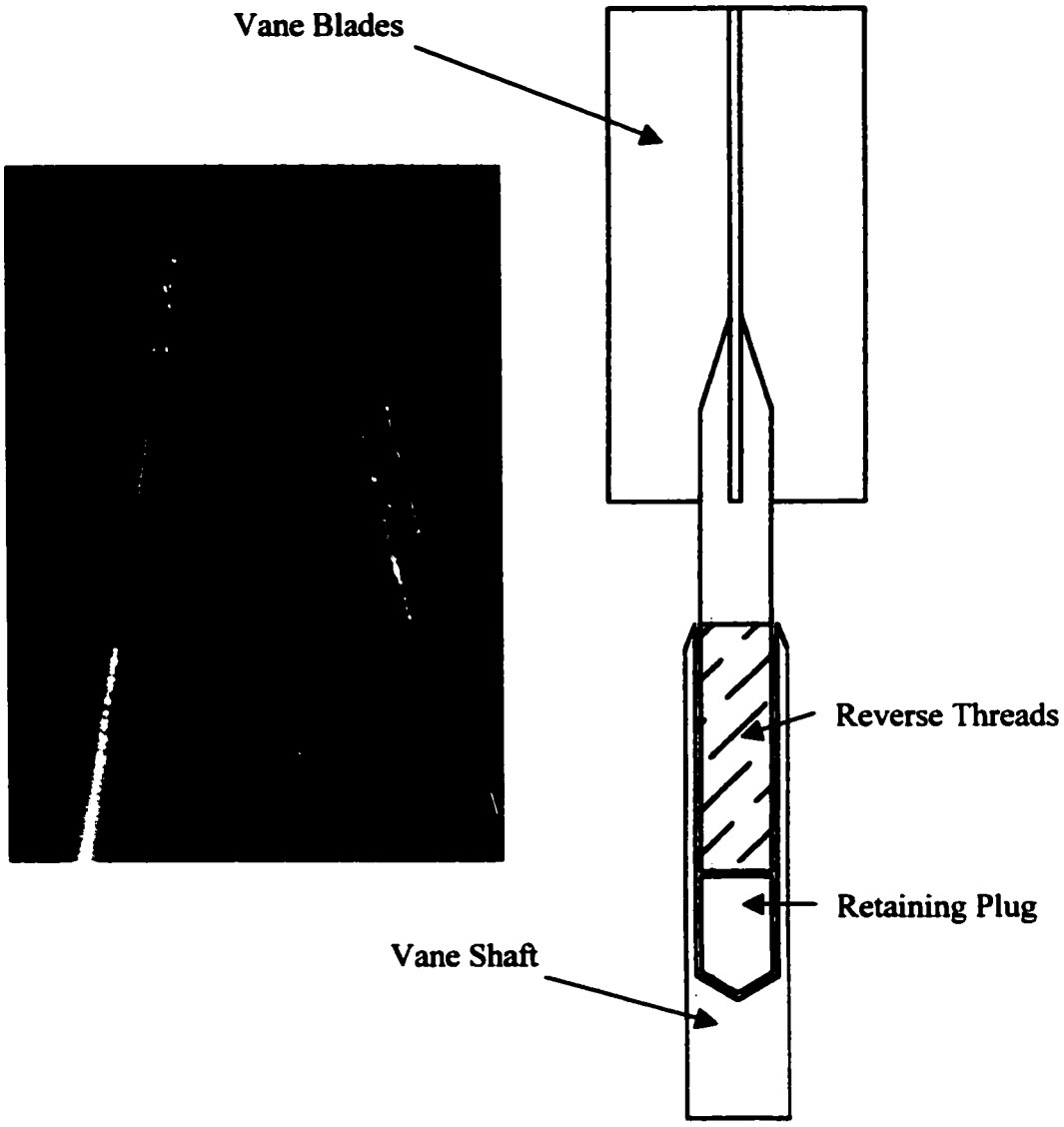

Figure 3.3: Vane Configuration

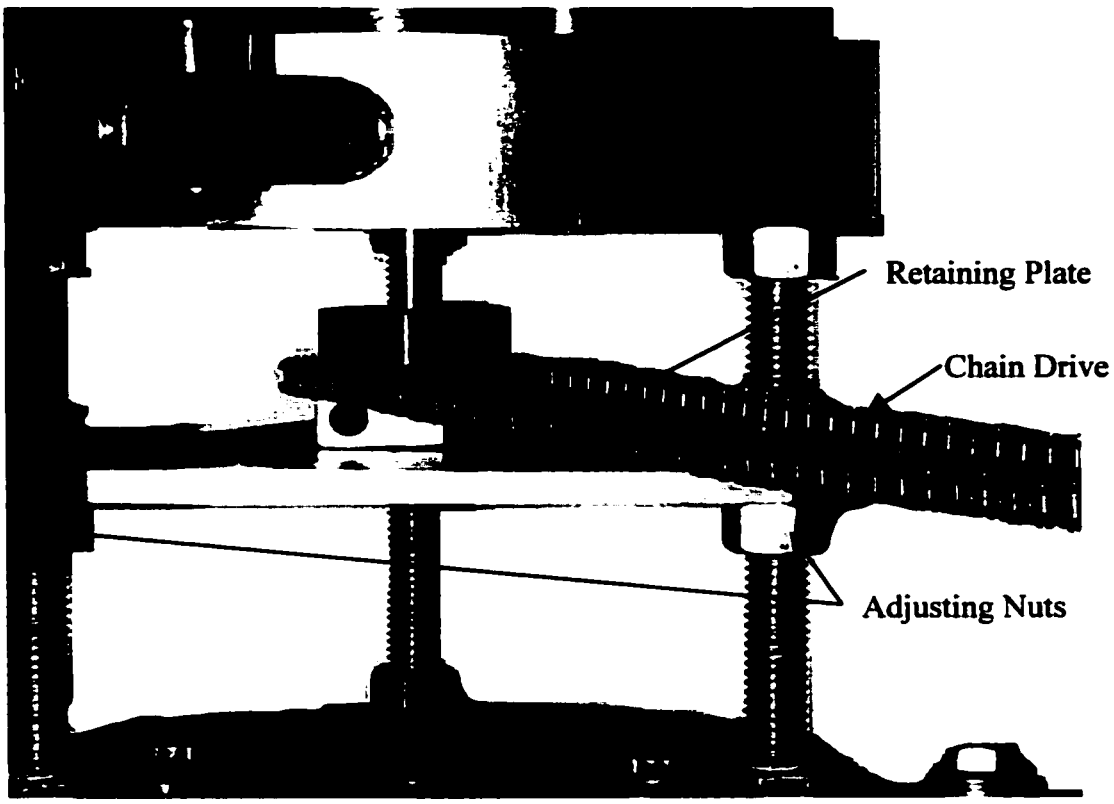

Figure 3.4: Vane Retaining Plate

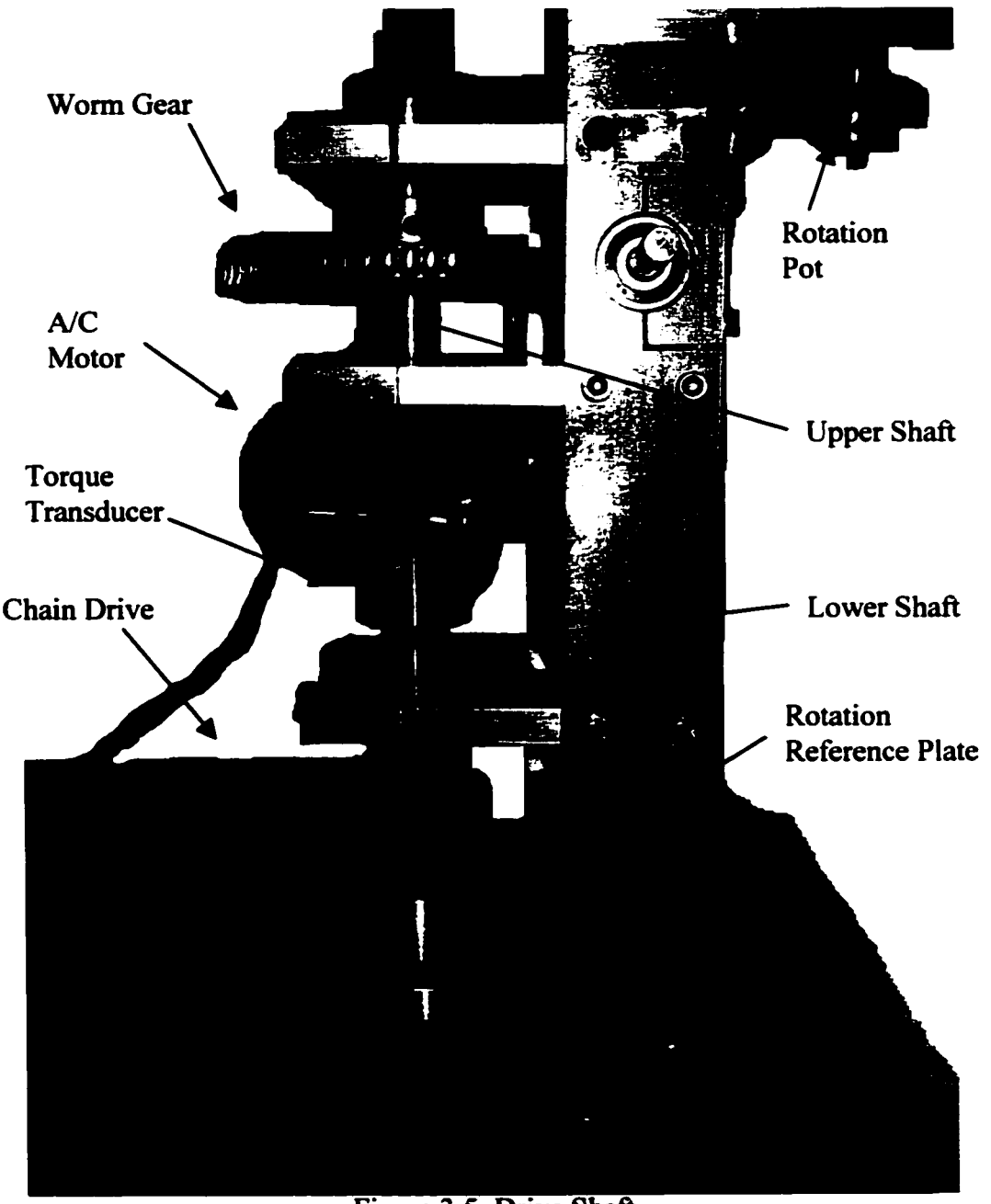

Figure 3.5: Drive Shaft

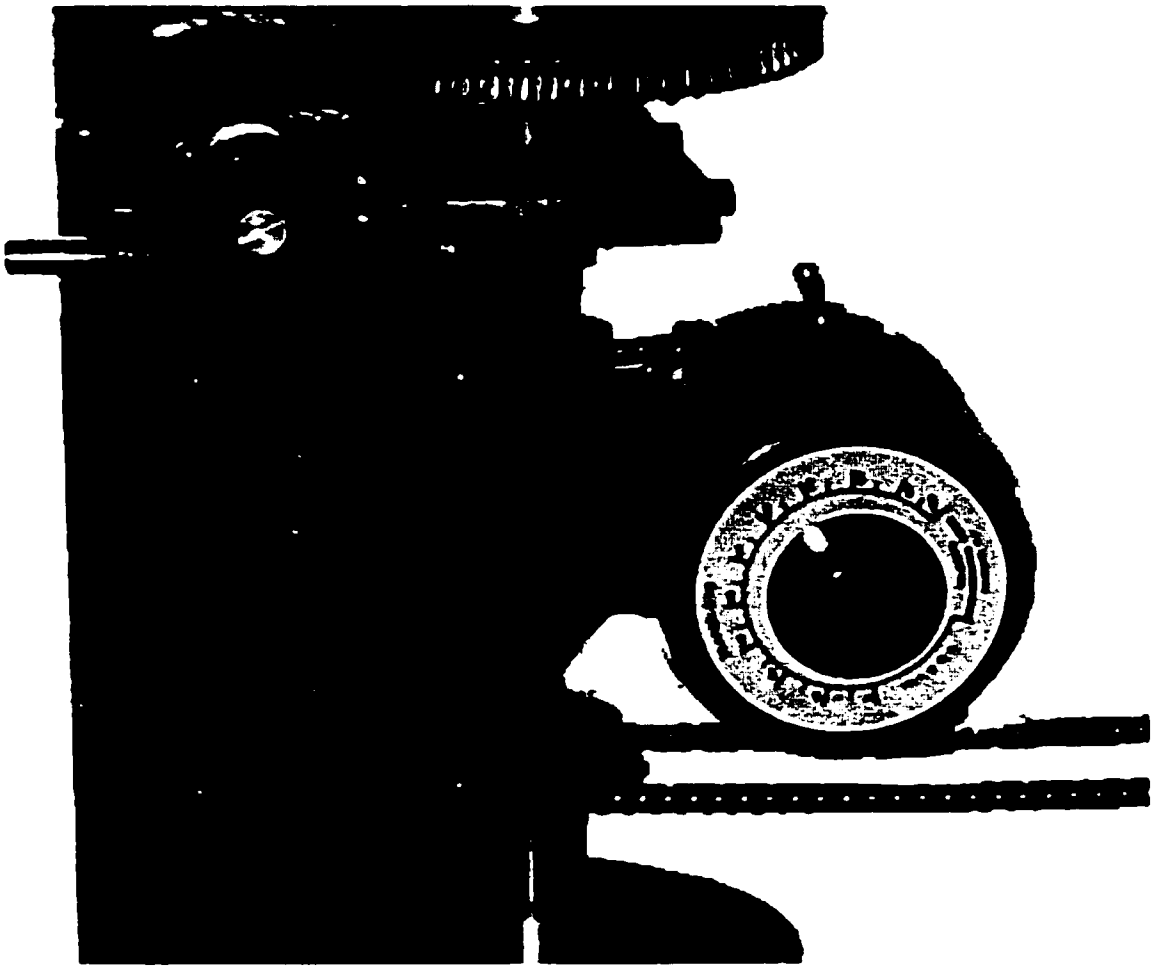

Figure 3.6: A/C Motor and Variable Speed Control Unit

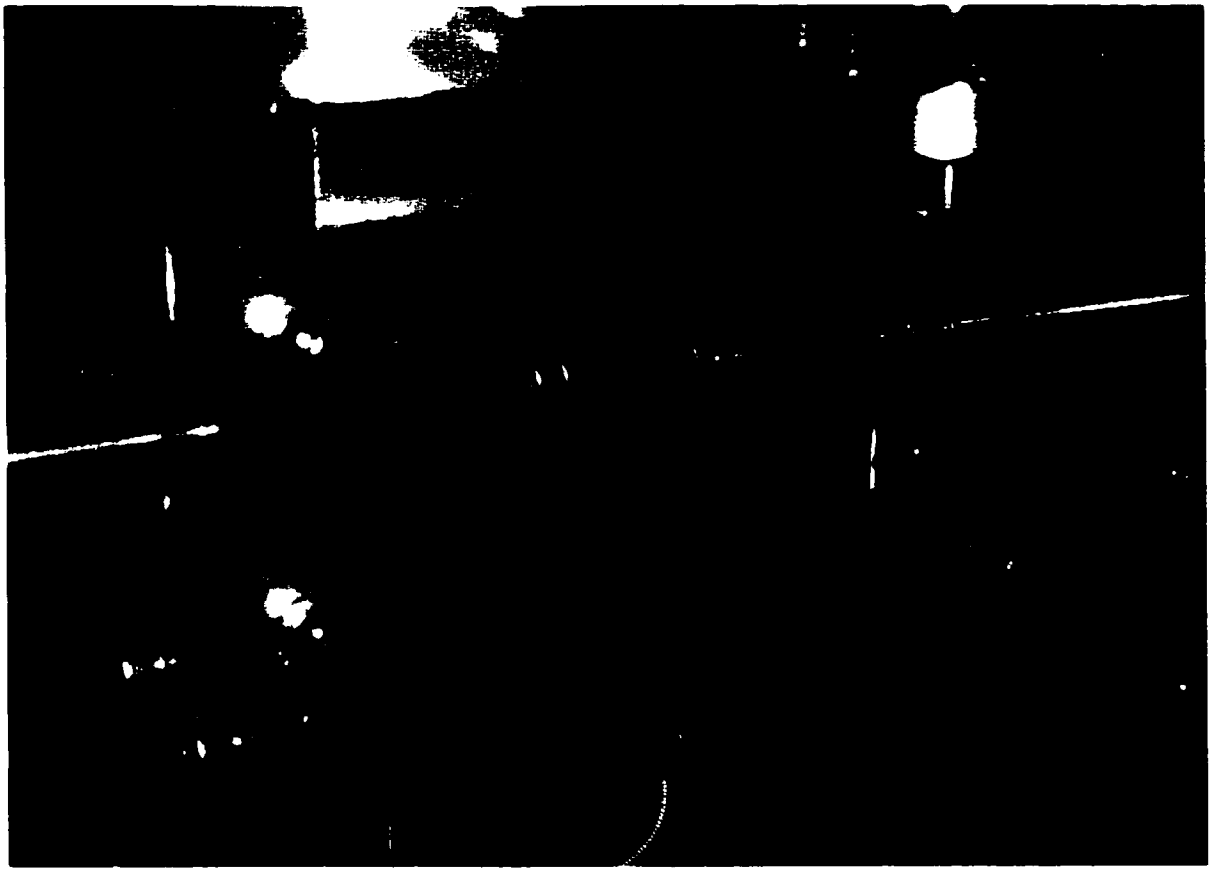

Figure 3.7: Worm Gear

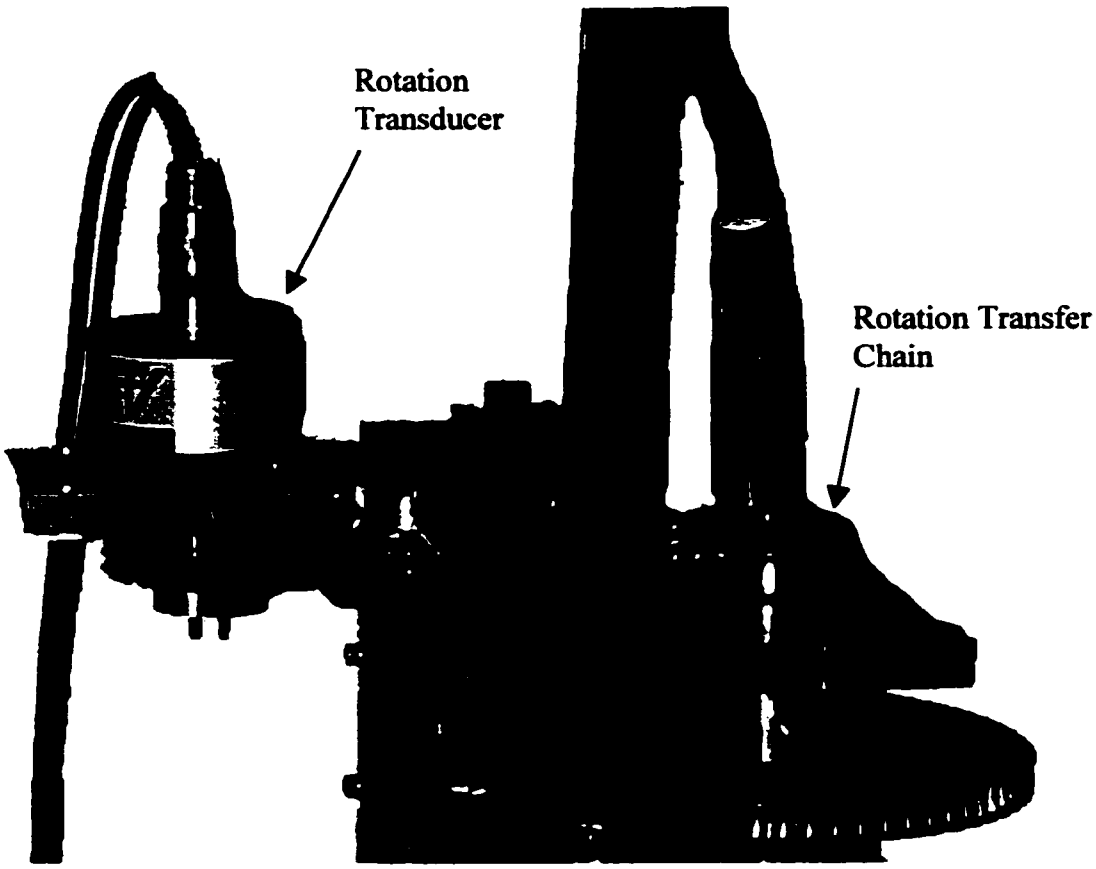

Figure 3.8: Rotation Transducer

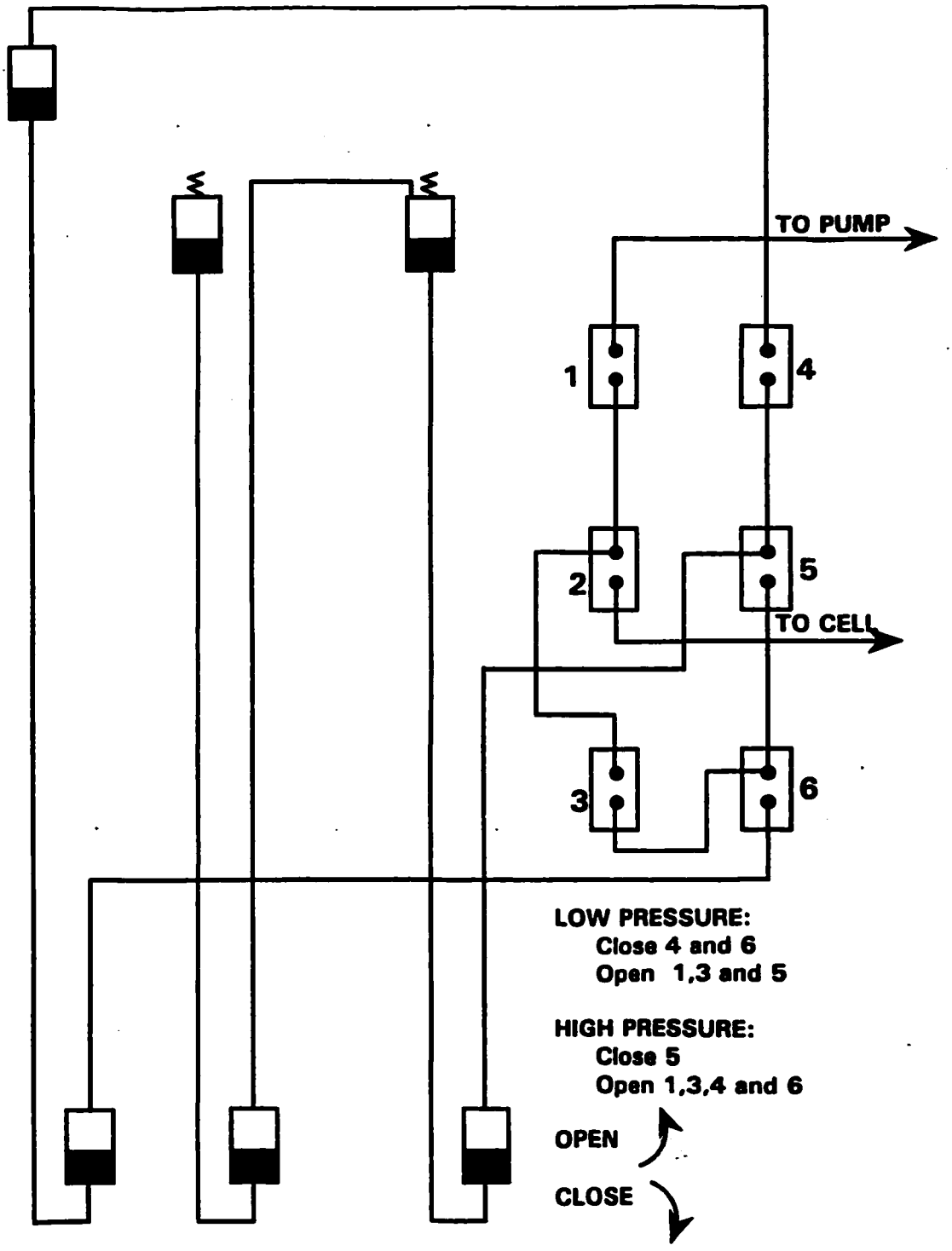

Figure 3.9: Mercury Pressure System Schematic

Figure 3.10: Valve Configuration

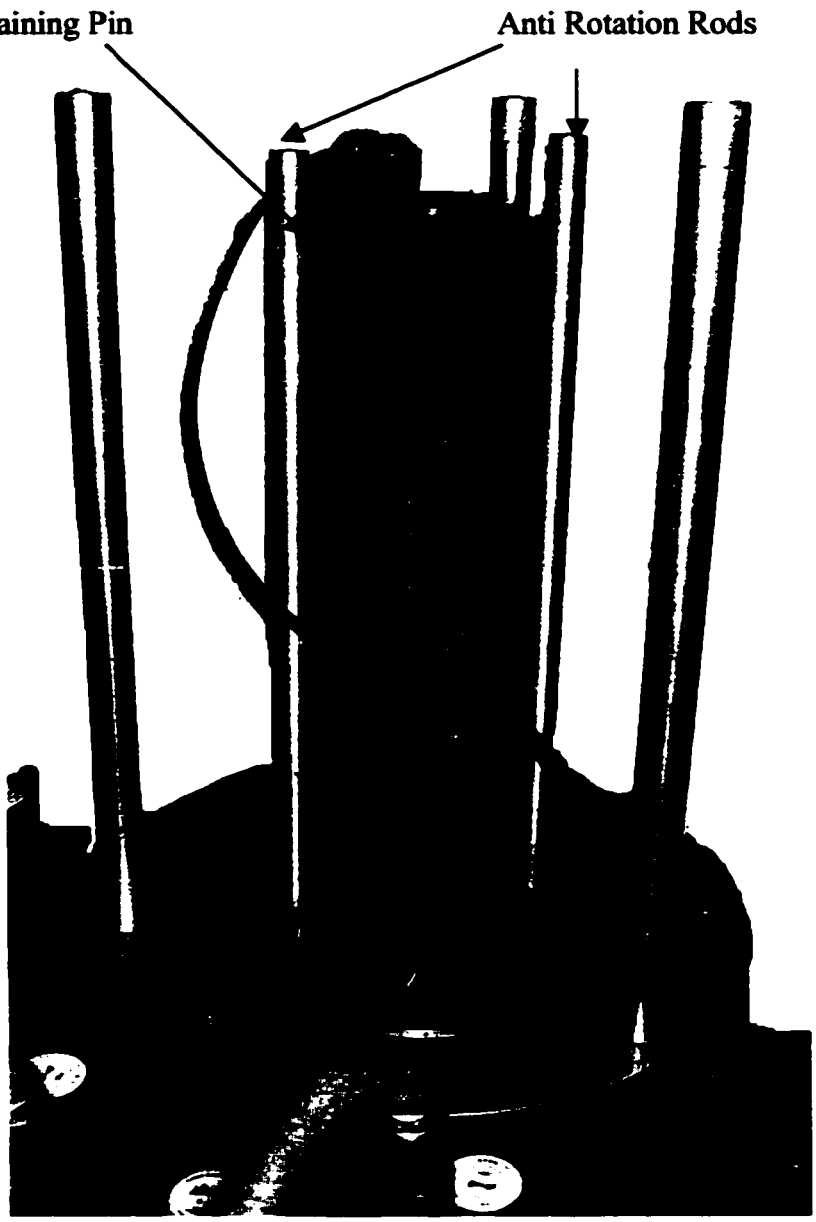

Figure 3.11: Location of Anti Rotation Rods

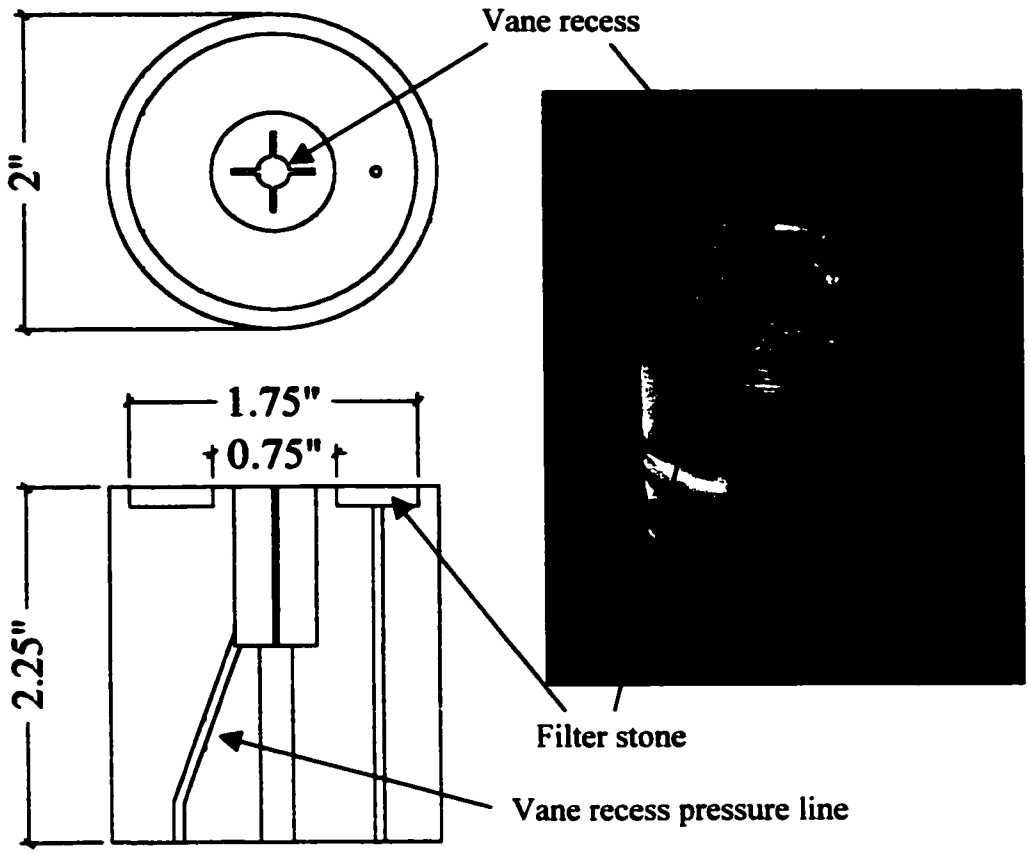

Figure 3.12: Clay Base

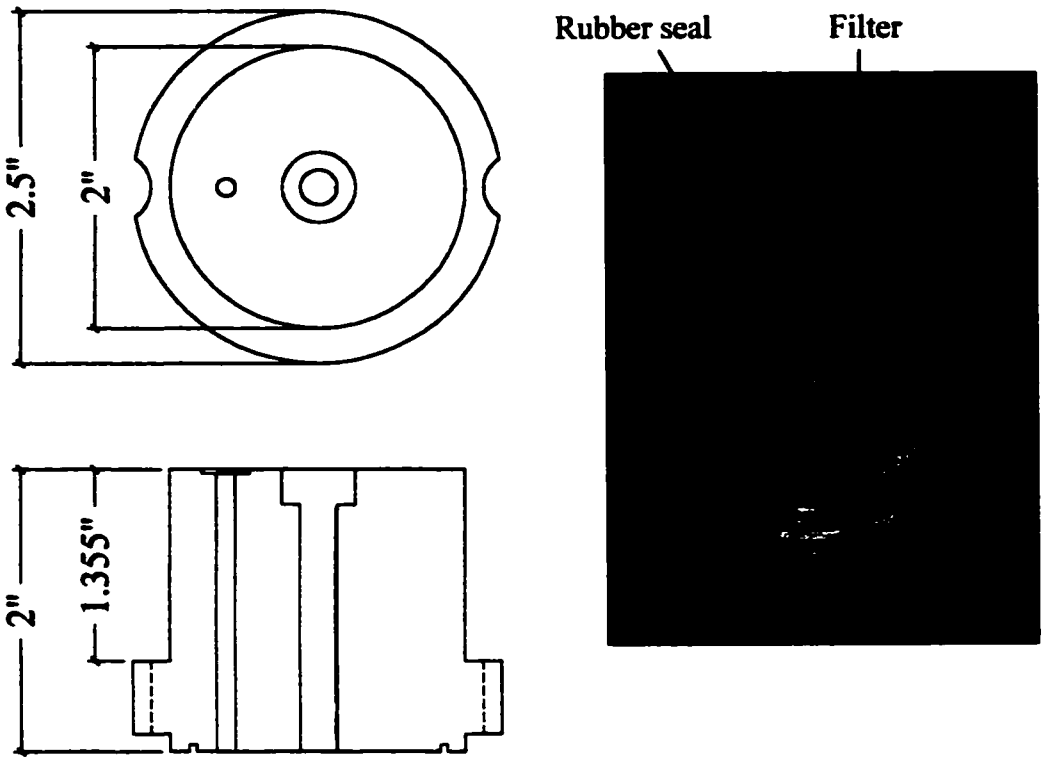

Figure 3.13: Sand Base

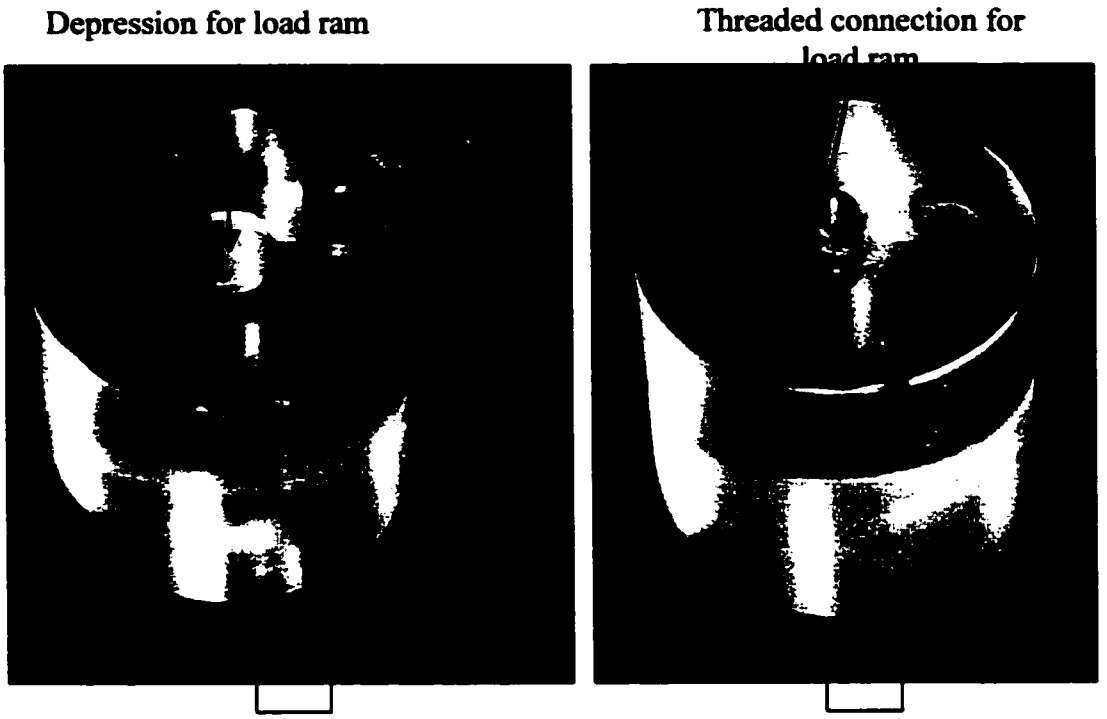

Figure 3.14: a) Compression Cap, b) Extension Cap

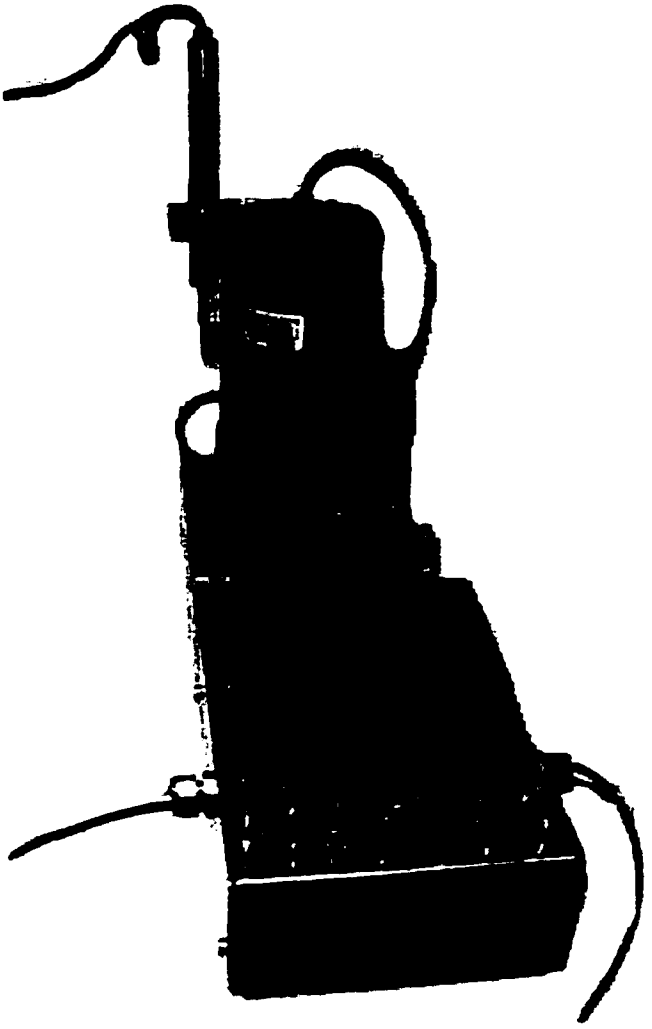

Figure 3.15: Volume Gauge

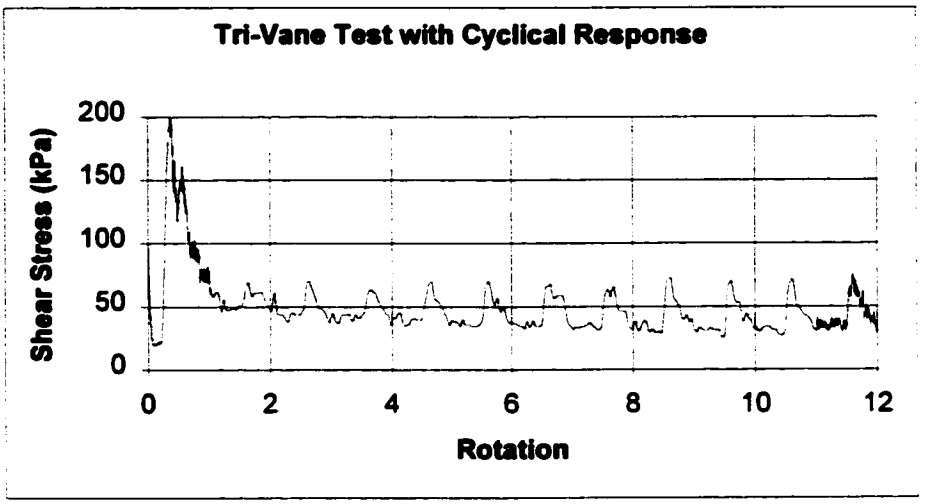

a)

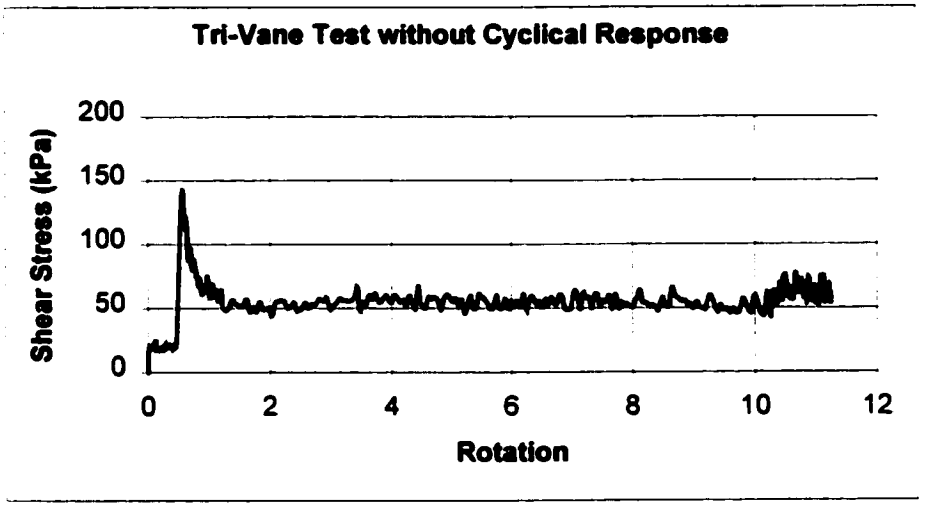

b)

Figure 3.16: Test results a) with a cyclical response due to shaft damage and b) without a cyclical response after repair

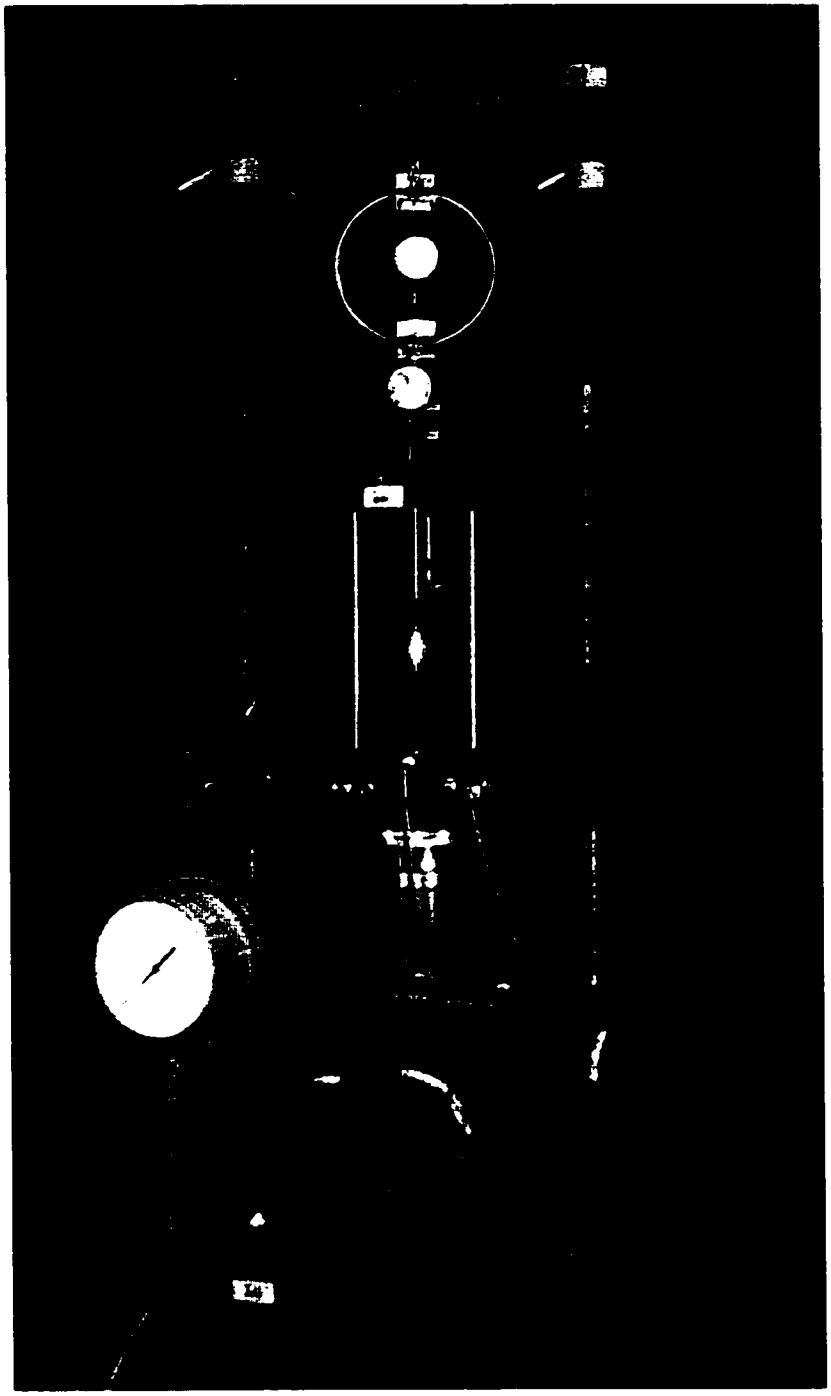

Figure 3.17: Triaxial Equipment used during conventional testing

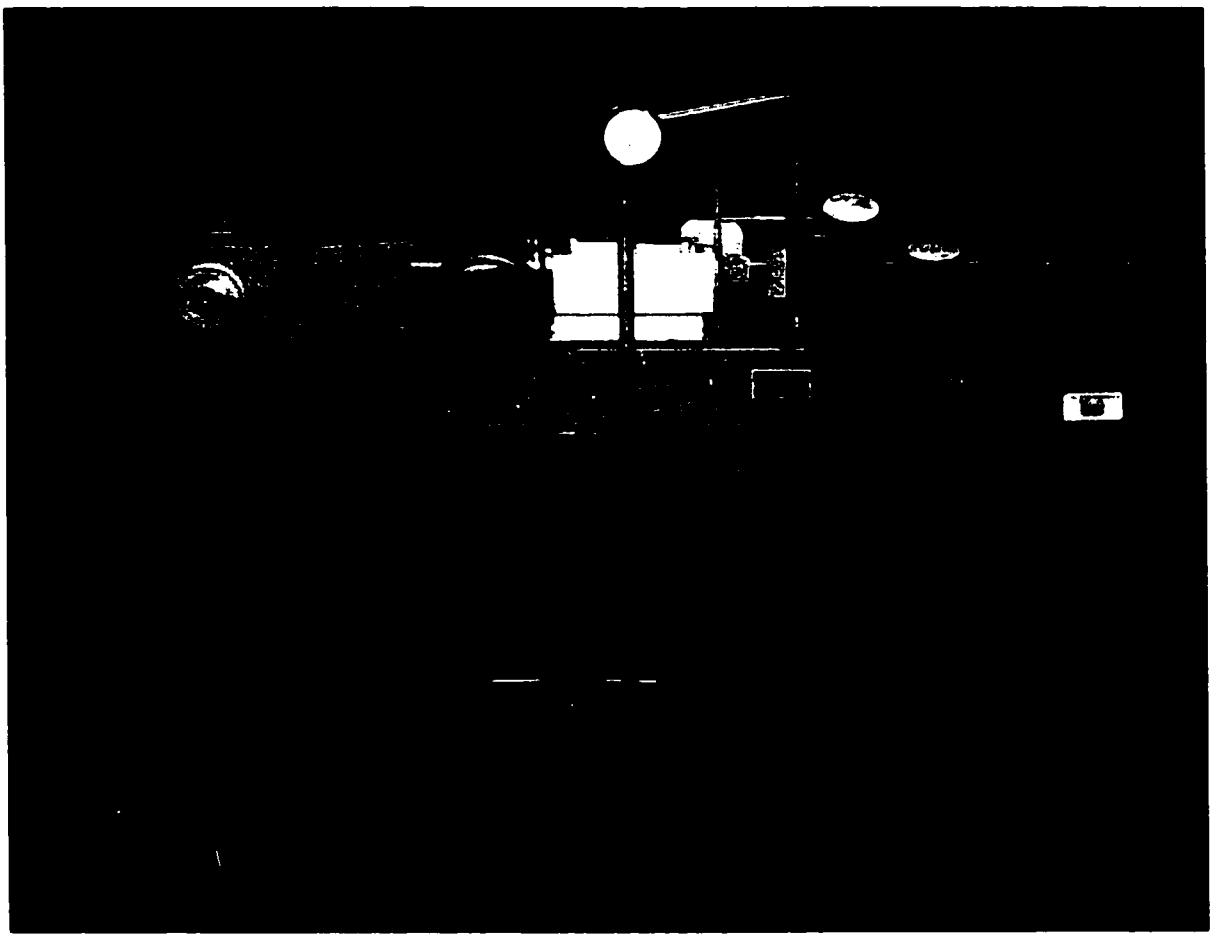

Figure 3.18: Direct Shear equipment used during conventional testing

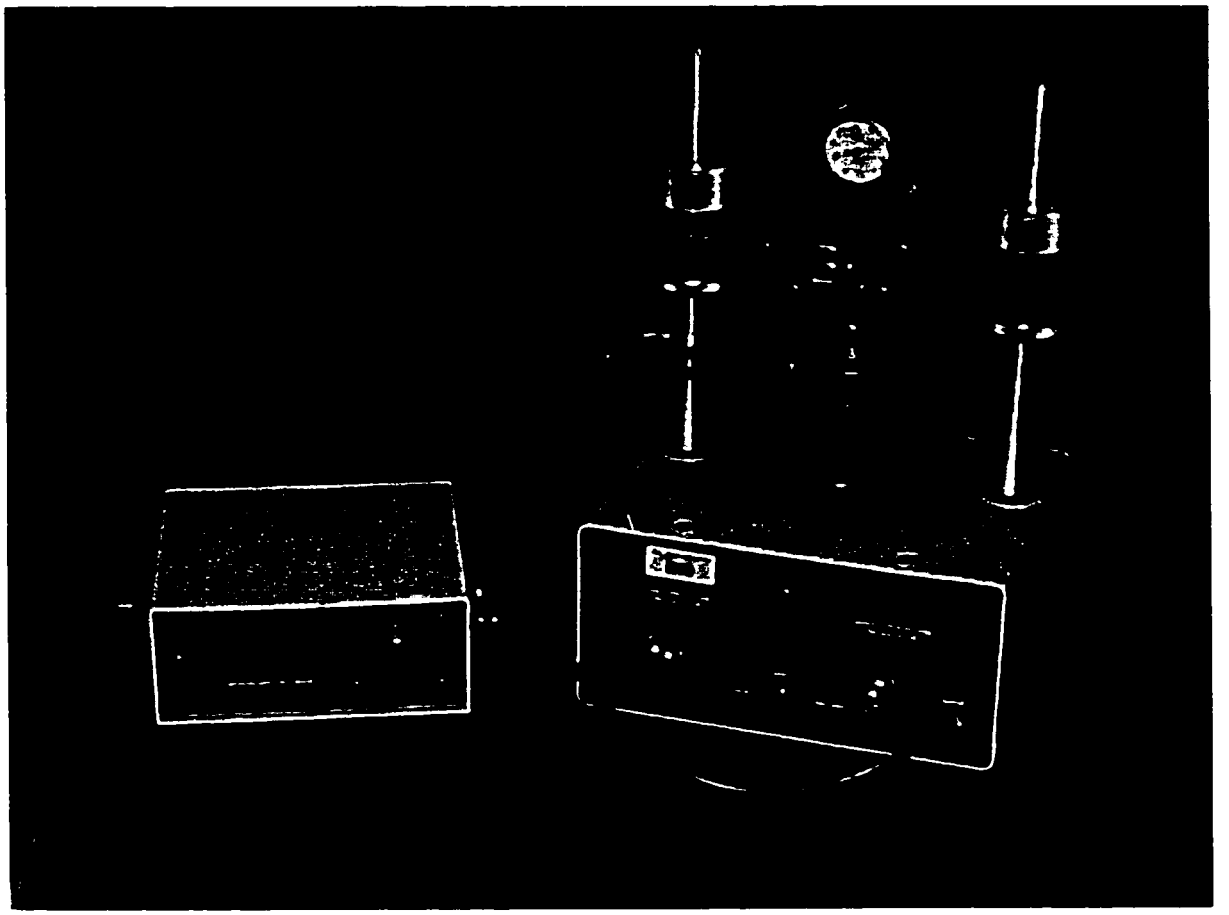

Figure 3.19: Odeometer used during conventional testing

Chapter 4: Sample Preparation

The Triaxial Vane Apparatus used in this research has been designed to accommodate both sand and clay samples. The method for preparing these different samples requires not only different preparation methods but also a change in the physical setup of the apparatus. Although the experimental program undertaken in this research was done on sand, the method for preparing both types of samples will be discussed in this chapter.

4.1 Clay Samples

4.1.1 Apparatus Set Up

The first step in making a clay sample is to ensure that the clay base in mounted in the Triaxial Vane Apparatus. The vane is placed into position, passing through the base of the cell and the vane retaining plate. The retaining plate is then positioned, such that the end of the vane shaft does not extend below the base of the plate when the vane is raised to the testing position. The vane is initially placed such that the vane blades are in the base. The porous stone in the sample base is removed and boiled in de-aired water to ensure full saturation of the stone and then replaced into the base.

4.1.2 Sample Set Up

The clay block sample is first cut with a 50mm diameter sample cutter. Next the sample is trimmed to a 100mm length. A piece of filter paper is cut into two 50mm diameter circles and a 100mm X 150mm grid. One of the circular filter papers is placed on the base and the clay sample is then placed into position on the base. The grid filter paper is wetted and then placed around the circumference of the sample, ensuring that no air pockets are trapped beneath the paper. A 0.30mm membrane is stretched into position using a membrane stretcher, again ensuring that no air is trapped below the membrane. The second circular filter paper is then placed on the top of the sample and the top cap is set in place. The membrane is then sealed on the base and the cap using O-rings. Anti

rotation rod are inserted on either side of the sample, just making contact with pins inserted into the cap. The remainder of the outer cell is then assembled around the sample and filled with water.

4.1.3 Testing Set Up

The cell is initially pressurized to approximately 20 kPa and a back pressure of approximately 10 kPa is applied to the sample. Cell pressure and back pressure are raised simultaneously until the back pressure is 600 kPa, the cell pressure is then increased until the desired consolidation pressure is reached. The sample is then left under pressure until consolidation is complete, at which time the back pressure valves are closed. If an anisotropically consolidated test is being set up, the loading ram can be adjusted to provide the required vertical load once the required horizontal consolidation stress is reached in the cell. Since the volume change is constantly monitored by the data acquisition system, the end of consolidation can easily be ascertained. Once consolidation is finished, the vane can be pushed up into position in the middle of the sample, with the retaining plate ensuring that the vane is not pushed to far up into the sample. The chain sprocket attached to the vane is then tightened onto the vane shaft and the test can proceed. As the vane is pushed into the sample, excess pore pressures will be generated, however, since the back pressure valves have been closed off, this pressure will not dissipate.

4.2 Sand Samples

4.2.1 Apparatus Set Up

As with the clay sample, the first step in setting up the sand sample is to ensure that the proper base is placed in the apparatus. Next the vane is placed into position. For the sand sample, the vane is placed so that the middle of the vane blades are located 50mm above the sample base, ie in the middle of the sample volume. **Figure 4.1** shows the proper positioning of the vane at this stage of sample preparation.

4.2.2 Sample Set Up

A measured amount of sand, approximately 255g, is placed into a pycnometer and filled with de-aired water. The pycnometer is then boiled to ensure full saturation of the sand sample, as shown in **Figure 4.2**. A 0.62mm membrane is placed into position over the sample base and a three-piece mold is assembled around the base. Suction is applied to the sample mold to retract the membrane tight to the mould. The mold is then filled with de-aired water. After the pycnometer has sufficiently cooled to be handled, the sand is hydro pluvated into the mold. The pluvated sample is shown in **Figure 4.3**. The sample cap is placed into position and the membrane is sealed. A 10 kPa suction is applied to the sample, the mold is removed and the anti rotation rods are set in place. The completed sample is shown in **Figure 4.4**. The remainder of the outer cell is then assembled around the sample and filled with water. The fully assembled cell is shown in **Figure 4.5**.

4.2.3 Testing Set Up

As with the clay sample, the cell is initially pressurized to approximately 20 kPa and a back pressure of approximately 10 kPa is applied to the sample. Cell pressure and back pressure are raised simultaneously until the back pressure is 600 kPa, the cell pressure is then increased until the desired consolidation pressure is reached. The sample is then left under pressure until consolidation is finished. If an anisotropically consolidated test is being set up, the load ram can now be adjusted to the proper vertical load. Since the volume change is constantly monitored by the data acquisition system, the end of consolidation can easily by ascertained and is usually reached within several minutes after the pressure has been applied. However, as suggested by Zhang (1997), the sand samples were left under the 600 kPa back pressure overnight to ensure total saturation. Shearing can then proceed.

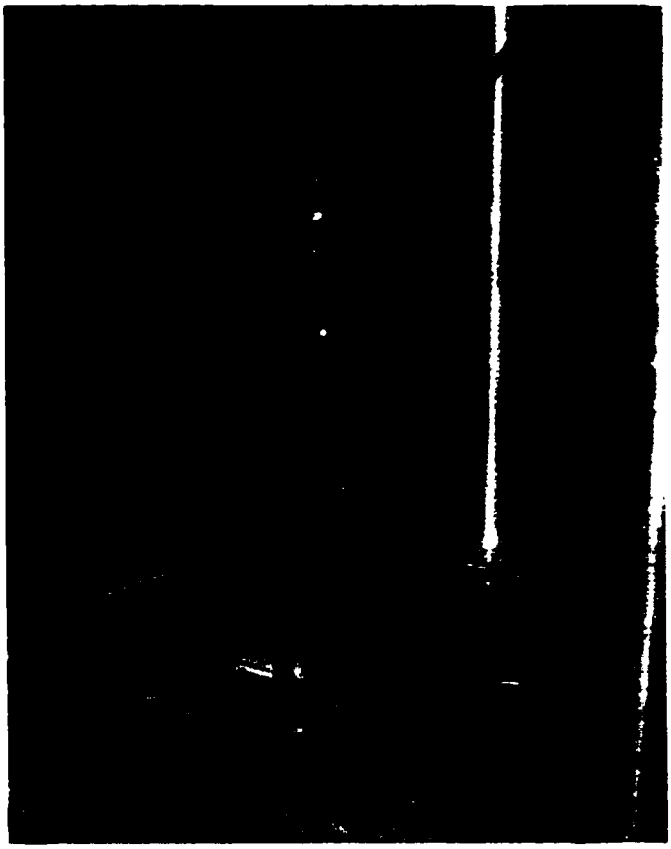

Figure 4.1: Vane in position for sand sample

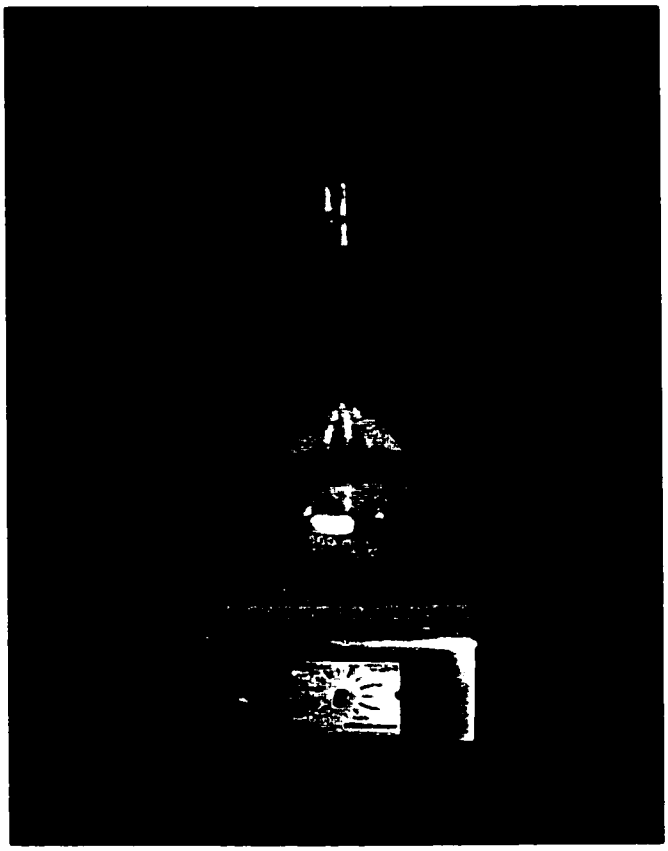

Figure 4.2: Boiling sand in a pycnometer to ensure saturation

Figure 4.3: Pluvated sample

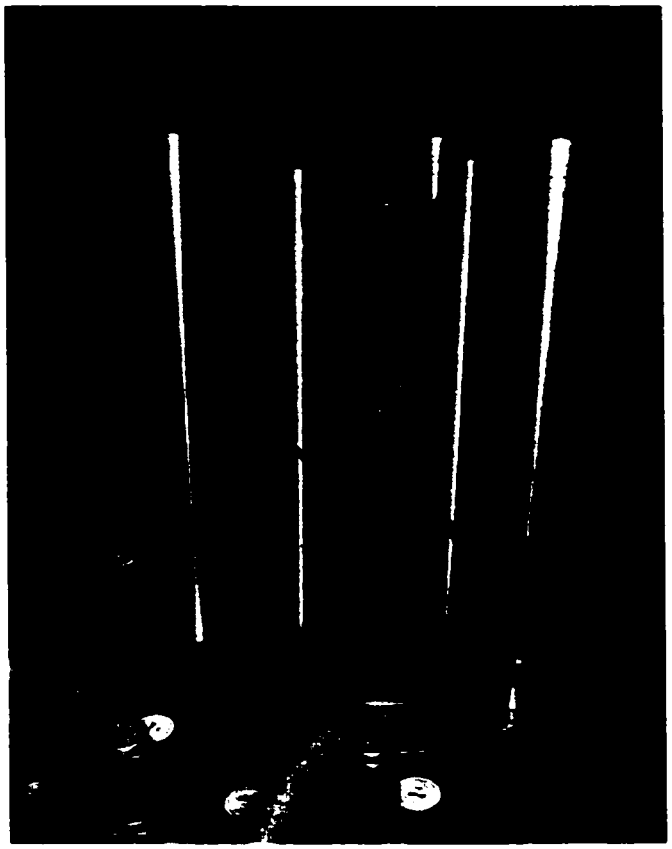

Figure 4.4: Completed sand sample

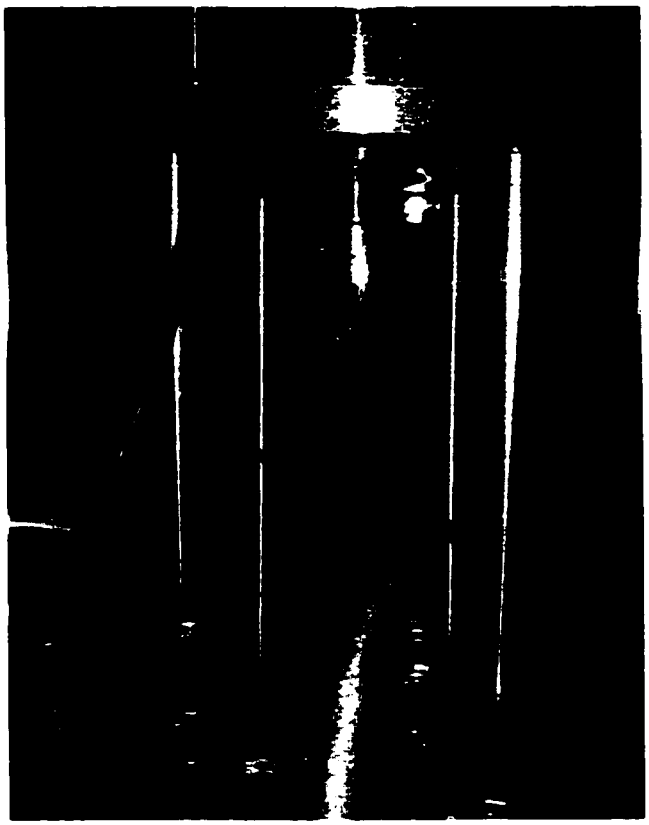

Figure 4.5: fully assembled cell with sand sample

Chapter 5: Material Tested and Density Verification Tests

This chapter describes the material used in the testing program and the various testes undertaken to verify the adequacy of the sample preparation technique. Since the density of the material can significantly affect the shear strength, verification of the uniform density of the sample with depth was critical.

5.1 Material Tested

The material selected for use in this testing program was the Unimin 2010 sand. This is an angular, medium crushed quartz obtained from St. Canut, Quebec, Canada. This material was selected for testing due to its previous use for research purposes at the University of Ottawa (Zhang, 1997; Sedano, 1998). As such the properties of the sand have been well studied using standard testing techniques and the results from the Tri Vane Apparatus have be compared to these established properties.

The Unimin 2010 sand has a specific gravity of 2.665, with a maximum dry density, ρ_{dmax}, of 1.610 t/m^3 and a minimum dry density, ρ_{dmin}, of 1.308 t/m^3. These values correspond with a minimum void ration, e_{min}, of 0.665 and a maximum void ration, e_{max}, of 1.037.

To help maintain a consistent sand gradation and to remove any possible effects from fine material, the Unimim 2010 sand was sieved to remove any particles smaller than 75μm (#200 sieve). The original grain size curve is shown in **Figure 5.1**. As can be seen from this curve, the amount of material removed by sieving was small and did not affect any of the previously stated soil properties.

5.2 Density Verification Tests

To properly verify the uniformity of a sample with depth, a method to solidify it, without altering the sample is required. Then individual slices of the sample can be taken and analyzed to create a density profile. It is possible to solidify the sample using a gelatin solution, proposed by Vaid and Negussey(1988). The gelatin solution permeates the pores; subsequently, after the gelatin solidifies, the sample can be sliced into layers with a specific thickness, and hence a known volume of each slice. The gelatine can then be washed away in water and the weight of the solids in each slice, and hence the density, can be determined.

5.2.1 Gelatin Concentration

The selection of a proper gelatin solution is critical to achieving accurate density distribution results. The solution must be fluid enough the flow easily but also have a high enough gelatin concentration to properly solidify the sample. Previous tests investigating the use of a gelatin mixture to solidify the Unimin 2010 sand (Sedano, 1998) found that a 1g / 10ml gelatin to water mixture was adequate to produce firm, yet easy to slice samples with no loss of material. As such, the same concentration has been used in this research. The gelatin material used was a commercial grade, flavorless gelatin powder mixed with hot de-aired water.

5.2.2 Gelatin Sample Preparation

Previous uses of a gelatin solution to solidify sand samples (Vaid and Negussey, 1988; Sedano, 1998) worked by first preparing the soil sample and then saturating the sample through the base of the specimen with the solution. In this research, due to the methodology used to prepare the soil sample, a different method was used. Since the samples were being prepared using a hydro pluvation method, water was replaced with the gelatin solution. The sample was made by first boiling the sand with the gelatin de-

aired water solution. This mixture was then hydro pluvated into a special mold (**Figure 5.2**), which was also filled with the gelatin de-aired water solution.

5.2.3 Sample Recovery and Filtration

Once the sample had solidified, the handle of the mold was turned to push the sample exactly 6.35 mm (1/4 inch) past the edge of the mold. The sample was then cut along the edge with a sharp knife. The sliced samples were collected in beakers and mixed with boiling water. The contents of the beaker were then placed into a suction filtration device (**Figure 5.3**) to remove any water, and thus any gelatin from the sample. The sample was then washed and filtered twice more with boiling water. Finally, the sample was oven dried and weighed.

5.2.4 Results of Density Verifcation

The results of the density verification tests are shown in **Figure 5.4**. The results of the tests show an average density of 0.894 t/m^3 with a standard deviation of 2.2%. This compares reasonably to the 3% standard deviation reported by Vaid and Negussey (1988) for water pluvated sand samples. Variation of density with depth is uniform and is repeatable. There does appear to be minor variation at the very top and bottom of the samples, however these are not inside the shear zone in the Tri Vane tests and will not cause significant variations in measured shear strength. The measured dry densities in the gelatin samples are lower than the minimum density given previously for the sand, however this reduction in believed to be caused by the use of the gelatin solution as the pluvation medium, where the higher viscosity of the solution results is a less tightly pack grain structure.

These results indicate that the water pluvation sample preparation technique is capable of creating samples with a uniform density throughout the sample, although the exact density can vary slightly between different samples.

5.3 Factors Affecting Density Distibution

During the course if the present research, two comments were raised concerning the ability to produce a uniform sand sample. These comments centered on the presence on the vane during sample preparation and were as follows:

1. Will the presence on the vane cause turbulence during the hydropluvation, and,
2. Will any flow disturbance caused by the presence on the vane results in density variations within the sample and could the results of the density investigation undertaken during this research, where the vane was not present during sample preparation, be compared to the sample preparation used during the testing where the vane was present during sample preparation.

5.3.1 Presence on Turbulence

The presence of the vane in the sample mould does present the possibility of turbulence generation. However the actual existence of turbulent flow can be determined through the use of fluid flow theory. Observations made during sample preparation indicated that the average time to fully pluvate a sample was approximately 30 seconds. Using the dimensions of the sample mould and this time, an average fluid flow velocity of 0.01 ft/sec can be calculated. From the fluid velocity and the vane dimensions, the Reynolds number can then be calculated as Re = 3.85. Finally, from the Reynolds number and the vane dimensions, the friction drag coefficient, CD, can be calculated as CD = 0.034. Turbulence is deemed to occur at the Reynolds number where an abrupt change occurs in the drag coefficient. **Figure 5.5** indicates that the transition from laminar flow to turbulent flow, when subject to foreign intrusion, exists between the range of 10^5<Re<10^6. Since the Reynolds number for flow around the vane is significantly less than the indicated laminar-turbulent boundary, it is apparent that the presence of the vane within the sample mould does not cause any significant turbulence.

5.3.2 Effect of Flow Disturbance and the Presence of the Vane During Sample Preparation

At the onset of this research, it was apparent that the uniformity of the sample was of paramount importance. Upon reviewing the hydropluviation method to be used for sample preparation during this research, two areas for potential problems were noted. The first problem concerns the placement of the sand during hydropluviation. If the flow rate of the sand out of the pycnometer is not controlled at a constant rate throughout the placement process, density layering will occur. The second problem is the potential that the vane will create disturbances during the pluvation, which will create a difference in the density of the sand around and under the vane compared to the sand above the vane.

The density testing conducted during this research used a hollow cylinder, without the vane being present. This was done deliberately. The purpose of this density testing was to investigate the first density problem as indicated above. The results presented earlier in this chapter do show that a uniform sample could be consistently produced, indicating that a consistent flow rate could be maintained during sample preparation. This removes one of the two potential problems completely.

The second potential problem, that of disturbance caused by the presence of the vane, is much more difficult to prove or disprove. The only method to accurately determine the density distribution within the sample is that described earlier, by solidifying the sample, slicing it into thin segments and determining the density of each individual segment. However, this presents an obvious problem if the vane is in the sample when it is solidified, as the vane itself cannot be sliced with the segments.

Attempts were made to determine the density of the sample with the vane in place. The first method attempted was to cut the sample segments from around the vane. Unlike cutting the segments when no vane was present, when the top of the hollow cylinder could be used to guarantee flat, straight, accurate cuts could be made every time, the cuts

around the vane had to be made by hand without any guide to ensure a proper cut. As a result, the cuts tended to be crooked, so that the volume could not be accurately calculated. Additionally, these smaller pieces tended to fall apart due to their small size, and the entire mass could not be guaranteed to be collected. This led to an inability to properly measure the density of each segment. Also, the gelatin tended to securely bond with the vane itself, leading to pieces that were adhered so tightly to the vane, they could not be removed, further increasing the error associated with any density calculations made from these samples.

The second method attempted was to push the vane out of the sample before being cut into segments so as to avoid the need to cut around the vane. However, as mentioned above, the gelatin bonded with the vane so tightly, that the sample was ripped apart while the vane was being pushed out. In order to prevent the bonding of the gelatin to the vane, a layer a silicon lubricant was place on the vane before it was placed in the cylinder. However, since the gelatin had to be placed in the cylinder hot to maintain its liquid state, the lubricant tended to be softened and washed away from the vane, allowing the gelatin to bond with the vane. In order to prevent this, a very thick layer of a lubricant was required, making any accurate measurements of volume, and thus density, impossible.

Although, the exact effect of having the vane in place could not be measured during the density tests, an attempt was made to mitigate the effect of vane-induced disturbance. As the sand was being placed into the mould, the pycnometer was kept to the outside edge of the mould. In this position, the sand flowed past the side of the vane and then settled in around it, avoiding the vane and any possible disturbance caused by the vane. This is confirmed by visual observation of the sand as it was pluviated into the mould during sample preparation. The sand did indeed follow this pluvation pattern and there was no visible movement of the sand grains due to vane-induced disturbance. Additionally, the shape of the vane used in the Triaxial Vane Apparatus reduces the vane-induced disturbance. The flat edge on the top and bottom of the vane designed used in this research causes less turbulence than a vane with an angled edge.

Additionally, if the turbulence around the vane caused a zone of sand with a different density, then the calculated overall density would be different for samples created with the vane in place than for sample created when the sample was not in place. During this research, in order to investigate shaft friction, several samples were prepared without the vane blades in place, but with the shaft. Comparison of the densities of these samples (the Friction XX tests) and the densities of the isotropically consolidated (IC-D and IC-U) sample shows that there is no significant difference between the overall density of the samples created with the vane in place and those created without the vane. The difference between the average densities with and without the vane blades is less than the standard deviation of the spread of the values with in the two groups. As a result, it can be reasonably inferred that the presence of the vane has a negligible effect on the density and the density distribution for the samples created in this research.

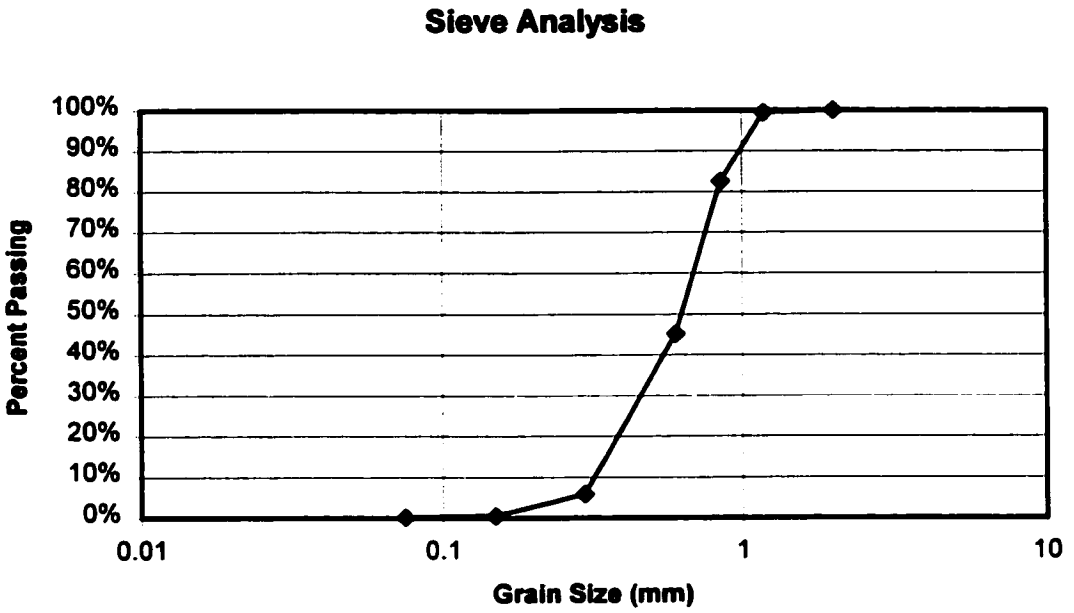

Figure 5.1: Grain size distribution of Unimin 2010 sand

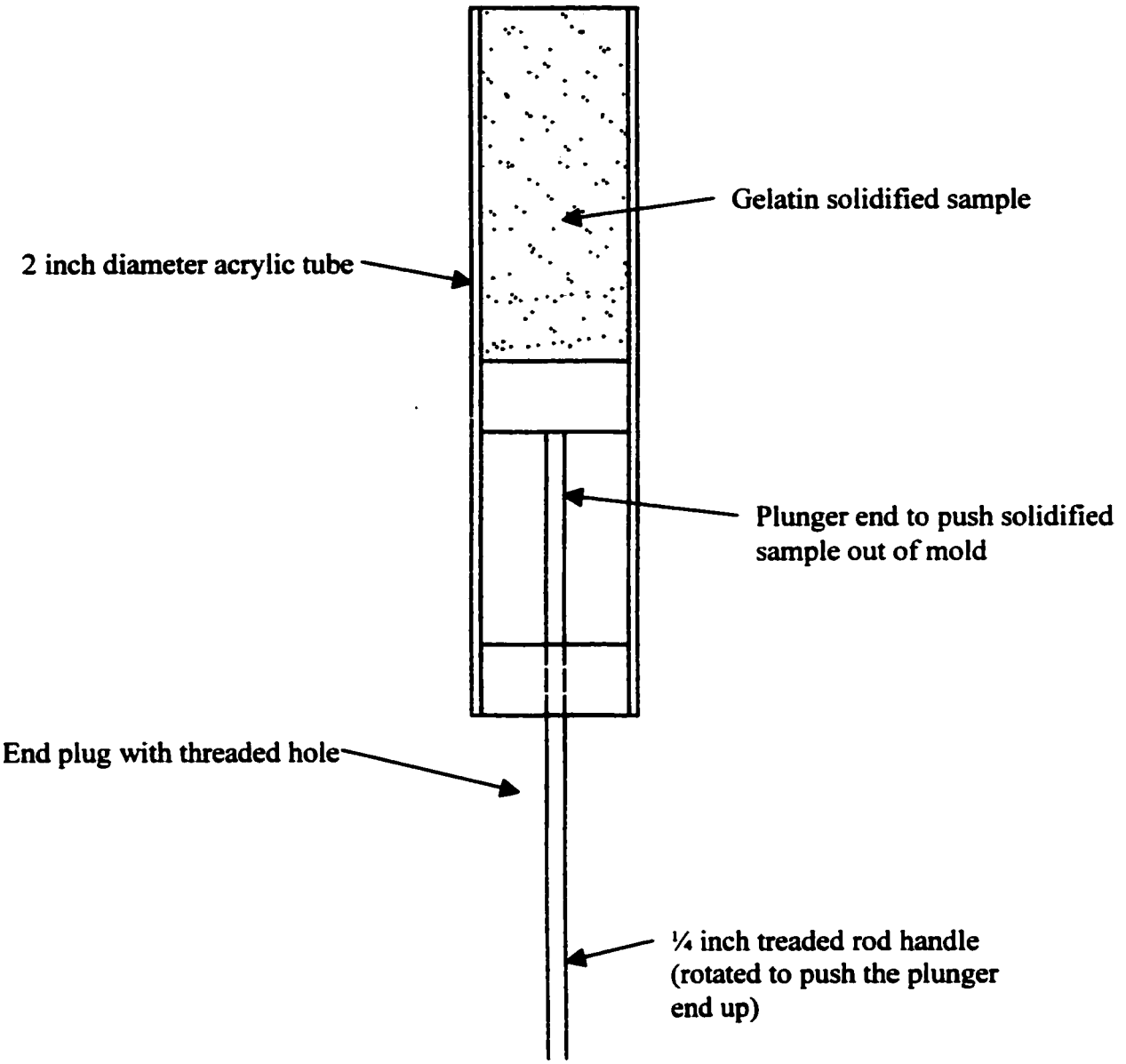

Figure 5.2: Gelatin sample mold

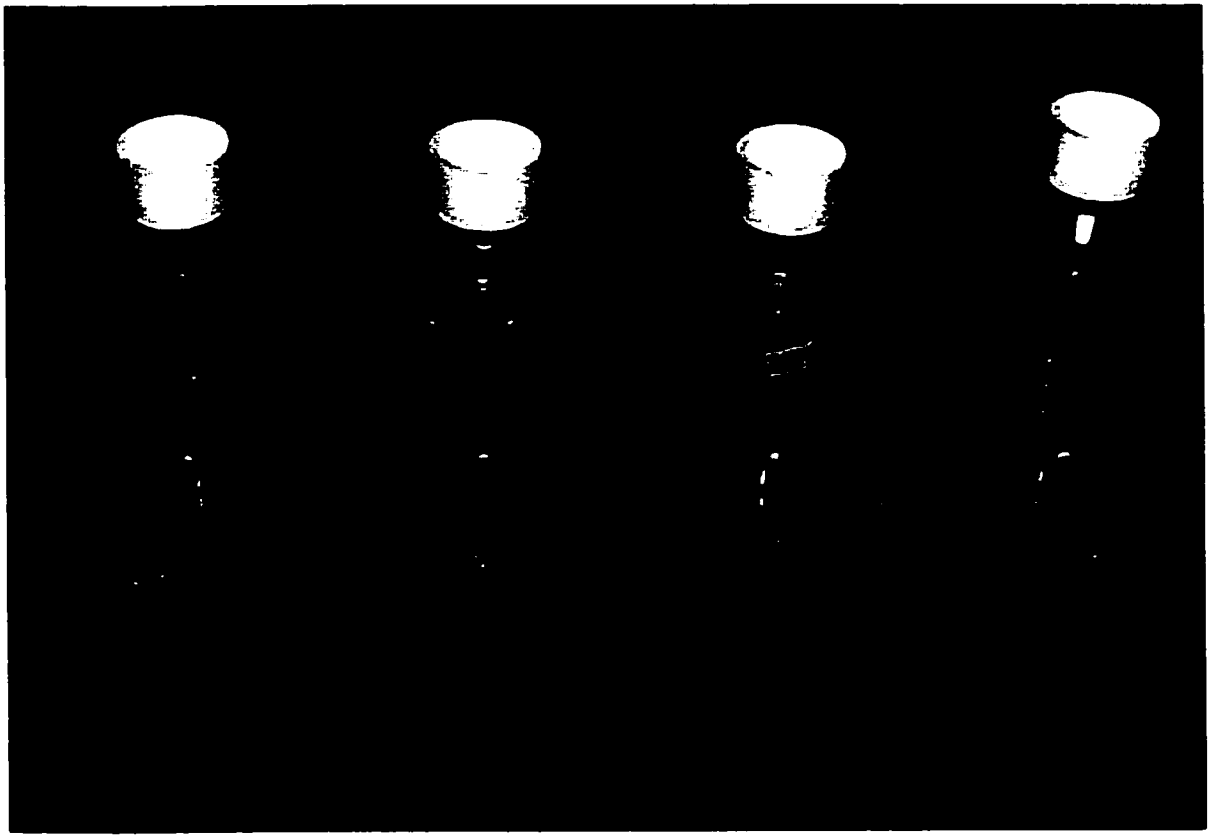

Figure 5.3: Suction filtration device

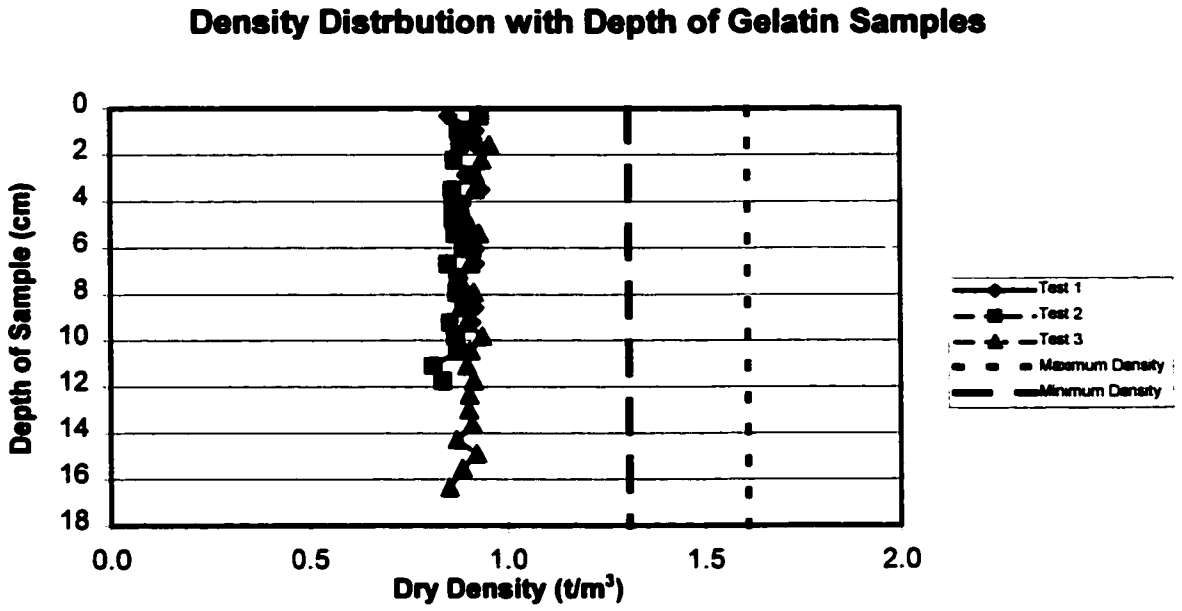

Figure 5.4: Density verification results

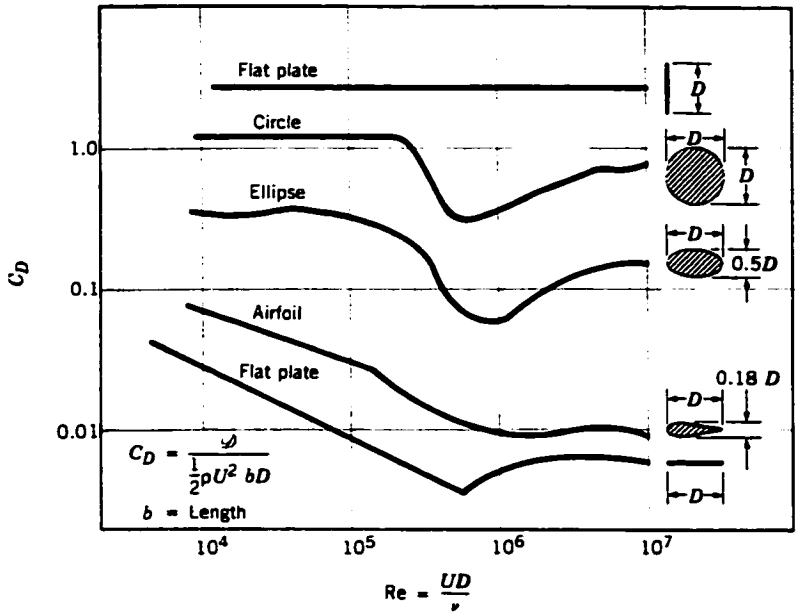

Figure 5.5: Character of the drag coefficient as a function of Reynolds number for objects with various degrees of streamlining (from Munson, Young and Okiishi, 1994)

Chapter 6: Test Program and Experimental Results

This chapter describes the test program undertaken during the course of this research program.

6.1 Test Program

The test program undertaken is presented in **Tables 6.1 and 6.2**. Table 6.1 shows the conventional tests that were conducted and Table 6.2 shows the Triaxial Vane tests.

The test program was designed to investigate the following:

1) The shear strength of the Unimin 2010 sand as determined by conventional tests, both the triaxial test and the direct shear test
2) The influence of initial void ratio on shear strength measured by the Triaxial Vane Apparatus
3) The influence of vane shaft friction in the Triaxial Vane Apparatus
4) The influence of shear rate on Triaxial Vane strength
5) The applicability of the Triaxial Vane Apparatus for determining the shear strength of sand in the following modes:
    a. Peak strength
    b. Residual strength
    c. Drained strength
    d. Undrained strength
    e. Isotropic consolidation
    f. Anisotropic consolidation

As mentioned previously, all testing in this research was conducted on Unimin 2010 sand. This material was selected since the same material had been used by Zhang (1997) and Sedano (1998). Thus many of the properties that have been investigated using the Triaxial Vane Apparatus have been studied using alternate equipment and the results can be compared to determine the applicability of the Triaxial Vane Appparatus.

For convenience, the following abbreviations are used in describing the tests:

IC-D: Isotropically consolidated drained tests

IC-U: Isotropically consolidated undrained tests

AC-D: Anisotropically consolidated drained tests

AC-U: Anisotrpically consolidated undrained tests

Additionally, the numbers following these abbreviations indicate the consolidation stress.

6.2 Experimental Results

6.2.1 Conventional Testing

The shear strength properties of the Unimin 2010 sand was determined using both the triaxial test and the direct shear test. **Figure 6.1** and **Figure 6.2** show the drained and undrained triaxial test results conducted on saturated material. The triaxial tests show a peak strength drained friction angle of 36° and a peak strength undrained friction angle of 37.4°. **Figure 6.3** shows the direct shear results, which indicate a peak strength friction angle of 38.5°. Both the triaxial and direct shear tests were conducted in accordance with ASTM standard procedures; however, the triaxial tests were analyzed as outline by Zhang (1997). The direct shear tests were conducted as saturated, drained tests so that a common failure mode would be compared for all test methods. Additionally, an odeometer test was carried out to determine the consolidation characteristics to be used in the Hansen and Gibson model (as described in Chapter 2). Individual test results are shown in Appendix 2.

6.2.2 Triaxial Vane Test Procedures and Analysis Method

To ensure that all Triaxial Vane tests were conducted in a similar manner, a standard test procedure was established and follow in all cases, except where specifically noted. The procedure was as follows:

1) Prepare sample as outlined in Chapter 4.
2) Allow sample to consolidate overnight with a 600 kPa back pressure and appropriate cell pressure (Zhang (1997) found that this back pressure was necessary to ensure full saturation).
3) For isotropically consolidated testing, the load ram was then lowered until it just made contact with the sample cap and then the ram is lock in place. This movement and the total change in volume measured by the volume gauge then allowed for the calculation of the consolidated sample dimensions.
4) Close back pressure valves. At this time the cell pressure was then increased by 100 kPa and the resulting increase in pore pressure was measured to determine the B value (and hence the degree of saturation). The cell pressure was then reduced back down. If a drained test was being conducted, the back pressure valve were opened.
5) Start vane rotation at 60° / min (Note: this speed was selected as it corresponds with the speed prescribed by ASTM 4648 for miniature vane tests in clays)
6) Allow vane to rotate at this speed for one full rotation or until the computer display indicated that peak strength had been exceeded, whichever was greater.
7) Turn off the motor and set the speed at maximum, corresponding to a rotation rate of 1100° / min. Restart the motor. This was accomplished with no more than 5 seconds of rest time (i.e. the time that there was no vane rotation)
8) Allow the vane to rotate at the higher speed for ten full rotations.
9) Turn off the motor and reset the speed to a rotation rate of 60° / min. Restart the motor. This was accomplished with no more than 5 seconds of rest time.
10) Allow the vane to rotate through one full rotation to measure residual strength.
11) For drained, isotropically consolidated testing, the load ram was then lower again until it just made contact with the sample cap. This allowed for the calculation of the change in sample dimensions during testing.

After the test was complete the vane torque measurements were converted to shear strength using the analysis method given in ASTM 4648 and described in Chapter 2.

6.2.3 Variation in Vane Shaft Friction

Figure 6.4 shows the results of IC-D tests investigating vane shaft friction. The standard test procedure was used for all tests in this series except that the vane blades were not attached to the shaft, only the shaft itself was inserted in to sample. The results show that the shaft friction varies not only with consolidation stress but also with rotation. As consolidation stress increases, the initial shaft friction (corresponding to friction at peak strength) increases fairly consistently. However, after peak strength has been exceeded, the shaft friction corresponding to the friction at residual strength behaves differently. At low confining stresses, the shaft friction initially decreases with increasing confining stress until confining stress reaches 100 kPa. The shaft friction then maintains a constant value of approximately 10 kPa, regardless of consolidation stress. However, since the majority of the data points support a constant vane shaft friction at residual strength, the constant value of 10 kPa was assumed for all residual tests. Consequentially, the shaft friction measured at the beginning of the test (by using the reverse thread on the vane) is the friction value used to adjust the peak strength and the constant value, 10 kPa, is used to adjust the residual strength value. Individual test results are shown in Appendix 3.

6.2.4 Effects of Initial Void Ratio

Figure 6.5 shows the results of IC-D tests to investigate the effects of variation of initial void ratio on measured drained shear strength. For convenience, void ratio has been converted to relative density. All tests were conducted in accordance with the standard test procedures with one addition. When preparing the sample, it was prepared as described in Chapter 4, and then the samples were vibrated for different periods of time to achieve higher relative densities. All samples in this test series were then consolidated to a 100 kPa consolidation pressure. Individual test results are shown in Appendix 3.

From the data shown in Figure 6.5, it can be concluded that the peak strength measured by the Triaxial Vane Apparatus is linearly proportional to the initial relative density, with a ratio of 1% change in relative density to 2 kPa change in peak shear strength. Consequentially, the results from multiple tests can be adjusted to the same relative density through a simple conversion to eliminate the effects of different initial void ratio.

Additionally, Figure 6.5 shows that the residual strength is unaffected by the initial void ratio.

6.2.5 Influence of Shear Rate

Figure 6.6 shows the results of IC-D tests investigating the effects of shear rate in the Triaxial Vane Apparatus. All tests conducted in this series followed the standard procedure with one modification. The rotation rate was set at the beginning of the test and maintained at the same rate for the entire duration of the test. Additionally, all tests were conducted at the same consolidation stress of 100 kPa. As can be seen from the data, the rate of shear has no effect of the residual strength measured by the Triaxial Vane Apparatus.

However, the measured peak strength appears to be affected by the shear rate. As the shear rate increases, the measured shear strength decreases. Although these tests are drained, it is believed that in the area directly around the vane, the rotation of the vane generates a localized pore pressure increase. This increase in pore pressure thereby reduces the local effective stress and thus the shear strength along the failure surface. Since all other tests done with the Triaxial Vane Apparatus are conducted using the lower shear rate, no adjustment of the measured strengths are required. Individual test results are shown in Appendix 3.

6.2.6 Isotropically Consolidated Drained Tests (IC-D)

Figure 6.7 shows the results from a typical IC-D Triaxial Vane test. As can be seen from the volumetric strain line shown in this typical result, steady state conditions are reached after approximately 6 full rotations. **Figure 6.8** shows the complete results of all the IC-D tests preformed during the course of this research. All tests conducted in this series followed the standard testing procedures. This figure shows both the peak and residual strength values. As can be seen from the data, the residual strength values show very little scatter about the tread line with a friction angle of 31.9°. The peak value, while showing a somewhat larger scatter, still shows a reasonable trend (with the exception of one data point) with a friction angle of 37.6°. Of noticeable importance is that for peak strengths, there is a zero effective stress intercept (i.e. an apparent cohesion). Since previous tests, including the conventional tests conducted in this research and the results of Zhang (1997) and Sedano (1998), show that the material does not have a cohesion value, this is believed to be an effect caused by the Triaxial Vane Apparatus. **Figure 6.9** shows the results of the Hansen and Gibson model (modified to included volumetric change). The predicted friction angle of 37.1° is in very close agreement with the actual value obtained during the experimental study. It should be noted that the Hansen and Gibson model requires an initial soil friction angle to predict the results of the vane test; this initial value was taken as the friction angle determined by the triaxial test . Individual test results are shown in Appendix 4.

6.2.7 Isotropically Consolidated Undrained Tests (IC-U)

Figure 6.10 shows the results from a typical IC-U Triaxial Vane test. As can be seen from the effective stress line shown in this typical result, the pore pressures measures during the test do shows fluctuations, however the trend is readily apparent and steady state conditions are reached after approximately 6 full rotations. **Figure 6.11** shows the complete results of all the IC-U tests preformed during the course of this research. This figure shows both the peak and residual strength values. As can be seen from the data, the residual strength values show very little scatter about the tread line with a friction angle

of 28.4°. The peak value shows a friction angle of 40.6°, however there is a large scatter in the data. This scatter is believed to be a result of localized pore pressure increase. The design of the Triaxial Vane Apparatus allows for the pore pressure to be measured only at the top and bottom of the sample. As the vane rotates, there is believed to be a larger pore pressure developed at the failure surface, which is then dissipated through the sample. If these pore pressure could be measured, it is believed that a much lower scatter in the data would be observed. As in the drained tests there is also a zero effective stress intercept (i.e. an apparent cohesion) in the peak strength line. Since this value is similar to the value noticed in the IC-D tests, the conclusion that this is a systemic problem is further reinforced. Individual test results are show in Appendix 5.

6.2.8 Anisotropically Consolidated Drained Tests (AC-D)

Figure 6.12 shows the results from a typical AC-D Triaxial Vane test. **Figure 6.13** shows the results of the AC-D test performed during the course of this research and the results of the Hansen and Gibson analysis. The figure is a plot of the normalized shear strength, τ / τ_o, vs. the anisotropic stress ratio, K (σ_3 / σ_1), where τ_o is taken as the shear strength at K = 1. Based on the results of Figure 6.12, it is apparent that the predictions of the Hansen and Gibson model are valid for the residual shear strength of the sand between the values of K = 1 to 0.55. However, at K < 0.55, the actual residual shear strength begins to diverge from the predicted values. The Hansen and Gibson model was developed based on the known performance of the vane shear test in 1954. Menzies and Merrifield (1980) and Wroth (1984) showed the vane test in sand has a greater dependency on the vertical stress than is found in clay, as shown in Chapter 2. Thus, as the vertical stress increases, the error caused by this underestimation of the influence of the vertical stress also increases, causing the divergence between the predicted results and the actual results.

Additionally, it can be seen in Figure 6.12 that the Hansen and Gibson model greatly underestimates the peak strength values of the sand. Also, at K = 0.5, the normalized peak strength values start to drop instead of continuing to increase as predicted by the

Hansen and Gibson model and seen in the residual strength. This divergence is believed to be caused by the axial loading in the Triaxial Vane Apparatus. At the lower K values (and hence higher σ_1 values), the sample approaches the point of failure in axial compression. As the vane begins to rotate, the localized pore pressure increases, thereby reducing the effective stress, and thus shear strength, to a point where axial failure occurs. At higher σ_1 levels, the sample is brought closer to failure and the torque required by the vane to exceed this failure point becomes less, thus creating the drop in shear strength shown in Figure 6.12. The Hansen and Gibson model does not account for axial failure, only failure along the vane surface and thus cannot predict this phenomenon. Individual test results are shown in Appendix 6.

6.2.9 Anisotropically Consolidated Undrained Tests (AC-U)

Attempts were made to use the Triaxial Vane Apparatus in an anisotropically consolidated undrained mode. However, as soon as the vane began to rotate, the increase in pore pressure resulted in liquefaction of the entire sample, which then collapsed under the axial loading.

6.3 Comparison and Discussion of Test Results

As mentioned earlier, the Unimin 2010 sand was chosen as the material to be used in this research since it had been used previously at the University of Ottawa and, as such, the properties had been studied extensively. **Table 6.3** compares the results of the Triaxial Vane Apparatus to those determined by Zhang (1997) and Sedano (1998) as well as the results of the conventional testing undertaken during the course of this research.

6.3.1 Drained Peak Strength

The drained peak strength friction angle measured by the Triaxial Vane Apparatus shows very good agreement to the conventional testing. Additionally, the predicted vane shear

friction angle from the Hansen and Gibson model is nearly identical to the actual value. All values are within 1.8° and the results have a standard deviation of only 0.78.

6.3.2 Undrained Peak Strength

The undrained peak strength friction angle measured by the Triaxial Vane Apparatus is reasonable close to the results of the conventional testing, the difference being only 3.2°. As mentioned earlier, it is believed that the scatter caused by the inability to accurately measure the pore pressure at the failure surface is responsible for this difference.

6.3.3 Residual Shear Strength

The drained residual strength friction angle measured by the Triaxial Vane Apparatus is very close to the results of the results of Sedano (1998) and Zhang (1997). The undrained residual friction angle, although it should be the same and the drained friction angle, is 2.5° lower. As mentioned earlier, it is believed that is caused by the inability to accurately measure the pore pressure at the failure surface.

6.3.4 Steady State Line

Figure 6.14 shows the steady state line as determined by the Triaxial Vane Apparatus, Sedano (1998) and Zhang (1997). This figure shows close agreement between the steady state lines determine by the constant volume ring shear (Sedano, 1998), the triaxial CU compression tests (Zhang, 1997) and the drained Triaxial Vane tests. The undrained Triaxial Vane tests plot below the other data sets, however, as with the residual shear strength, this is believed to be caused by the inability to accurately measure the pore pressure at the failure surface.

6.3.5 Effect of Initial Void Ratio

Deschenes (1978) investigated the effect of void ratio on shear strength measured in a shear box on a sand similar to the Unimin 2010 sand used in this investigation. These results are shown in **Figure 6.15**. The figure shows that the effect of the void ratio depends on the normal stress applied to the sample. However, for the stress range used in the Triaxial Vane research, 50-200 kPa, Figure 6.15 shows that the shear strength increases approximately 1.5 kPa for every 1% increase in relative density. This is consistent with the 2 kPa increase found with the Triaxial Vane Apparatus.

6.3.6 Effect of Vertical Stress

Law (1978) used the NRC Triaxial Vane to investigate the effect of different K values on the strength in clays measured by the vane test. In 1978 tests, Law first maintained a constant horizontal stress of 37.3 kPa and then conducted tests increasing the vertical stress from 37.3 to 83.4 kPa. Across this stress increase, Law measured only a 5% increase in measured shear strength, compared to a 50% increase measured shear strength when holding the vertical stress constant and increasing the horizontal stress within similar stress ranges as in the first series of tests. From this, Law determined that:

> *...the apparent vane strength interpreted using strength isotropy is relatively insensitive to a change in vertical consolidation pressure...*

However, from the anisotropic tests conducted in the current research, it can be seen that the measured vane shear strength increases of over 15% for a similar increase in vertical stress as used by Law. However, as mentioned in Chapter 2 and Section 6.2.8, this increase in the effect of the vertical stress was expected when the difference in stress distributions on the horizontal surface between sand and clay is considered.

6.3.7 Apparent Cohesion

Figures 6.8 and 6.11 show a very interesting results, as both figures show a cohesion intercept of 50 kPa for the strength envelopes. However, it is known that is sand does not have cohesion, and as a result this intercept or "apparent cohesion" is misleading. It is believed by this researcher that this "apparent cohesion" value of 50 kPa is not a measurement of the shear strength of the sand but is actually a result of the initial inertia of the embedded Vane Apparatus itself. As the vane blades begin to rotate, an initial force is required to overcome the inertia and to start the rotation. It is this initial force is what is being shown as the "apparent cohesion" in the test results. The result of this force would be a vertical shift in the failure envelope only and would have *no effect* on the angle of friction. As the peak shear stress occurs quickly after vane rotation starts, this initial force is indistinguishable from the peak strength in the individual test results and only becomes apparent when the results are compiled in a failure envelope diagram.

The tests results themselves also tend to indicate that this "apparent cohesion" is caused by an internal system force and not by the shear resistance of the sand. Both the drain and undrained isotropically consolidated sand samples (IC-D and IC-U tests) have the same intercept value. The fact that the values are the same tends to lead to the conclusion that the same phenomenon is at work causing this shift for both test types. Additionally, the fact that the values are the same for the drained and undrained cases also indicate that the mechanism causing this shift is independent of pore water pressure. Only a load transfer within the Triaxial Vane Apparatus can account for this additional loading. Further credence to the validity of values of residual strength (at large strain) measured in this triaxial apparatus is provided by comparison of residual strength measured in the modified Ottawa ring shear apparatus (Sedano, 1998), and by the values obtained by Zhang (1997) in carefully controlled triaxial tests. The same Unimin no. 2010 sand was used in all of these investigations. The residual strength envelopes from the three independent investigations are very similar. There is no apparent cohesion intercept at zero effective stress in any of these results. This clearly shows that the initial inertia force of 50 kPa does not act at large strain, otherwise different intercepts and strength values would have been obtained.

It was for this reason that *only* the angle of friction was used for comparison of the test results to conventional testing techniques. This intrinsic system force could have been removed from the records, however, this researcher decided to leave the shift in the results in order to present a complete record of all test results.

	Consolidation State			Measured Shear Strength	
Test ID	Relative Density	σ_1 (kPa)	σ_3 (kPa)	Peak Shear Strength (kPa)	Effective Confining Stress at Peak (kPa)
Triaxial Tests					
Triaxial Drained 100	39	100	100	308	
Triaxial Drained 200	35	200	200	584	
Triaxial Undrained 100	32	100	100	118	33
Triaxial Undrained 200	31	200	200	148	106
Triaxial Undrained 300	18	300	300	203	161
Direct Shear					
Direct Shear Test 1		120		86	
Direct Shear Test 2		224		165	
Direct Shear Test 3		330		257	
Direct Shear Test 4		16		6	
Direct Shear Test 5		51		37	
Oedometer					
C_c	2.57E-05				
C_{cr}	6.87E-06				
C_s	4.46E-06				

Table 6.1: Conventional Test Program

	Consolidation State			Triaxial Vane Measured Shear Strength				
Test ID	Relative Density	σ_1 (kPa)	σ_3 (kPa)	Peak Strength (kPa)	Effective Confining Stress at Peak (kPa)	Residual Strength (kPa)	Effective Confining Stress at Residual (kPa)	Comments
Isotropic Tests								
IC-D-50a	30	50	50	65		34	50	
IC-D-100a	23	106	106	117		66	107	
IC-D-150a	27	150	150	261		90	150	
IC-D-200a	32	201	201	199		122	201	
IC-U-50a	25	48	48	39	26	7	0	
IC-U-100a	20	94	94	97	73	6	9	
IC-U-150a	24	148	148	125	102	13	14	
IC-D-50	32	51	51	75		39		
IC-D-100	38	104	104	130		72		
IC-D-150	41	148	148	173		89		
IC-D-200	36	200	200	220		132		
IC-U-50	34	51	51	38	27	6	0	
IC-U-100	32	100	100	63	60	8	3	
IC-U-150	39	154	154	154	119	20	24	
IC-U-200	42	203	203	137	142	20	29	
IC-D-50b	35	51	51	62		39		
IC-D-100b	49	96	96	92		70		
IC-D-150b	38	147	147	146		97		
IC-D-200b	53	199	199	185		128		
IC-U-50b	50	47	47	67	37	8	0	
IC-U-100b	40	99	99	80	68	10	7	
IC-U-150b	40	153	153	144	119	19	24	
IC-U-200b	38	202	202	159	150	32	43	
Anisotropic Tests								
AC-D-100-70	55	169	99	93		70		
AC-D-100-88	39	191	103	134		82		
AC-D-100-116	28	222	106	156		87		
AC-D-100-172	27	276	104	135		98		
AC-D-100-201	34	301	100	120		106		
Rotation Rate Tests								

IC-D-100 SPEED 10	29	92	104	41	71 deg/min
IC-D-100 SPEED 20	29	101	93	47	192 deg/min
IC-D-100 SPEED 40	18	102	101	45	427 deg/min
IC-D-100 SPEED 60	18	101	96	41	720 deg/min
IC-D-100 SPEED 80	21	104	76	41	942 deg/min
IC-D-100 SPEED 100	13	105	82	41	1080 deg/min
Initial Density Tests					
Density 10s	31	101	100	72	
Density 15s	48	104	137	70	
Density 20s	59	101	154	69	
Density 30s	54	100	151	62	
Shaft Friction Tests					
Friction 50	32	48	16	11	
Friction 100	30	103	17	10	
Friction 150	32	142	18	10	
Friction 200	32	187	18	10	

Table 6.2: Triaxial Vane Apparatus Test Program

Peak Strength	
Drained	
Triaxial Vane	37.6°
Direct Shear	38.5°
Triaxial	36.7°
Hansen and Gibson Model	37.1°
Undrained	
Triaxial Vane	40.6°
Triaxial	37.4°
Residual Strength	
Triaxial Vane (Drained)	30.9°
Triaxial Vane (Undrained)	28.4°
Zhang (1997)	33.6°
Sedano (1998)	31.0°

Table 6.3: Comparison of Triaxial Vane Results to Previous Results

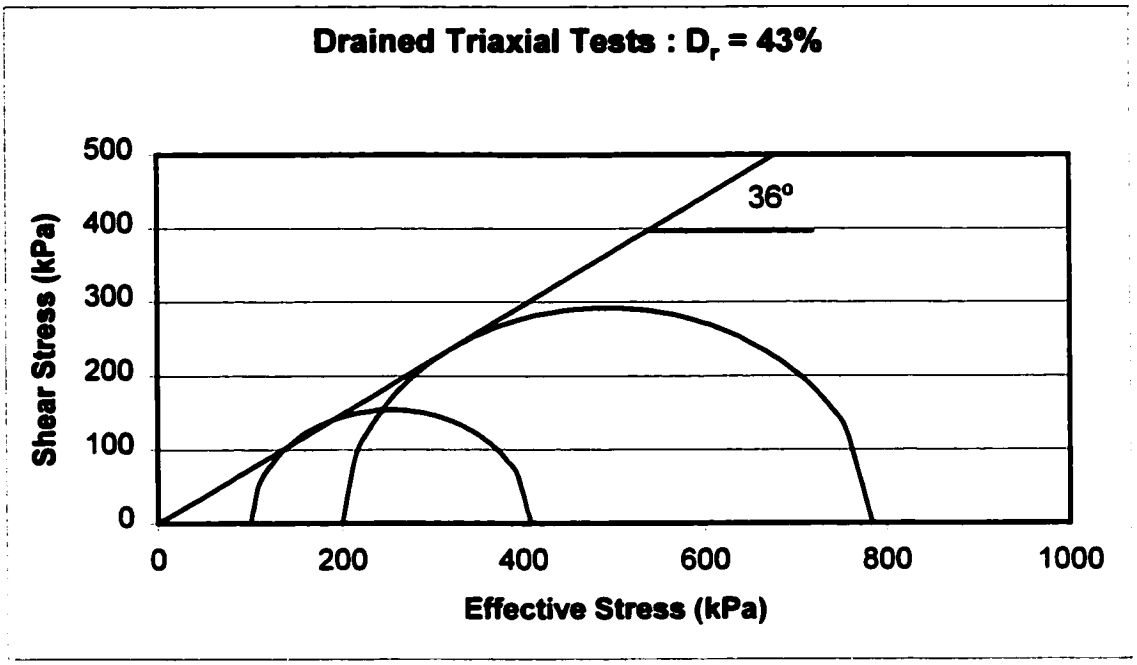

Figure 6.1: Drained Triaxial Tests Results

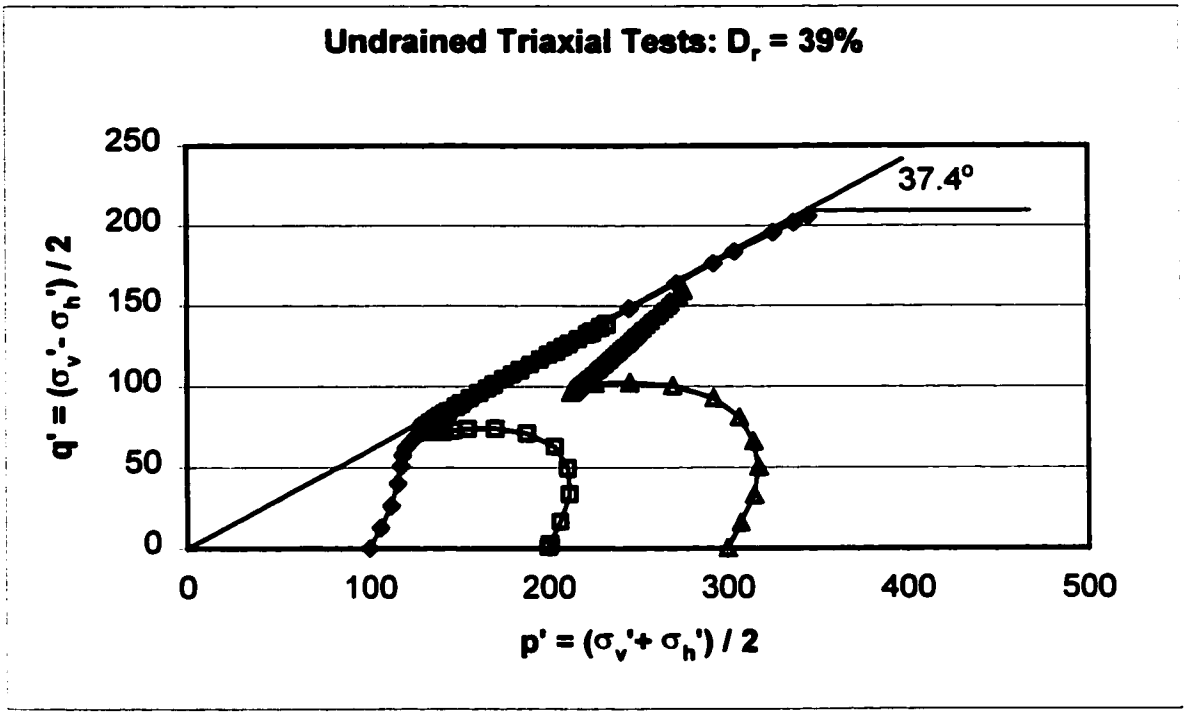

Figure 6.2: Undrained Triaxial Test Results

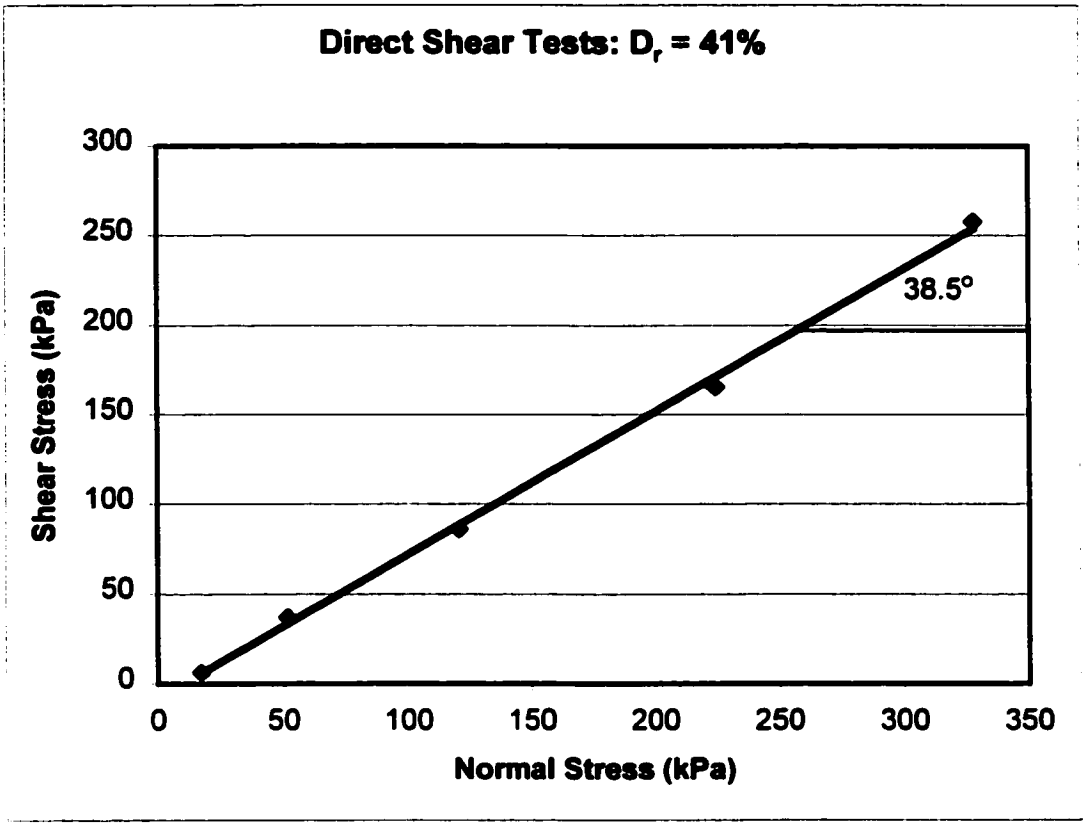

Figure 6.3: Drained Direct Shear Test Results

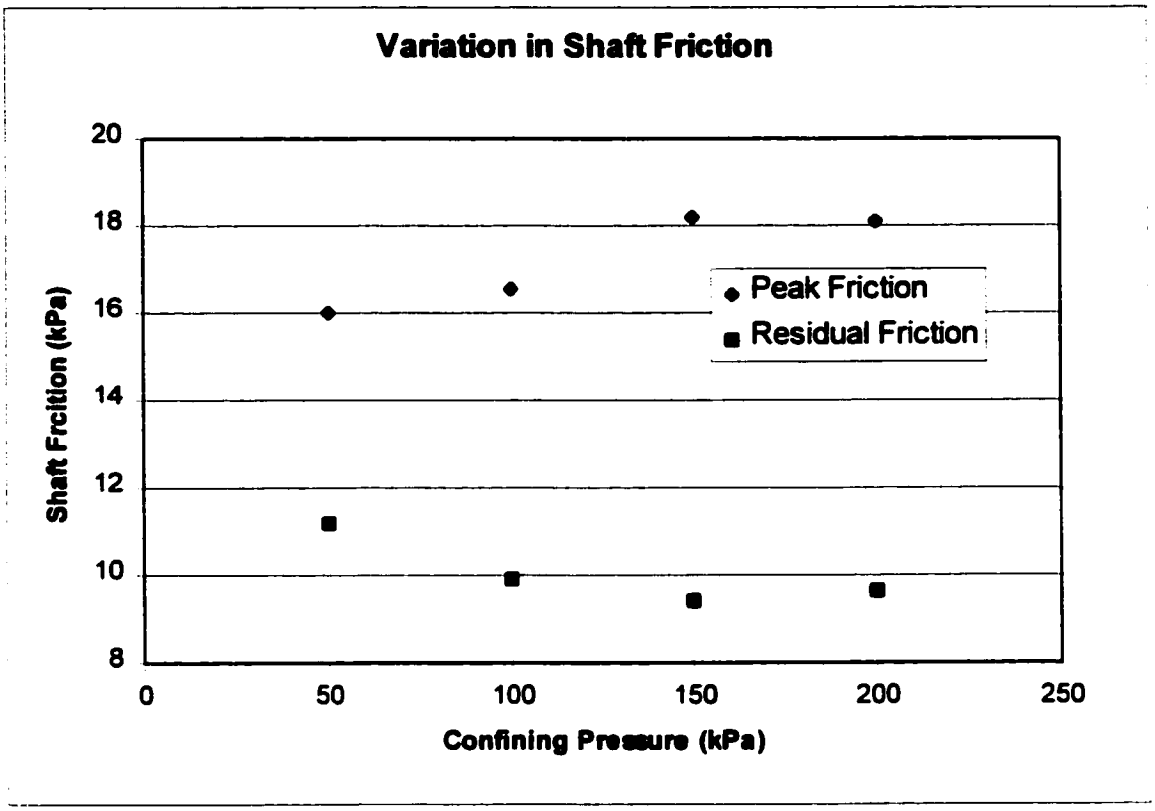

Figure 6.4: Variation in Shaft Friction

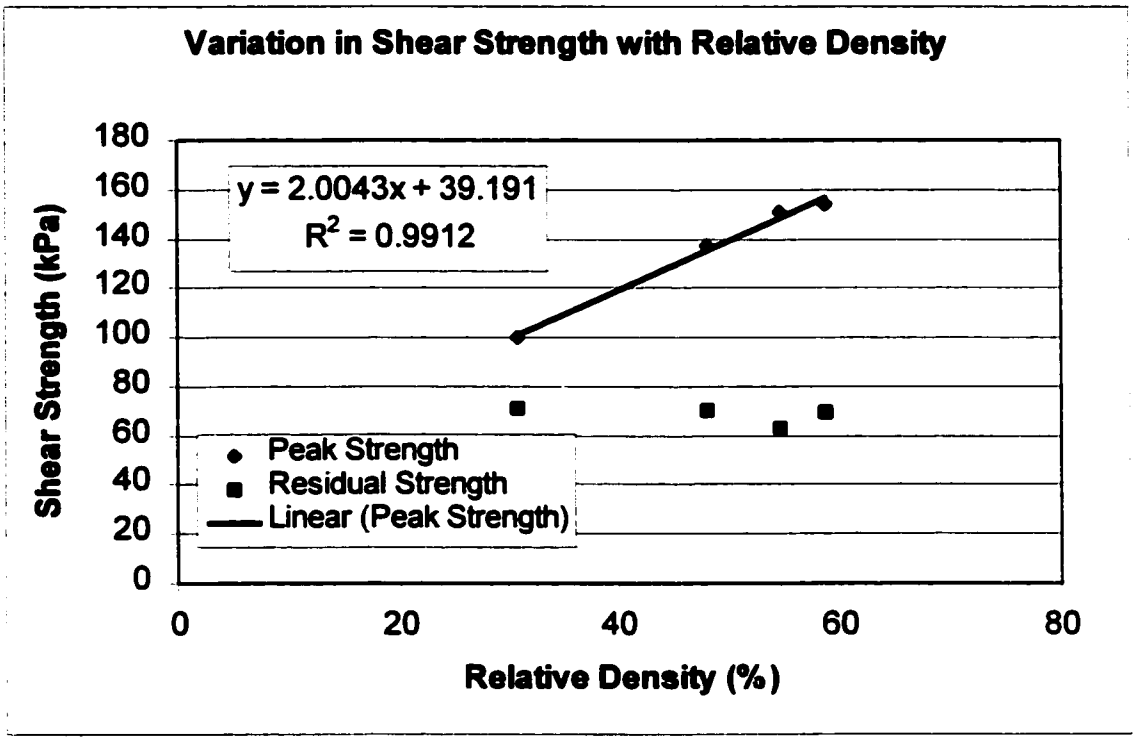

Figure 6.5: Effects of Initial Void Ratio on Drained Shear Strength Measured by the Triaxial Vane

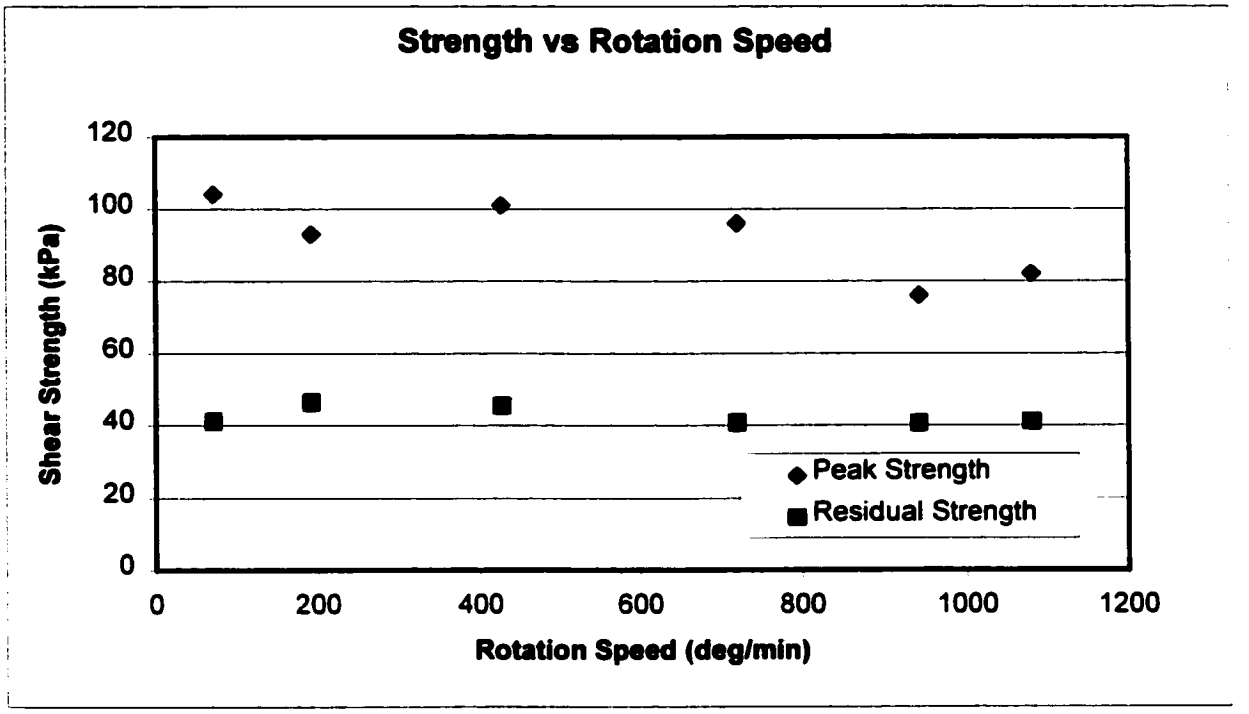

Figure 6.6: Influence of Shear Rate

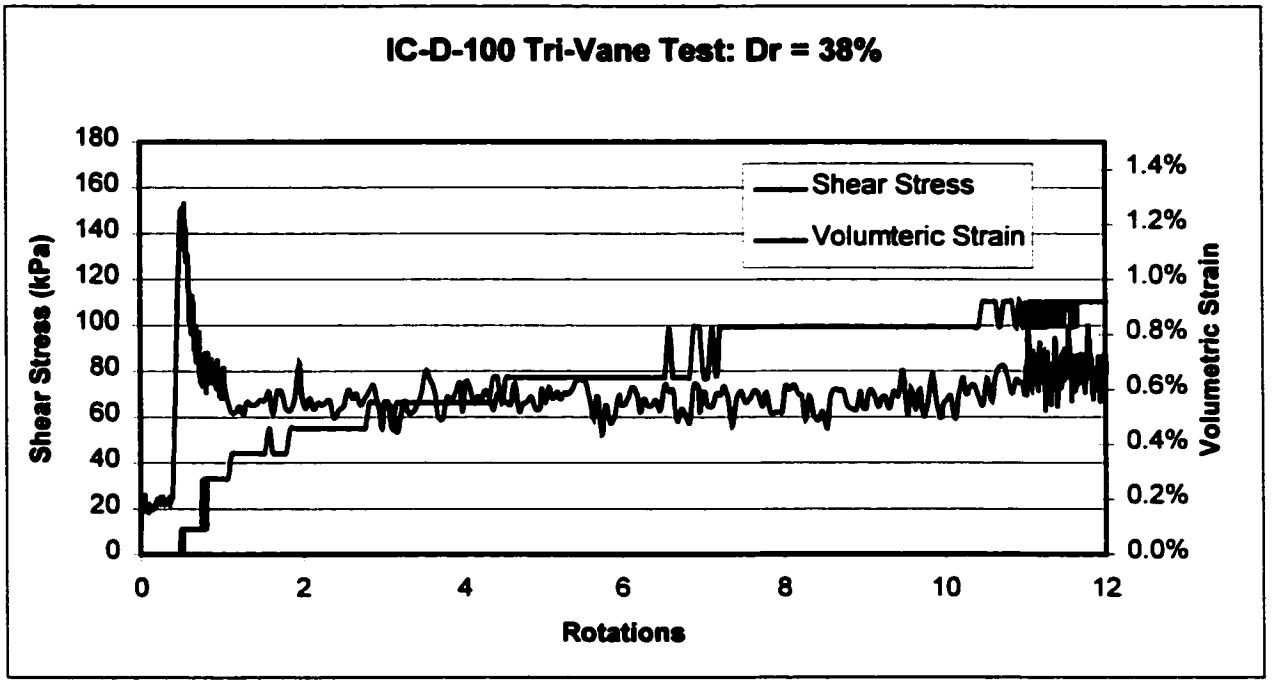

Figure 6.7: Typical IC-D Triaxial Vane test results

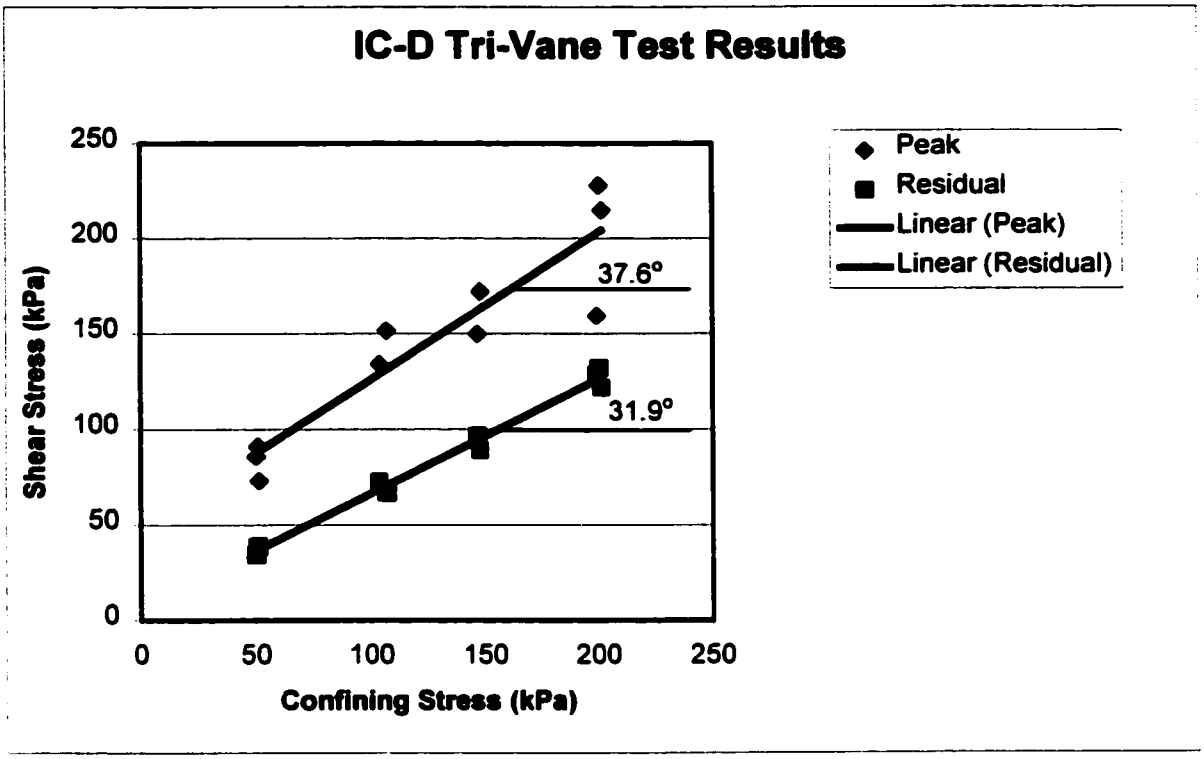

Figure 6.8: IC-D Triaxial Vane Results

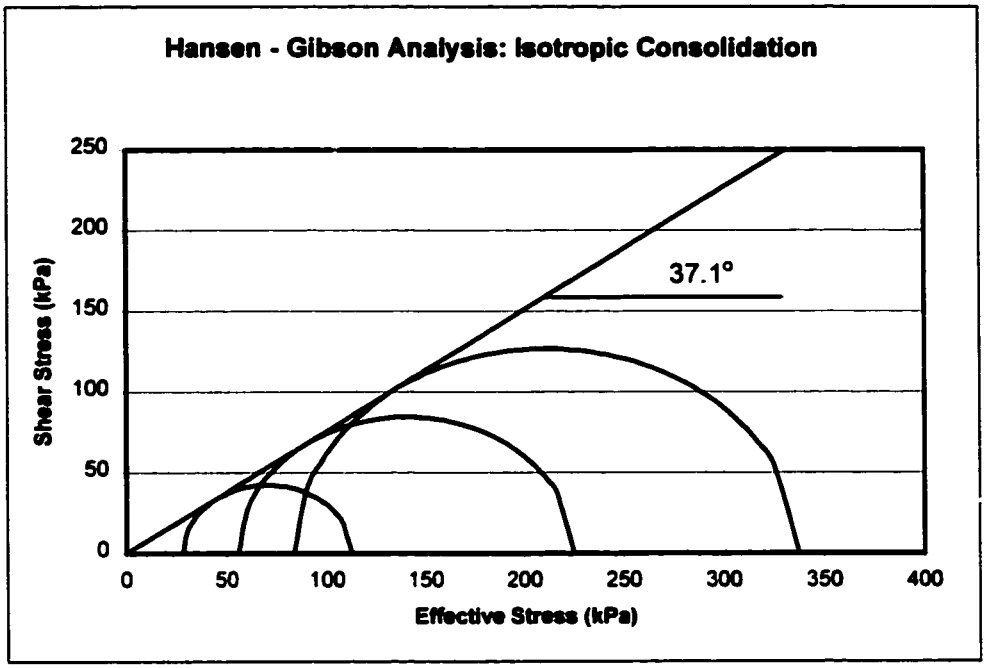

Figure 6.9: Hansen and Gibson Analysis for Isotropically Consolidated Sand

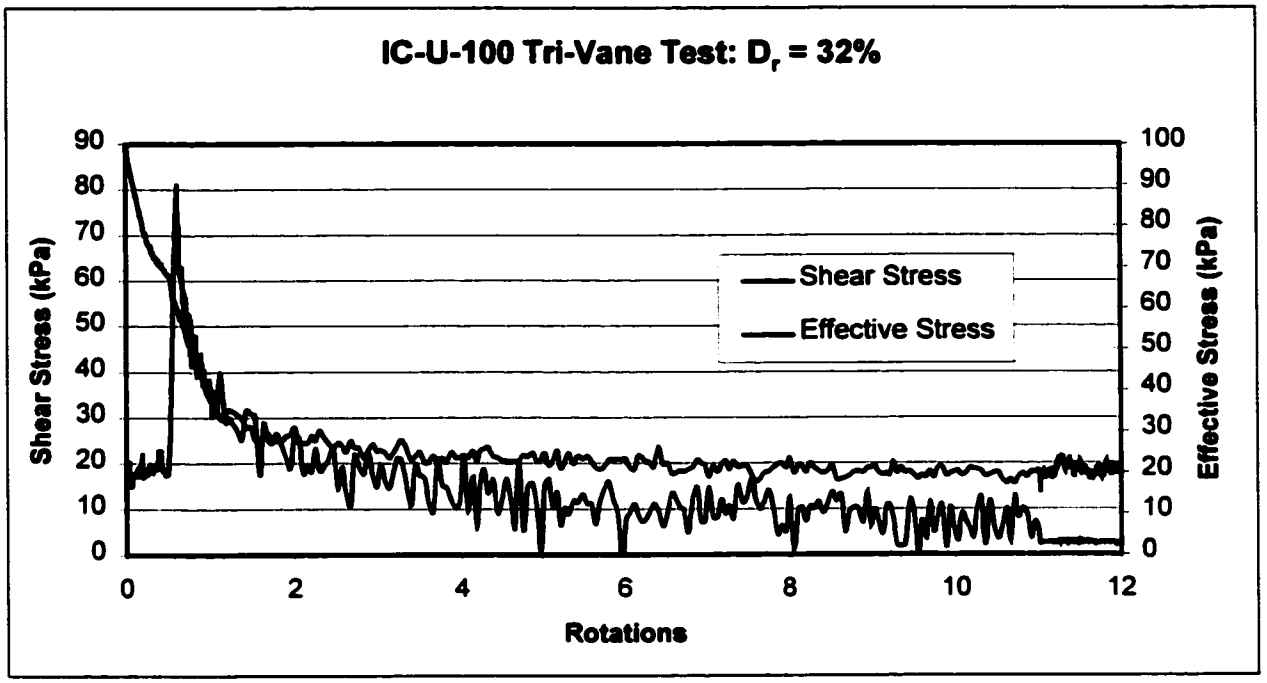

Figure 6.10: Typical IC-U Triaxial Vane test results

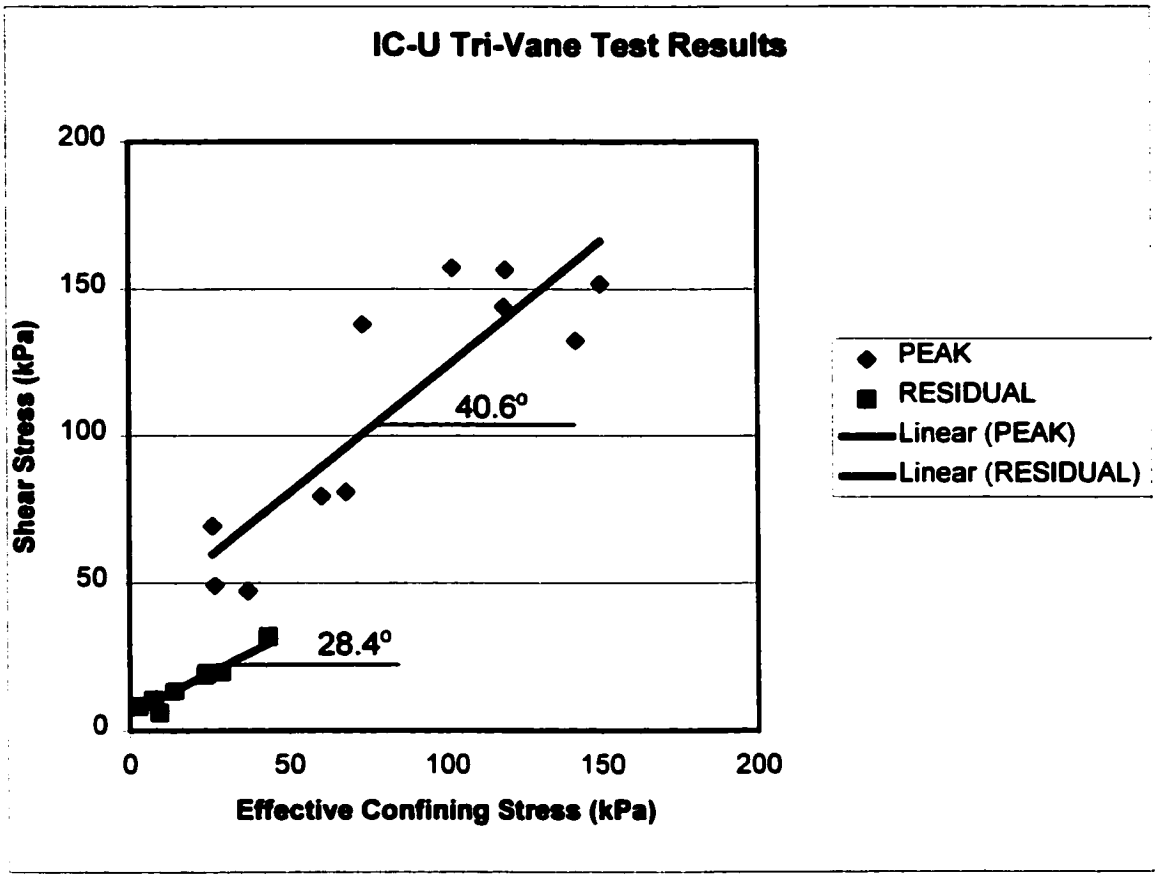

Figure 6.11: IC-U Triaxial Vane Results

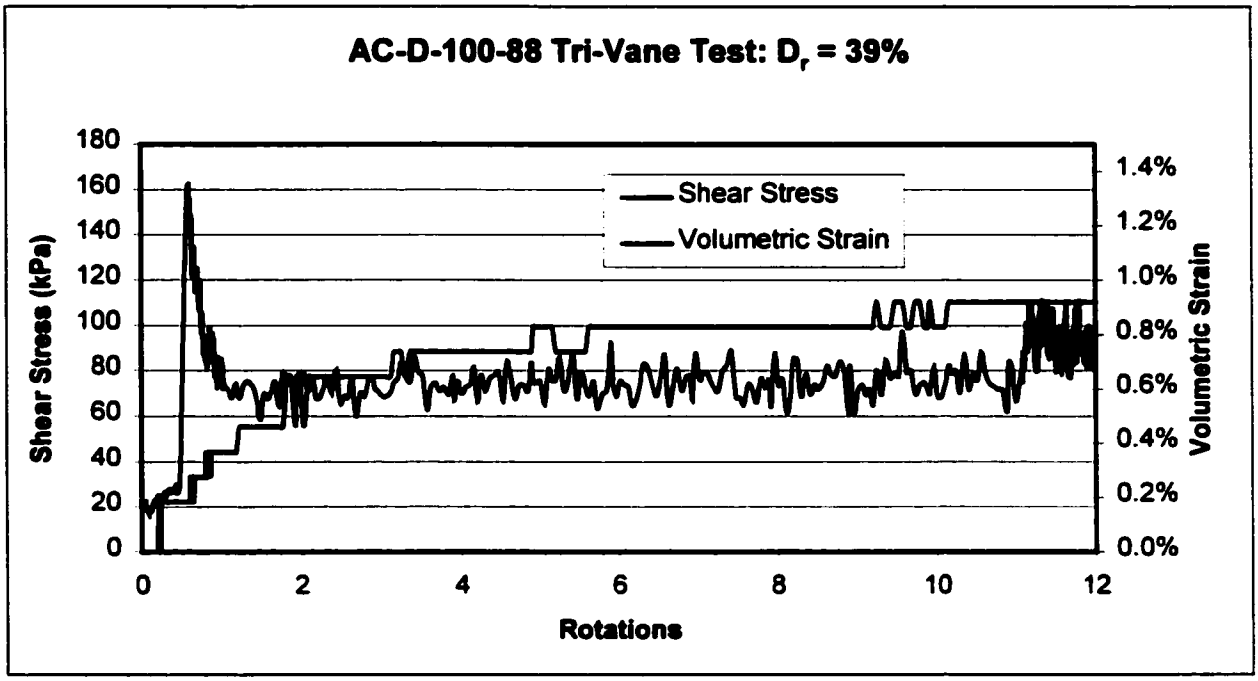

Figure 6.12: Typical AC-D Triaxial Vane test results

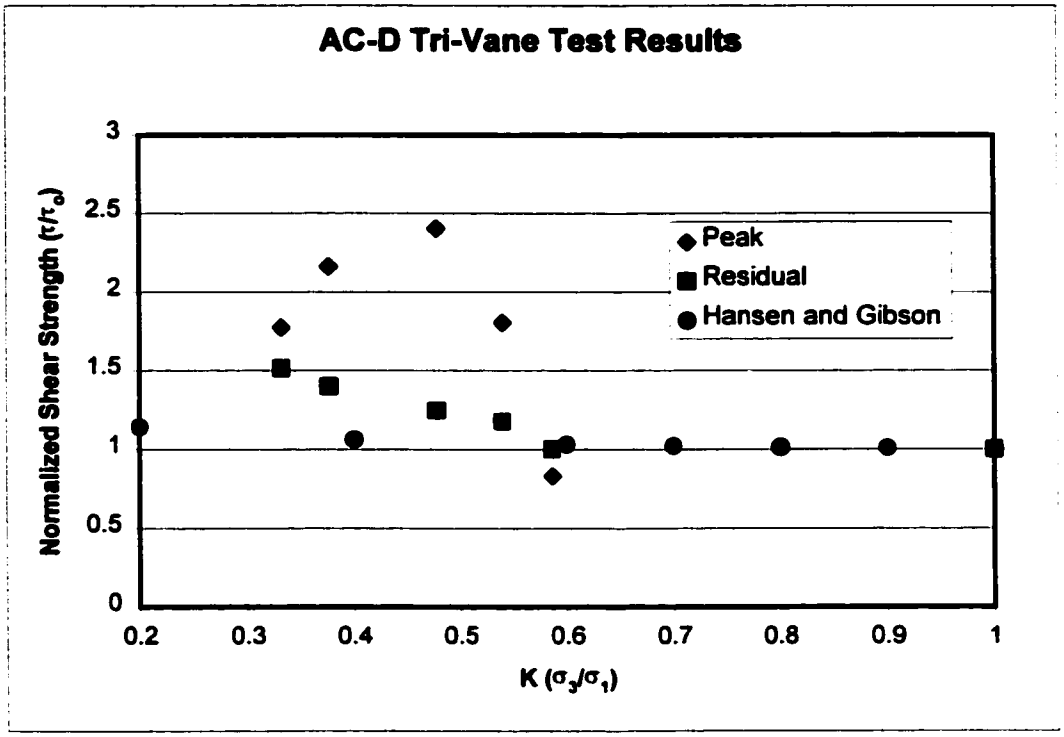

Figure 6.13: AC-D Triaxial Vane Results

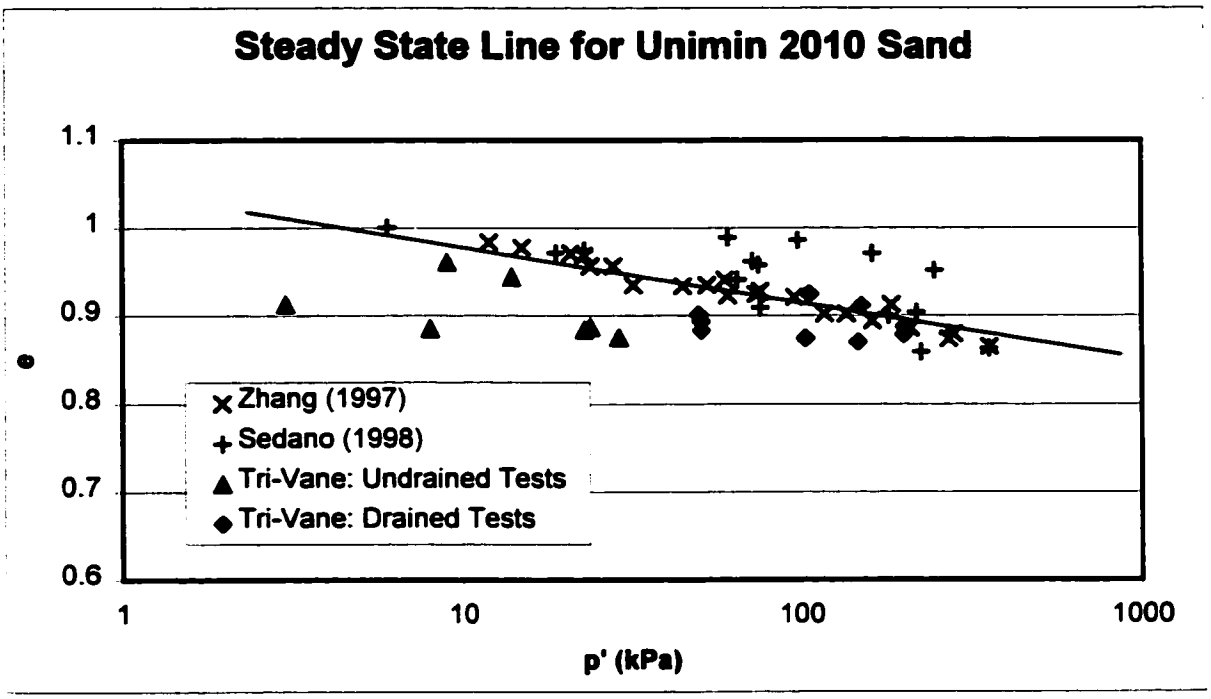

Figure 6.14: Steady State Line for Unimin 2010 Sand

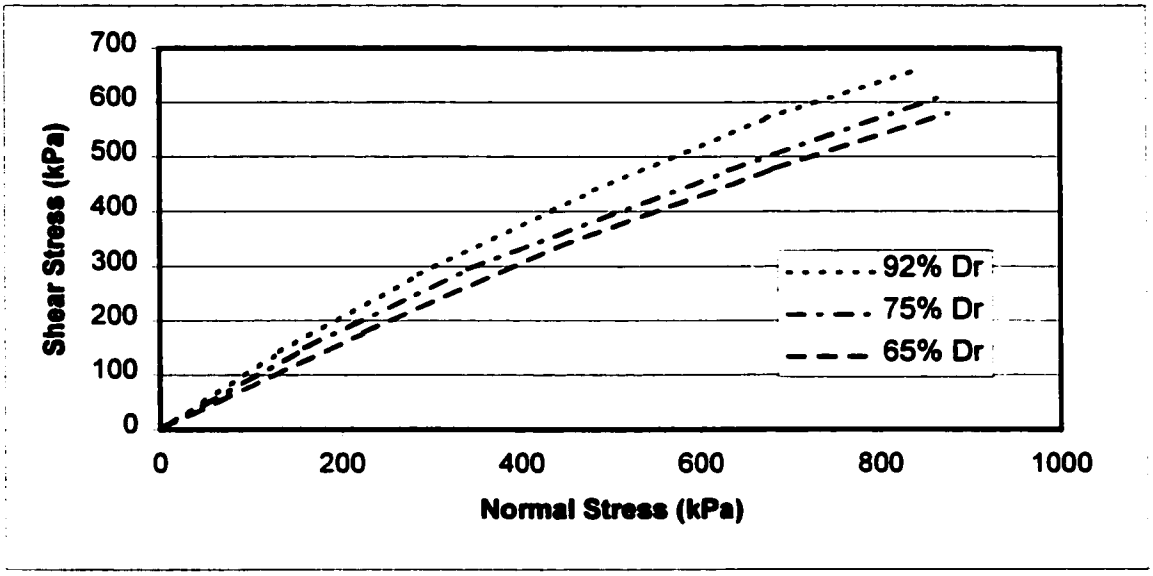

Figure 6.15: Effect of Relative Density on Shear Strength (Deschenes, 1978)

Chapter 7: Conclusions and Recommendations

7.1 Conclusions

The following conclusions may be made from the results of the tests performed:

1) The current Triaxial Vane design meets all the requirements given at the beginning of the research
2) The vane shaft friction is lower at residual strength than at peak strength in saturated sand samples
3) The initial void of saturated sand samples affects the peak strength as measured by the Triaxial Vane Apparatus but not the residual strength
4) The vane rotation rate does not affect the measured residual strength of saturated sand samples
5) The drained peak shear strength measured by the Triaxial Vane Apparatus is similar to those obtained by conventional test methods for saturated sand samples
6) The drained residual shear strength measured by the Triaxial Vane Apparatus is similar to those obtained in the triaxial test (Zhang, 1997) and the ring shear test (Sedano, 1998) for sand samples

7.2 Recommendations for Further Research

Further research on the following topics related to the Triaxial Vane Apparatus is suggested:

1) Modification of the design to allow for pore pressure measurements to be taken directly at the failure surface
2) Additional testing to investigate the shear strength of the saturated sand sample under extension loading
3) Additional investigation into the stress distribution around the vane blades

References

ASTM, (2000) D-2573-94, "*Standard Test Method for Field Vane Shear Tests in Cohesive Soil*", ASTM Standards Vol 04.08, Soil and Rock (I); pp.260-262.

ASTM, (2000) D-4648-94, "*Standard Test Method for Field Vane Shear Tests in Cohesive Soil*", ASTM Standards Vol 04.08, Soil and Rock (I); pp. 799-804.

Atkinson J.H., Jessett, J.H, (1990) "*Measurement of Relative Density of Saturated Sand Using the Piezovane*," Field Testing in Engineering Geology, Engineering Geology Special Publication 6, pp. 229-233.

Bishop, A.W., Webb, D.L. and Skinner, A.E., (1965) "*Triaxial Tests on Soil at Elevated Cell Pressures*," Proceedings of the Sixth International Conference on Soil Mechanics, Montreal, Vol 1, pp. 170-174.

Bjerrum, L. (1973) "*Problems of Soil Mechanics and Construction on Soft Clays and Structually Unstable Soils (Collapible, Expansive and Others),* " Procceding of the Eighth International Conference on Soil Mechanics and Foundation Engineering , Moscow, Session 4, Vol 3, pp111-190.

Cadling L. and Odenstad, S (1948). "*The Vane Borer*," Royal Swedish Geotechnical Institute, Proceedings No 2.

Casagrande, A., (1936) "*Characteristics of Cohesionless Soils Affecting the Stability of Earth Fills*," Contributions to Soil Mechanics 1925-1940, Boston Society of Civil Engineers, 1940, pp.257-276. (Originally published in the Journal of Boston Society of Civil Engineers, 1936)

Casagrande, A., (1938) "*The Shearing Resistance of Soils and its Relation to the Stability of Earth Dams*," Proceedings of the Soils and Foundation Conference of the U.S. Engineering Department.

Casagrande, A., (1975) "Liquefaction and Cyclic Deformations of Sand: A Critical Review," Harvard Soil Mechanics Series No 88, Harvard University, 1976. (Originally presented at the Fifth Pan-American Conference on Soil Mechanics and Foundation Engineering, 1975, Buenos Aires, Argentina)

Castro, G., (1969) "Liquefaction of Sands," Ph.D. thesis, Havard University, Cambridge, Mass. USA.

Castro, G., Poulos, S.J., (1977) "*Factors Affecting Liquefaction and Cyclic Mobilty*," Journal of Geotechnical Engineering, Vol 103, No 6, pp. 501-516.

Castro, G., Poulos, S.J., France, J.W., and Enos, J.L., (1982) "*Liquefaction Induced by Cyclic Loading*," Report to National Science Foundation, Washington D.C.

Chandler, R.J. (1988) "*The In-Situ Measurement of Undrained Shear Strength of Clays Using the Field Vane*," Vane Shear Strength Testing in Soils: Field and Laboratory Studies, ASTM STP 1014, A.F. Richards, Ed., American Society for Testing and Materials, Philadelphia, 1988, pp. 13-44.

Charlie, W.A et al, (1994) "*Liquefaction Evaluation with the CSU Piezovane*," Proceeding of the Thirteenth International Conference on Soil Mechanics and Foundation Engineering, Vol 1, pp. 197-200.

Charlie , W.A. et al, (1995) "*Estimating Liquefaction Potential of Sand Using the Piezovane*," Geotechnique, Vol 45, No 1, pp. 55-67.

Deschenes, J. (1978) "*Bearing Capacity of Footings Close to Slopes of Cohesionless Soil*", Ph.D. Thesis, University of Ottawa, Ottawa, Ontario, Canada.

Donald, I. B., Jordan, D.O., Parker, R. J., and Toh, C.T. (1977) "*The Vane Test – A Critical Appraisal*," Proceedings of the Ninth International Conference on Soil Mechanics and Foundation Engineering, Vol 1, 1977, pp. 81-88.

Hansen, J.B., Gibson, R.E., (1954) "*Undrained Shear Strength of Anisotropically Consolidated Clays*" Geotechnique, Vol 4, No 3, pp. 124-204.

Hvorslev, M.J., (1937) "*Uber die Festigkeitsiegenschaften gestorter bindiger Boden*," Ingeniorvidenskabelige Skrifter. A. No 45. Danmark Naturvid. Samfund.

Kenny, T.C., Landva, A., (1965) "*Vane-Triaxial Apparatus*", Proceeding of the Sixth International Conference on Soil Mechanics and Foundation Engineering, Vol 1, Divisions 1-2, pp. 269-272.

Khan, M.A., Garga, V.K., (1994) "A Simple Design for Hydraulic Consolidometer and Volume Gauge," Canadian Geotechnical Journal, Vol 31, No. 5, pp. 769-772.

Law, K.T., (1978) "*Triaxial Vane Tests on a Soft Marine Clay*," Canadian Geotechnical Journal, Vol 16, pp. 11-18.

Menzies, B.K., Merrifield, C.M., (1980) *Measurements of Shear Stress Distribution on the Edges of a Shear Vane Blade*," Geotechnique, Vol 30, 1980, pp. 314-318.

Munson, B.R., Young, D.F. and Okiishi, T.H., (1994) *Fundamentals of Fluid Mechanics Second Edition*, Chapter 9, John Wiley & Sons, Inc., New York.

Pamukcu, S., Suhayda, J., (1988) "Low Strain Shear Measurements Using a Triaxial Vane Device," Vane Shear Strength Testing in Soils: Field and Laboratory Studies,

ASTM STP 1014, A.F. Richards, Ed., American Society for Testing and Materials, Philadelphia, 1988, pp. 193-208.

Poulos, S.J., (1971) The Stress Strain Curves of Soils, Geotechnical Engineers Inc., Winchester, Mass, pp. 1-80.

Poulos, S.J., (1981) "*The Steady State of Deformation*," Journal of Geotechnical Engineering, Vol 107, No. 5, pp. 553-562.

Poulos, S.J., (1997) "*Comments on Laboratory Determination of Undrained Steady State Shear Strength*," National Science Foundation Workshop: Post Liquefaction Shear Strength of Granular Soils Workshop, April 17, Urbana, Illinois, USA, pp. 147-153.

Rosco, K.H., Schofield, A.N. and Wroth, C.P., (1958) "*On the Yielding of Soils*," Geotechnique, Vol 8, No. 1, pp. 22-53.

Roy, M., Leblanc, A., (1988) "*Factors Affecting the Measurments and Interpretation of the Vane Strength in Soft Sensitive Clays*" Vane Shear Strength Testing in Soils: Field and Laboratory Studies, ASTM STP 1014, A.F. Richards, Ed., American Society for Testing and Materials, Philadelphia, 1988, pp. 117-128.

Sedano, J. (1998) "*Constant Volume Ring Shear Test for Sand*", M.A.Sc. Thesis, University of Ottawa, Ottawa, Ontario, Canada.

Sharifounnasab, M., Ullrich, C.R., (1984) "*Rate of Shear Effects on Vane Shear Strength*," Journal of Geotechnical Engineering, Vol 3, No 1, pp. 135-139.

Tatsuoka, F., Ochi, K., Fujii, S., and Okamoto, M., (1986) "*Cyclic Undrained Triaxial and Torsional Shear Strength of Sands for Different Sample Preparation Methods*," Soils and Foundations, Vol 26, No 3, pp. 23-41.

Tatsuko, F., Sakamoto, M., Kawamura, T., and Fukushima, S., (1986) "*Strength and Deformation Characteristics of Sand in Plane Strain Compression at Extremely Low Pressures*," Soils and Foundations, Vol 26, No 1, pp. 65-84.

Taylor, D.W., (1948) Fundamentals of Soil Mechanics, Chapter 14. John Wiley and Sons Inc, New York.

Torstensson, B.A., (1977) "*Time Dependent Effects in the Field Vane Test*," International Symposium on Soft Clay, 1977, pp. 387-397.

Vaid, Y.P, (1988) "Preparation of Reconstituted Sand Specimens," Advanced Triaxial Testing of Soil and Rock, ASTM STP 977, American Society for Testing and Materials, Philadelphia, 1988, pp. 405-417.

Weisel, C.E., (1973) "*Some Factors Influencing In Situ Vane Results*" Procceding of the Eighth International Conference on Soil Mechanics and Foundation Engineering , Moscow, Vol 1.2, pp 475-479

Wilson, N.E., (1963) "*Laboratory Vane Shear Tests and the Influence of Pore Water Stresses*," Laboratory Shear Testing of Soils, ASTM STP 361, American Society for Testing and Materials, Philadelphia, 1963, pp.377-385.

Wroth, C.P., (1984) "*The Interpretation in In-Situ Soil Tests*", Geotechnique, Vol 34, No 4, pp. 449-489.

Zhang, H. (1997) "*Steady State Behaviour of Sands and Limitations of the Triaxial Test*", Ph.D. Thesis, University of Ottawa, Ottawa, Ontario, Canada.

Appendix 1: Calibration

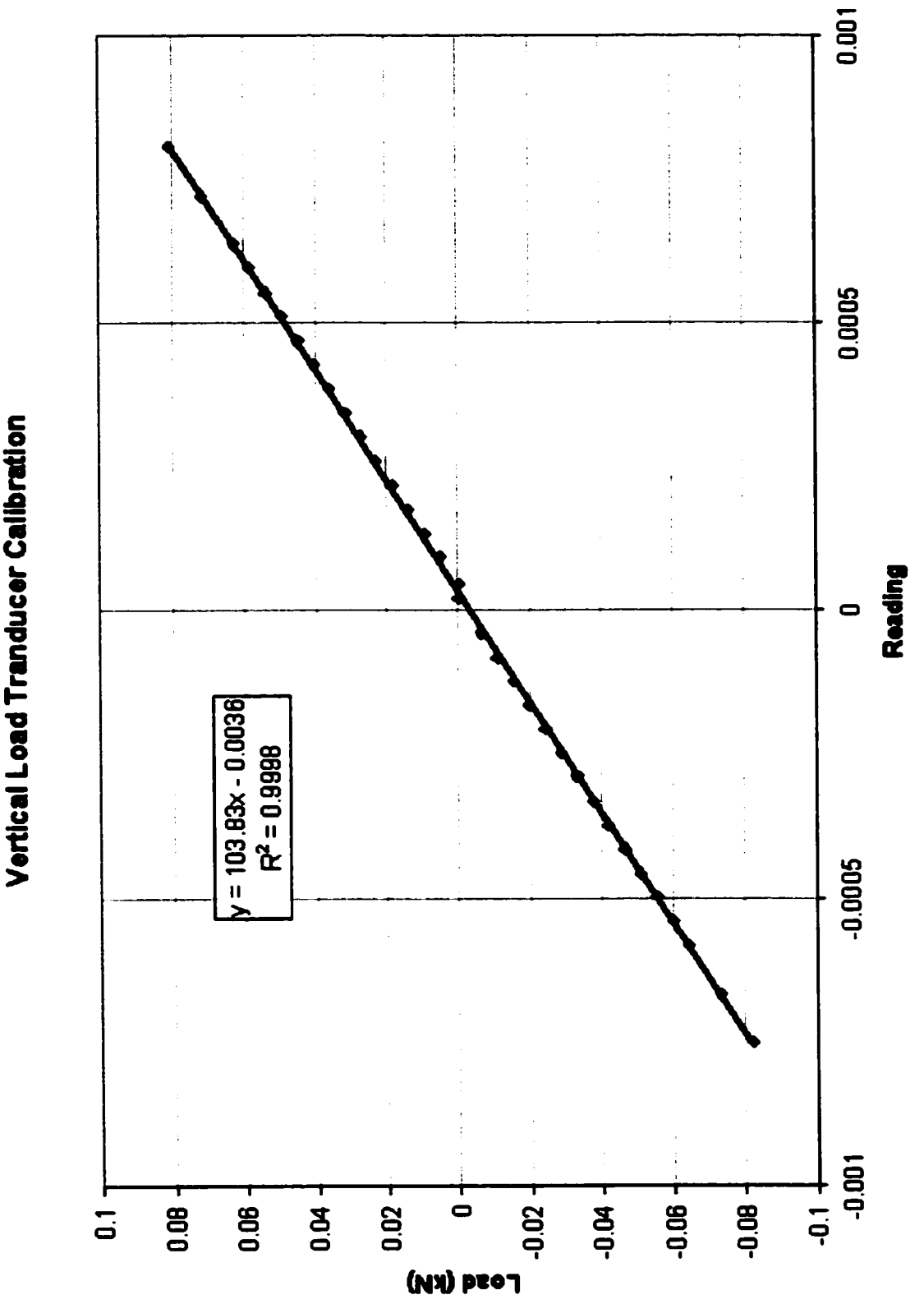
Vertical Load Tranducer Calibration
y = 103.83x - 0.0038
R² = 0.9988
Load (kN)
Reading
0.1
0.08
0.06
0.04
0.02
0
-0.02
-0.04
-0.06
-0.08
-0.1
-0.001
-0.0005
0
0.0005
0.001

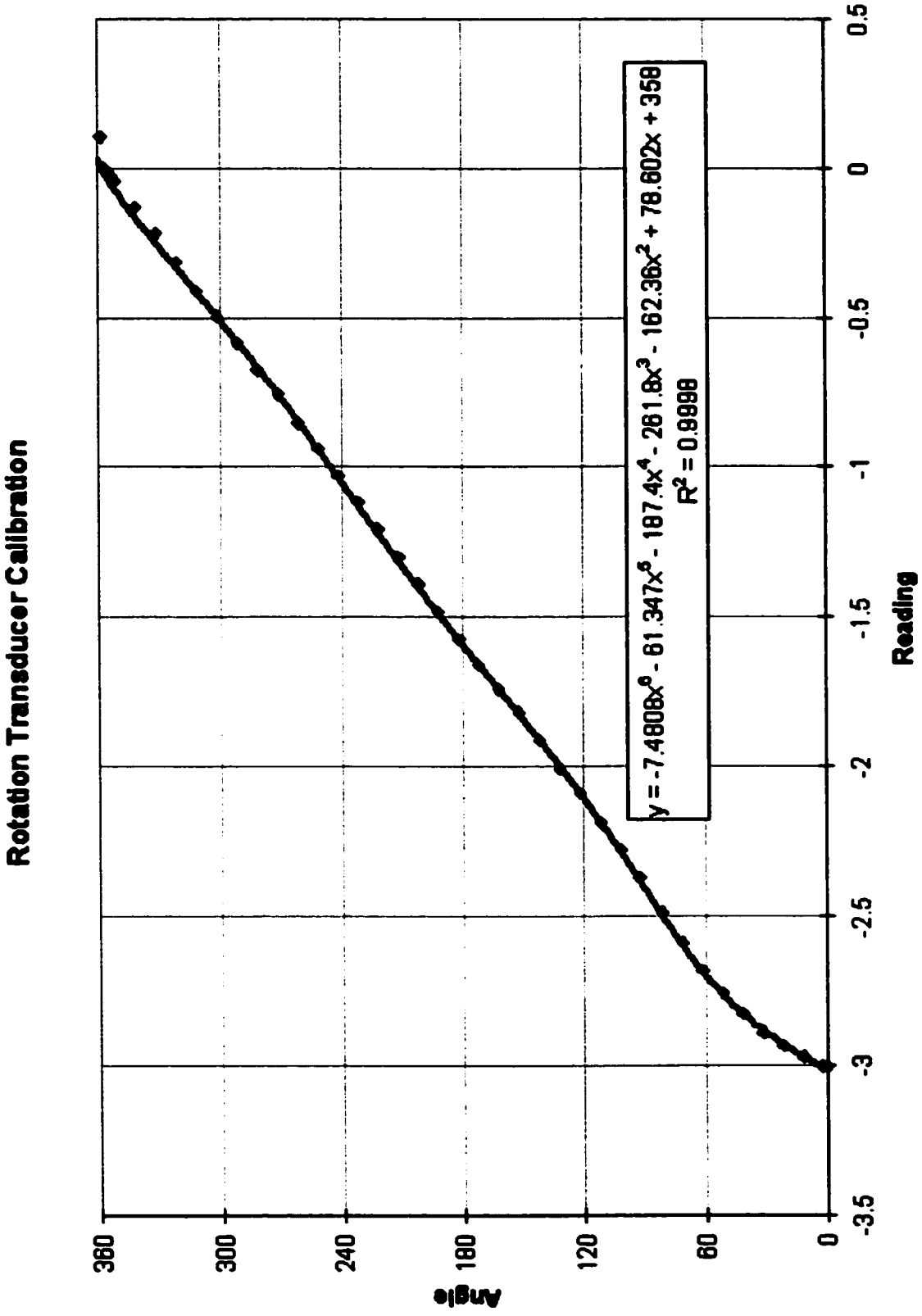
Rotation Transducer Calibration
Angle
Reading
360
300
240
180
120
60
0
0.5
0
-0.5
-1
-1.5
-2
-2.5
-3
-3.5
y = -7.4808x⁶ - 81.347x⁵ - 187.4x⁴ - 261.8x³ - 162.36x² + 78.602x + 358
R² = 0.9998

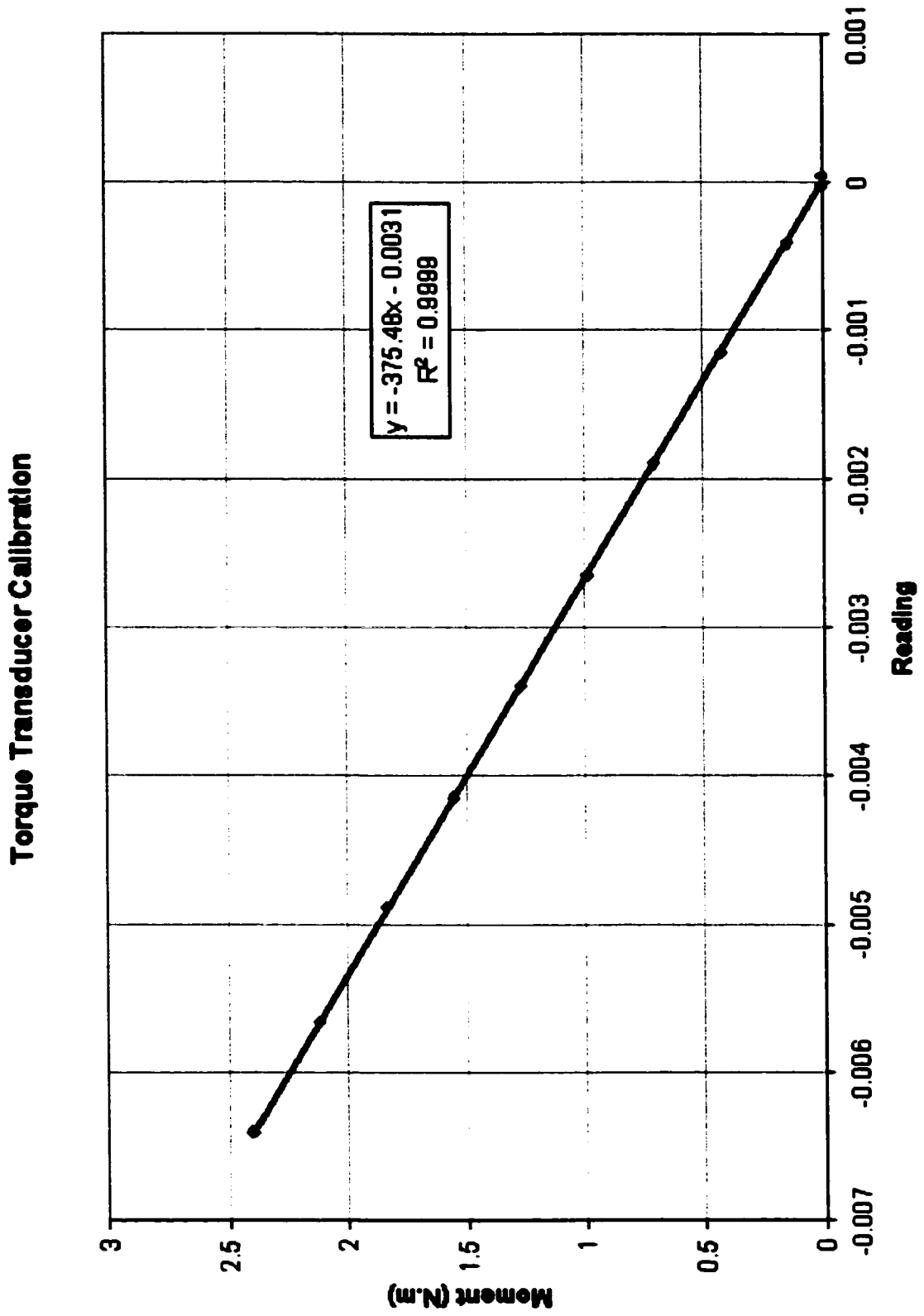
Torque Transducer Calibration
y = -375.48x - 0.0031
R² = 0.9999
Moment (N.m)
Reading
3
2.5
2
1.5
1
0.5
0
-0.007
-0.006
-0.005
-0.004
-0.003
-0.002
-0.001
0
0.001

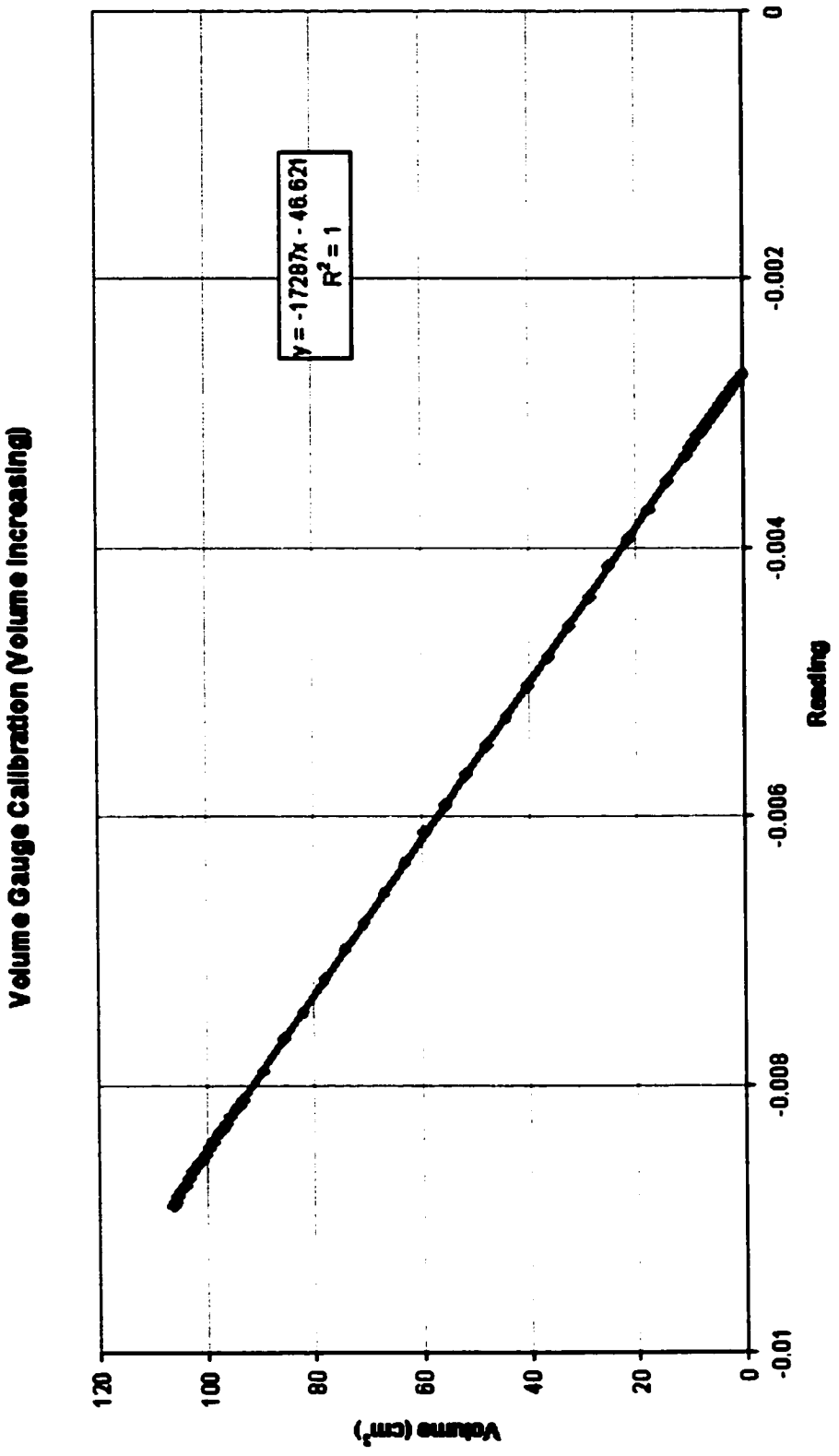
Volume Gauge Calibration (Volume Increasing)
y = -17287x - 46.621
R² = 1
Volume (cm³)
Reading
120
100
80
60
40
20
0
-0.01
-0.008
-0.006
-0.004
-0.002
0

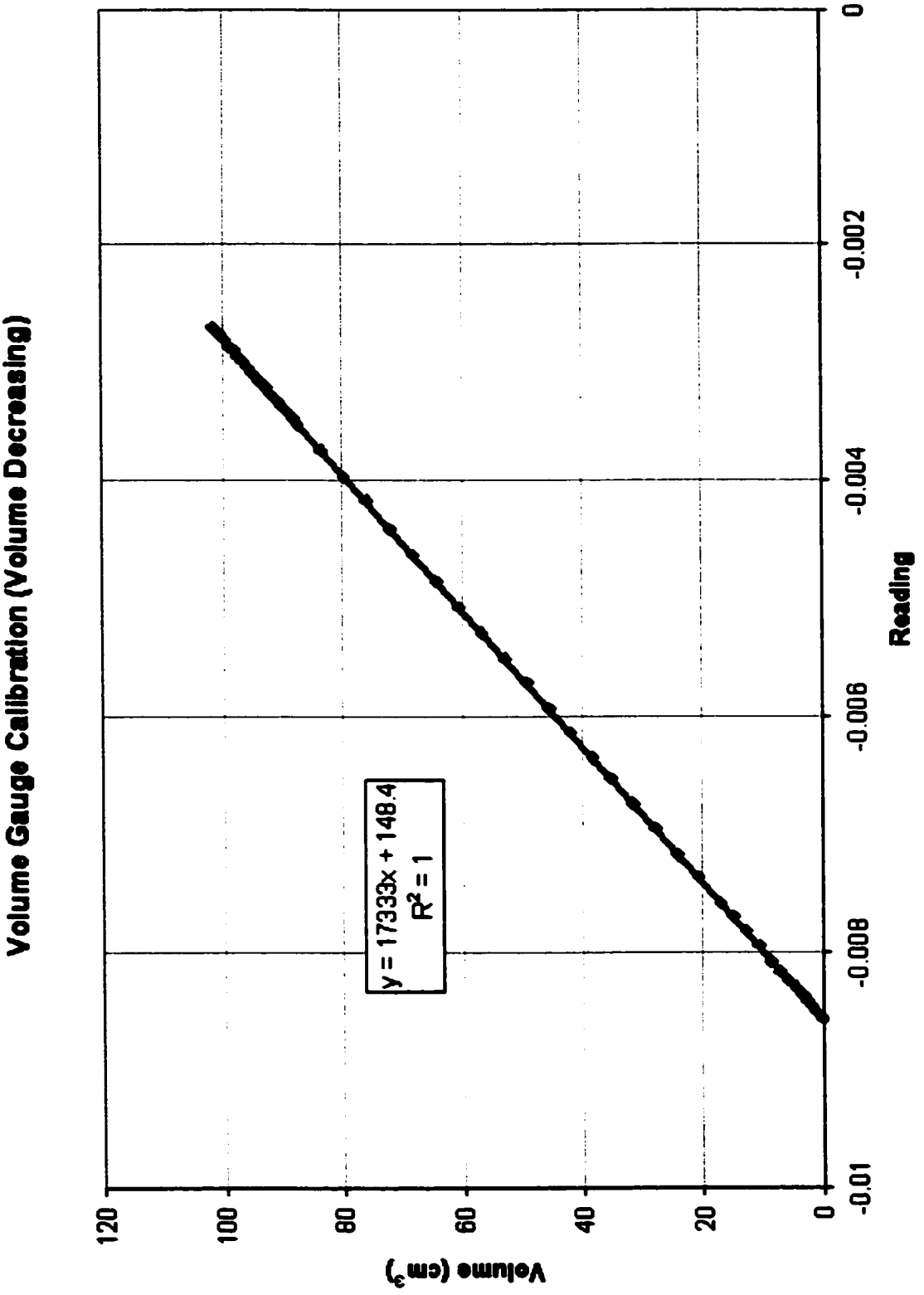
Volume Gauge Calibration (Volume Decreasing)
y = 17333x + 148.4
R² = 1
Volume (cm³)
Reading
120
100
80
60
40
20
0
-0.01
-0.008
-0.006
-0.004
-0.002
0

Appendix 2: Conventional Tests

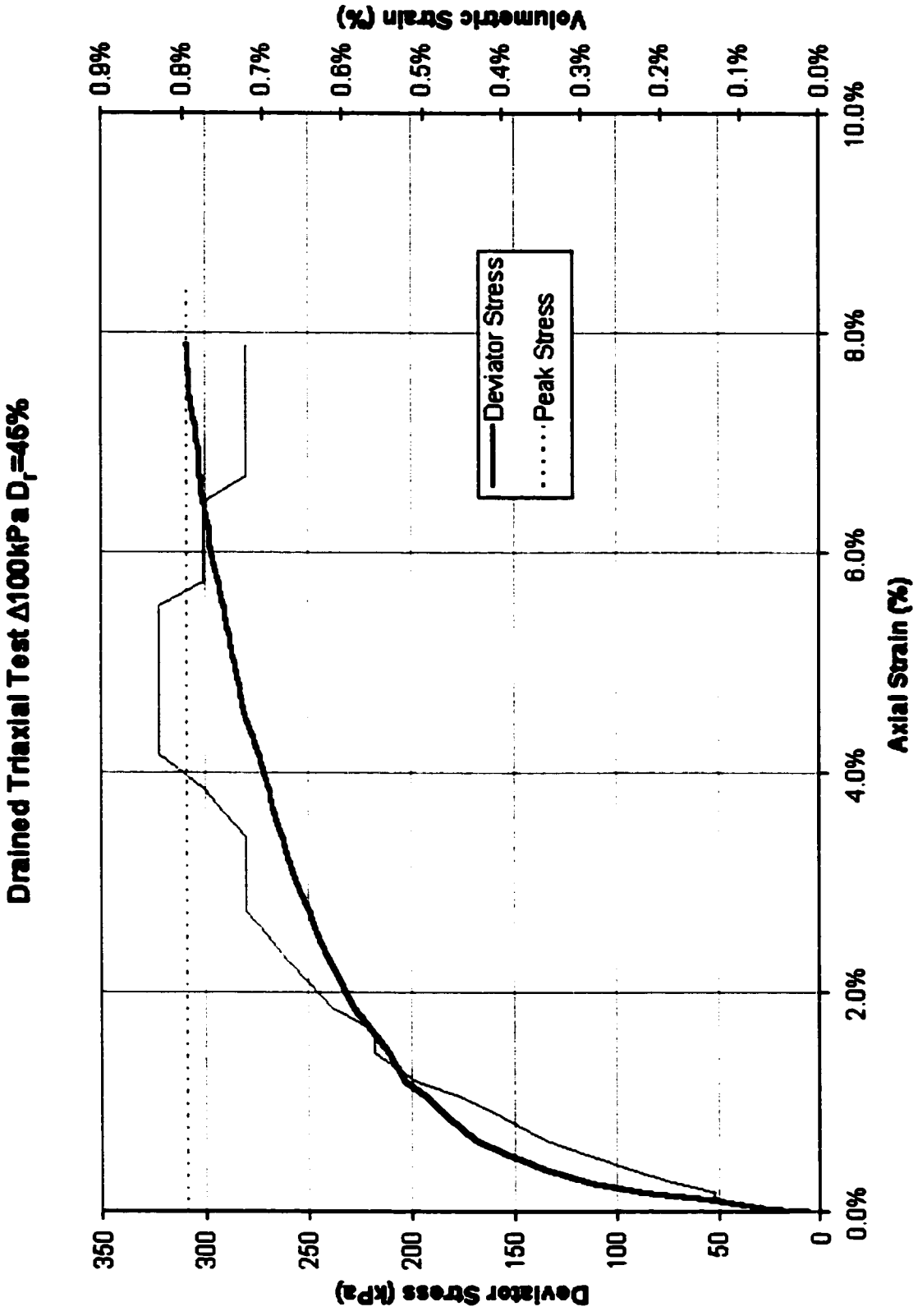
Drained Triaxial Test Δ100kPa D_r=46%
Deviator Stress (kPa)
Volumetric Strain (%)
Axial Strain (%)
Deviator Stress
Peak Stress
0
50
100
150
200
250
300
350
0.0%
0.1%
0.2%
0.3%
0.4%
0.5%
0.6%
0.7%
0.8%
0.9%
0.0%
2.0%
4.0%
6.0%
8.0%
10.0%

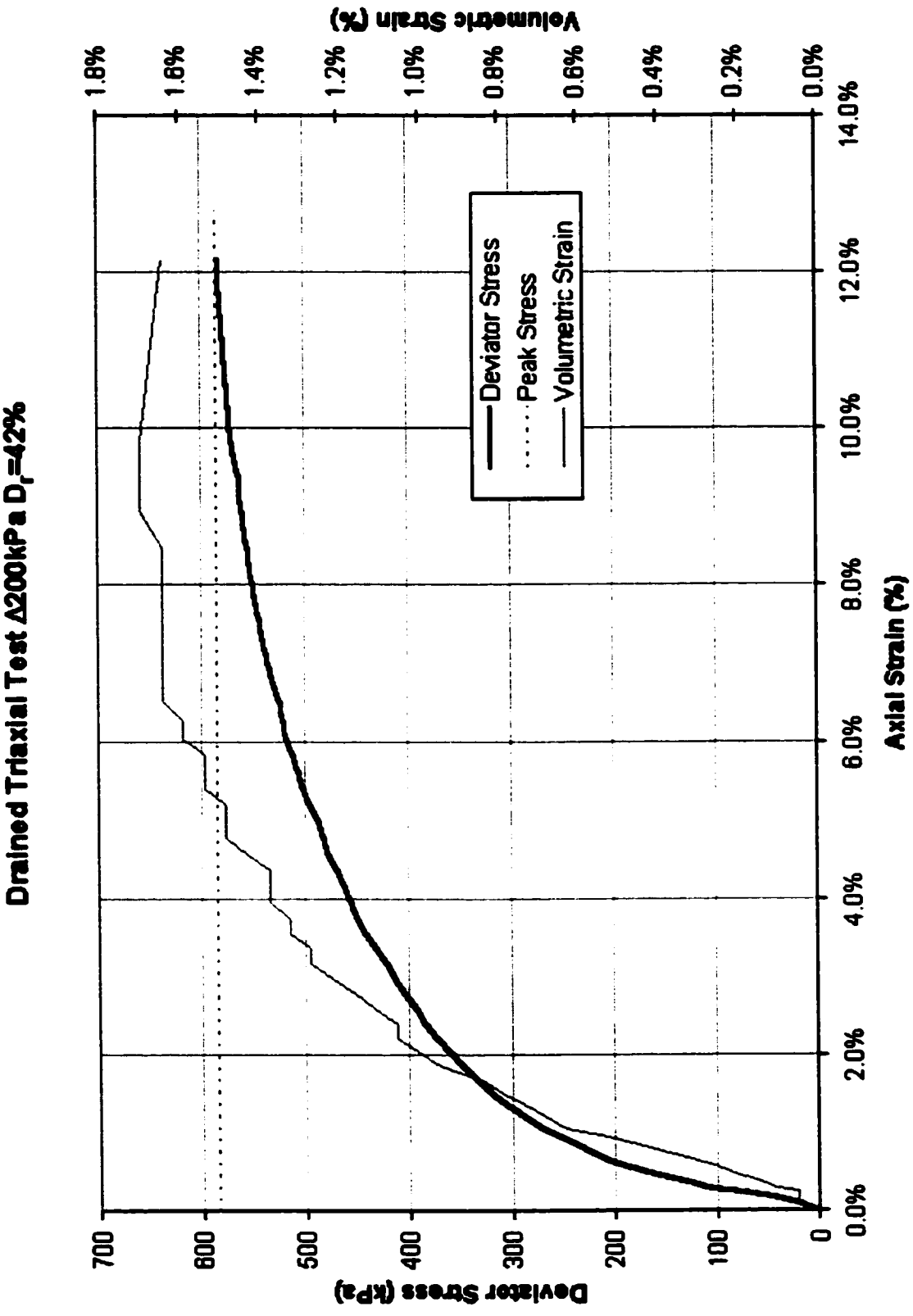
Drained Triaxial Test Δ200kPa D_r=42%
Deviator Stress (kPa)
Volumetric Strain (%)
Axial Strain (%)
Deviator Stress
Peak Stress
Volumetric Strain
0
100
200
300
400
500
600
700
0.0%
0.2%
0.4%
0.6%
0.8%
1.0%
1.2%
1.4%
1.6%
1.8%
0.0%
2.0%
4.0%
6.0%
8.0%
10.0%
12.0%
14.0%

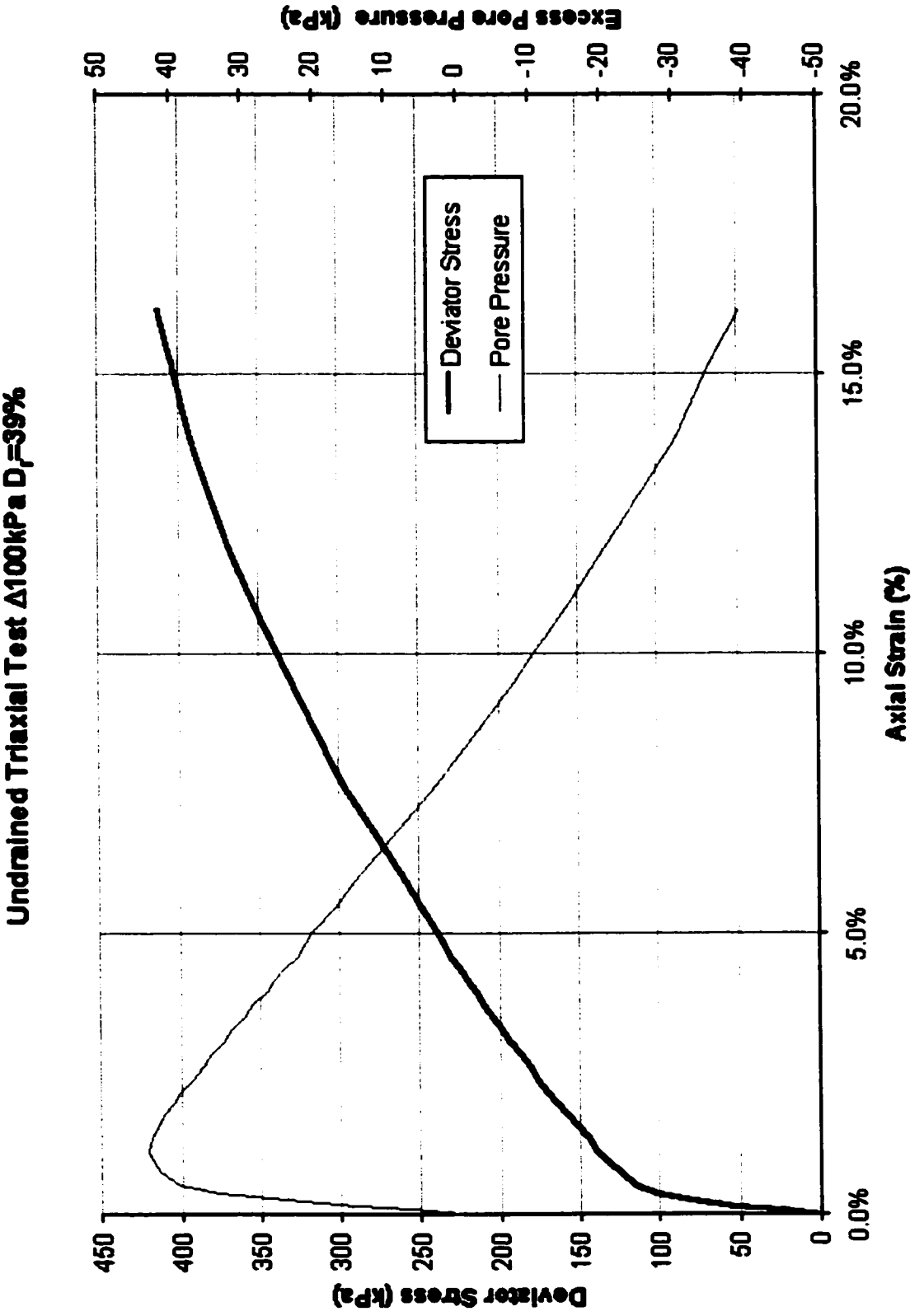
Undrained Triaxial Test Δ100kPa D_r=39%
Deviator Stress (kPa)
Excess Pore Pressure (kPa)
Axial Strain (%)
Deviator Stress
Pore Pressure
450
400
350
300
250
200
150
100
50
0
50
40
30
20
10
0
-10
-20
-30
-40
-50
0.0%
5.0%
10.0%
15.0%
20.0%

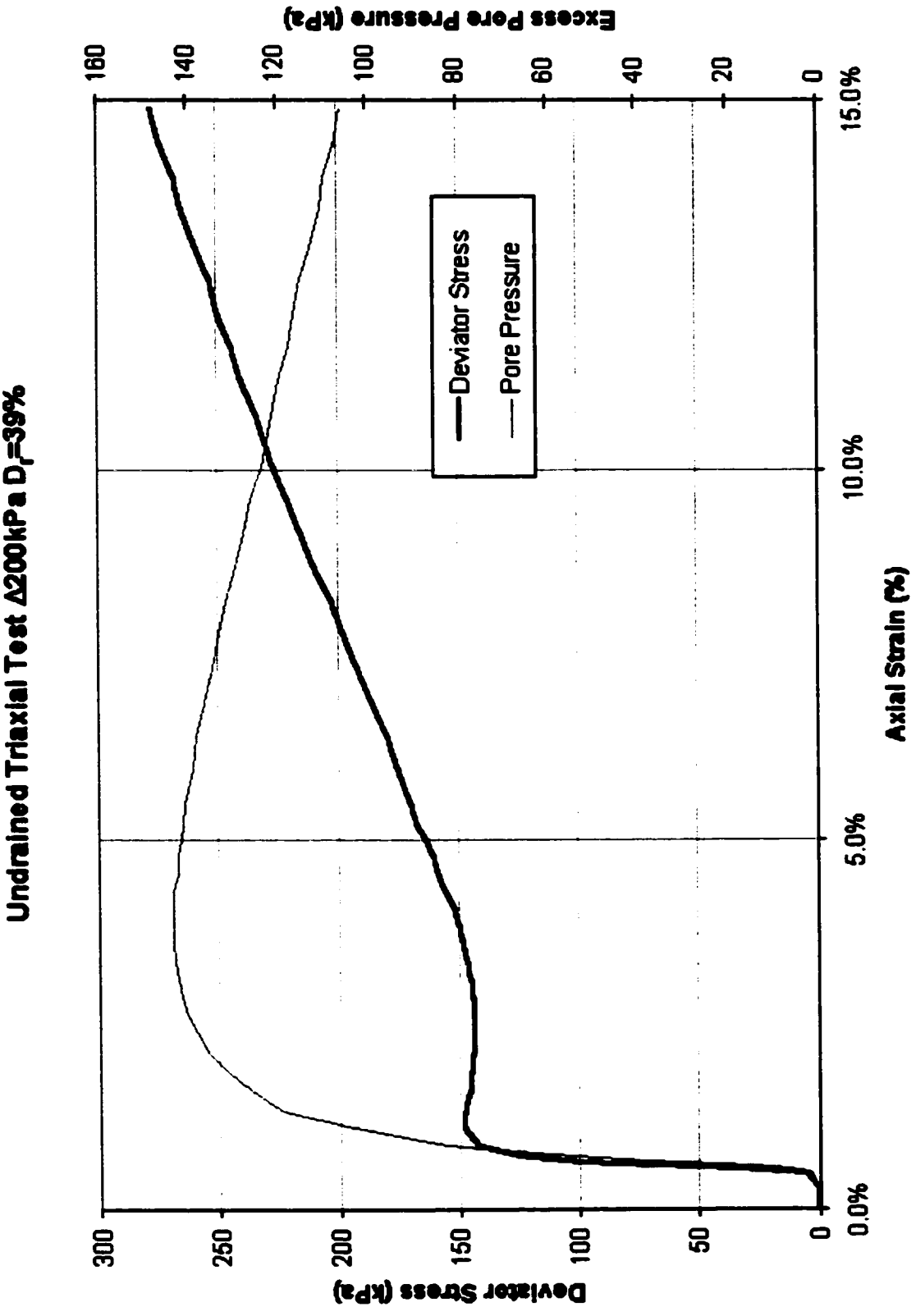
Undrained Triaxial Test Δ200kPa D_r=39%
Deviator Stress (kPa)
Excess Pore Pressure (kPa)
Axial Strain (%)
Deviator Stress
Pore Pressure
0
50
100
150
200
250
300
0
20
40
60
80
100
120
140
160
0.0%
5.0%
10.0%
15.0%

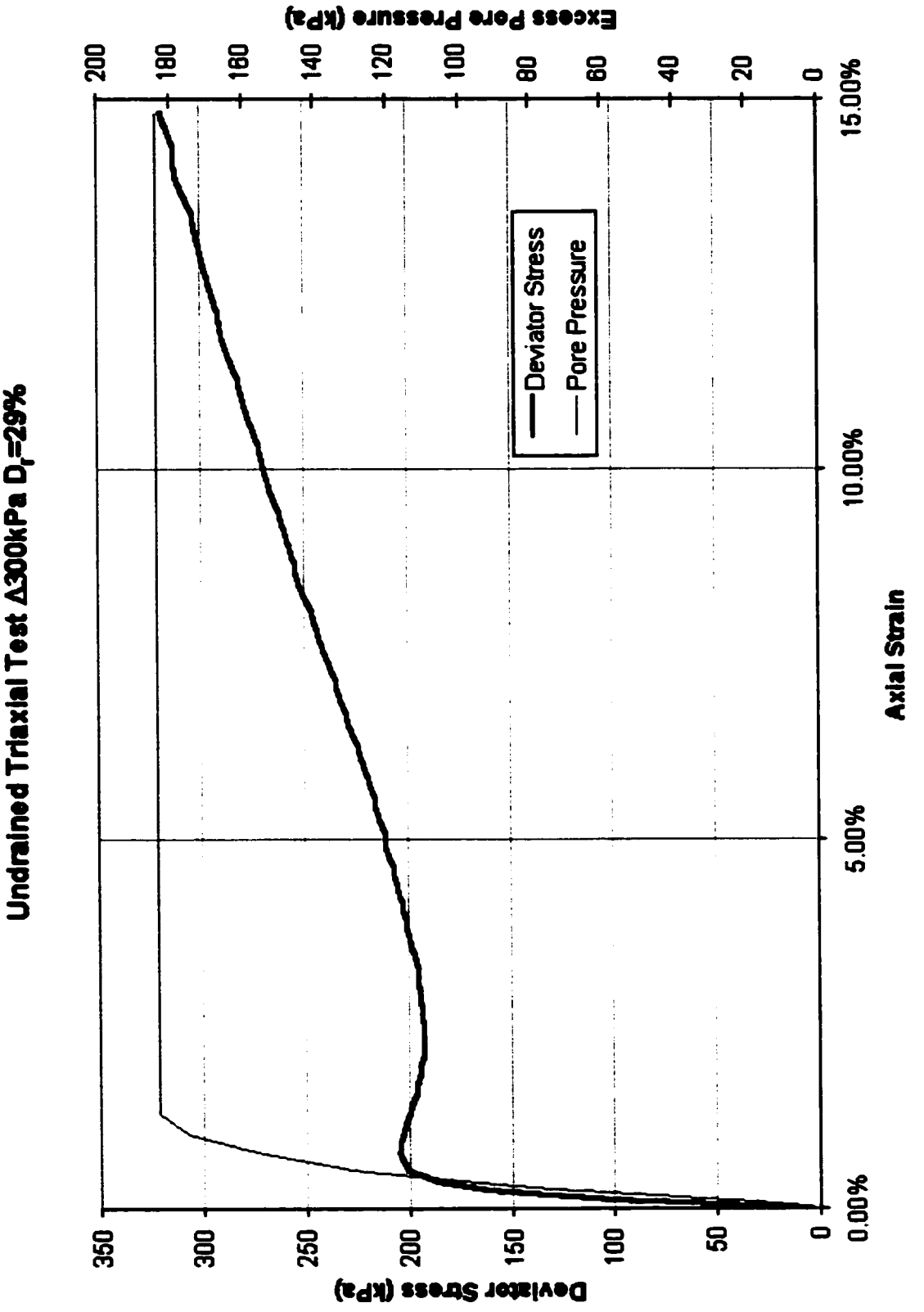
Undrained Triaxial Test Δ300kPa D_r=29%
Deviator Stress (kPa)
Excess Pore Pressure (kPa)
Axial Strain
Deviator Stress
Pore Pressure
350
300
250
200
150
100
50
0
200
180
160
140
120
100
80
60
40
20
0
0.00%
5.00%
10.00%
15.00%

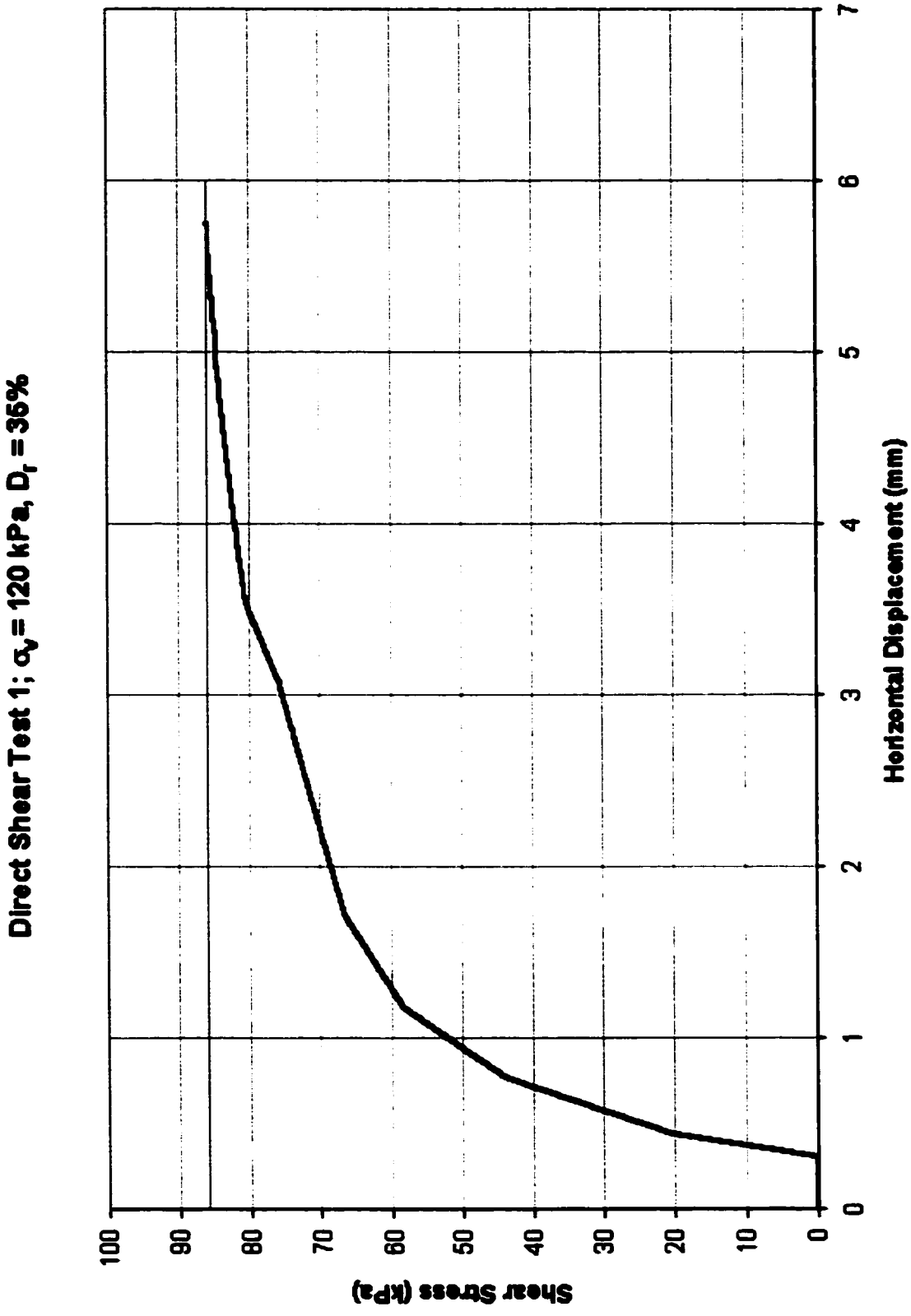
Direct Shear Test 1; σ_v = 120 kPa, D_r = 35%
Shear Stress (kPa)
0
10
20
30
40
50
60
70
80
90
100
Horizontal Displacement (mm)
0
1
2
3
4
5
6
7

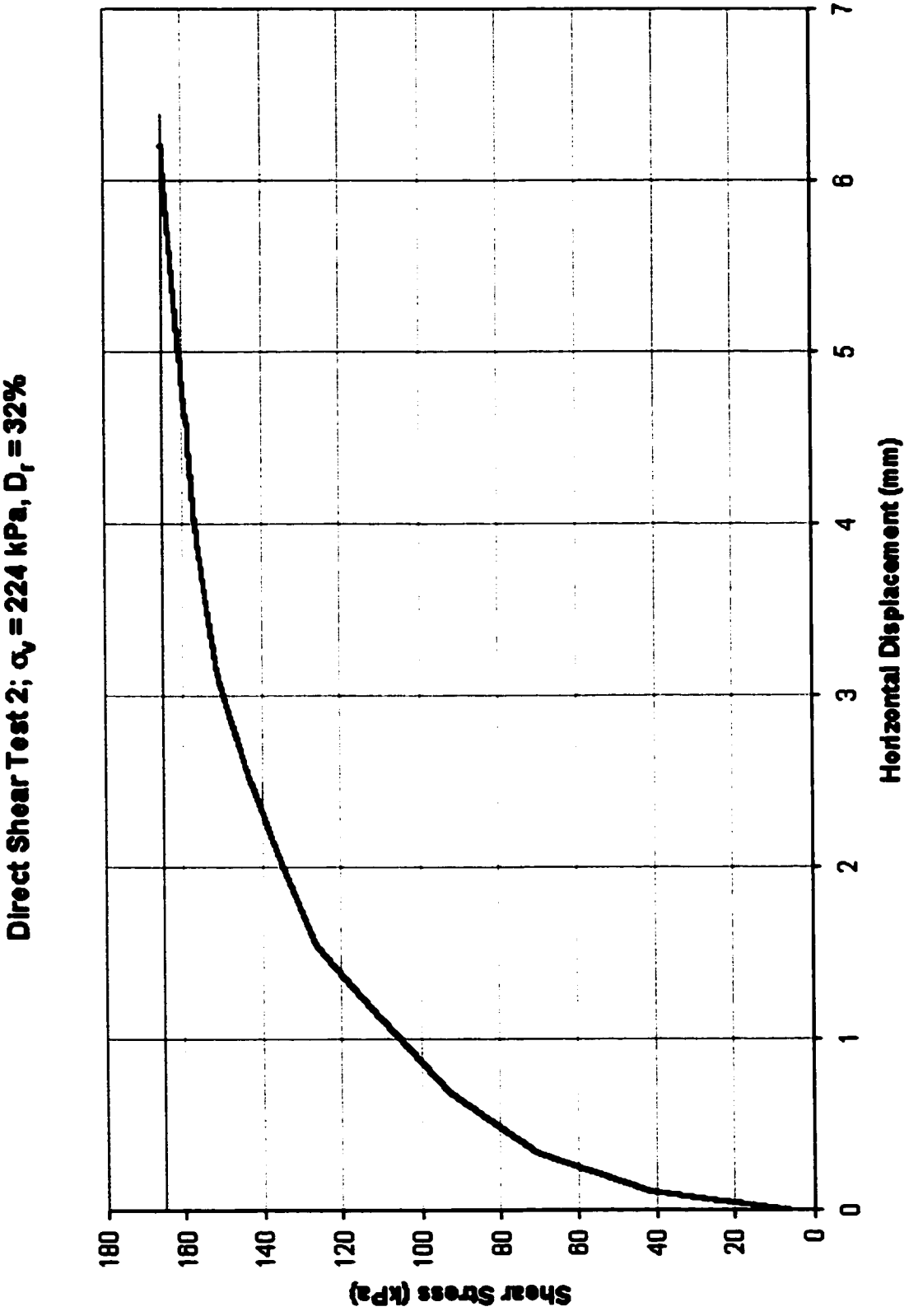
Direct Shear Test 2; σ_v = 224 kPa, D_r = 32%
Shear Stress (kPa)
0
20
40
60
80
100
120
140
160
180
Horizontal Displacement (mm)
0
1
2
3
4
5
6
7

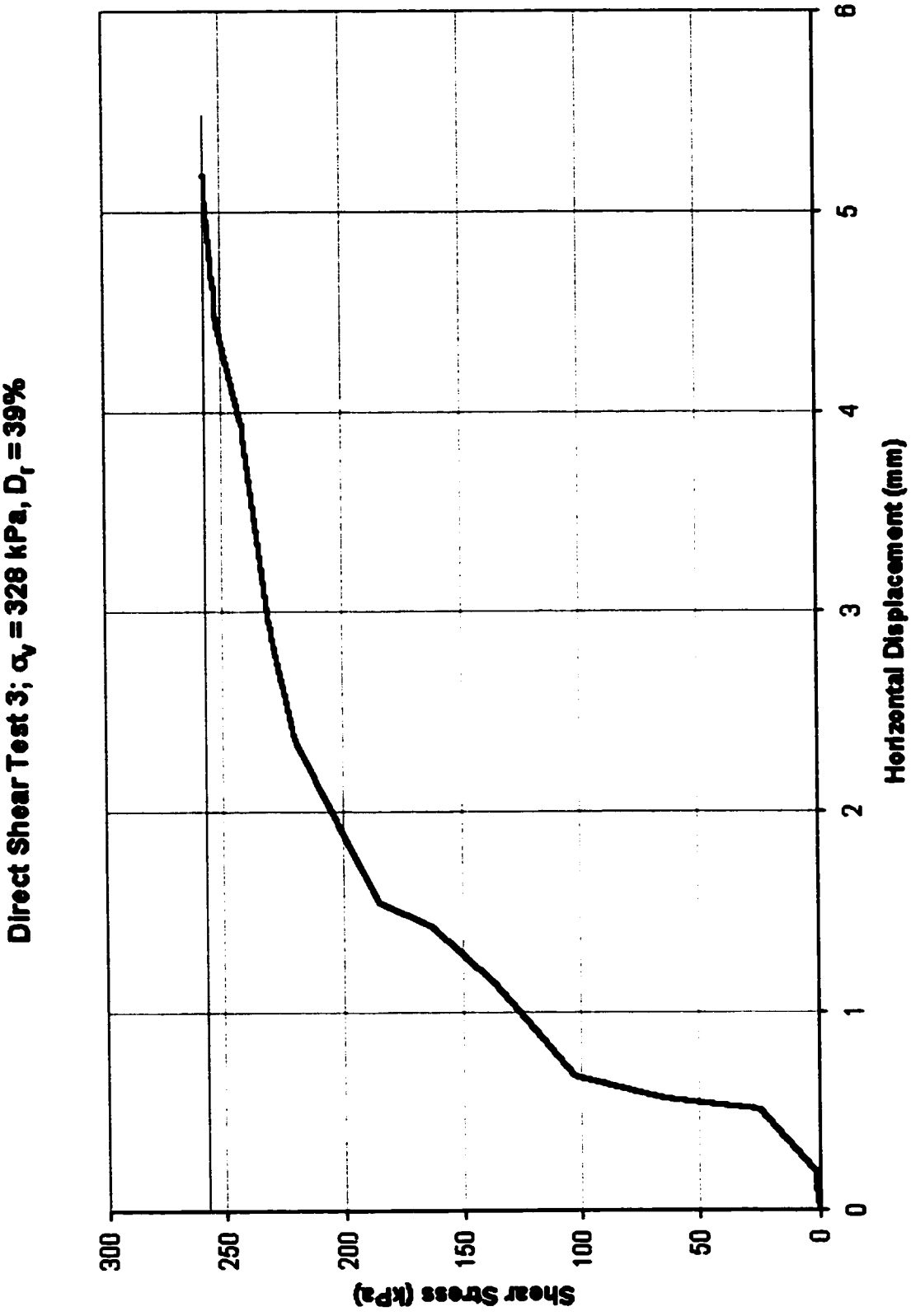
Direct Shear Test 3; σ_v = 328 kPa, D_r = 39%
Shear Stress (kPa)
300
250
200
150
100
50
0
0
1
2
3
4
5
6
Horizontal Displacement (mm)

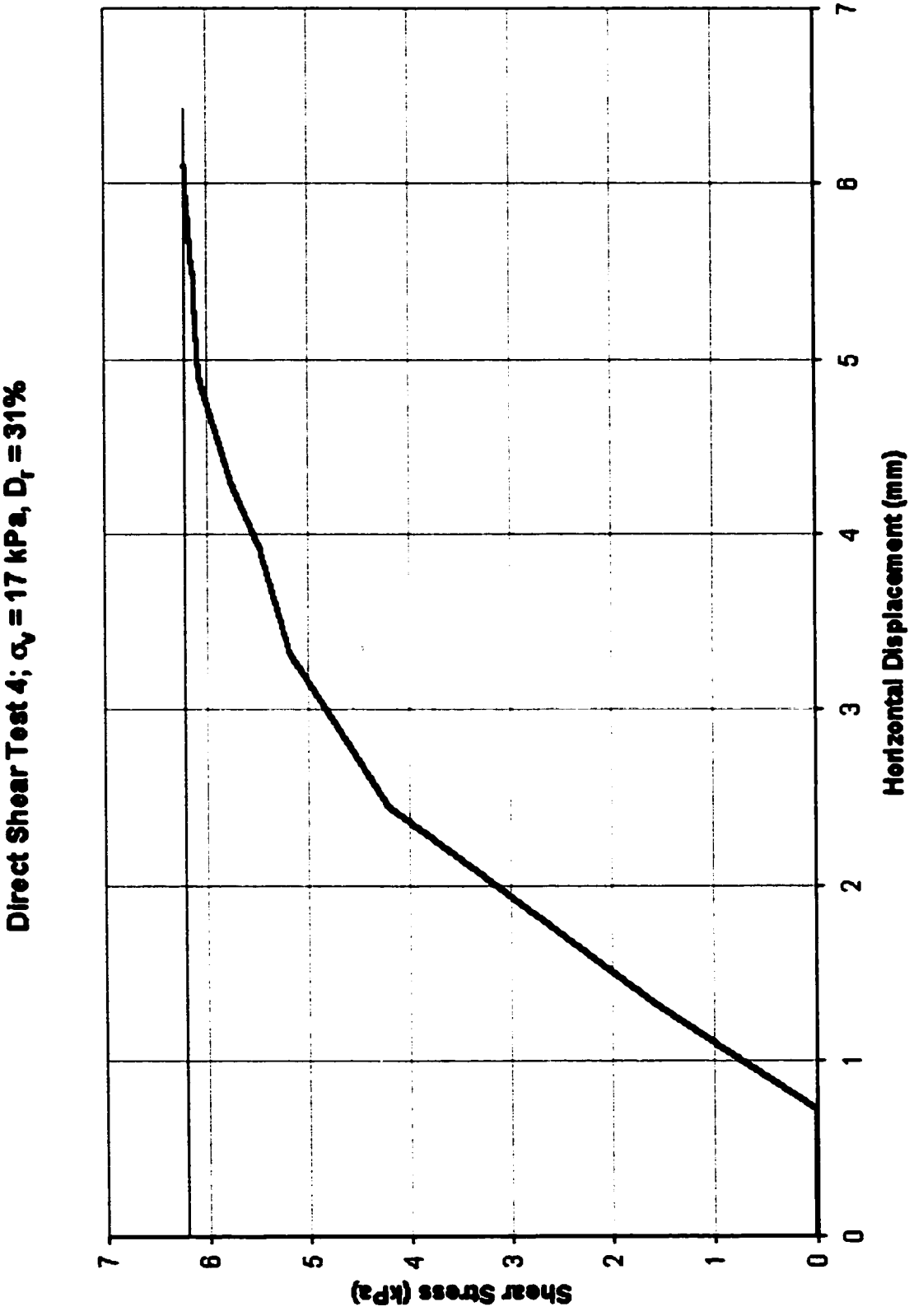
Direct Shear Test 4; σ_v = 17 kPa, D_r = 31%
Shear Stress (kPa)
Horizontal Displacement (mm)
0
1
2
3
4
5
6
7
8

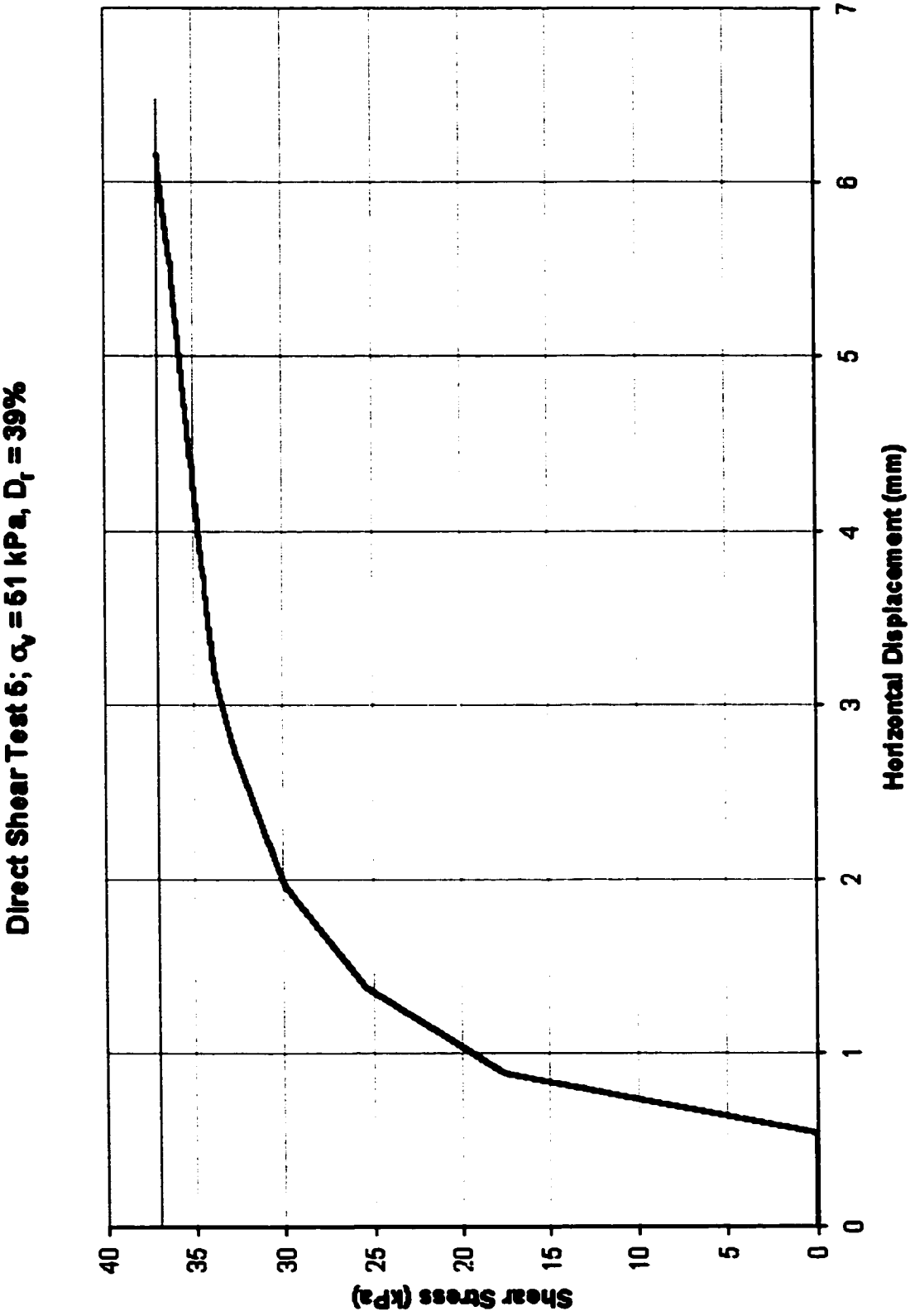
Direct Shear Test 6; σ_v = 61 kPa, D_r = 39%
Shear Stress (kPa)
0
5
10
15
20
25
30
35
40
Horizontal Displacement (mm)
0
1
2
3
4
5
6
7

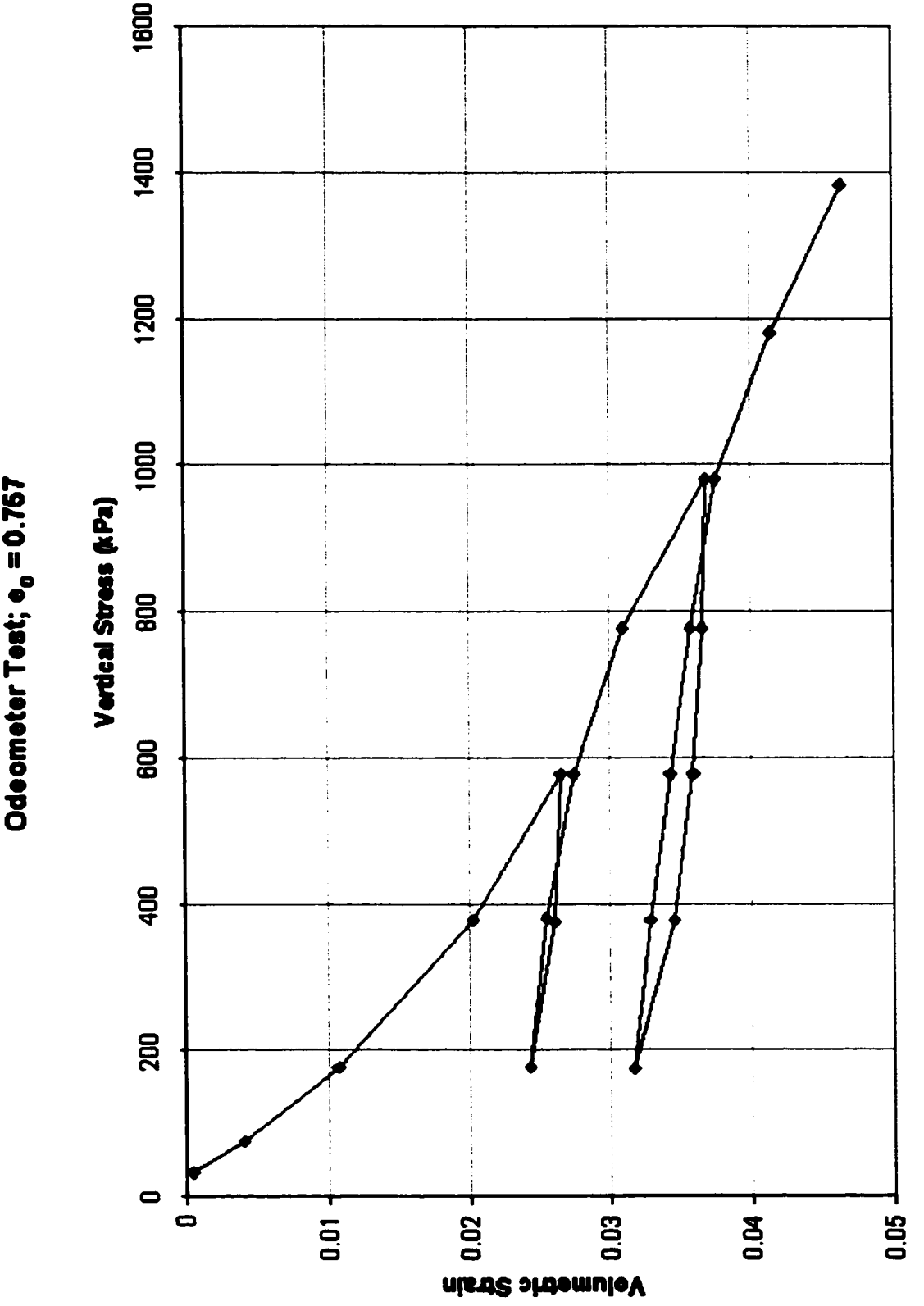
Odeometer Test; $e_o = 0.757$
Vertical Stress (kPa)
0
200
400
600
800
1000
1200
1400
1600
Volumetric Strain
0
0.01
0.02
0.03
0.04
0.05

Appendix 3: Effects of Shaft Friction, Density and Rotation Rate

Friction 50 kPa

Consolidation Pressure	47 kPa

Start of Test	
Dry Density	1.38 g / cm3
Saturated Density	1.86 g / cm3
e	0.93
Dr	0.28
After Consolidation	
Dry Density	1.39 g / cm3
Saturated Density	1.87 g / cm3
e	0.91
Dr	0.32
After Test	
Dry Density	1.40 g / cm3
Saturated Density	1.87 g / cm3
e	0.90
Dr	0.35
Shear Strength	
Peak Friction	16 kPa
Residucal Friction	11.21 kPa
Vane Speed	
Slow Testing	97.8 deg/min
Fast Testing	1062.6 deg/min

Friction 100 kPa

Consolidation Pressure 103 kPa

Start of Test	
Dry Density	1.37 g / cm3
Saturated Density	1.85 g / cm3
e	0.95
Dr	0.22
After Consolidation	
Dry Density	1.39 g / cm3
Saturated Density	1.87 g / cm3
e	0.92
Dr	0.30
After Test	
Dry Density	1.39 g / cm3
Saturated Density	1.87 g / cm3
e	0.91
Dr	0.33
Shear Strength	
Peak Friction	16.54 kPa
Residucal Friction	9.92 kPa
Vane Speed	
Slow Testing	97.8 deg/min
Fast Testing	1062.6 deg/min

Friction 150 kPa

Consolidation Pressure 143 kPa

Start of Test	
Dry Density	1.37 g / cm3
Saturated Density	1.85 g / cm3
e	0.95
Dr	0.23
After Consolidation	
Dry Density	1.39 g / cm3
Saturated Density	1.87 g / cm3
e	0.92
Dr	0.32
After Test	
Dry Density	1.40 g / cm3
Saturated Density	1.87 g / cm3
e	0.90
Dr	0.35
Shear Strength	
Peak Friction	18.16 kPa
Residucal Friction	9.42 kPa
Vane Speed	
Slow Testing	120 deg/min
Fast Testing	1062.6 deg/min

Friction 200 kPa

Consolidation Pressure 188 kPa

Start of Test	
Dry Density	1.37 g / cm3
Saturated Density	1.85 g / cm3
e	0.95
Dr	0.23
After Consolidation	
Dry Density	1.39 g / cm3
Saturated Density	1.87 g / cm3
e	0.91
Dr	0.32
After Test	
Dry Density	1.40 g / cm3
Saturated Density	1.87 g / cm3
e	0.91
Dr	0.34
Shear Strength	
Peak Friction	18.09 kPa
Residucal Friction	9.62 kPa
Vane Speed	
Slow Testing	97.8 deg/min
Fast Testing	1062.6 deg/min

Density 10s Vib

Consolidation Pressure	102 kPa

Start of Test	
Dry Density	1.37 g / cm3
Saturated Density	1.86 g / cm3
e	0.94
Dr	0.25
After Consolidation	
Dry Density	1.39 g / cm3
Saturated Density	1.87 g / cm3
e	0.92
Dr	0.31
After Test	
Dry Density	1.41 g / cm3
Saturated Density	1.88 g / cm3
e	0.89
Dr	0.38
B Value	0.98
Peak Strength	
Maximum Shear Strength	100.48 kPa
Effective Stress	101.66 kPa
Residual Strength	
Steady State Shear Strength	71.56 kPa
High Speed Steady State	61.26 kPa
Effective Stress	101.66 kPa
Vane Speed	
Slow Testing	84 deg/min
Fast Testing	1062.6 deg/min

Density 15s Vib

Consolidation Pressure	104 kPa

Start of Test	
Dry Density	1.43 g / cm3
Saturated Density	1.89 g / cm3
e	0.87
Dr	0.44
After Consolidation	
Dry Density	1.44 g / cm3
Saturated Density	1.90 g / cm3
e	0.85
Dr	0.48
After Test	
Dry Density	1.45 g / cm3
Saturated Density	1.91 g / cm3
e	0.84
Dr	0.53
B Value	0.97
Peak Strength	
Maximum Shear Strength	137.19 kPa
Effective Stress	104.18 kPa
Residual Strength	
Steady State Shear Strength	70.26 kPa
High Speed Steady State	56.16 kPa
Effective Stress	104.18 kPa
Vane Speed	
Slow Testing	84 deg/min
Fast Testing	1062.6 deg/min

Density 20s Vib

Consolidation Pressure 101 kPa

Start of Test	
Dry Density	1.44 g / cm3
Saturated Density	1.90 g / cm3
e	0.85
Dr	0.50
After Consolidation	
Dry Density	1.47 g / cm3
Saturated Density	1.92 g / cm3
e	0.81
Dr	0.59
After Test	
Dry Density	1.50 g / cm3
Saturated Density	1.94 g / cm3
e	0.77
Dr	0.69
B Value	N/A
Peak Strength	
Maximum Shear Strength	154.40 kPa
Effective Stress	101.43 kPa
Residual Strength	
Steady State Shear Strength	69.36 kPa
High Speed Steady State	52.26 kPa
Effective Stress	101.43 kPa
Vane Speed	
Slow Testing	84 deg/min
Fast Testing	1062.6 deg/min

Density 30s Vib

Consolidation Pressure 100 kPa

Start of Test	
Dry Density	1.45 g / cm3
Saturated Density	1.90 g / cm3
e	0.84
Dr	0.51
After Consolidation	
Dry Density	1.46 g / cm3
Saturated Density	1.91 g / cm3
e	0.83
Dr	0.55
After Test	
Dry Density	1.47 g / cm3
Saturated Density	1.92 g / cm3
e	0.81
Dr	0.59
B Value	0.96
Peak Strength	
Maximum Shear Strength	151.15 kPa
Effective Stress	100.29 kPa
Residual Strength	
Steady State Shear Strength	62.56 kPa
High Speed Steady State	54.56 kPa
Effective Stress	100.29 kPa
Vane Speed	
Slow Testing	100.8 deg/min
Fast Testing	1062.6 deg/min

IC-D-100 Speed 10

Consolidation Pressure 93 kPa

Start of Test	
Dry Density	1.36 g / cm3
Saturated Density	1.85 g / cm3
e	0.95
Dr	0.22
After Consolidation	
Dry Density	1.38 g / cm3
Saturated Density	1.86 g / cm3
e	0.93
Dr	0.29
After Test	
Dry Density	1.40 g / cm3
Saturated Density	1.87 g / cm3
e	0.91
Dr	0.34
Shear Strength	
Peak Strength	
Maximum Shear Strength	104.78 kPa
Effective Stress	92.77 kPa
Residual Strength	
Steady State Shear Strength	41.20 kPa
Effective Stress	92.77 kPa
Vane Speed	
Speed	71.4 deg/min

IC-D-100 Speed 20

Consolidation Pressure 101 kPa

Start of Test	
Dry Density	1.37 g / cm3
Saturated Density	1.86 g / cm3
e	0.94
Dr	0.25
After Consolidation	
Dry Density	1.38 g / cm3
Saturated Density	1.86 g / cm3
e	0.93
Dr	0.29
After Test	
Dry Density	1.39 g / cm3
Saturated Density	1.87 g / cm3
e	0.91
Dr	0.33
Shear Strength	
Peak Strength	
Maximum Shear Strength	93.28 kPa
Effective Stress	101.48 kPa
Residual Strength	
Steady State Shear Strength	46.50 kPa
Effective Stress	101.48 kPa
Vane Speed	
Speed	192 deg/min

IC-D-100 Speed 40

Consolidation Pressure 102 kPa

Start of Test	
Dry Density	1.34 g / cm3
Saturated Density	1.84 g / cm3
e	0.99
Dr	0.13
After Consolidation	
Dry Density	1.35 g / cm3
Saturated Density	1.84 g / cm3
e	0.97
Dr	0.17
After Test	
Dry Density	1.36 g / cm3
Saturated Density	1.85 g / cm3
e	0.95
Dr	0.22
Shear Strength	
Peak Strength	
Maximum Shear Strength	101.13 kPa
Effective Stress	102.09 kPa
Residual Strength	
Steady State Shear Strength	45.40 kPa
Effective Stress	102.09 kPa
Vane Speed	
Speed	427.8 deg/min

IC-D-100 Speed 60

Consolidation Pressure 101 kPa

Start of Test	
Dry Density	1.34 g / cm3
Saturated Density	1.84 g / cm3
e	0.99
Dr	0.13
After Consolidation	
Dry Density	1.35 g / cm3
Saturated Density	1.85 g / cm3
e	0.97
Dr	0.18
After Test	
Dry Density	1.37 g / cm3
Saturated Density	1.85 g / cm3
e	0.95
Dr	0.23
Shear Strength	
Peak Strength	
Maximum Shear Strength	96.93 kPa
Effective Stress	101.30 kPa
Residual Strength	
Steady State Shear Strength	40.80 kPa
Effective Stress	101.30 kPa
Vane Speed	
Speed	720 deg/min

IC-D-100 Speed 80

Consolidation Pressure	104 kPa

Start of Test	
Dry Density	1.35 g / cm3
Saturated Density	1.84 g / cm3
e	0.98
Dr	0.16
After Consolidation	
Dry Density	1.36 g / cm3
Saturated Density	1.85 g / cm3
e	0.96
Dr	0.21
After Test	
Dry Density	1.37 g / cm3
Saturated Density	1.86 g / cm3
e	0.94
Dr	0.25
Shear Strength	
Peak Strength	
Maximum Shear Strength	76.37 kPa
Effective Stress	104.01 kPa
Residual Strength	
Steady State Shear Strength	40.60 kPa
Effective Stress	104.01 kPa
Vane Speed	
Speed	942 deg/min

IC-D-100 Speed 100

Consolidation Pressure 105 kPa

Start of Test	
Dry Density	1.33 g / cm3
Saturated Density	1.83 g / cm3
e	1.01
Dr	0.08
After Consolidation	
Dry Density	1.34 g / cm3
Saturated Density	1.84 g / cm3
e	0.99
Dr	0.13
After Test	
Dry Density	1.35 g / cm3
Saturated Density	1.85 g / cm3
e	0.97
Dr	0.18
Shear Strength	
Peak Strength	
Maximum Shear Strength	82.43 kPa
Effective Stress	104.93 kPa
Residual Strength	
Steady State Shear Strength	41.10 kPa
Effective Stress	104.93 kPa
Vane Speed	
Speed	1080 deg/min

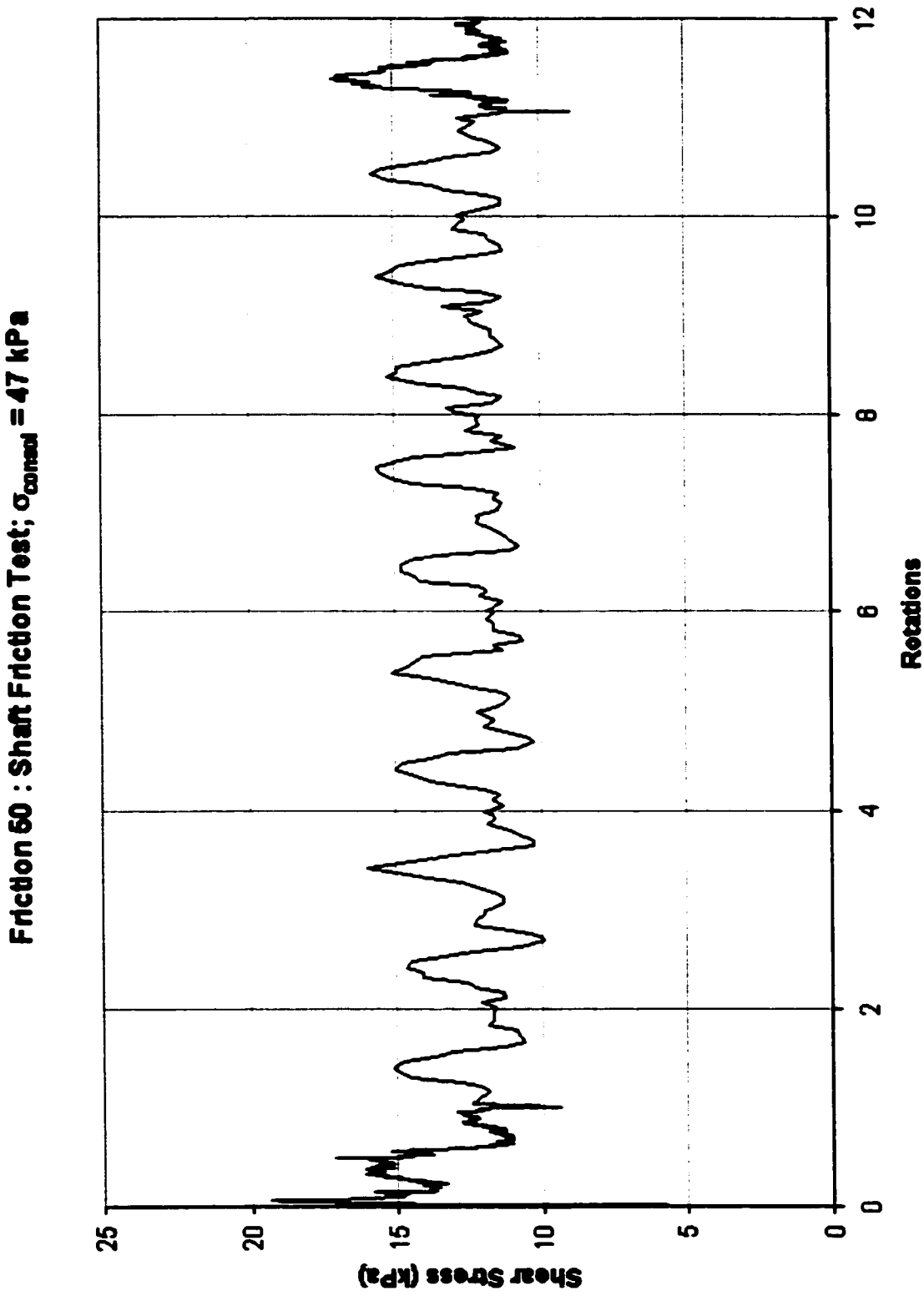
Friction 60 : Shaft Friction Test; σ_{consol} = 47 kPa
Shear Stress (kPa)
0
5
10
15
20
25
Rotations
0
2
4
6
8
10
12

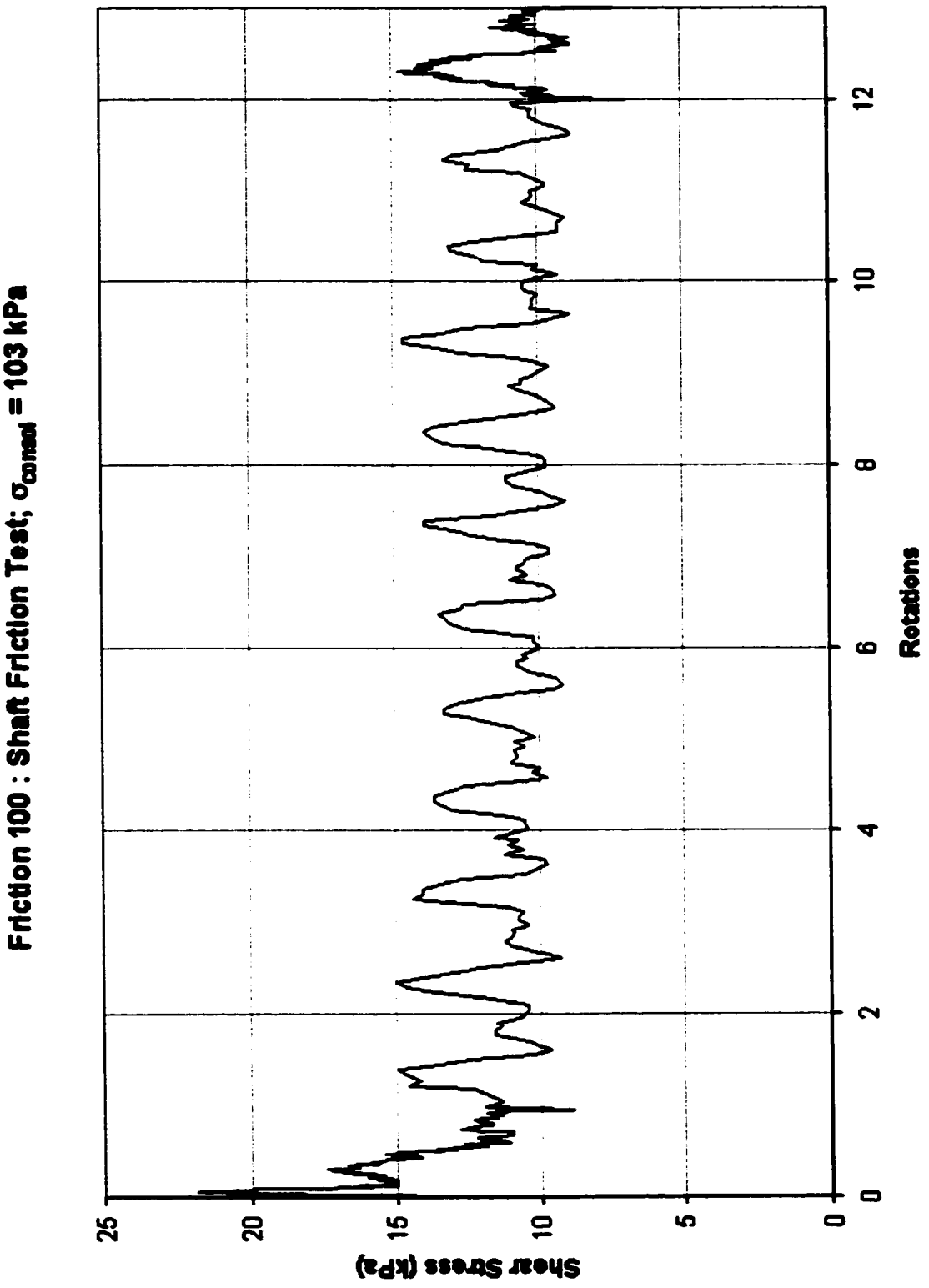
Friction 100 : Shaft Friction Test; σ_{consol} = 103 kPa
Shear Stress (kPa)
25
20
15
10
5
0
0
2
4
6
8
10
12
Rotations

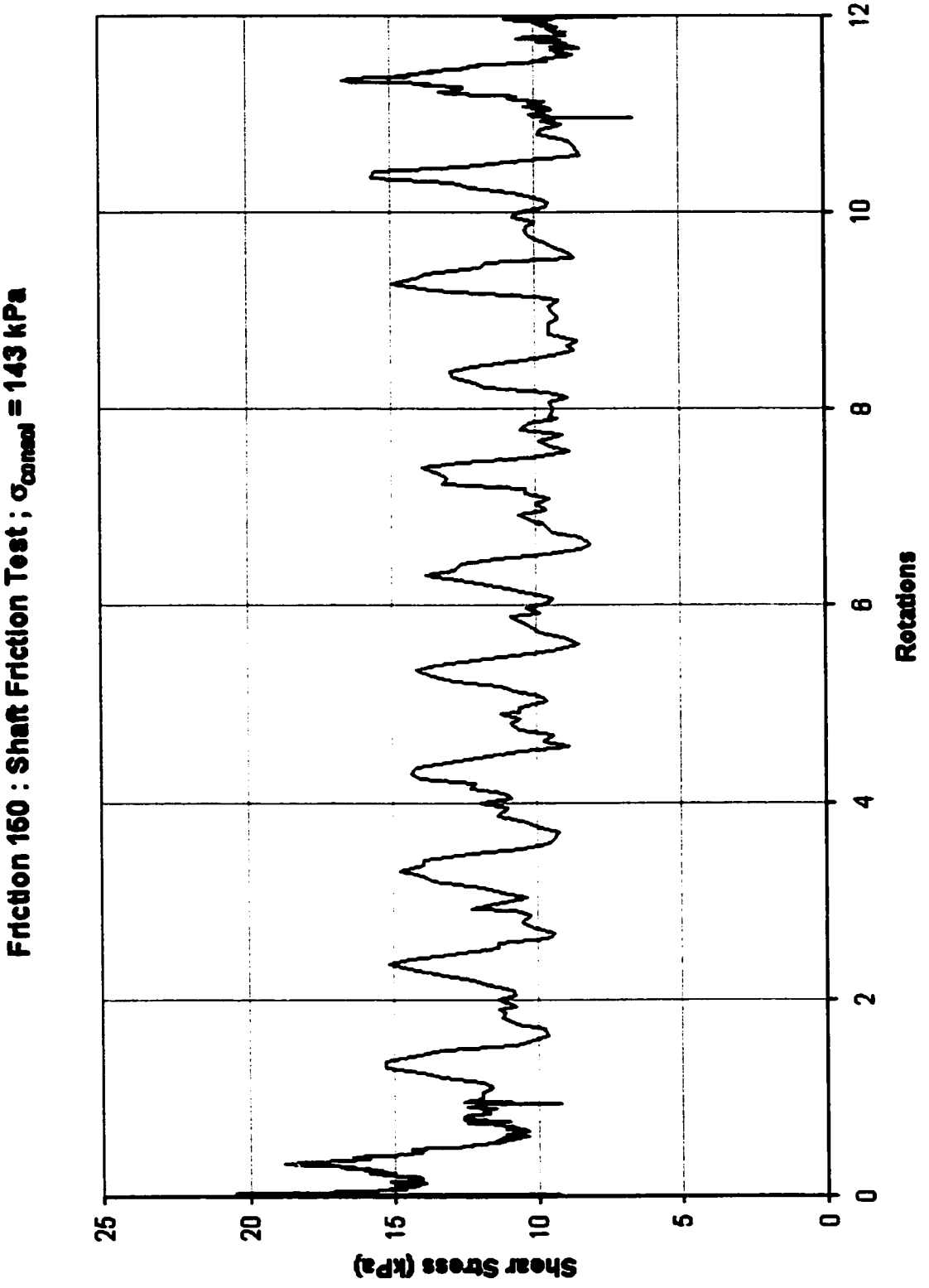
Friction 160 : Shaft Friction Test ; σconsol = 143 kPa
Shear Stress (kPa)
25
20
15
10
5
0
0
2
4
6
8
10
12
Rotations

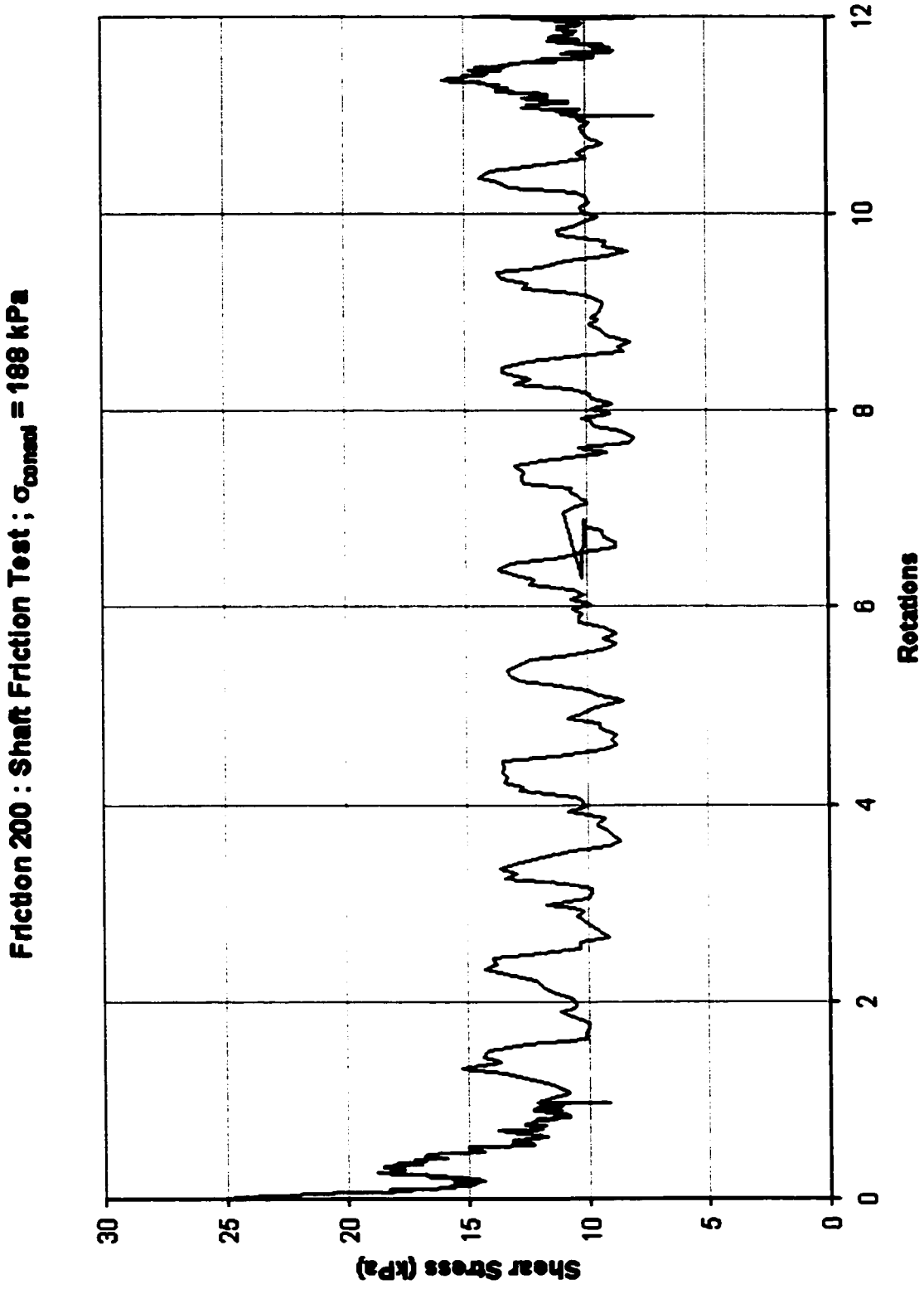
Friction 200 : Shaft Friction Test ; σ_{consol} = 188 kPa
Shear Stress (kPa)
0
5
10
15
20
25
30
Rotations
0
2
4
6
8
10
12

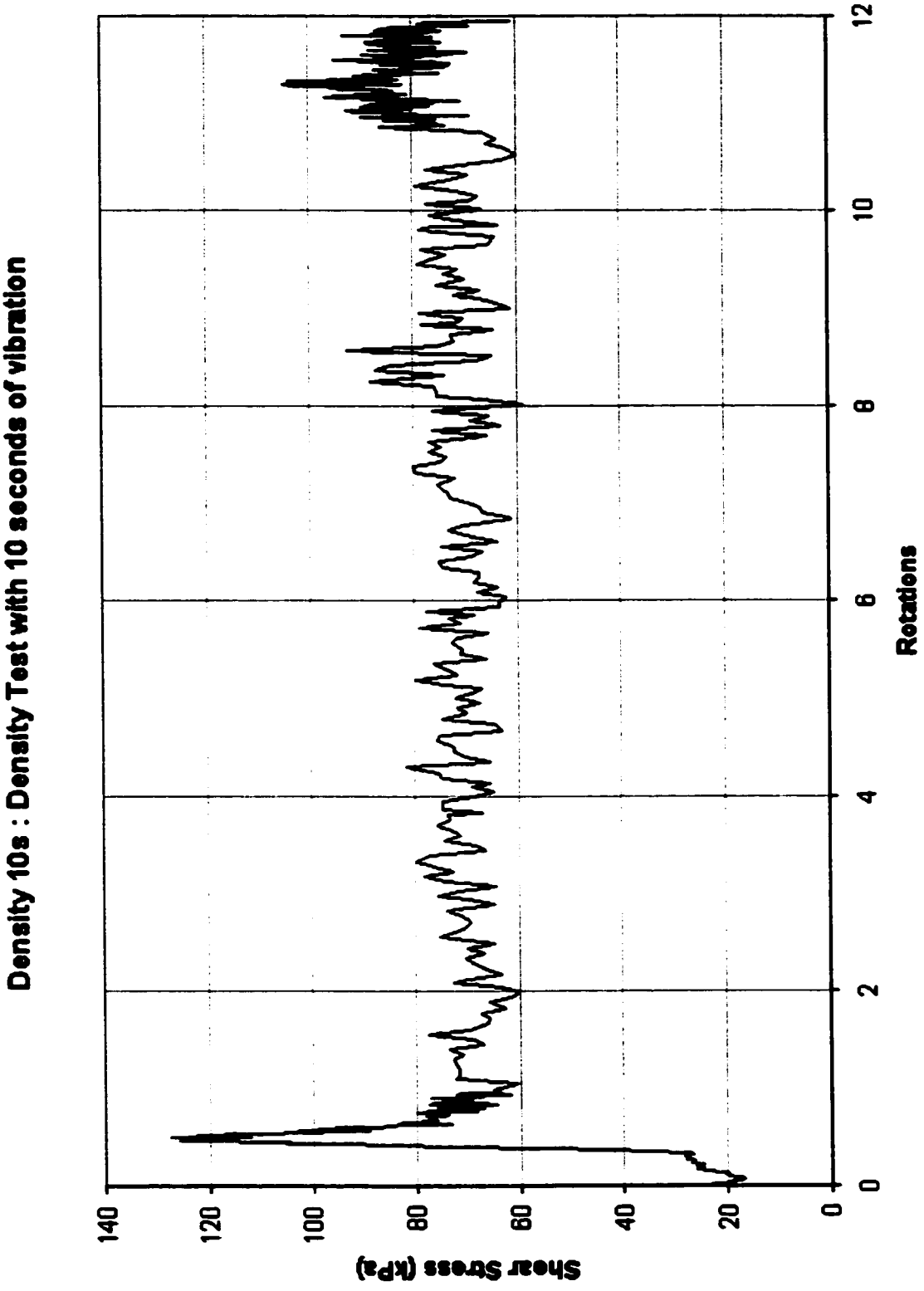
Density 10s : Density Test with 10 seconds of vibration
Shear Stress (kPa)
140
120
100
80
60
40
20
0
0
2
4
6
8
10
12
Rotations

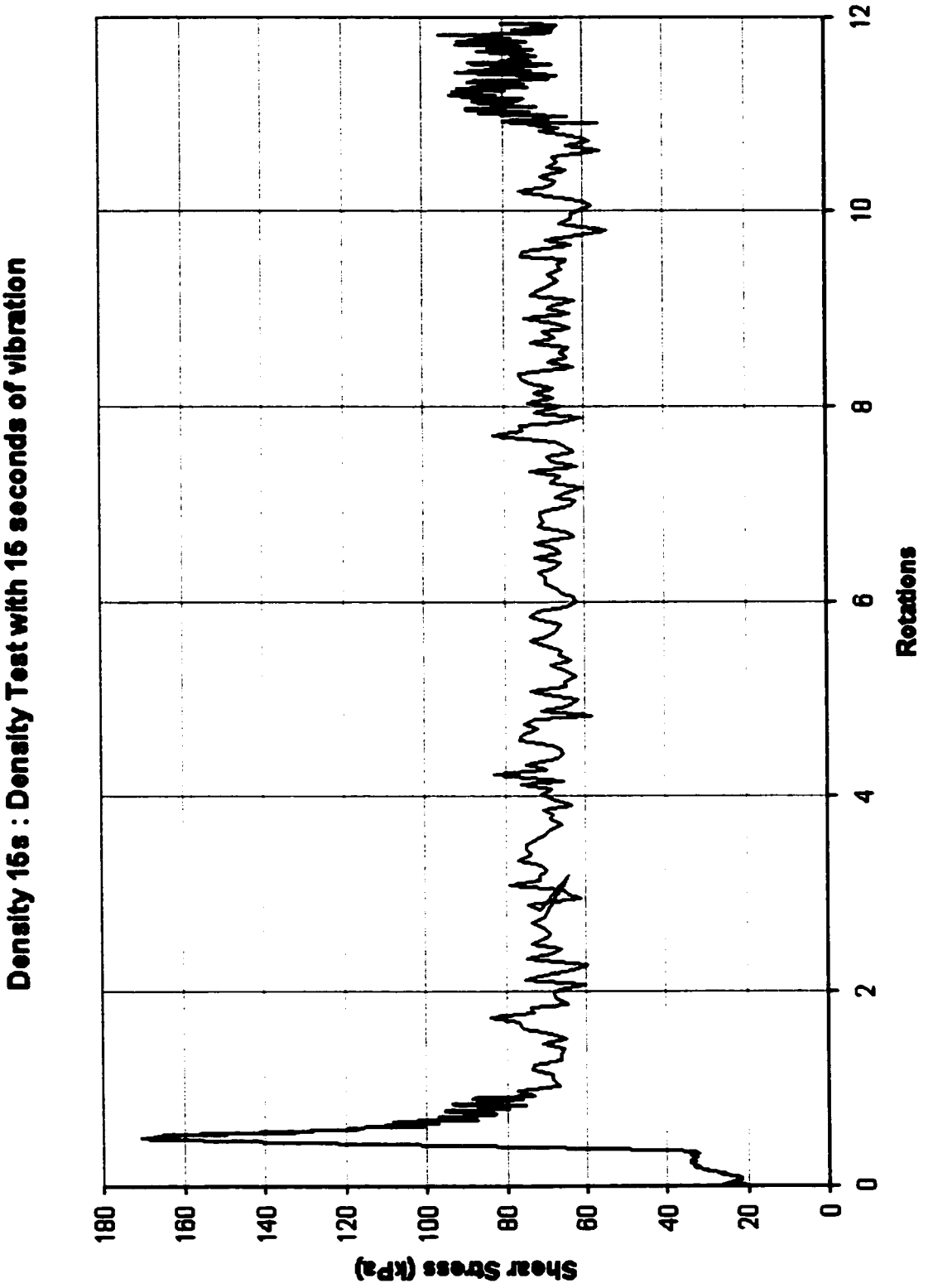
Density 16s : Density Test with 15 seconds of vibration
Shear Stress (kPa)
0
20
40
60
80
100
120
140
160
180
0
2
4
6
8
10
12
Rotations

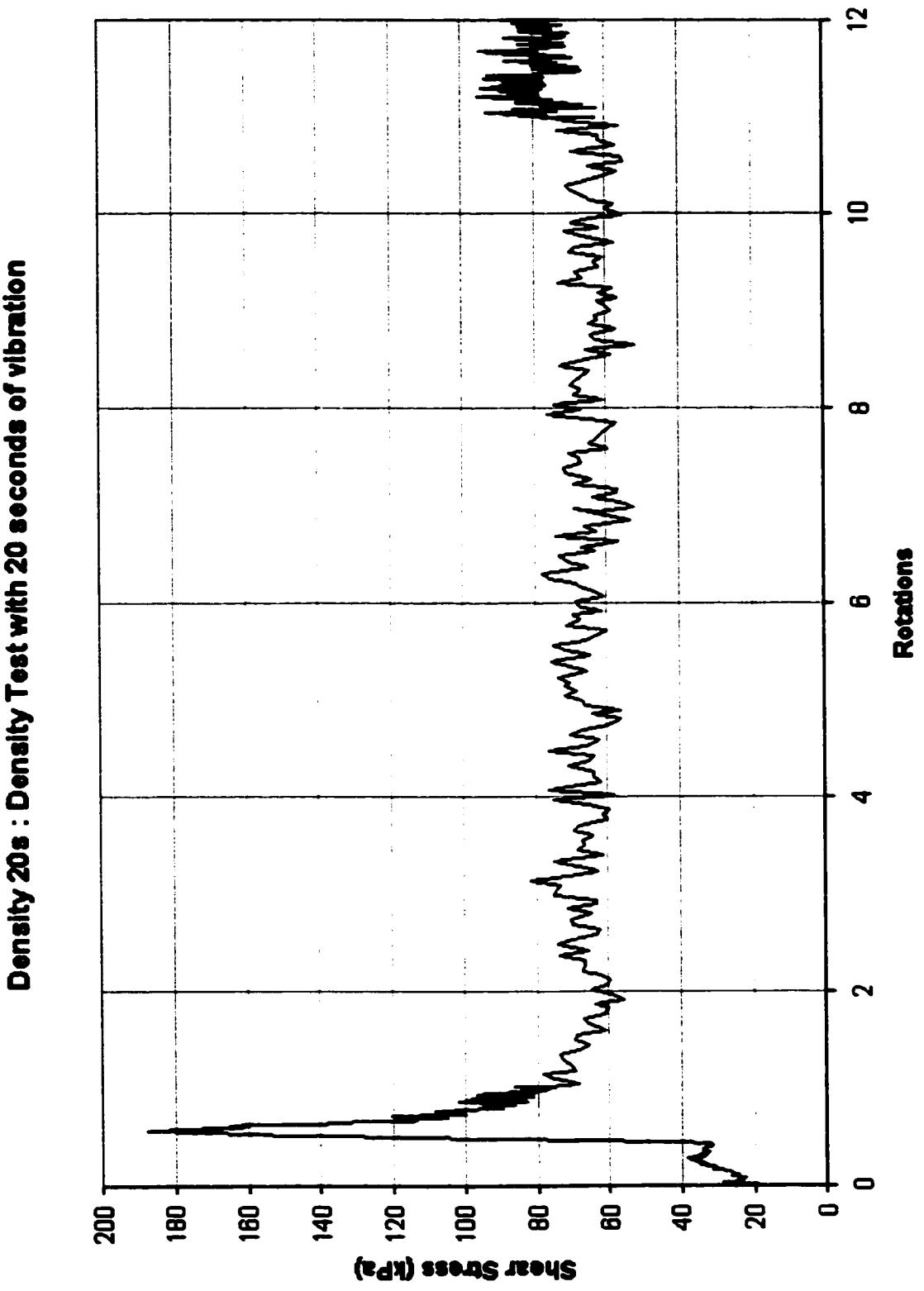
Density 20s : Density Test with 20 seconds of vibration
Shear Stress (kPa)
200
180
160
140
120
100
80
60
40
20
0
0
2
4
6
8
10
12
Rotations

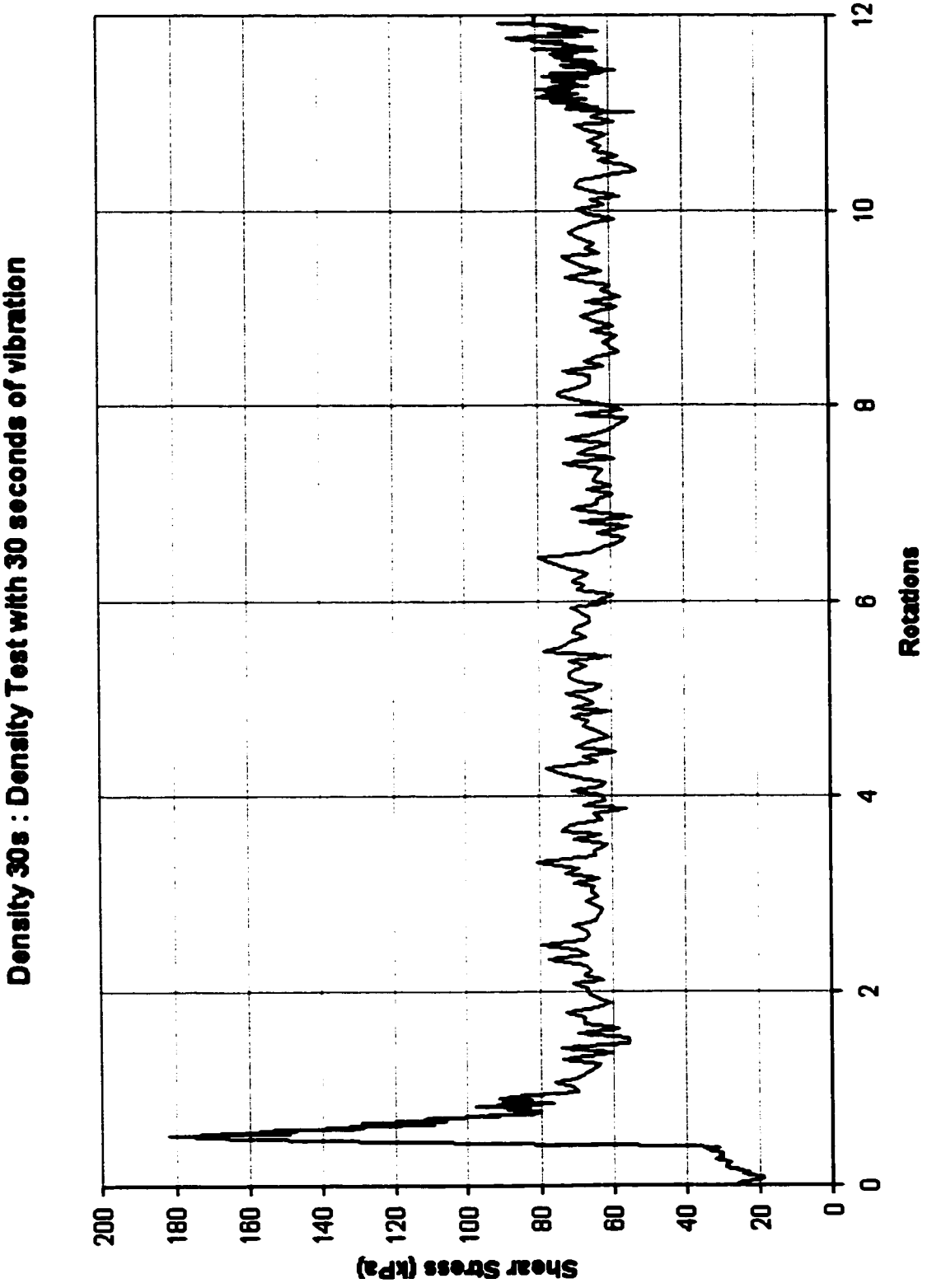
Density 30s : Density Test with 30 seconds of vibration
Shear Stress (kPa)
200
180
160
140
120
100
80
60
40
20
0
0
2
4
6
8
10
12
Rotations

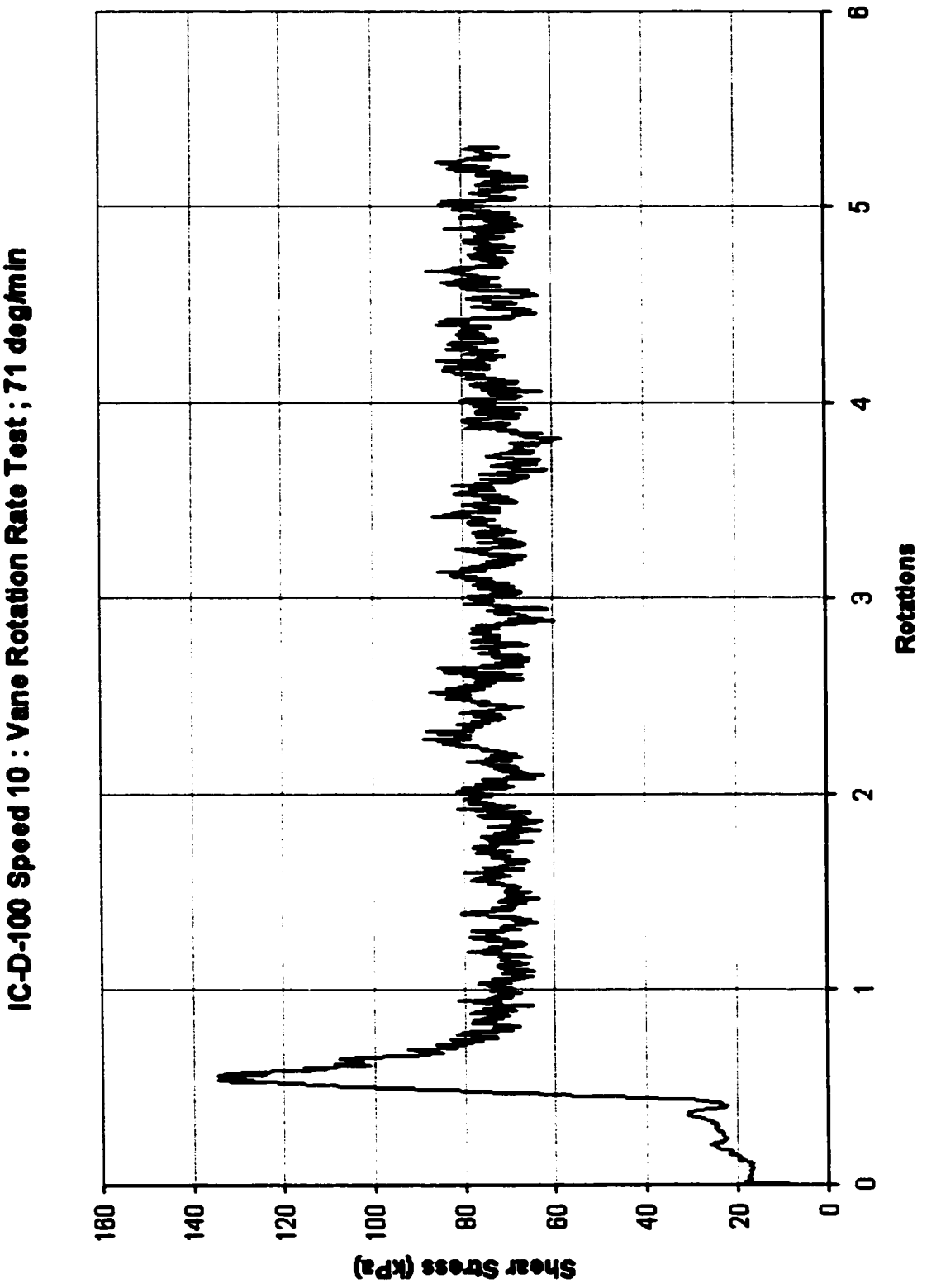
IC-D-100 Speed 10 : Vane Rotation Rate Test ; 71 deg/min
Shear Stress (kPa)
0
20
40
60
80
100
120
140
160
Rotations
0
1
2
3
4
5
6

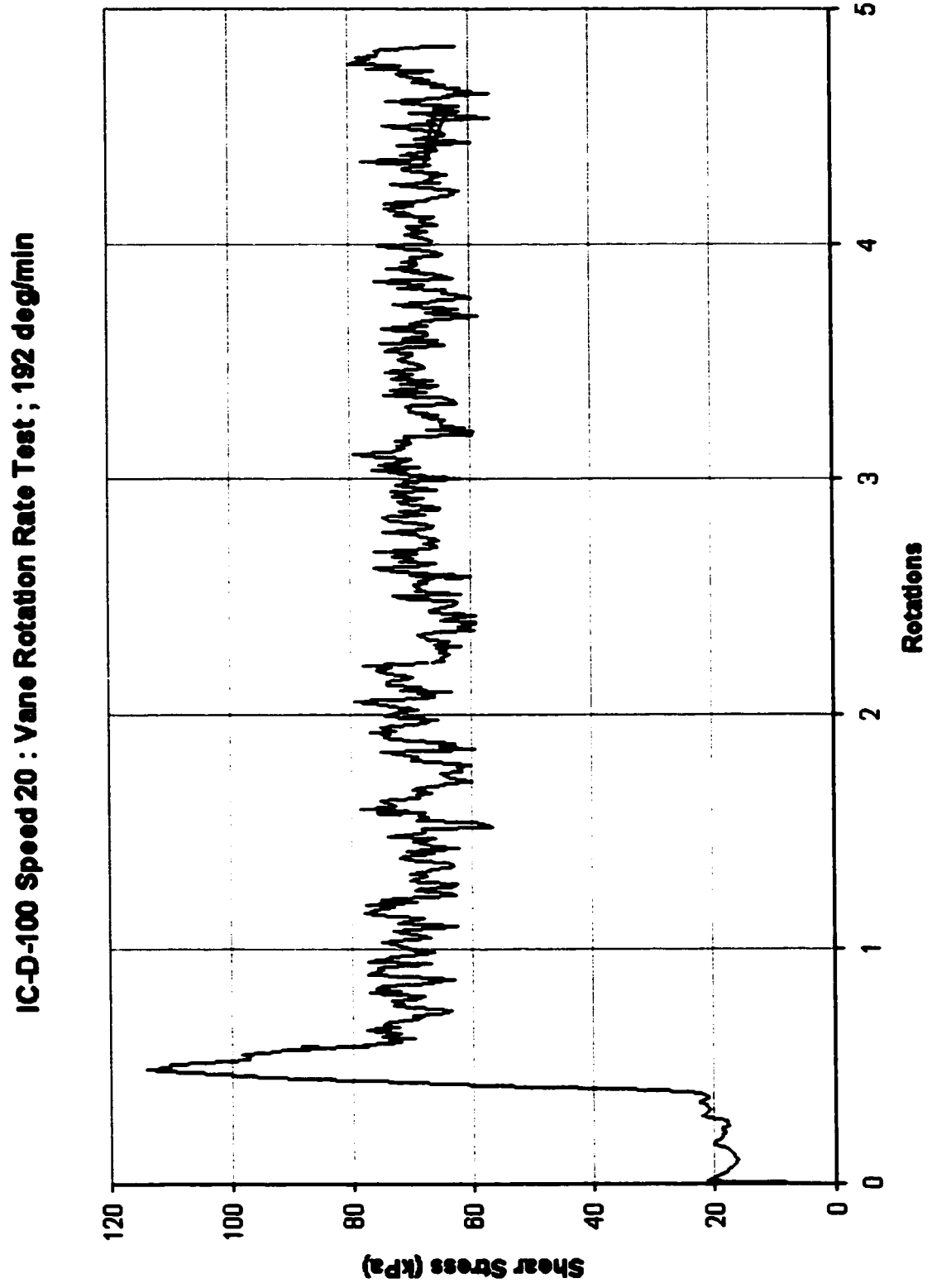
IC-D-100 Speed 20 : Vane Rotation Rate Test ; 192 deg/min
Shear Stress (kPa)
120
100
80
60
40
20
0
0
1
2
3
4
5
Rotations

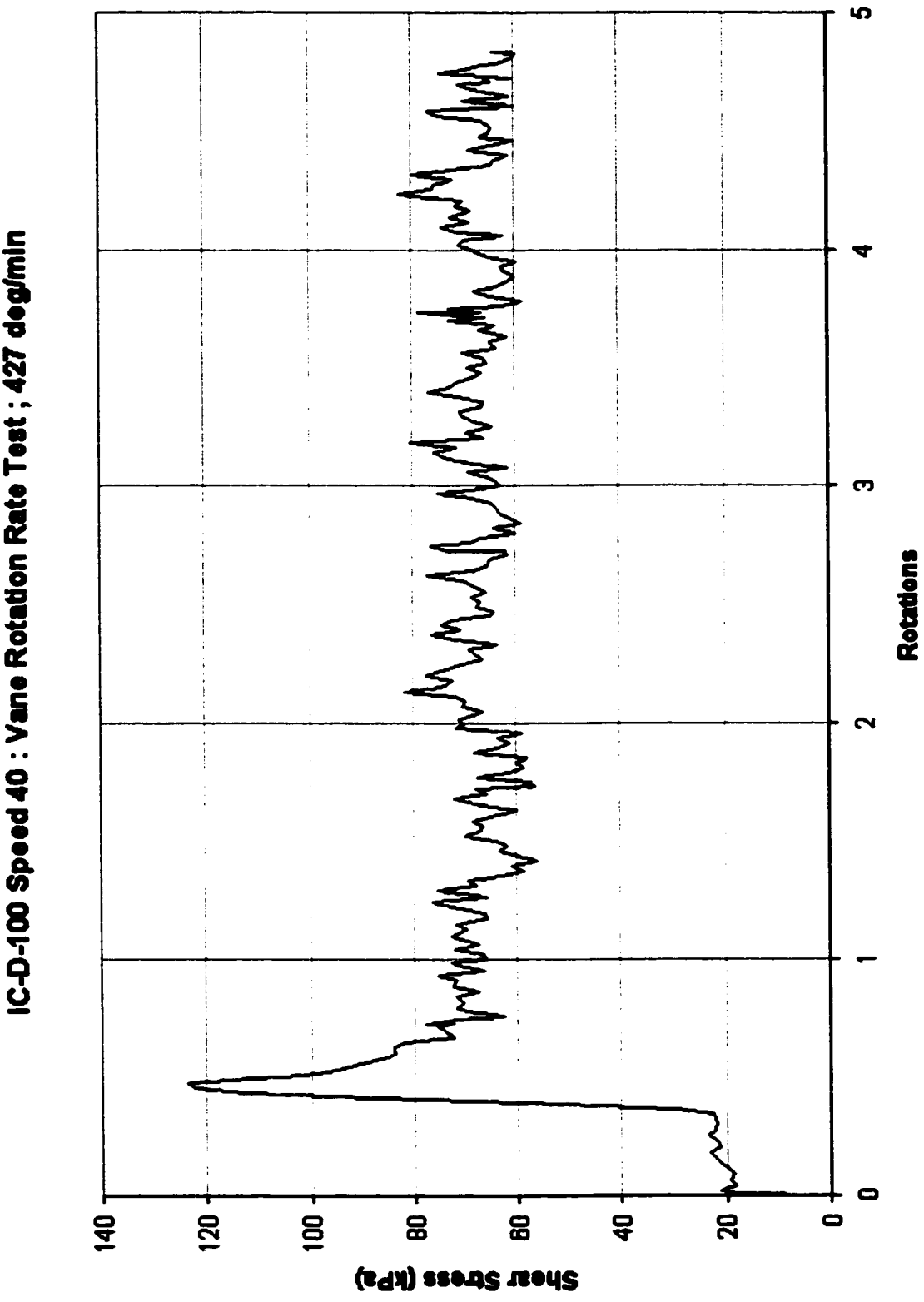
IC-D-100 Speed 40 : Vane Rotation Rate Test ; 427 deg/min
Shear Stress (kPa)
140
120
100
80
60
40
20
0
0
1
2
3
4
5
Rotations

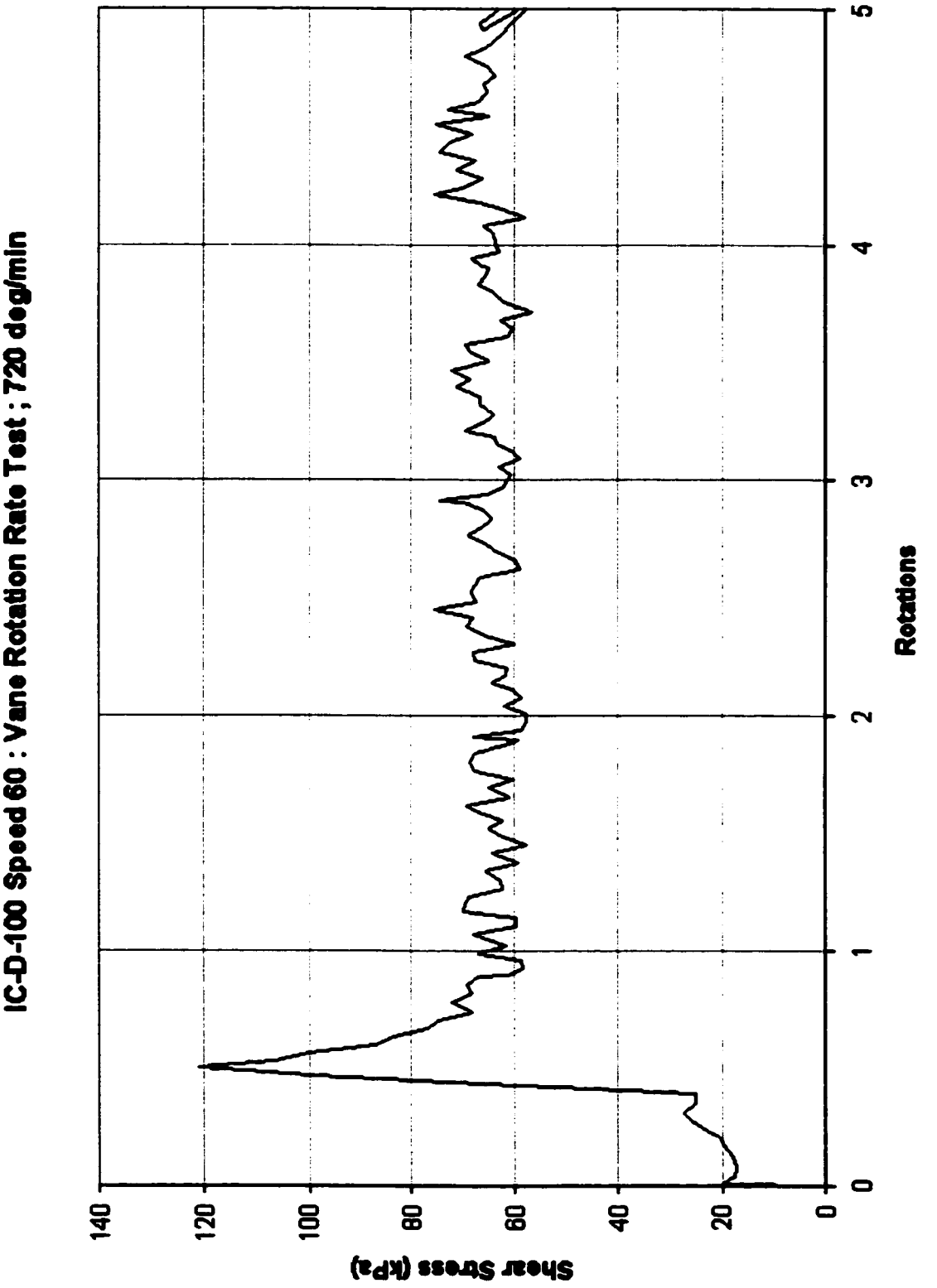
IC-D-100 Speed 60 : Vane Rotation Rate Test ; 720 deg/min
Shear Stress (kPa)
140
120
100
80
60
40
20
0
0
1
2
3
4
5
Rotations

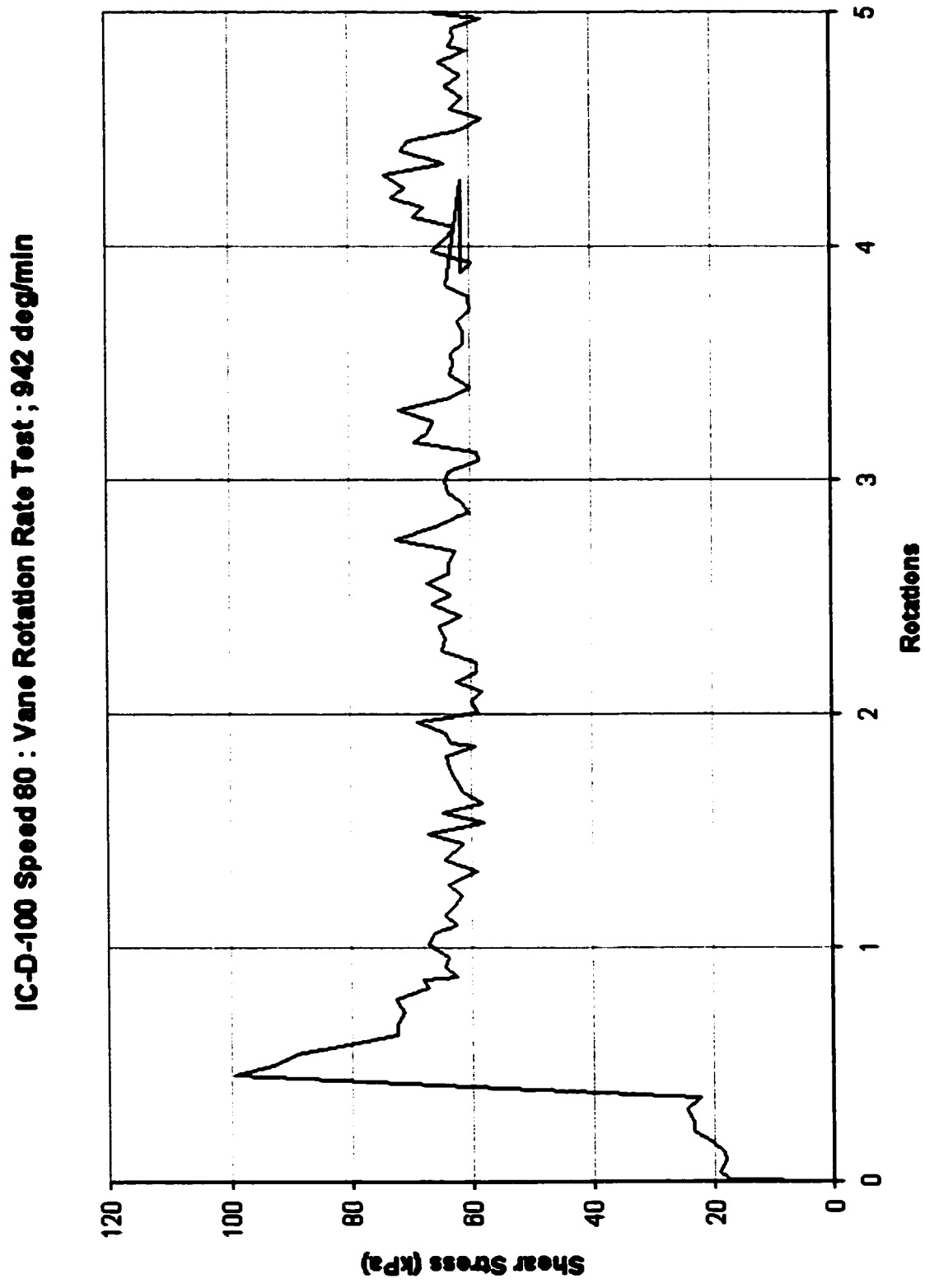
IC-D-100 Speed 80 : Vane Rotation Rate Test ; 942 deg/min
Shear Stress (kPa)
120
100
80
60
40
20
0
0
1
2
3
4
5
Rotations

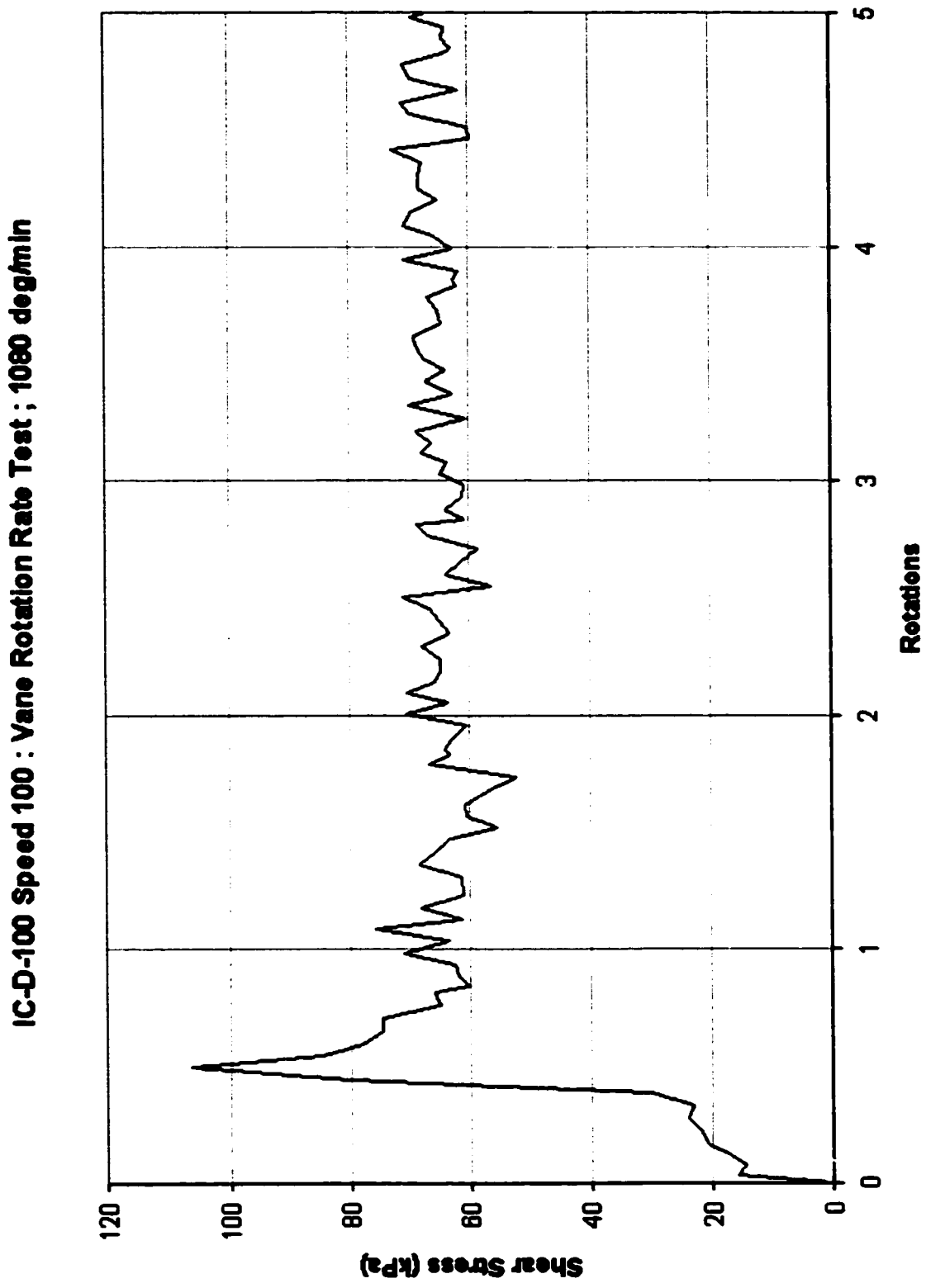
IC-D-100 Speed 100 : Vane Rotation Rate Test ; 1080 deg/min
Shear Stress (kPa)
120
100
80
60
40
20
0
0
1
2
3
4
5
Rotations

Appendix 4: IC-D Triaxial Vane Tests

IC-D-50

Consolidation Pressure	51 kPa

Start of Test	
Dry Density	1.38 g / cm3
Saturated Density	1.87 g / cm3
e	0.92
Dr	0.29
After Consolidation	
Dry Density	1.39 g / cm3
Saturated Density	1.87 g / cm3
e	0.91
Dr	0.32
After Test	
Dry Density	1.41 g / cm3
Saturated Density	1.88 g / cm3
e	0.89
Dr	0.38
B Value	0.99
Peak Strength	
Maximum Shear Strength	74.97 kPa
Effective Stress	50.79 kPa
Residual Strength	
Steady State Shear Strength	38.66 kPa
High Speed Steady State	30.36 kPa
Effective Stress	50.79 kPa
Vane Speed	
Slow Testing	90.6 deg/min
Fast Testing	1062.6 deg/min

IC-D-100

Consolidation Pressure	104 kPa

Start of Test	
Dry Density	1.39 g / cm3
Saturated Density	1.87 g / cm3
e	0.92
Dr	0.32
After Consolidation	
Dry Density	1.41 g / cm3
Saturated Density	1.88 g / cm3
e	0.89
Dr	0.38
After Test	
Dry Density	1.42 g / cm3
Saturated Density	1.89 g / cm3
e	0.87
Dr	0.43
B Value	1.00
Peak Strength	
Maximum Shear Strength	130.04 kPa
Effective Stress	103.60 kPa
Residual Strength	
Steady State Shear Strength	72.46 kPa
High Speed Steady State	56.96 kPa
Effective Stress	103.60 kPa
Vane Speed	
Slow Testing	60 deg/min
Fast Testing	1062.6 deg/min

IC-D-150

Consolidation Pressure	148 kPa

Start of Test	
Dry Density	1.39 g / cm3
Saturated Density	1.87 g / cm3
e	0.91
Dr	0.33
After Consolidation	
Dry Density	1.53 g / cm3
Saturated Density	1.96 g / cm3
e	0.74
Dr	0.79
After Test	
Dry Density	1.56 g / cm3
Saturated Density	1.97 g / cm3
e	0.71
Dr	0.85
B Value	1.00
Peak Strength	
Maximum Shear Strength	173.10 kPa
Effective Stress	147.99 kPa
Residual Strength	
Steady State Shear Strength	89.16 kPa
High Speed Steady State	75.76 kPa
Effective Stress	147.99 kPa
Vane Speed	
Slow Testing	73.8 deg/min
Fast Testing	1062.6 deg/min

IC-D-200

Consolidation Pressure	200 kPa

Start of Test	
Dry Density	1.38 g / cm3
Saturated Density	1.86 g / cm3
e	0.93
Dr	0.28
After Consolidation	
Dry Density	1.40 g / cm3
Saturated Density	1.88 g / cm3
e	0.90
Dr	0.36
After Test	
Dry Density	1.42 g / cm3
Saturated Density	1.89 g / cm3
e	0.88
Dr	0.41
B Value	0.96
Peak Strength	
Maximum Shear Strength	219.61 kPa
Effective Stress	200.35 kPa
Residual Strength	
Steady State Shear Strength	131.86 kPa
High Speed Steady State	102.26 kPa
Effective Stress	200.35 kPa
Vane Speed	
Slow Testing	43.8 deg/min
Fast Testing	1062.6 deg/min

IC-D-50a

Consolidation Pressure 50 kPa

Start of Test	
Dry Density	1.37 g / cm3
Saturated Density	1.86 g / cm3
e	0.94
Dr	0.25
After Consolidation	
Dry Density	1.39 g / cm3
Saturated Density	1.87 g / cm3
e	0.92
Dr	0.30
After Test	
Dry Density	1.40 g / cm3
Saturated Density	1.88 g / cm3
e	0.90
Dr	0.35
B Value	N/A
Peak Strength	
Maximum Shear Strength	64.97 kPa
Effective Stress	50.23 kPa
Residual Strength	
Steady State Shear Strength	34.36 kPa
High Speed Steady State	28.86 kPa
Effective Stress	50.23 kPa
Vane Speed	
Slow Testing	96.6 deg/min
Fast Testing	1062.6 deg/min

IC-D-100a

Consolidation Pressure 107 kPa

Start of Test	
Dry Density	1.35 g / cm3
Saturated Density	1.85 g / cm3
e	0.97
Dr	0.18
After Consolidation	
Dry Density	1.37 g / cm3
Saturated Density	1.85 g / cm3
e	0.95
Dr	0.23
After Test	
Dry Density	1.38 g / cm3
Saturated Density	1.87 g / cm3
e	0.92
Dr	0.29
B Value	N/A
Peak Strength	
Maximum Shear Strength	117.48 kPa
Effective Stress	106.75 kPa
Residual Strength	
Steady State Shear Strength	66.36 kPa
High Speed Steady State	54.86 kPa
Effective Stress	106.75 kPa
Vane Speed	
Slow Testing	88.8 deg/min
Fast Testing	984.6 deg/min

IC-D-150a

Consolidation Pressure 150 kPa

Start of Test	
Dry Density	1.36 g / cm3
Saturated Density	1.85 g / cm3
e	0.97
Dr	0.19
After Consolidation	
Dry Density	1.38 g / cm3
Saturated Density	1.86 g / cm3
e	0.94
Dr	0.26
After Test	
Dry Density	1.39 g / cm3
Saturated Density	1.87 g / cm3
e	0.91
Dr	0.33
B Value	0.94
Peak Strength	
Maximum Shear Strength	260.92 kPa
Effective Stress	150.01 kPa
Residual Strength	
Steady State Shear Strength	89.96 kPa
High Speed Steady State	73.16 kPa
Effective Stress	150.01 kPa
Vane Speed	
Slow Testing	60 deg/min
Fast Testing	1000.8 deg/min

IC-D-200a

Consolidation Pressure 201 kPa

Start of Test	
Dry Density	1.37 g / cm3
Saturated Density	1.86 g / cm3
e	0.95
Dr	0.24
After Consolidation	
Dry Density	1.39 g / cm3
Saturated Density	1.87 g / cm3
e	0.91
Dr	0.32
After Test	
Dry Density	1.41 g / cm3
Saturated Density	1.88 g / cm3
e	0.89
Dr	0.39
B Value	0.85
Peak Strength	
Maximum Shear Strength	199.36 kPa
Effective Stress	201.49 kPa
Residual Strength	
Steady State Shear Strength	121.66 kPa
High Speed Steady State	94.76 kPa
Effective Stress	201.49 kPa
Vane Speed	
Slow Testing	48.6 deg/min
Fast Testing	976.8 deg/min

IC-D-50b

Consolidation Pressure 51 kPa

Start of Test	
Dry Density	1.39 g / cm3
Saturated Density	1.87 g / cm3
e	0.92
Dr	0.31
After Consolidation	
Dry Density	1.40 g / cm3
Saturated Density	1.87 g / cm3
e	0.90
Dr	0.35
After Test	
Dry Density	1.42 g / cm3
Saturated Density	1.88 g / cm3
e	0.88
Dr	0.40
B Value	0.99
Peak Strength	
Maximum Shear Strength	62.47 kPa
Effective Stress	51.28 kPa
Residual Strength	
Steady State Shear Strength	38.96 kPa
High Speed Steady State	32.76 kPa
Effective Stress	51.28 kPa
Vane Speed	
Slow Testing	60 deg/min
Fast Testing	1062.6 deg/min

IC-D-100b

Consolidation Pressure	96 kPa

Start of Test	
Dry Density	1.38 g / cm3
Saturated Density	1.86 g / cm3
e	0.93
Dr	0.28
After Consolidation	
Dry Density	1.44 g / cm3
Saturated Density	1.90 g / cm3
e	0.85
Dr	0.49
After Test	
Dry Density	1.46 g / cm3
Saturated Density	1.91 g / cm3
e	0.82
Dr	0.56
B Value	1.00
Peak Strength	
Maximum Shear Strength	91.83 kPa
Effective Stress	96.03 kPa
Residual Strength	
Steady State Shear Strength	69.96 kPa
High Speed Steady State	60.86 kPa
Effective Stress	96.03 kPa
Vane Speed	
Slow Testing	81 deg/min
Fast Testing	1062.6 deg/min

IC-D-150b

Consolidation Pressure	147 kPa

Start of Test	
Dry Density	1.39 g / cm3
Saturated Density	1.87 g / cm3
e	0.92
Dr	0.32
After Consolidation	
Dry Density	1.41 g / cm3
Saturated Density	1.88 g / cm3
e	0.89
Dr	0.38
After Test	
Dry Density	1.43 g / cm3
Saturated Density	1.89 g / cm3
e	0.87
Dr	0.44
B Value	0.99
Peak Strength	
Maximum Shear Strength	146.50 kPa
Effective Stress	146.87 kPa
Residual Strength	
Steady State Shear Strength	96.66 kPa
High Speed Steady State	81.46 kPa
Effective Stress	146.87 kPa
Vane Speed	
Slow Testing	60 deg/min
Fast Testing	1062.6 deg/min

IC-D-200b

Consolidation Pressure	199 kPa

Start of Test	
Dry Density	1.40 g / cm3
Saturated Density	1.88 g / cm3
e	0.90
Dr	0.36
After Consolidation	
Dry Density	1.45 g / cm3
Saturated Density	1.91 g / cm3
e	0.83
Dr	0.53
After Test	
Dry Density	1.47 g / cm3
Saturated Density	1.92 g / cm3
e	0.81
Dr	0.59
B Value	0.98
Peak Strength	
Maximum Shear Strength	185.46 kPa
Effective Stress	199.47 kPa
Residual Strength	
Steady State Shear Strength	128.46 kPa
High Speed Steady State	100.96 kPa
Effective Stress	199.47 kPa
Vane Speed	
Slow Testing	70.2 deg/min
Fast Testing	1062.6 deg/min

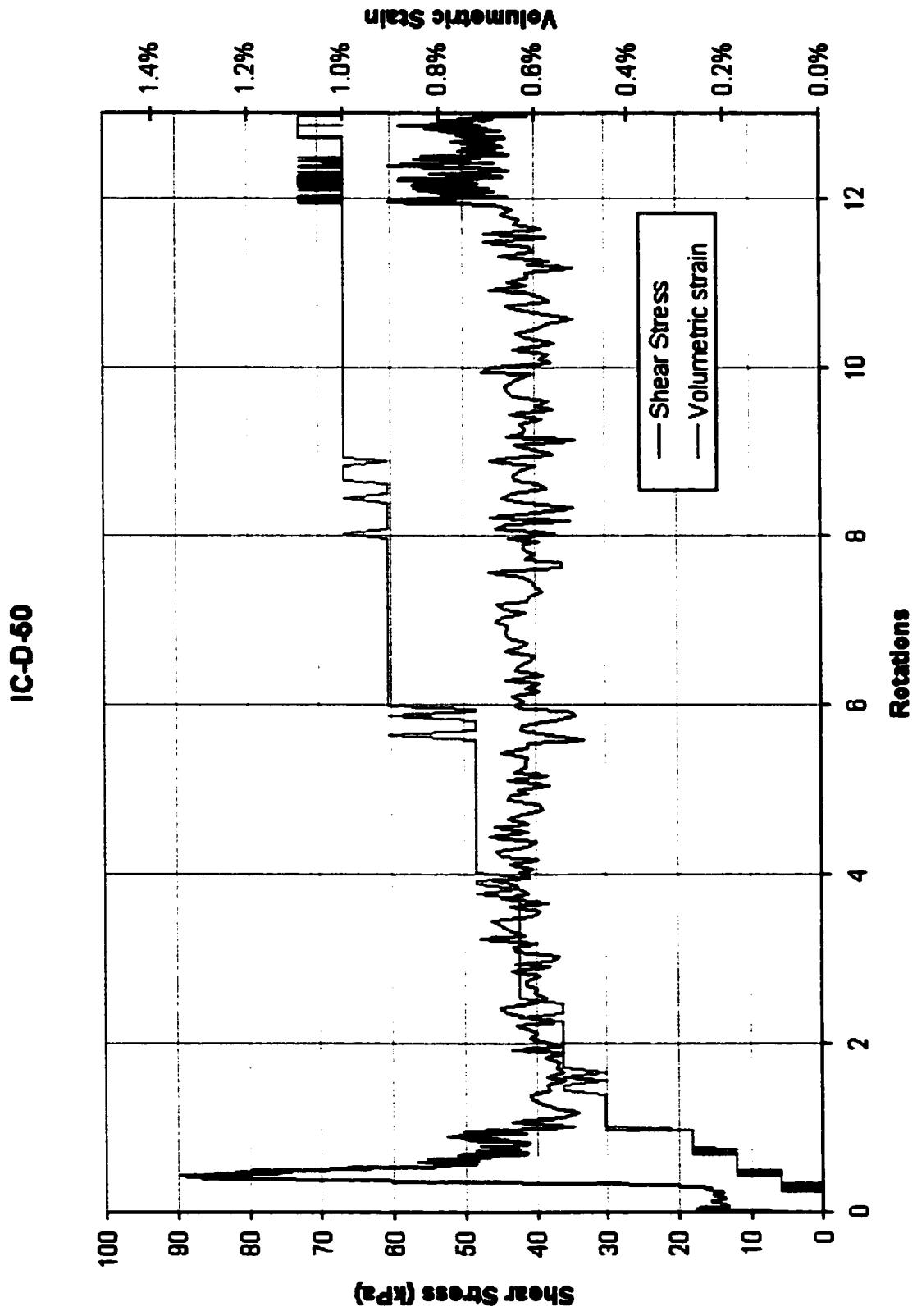
IC-D-60
Shear Stress (kPa)
Volumetric Strain
Rotations
Shear Stress
Volumetric strain
0
10
20
30
40
50
60
70
80
90
100
0.0%
0.2%
0.4%
0.6%
0.8%
1.0%
1.2%
1.4%
0
2
4
6
8
10
12

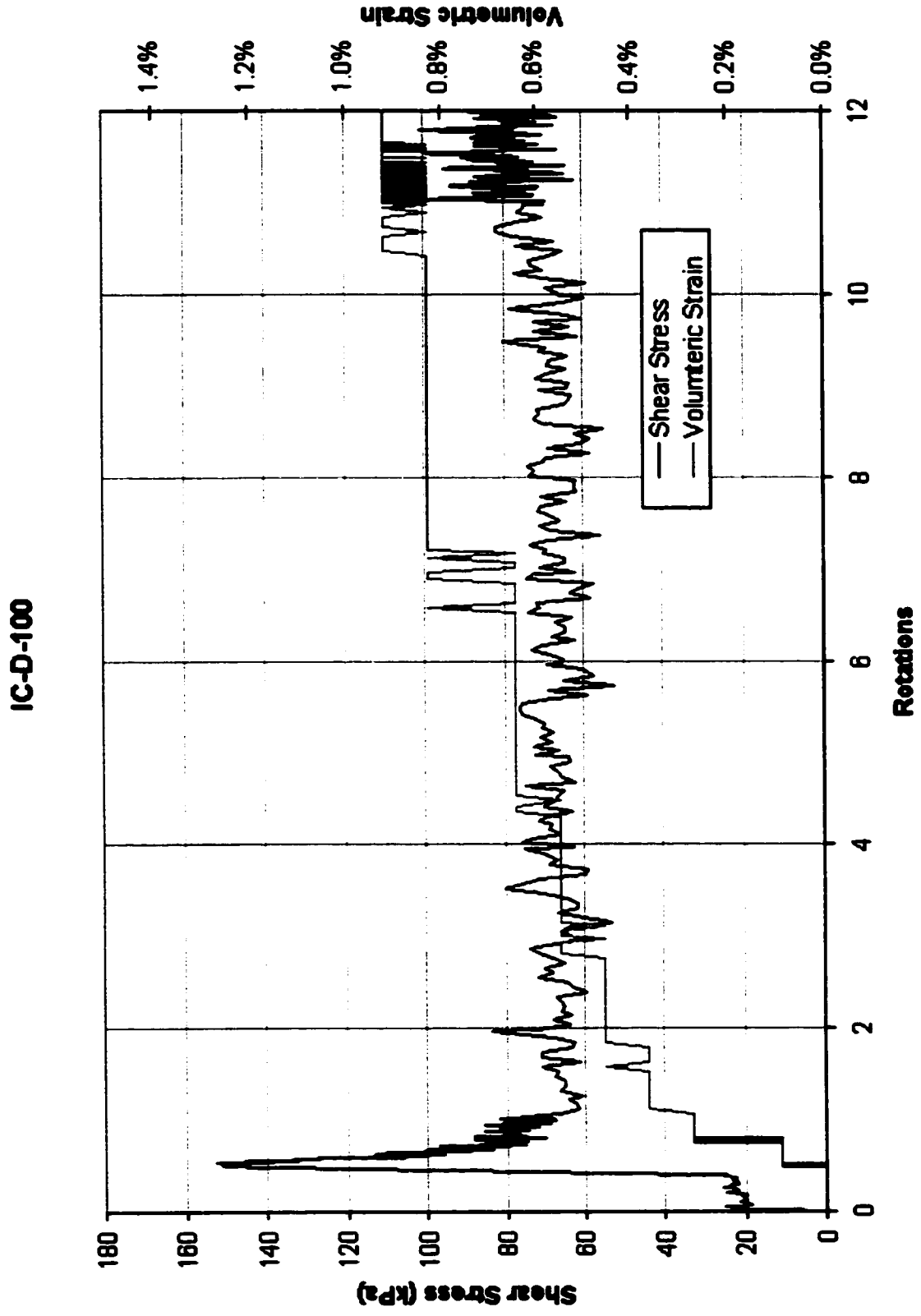
IC-D-100
Shear Stress (kPa)
Volumetric Strain
Rotations
Shear Stress
Volumteric Strain
0
20
40
60
80
100
120
140
160
180
0.0%
0.2%
0.4%
0.6%
0.8%
1.0%
1.2%
1.4%
0
2
4
6
8
10
12

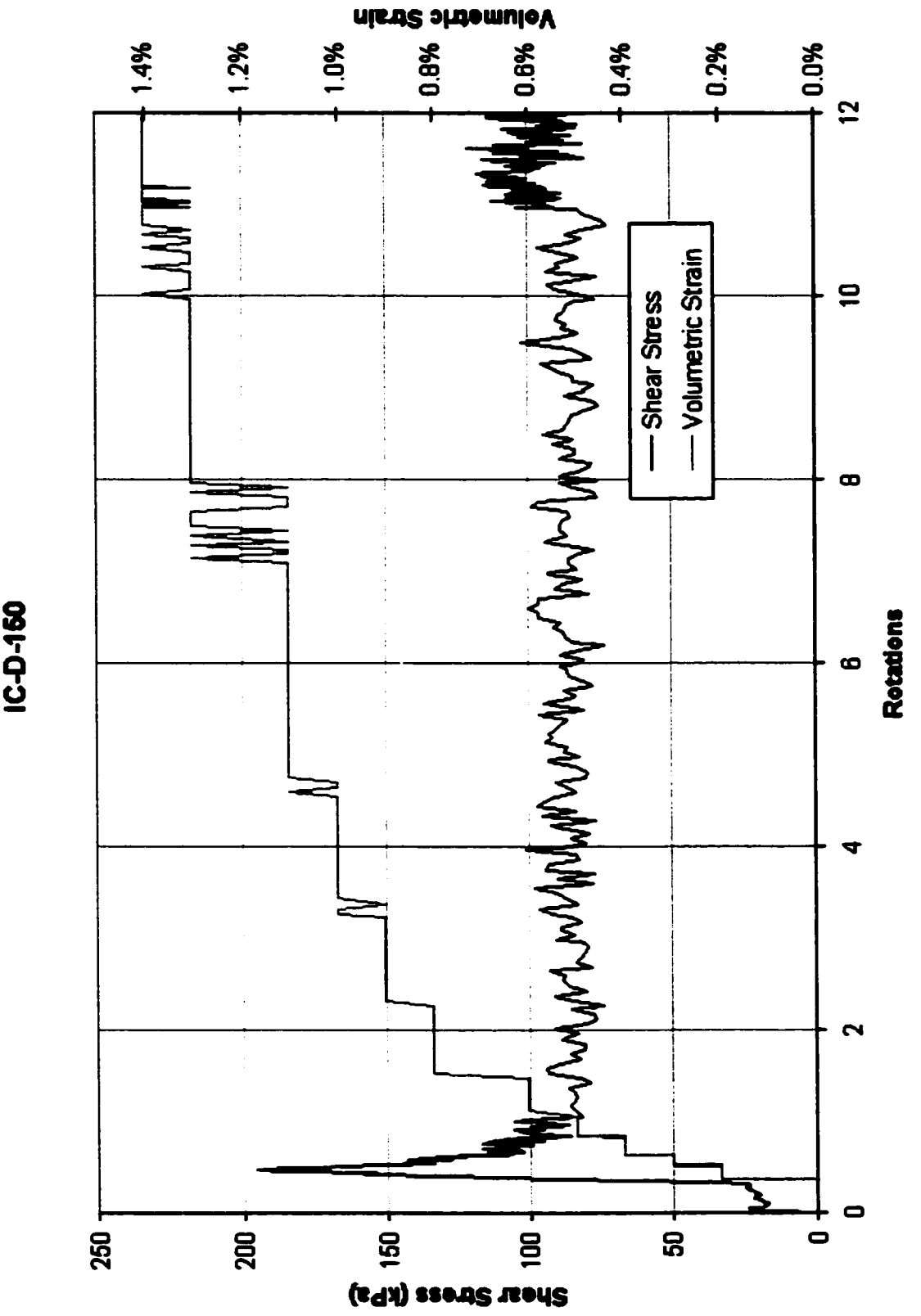
IC-D-160
Shear Stress (kPa)
Volumetric Strain
Rotations
Shear Stress
Volumetric Strain
0
50
100
150
200
250
0.0%
0.2%
0.4%
0.6%
0.8%
1.0%
1.2%
1.4%
0
2
4
6
8
10
12

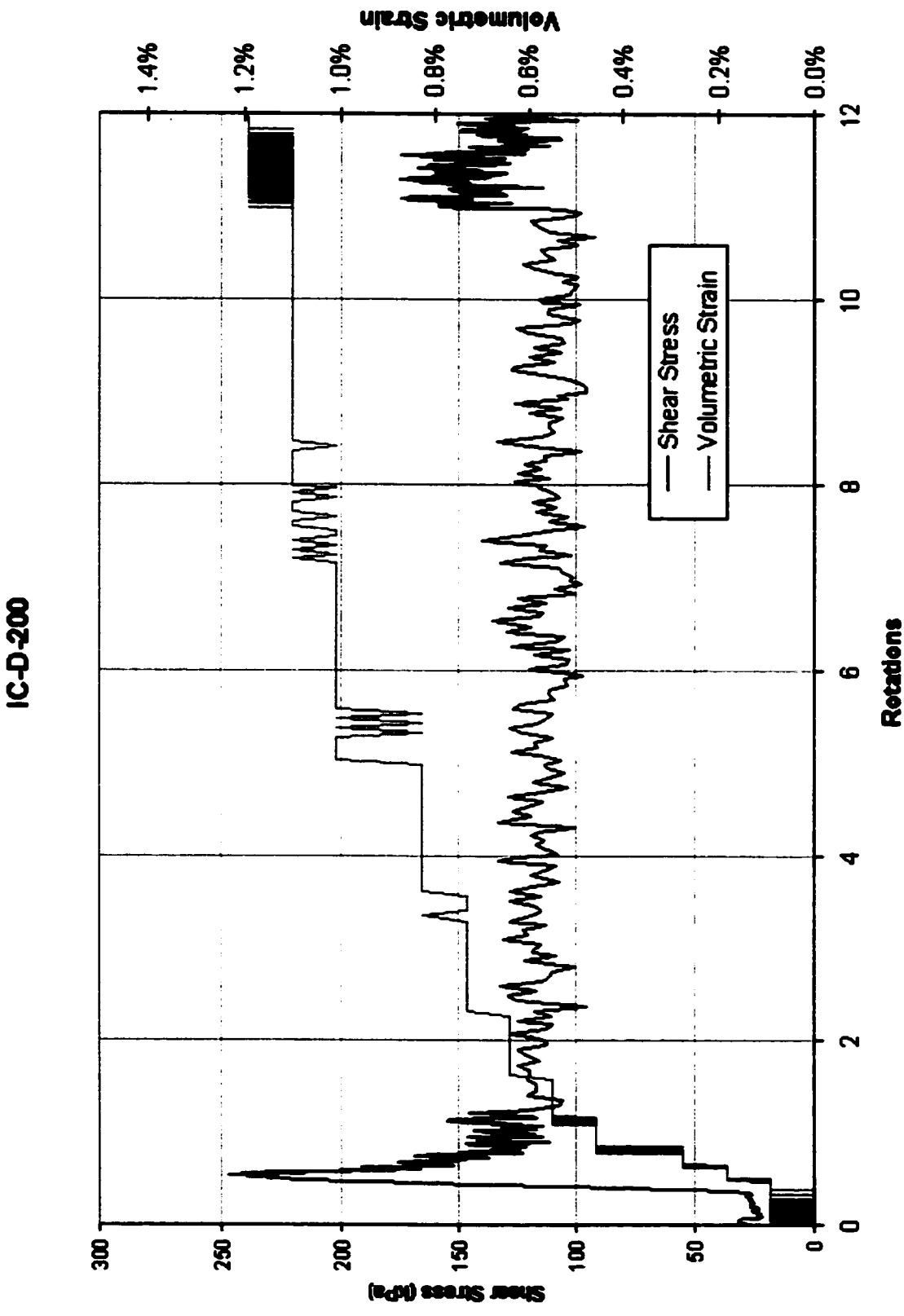
IC-D-200
Shear Stress (kPa)
Volumetric Strain
Rotations
Shear Stress
Volumetric Strain
0
50
100
150
200
250
300
0.0%
0.2%
0.4%
0.6%
0.8%
1.0%
1.2%
1.4%
0
2
4
6
8
10
12

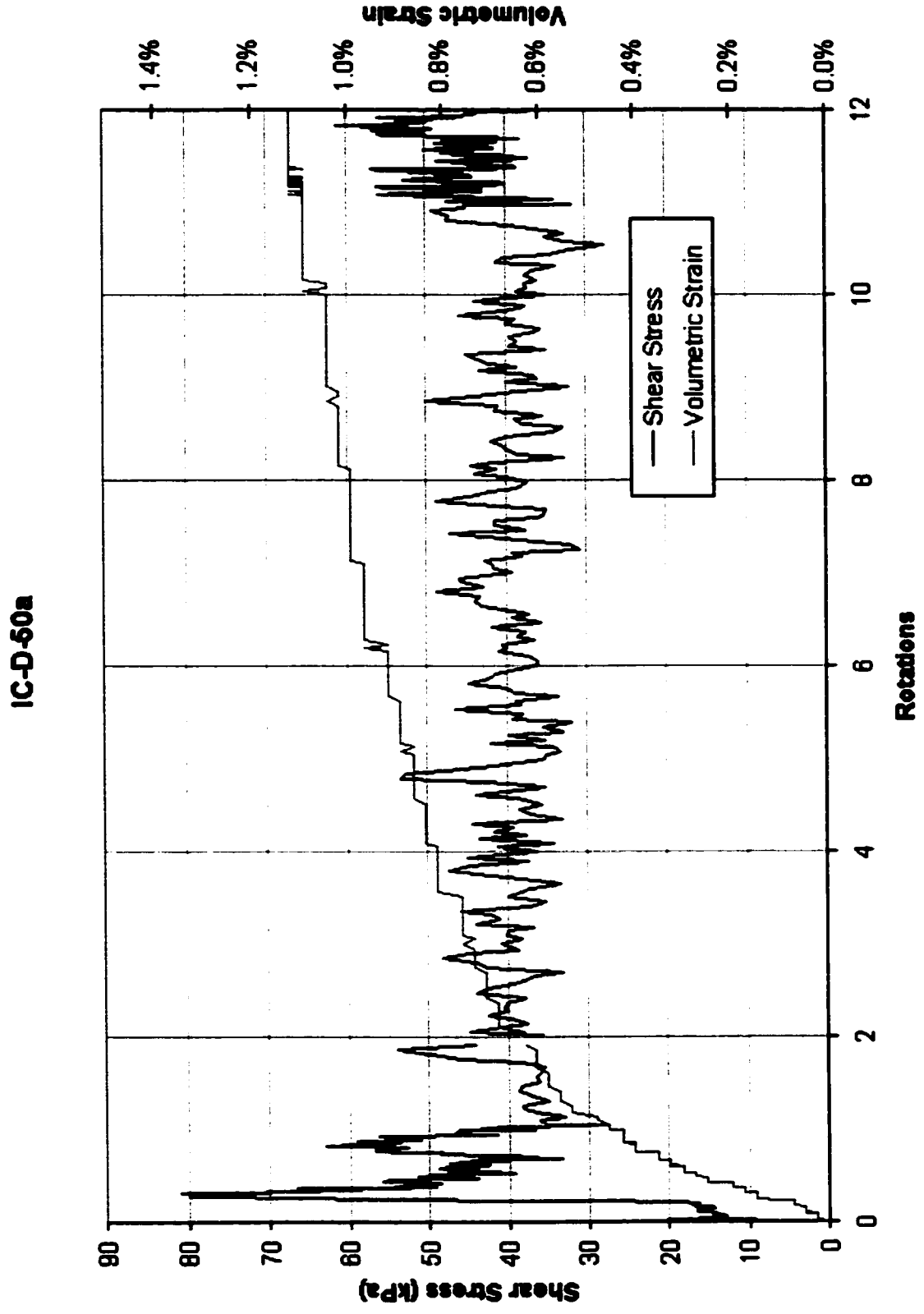
IC-D-60a
Shear Stress (kPa)
Volumetric Strain
Rotations
Shear Stress
Volumetric Strain
0
10
20
30
40
50
60
70
80
90
0.0%
0.2%
0.4%
0.6%
0.8%
1.0%
1.2%
1.4%
0
2
4
6
8
10
12

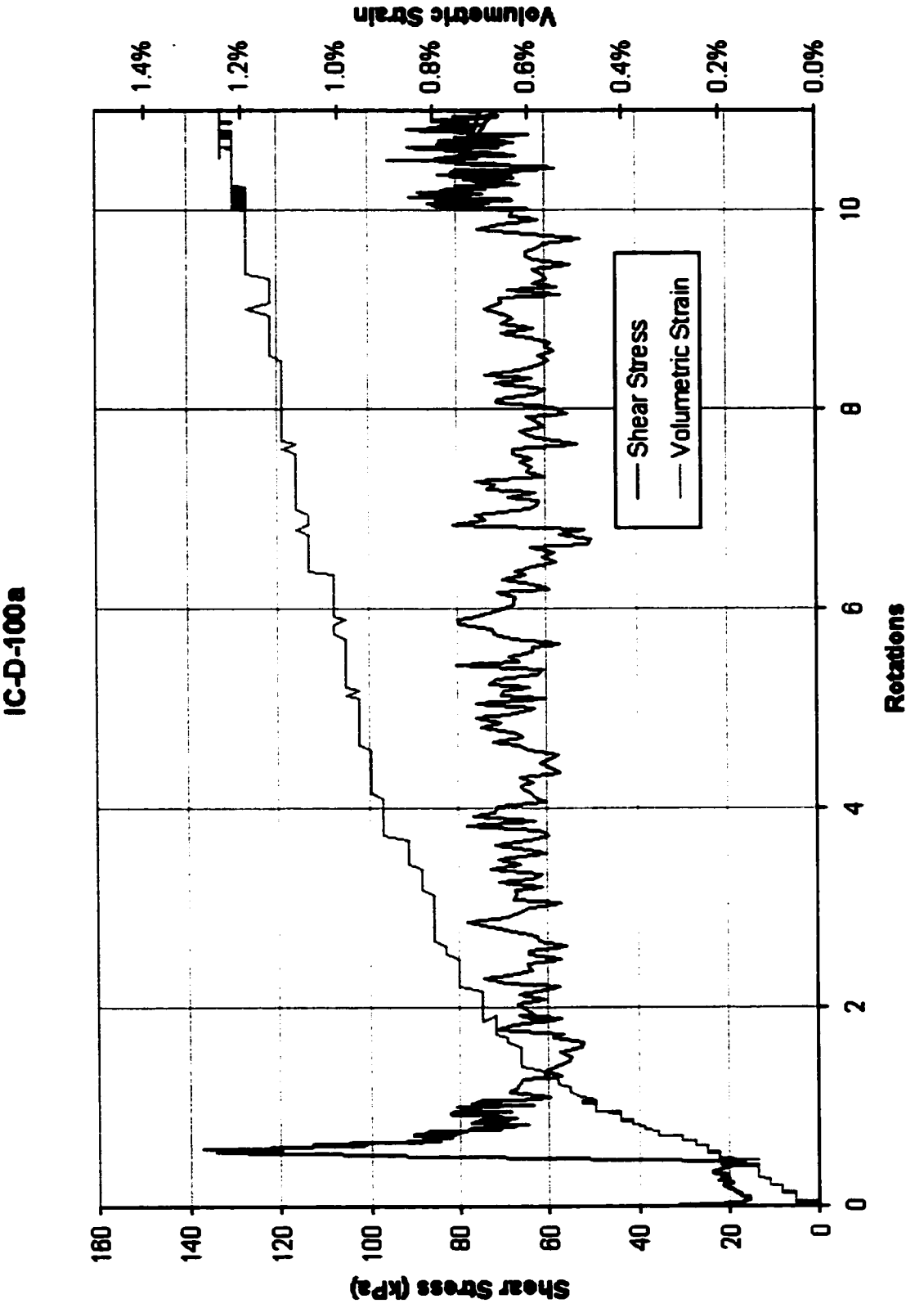
IC-D-100a
Shear Stress (kPa)
Volumetric Strain
Rotations
Shear Stress
Volumetric Strain
0
20
40
60
80
100
120
140
160
0.0%
0.2%
0.4%
0.6%
0.8%
1.0%
1.2%
1.4%
0
2
4
6
8
10

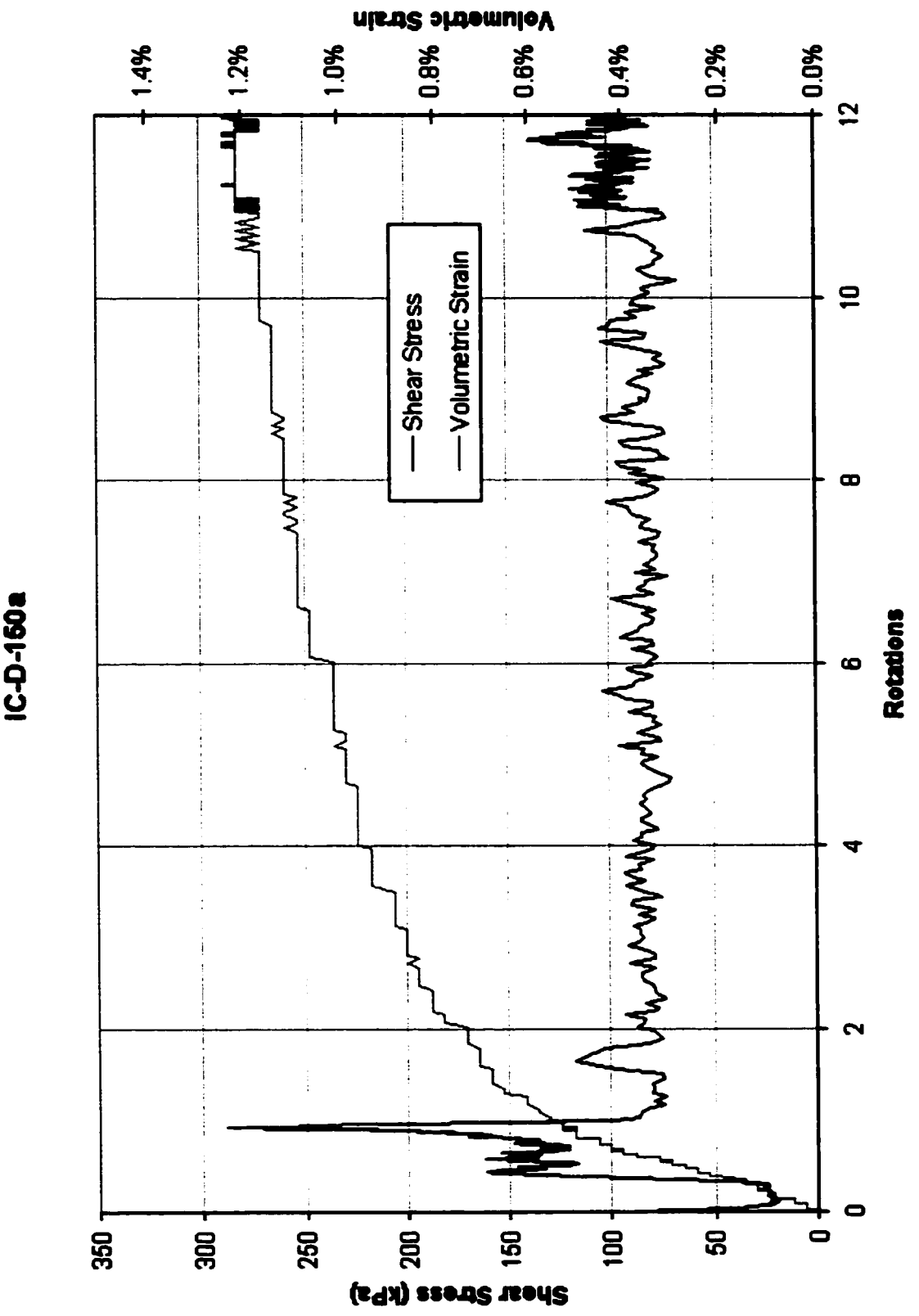
IC-D-150a
Shear Stress (kPa)
Volumetric Strain
Rotations
Shear Stress
Volumetric Strain
0
50
100
150
200
250
300
350
0.0%
0.2%
0.4%
0.6%
0.8%
1.0%
1.2%
1.4%
0
2
4
6
8
10
12

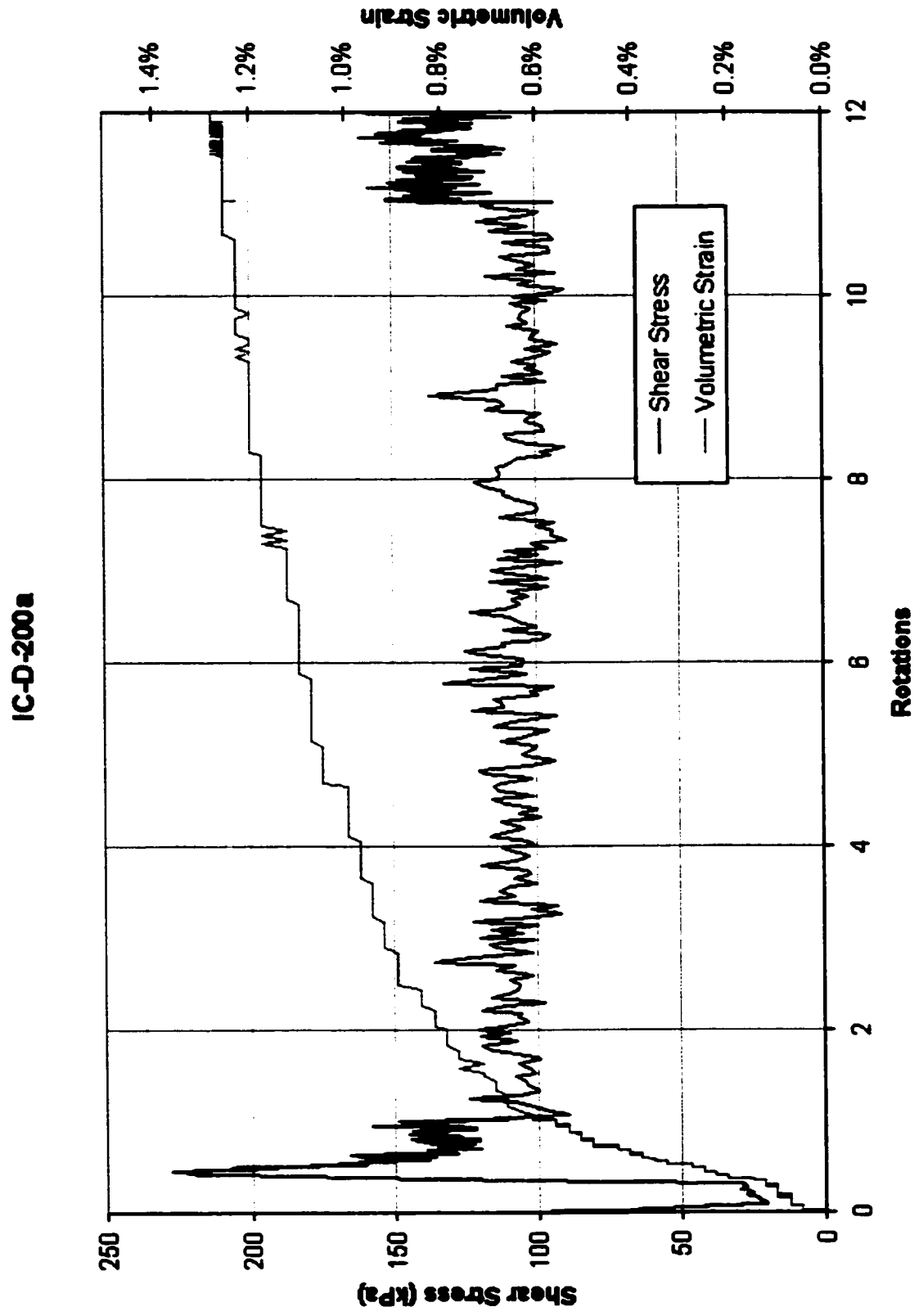
IC-D-200a
Shear Stress (kPa)
Volumetric Strain
Rotations
Shear Stress
Volumetric Strain
0
50
100
150
200
250
0.0%
0.2%
0.4%
0.6%
0.8%
1.0%
1.2%
1.4%
0
2
4
6
8
10
12

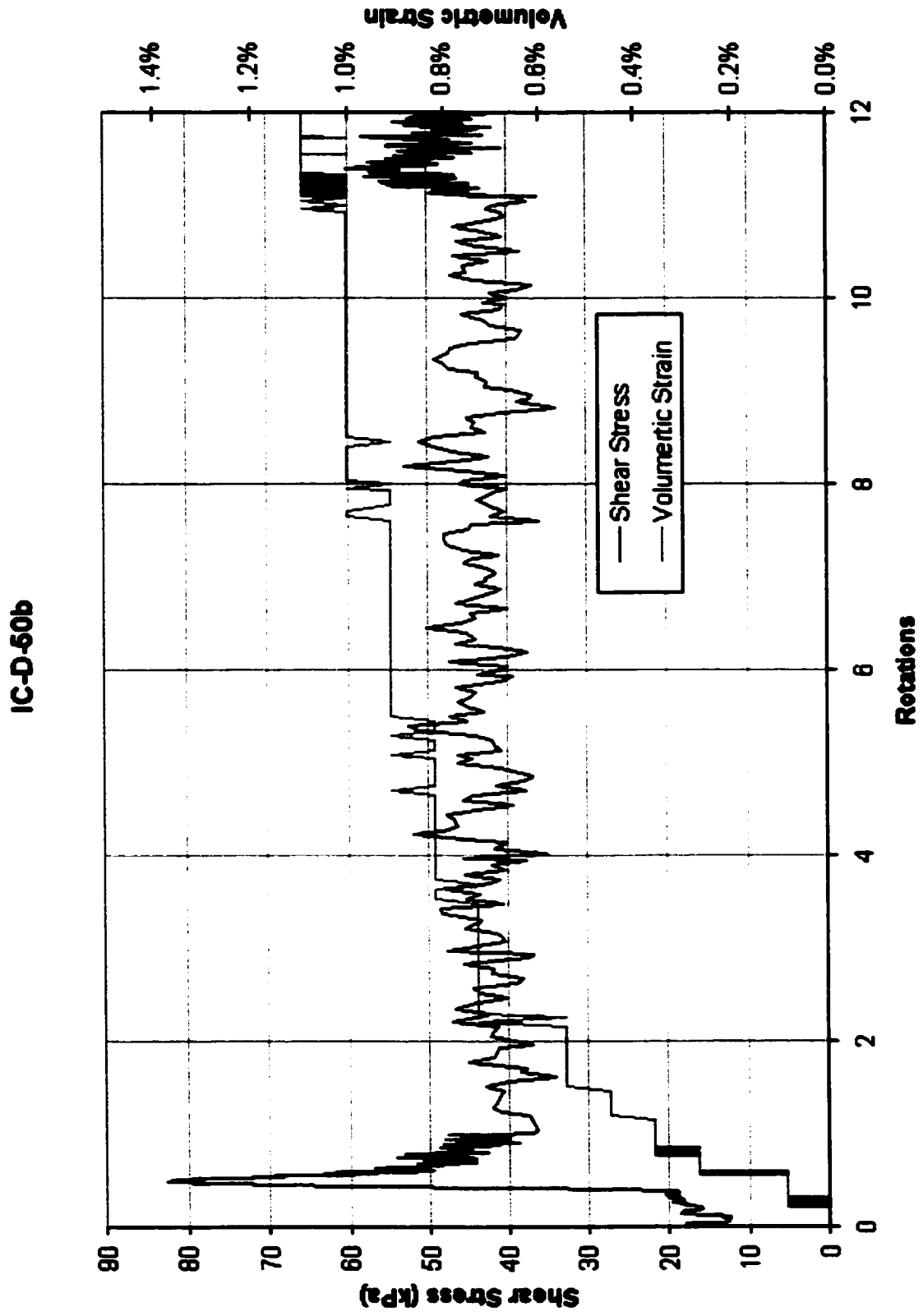
IC-D-60b
Shear Stress (kPa)
Volumetric Strain
Rotations
Shear Stress
Volumetric Strain
0
10
20
30
40
50
60
70
80
90
0.0%
0.2%
0.4%
0.6%
0.8%
1.0%
1.2%
1.4%
0
2
4
6
8
10
12

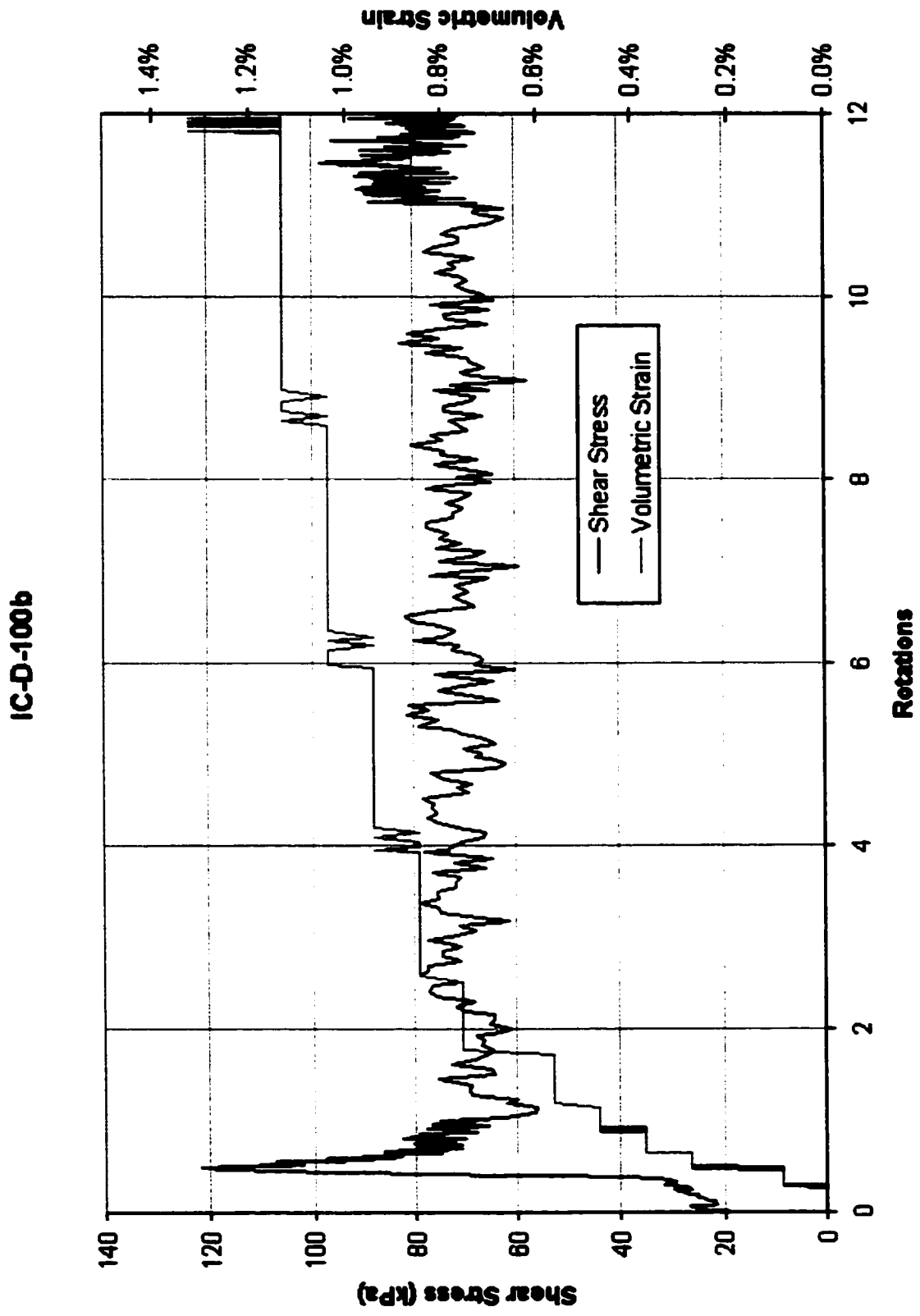
IC-D-100b
Shear Stress (kPa)
Volumetric Strain
Rotations
Shear Stress
Volumetric Strain
0
20
40
60
80
100
120
140
0.0%
0.2%
0.4%
0.8%
0.8%
1.0%
1.2%
1.4%
0
2
4
6
8
10
12

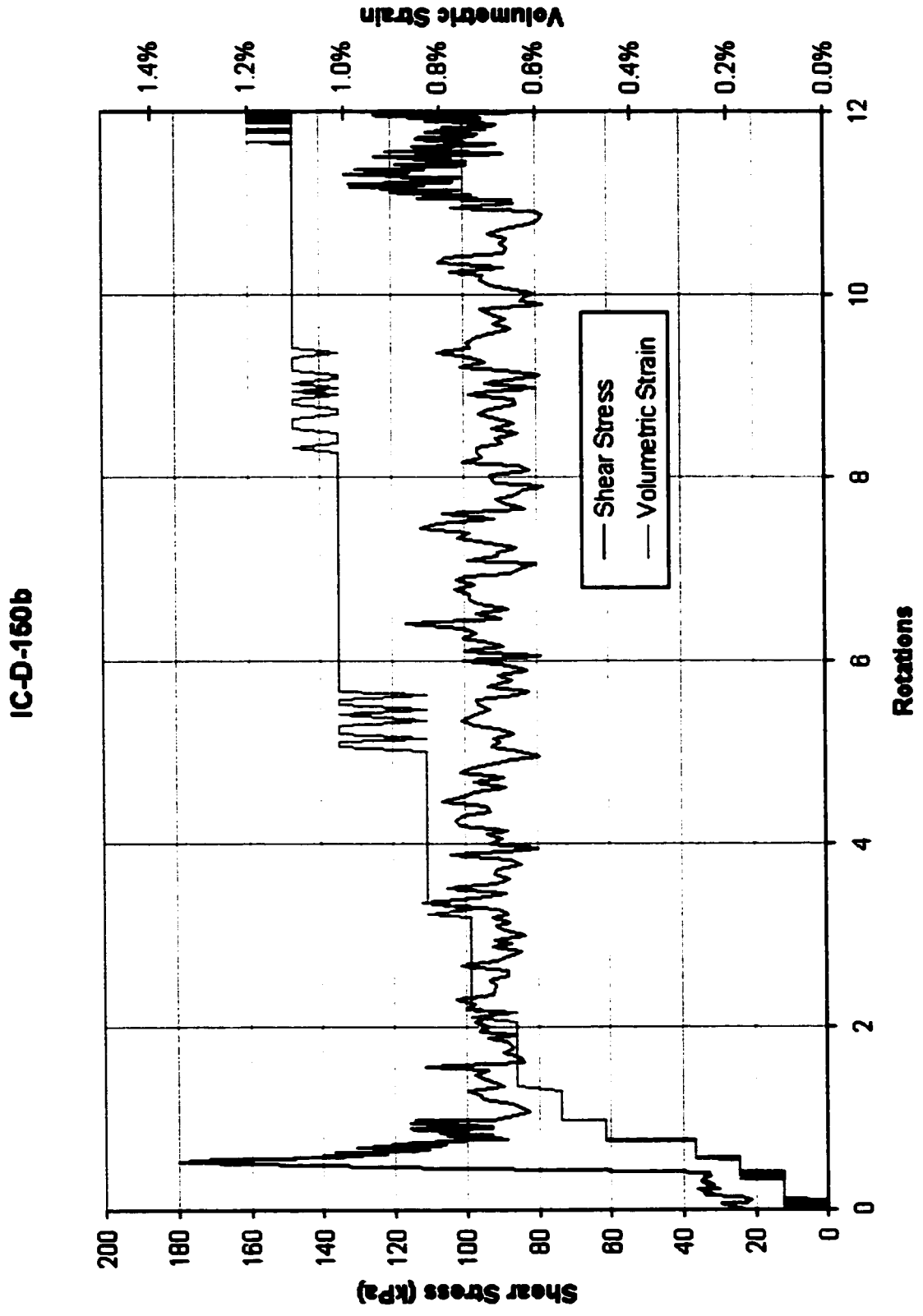
IC-D-160b
Shear Stress (kPa)
Volumetric Strain
Rotations
Shear Stress
Volumetric Strain
0
20
40
60
80
100
120
140
160
180
200
0.0%
0.2%
0.4%
0.6%
0.8%
1.0%
1.2%
1.4%
0
2
4
6
8
10
12

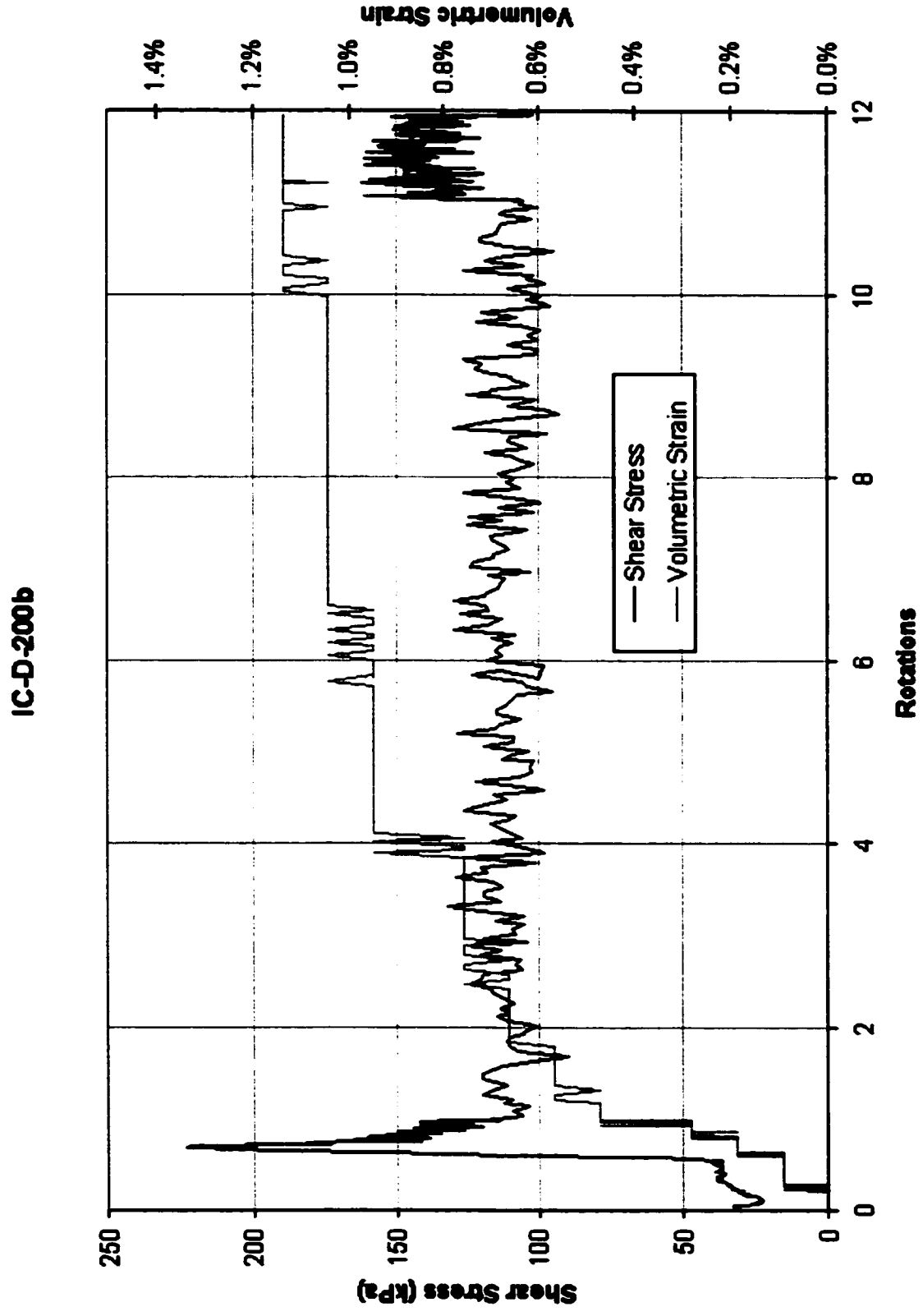
IC-D-200b
Shear Stress (kPa)
Volumetric Strain
Rotations
Shear Stress
Volumetric Strain
0
50
100
150
200
250
0.0%
0.2%
0.4%
0.6%
0.8%
1.0%
1.2%
1.4%
0
2
4
6
8
10
12

Appendix 5: IC-U Triaxial Vane Tests

IC-U-50

Consolidation Pressure 51 kPa

Start of Test	
Dry Density	1.39 g / cm3
Saturated Density	1.87 g / cm3
e	0.91
Dr	0.32
After Consolidation	
Dry Density	1.40 g / cm3
Saturated Density	1.87 g / cm3
e	0.91
Dr	0.34
After Test	
Dry Density	1.40 g / cm3
Saturated Density	1.87 g / cm3
e	0.91
Dr	0.34
B Value	1.00
Peak Strength	
Maximum Shear Strength	37.96 kPa
Effective Stress	26.63 kPa
Residual Strength	
Steady State Shear Strength	5.92 kPa
High Speed Steady State	4.77 kPa
Effective Stress	-1.08 kPa
Vane Speed	
Slow Testing	70.8 deg/min
Fast Testing	1062.6 deg/min

IC-U-100

Consolidation Pressure	100 kPa

Start of Test	
Dry Density	1.38 g / cm3
Saturated Density	1.86 g / cm3
e	0.93
Dr	0.28
After Consolidation	
Dry Density	1.39 g / cm3
Saturated Density	1.87 g / cm3
e	0.91
Dr	0.32
After Test	
Dry Density	1.39 g / cm3
Saturated Density	1.87 g / cm3
e	0.91
Dr	0.32
B Value	1.00
Peak Strength	
Maximum Shear Strength	63.27 kPa
Effective Stress	60.19 kPa
Residual Strength	
Steady State Shear Strength	8.36 kPa
High Speed Steady State	7.48 kPa
Effective Stress	2.90 kPa
Vane Speed	
Slow Testing	60 deg/min
Fast Testing	992.4 deg/min

IC-U-150

Consolidation Pressure	154 kPa

Start of Test	
Dry Density	1.40 g / cm3
Saturated Density	1.87 g / cm3
e	0.91
Dr	0.34
After Consolidation	
Dry Density	1.41 g / cm3
Saturated Density	1.88 g / cm3
e	0.89
Dr	0.39
After Test	
Dry Density	1.41 g / cm3
Saturated Density	1.88 g / cm3
e	0.89
Dr	0.39
B Value	0.97
Peak Strength	
Maximum Shear Strength	152.45 kPa
Effective Stress	119.15 kPa
Residual Strength	
Steady State Shear Strength	19.56 kPa
High Speed Steady State	16.56 kPa
Effective Stress	23.99 kPa
Vane Speed	
Slow Testing	60 deg/min
Fast Testing	1062.6 deg/min

IC-U-200

Consolidation Pressure	203 kPa

Start of Test	
Dry Density	1.40 g / cm3
Saturated Density	1.88 g / cm3
e	0.90
Dr	0.35
After Consolidation	
Dry Density	1.42 g / cm3
Saturated Density	1.89 g / cm3
e	0.88
Dr	0.42
After Test	
Dry Density	1.42 g / cm3
Saturated Density	1.89 g / cm3
e	0.88
Dr	0.42
B Value	0.95
Peak Strength	
Maximum Shear Strength	136.89 kPa
Effective Stress	141.84 kPa
Residual Strength	
Steady State Shear Strength	19.86 kPa
High Speed Steady State	15.86 kPa
Effective Stress	29.03 kPa
Vane Speed	
Slow Testing	60 deg/min
Fast Testing	1062.6 deg/min

IC-U-50a

Consolidation Pressure 48 kPa

Start of Test	
Dry Density	1.36 g / cm3
Saturated Density	1.85 g / cm3
e	0.95
Dr	0.22
After Consolidation	
Dry Density	1.37 g / cm3
Saturated Density	1.86 g / cm3
e	0.94
Dr	0.25
After Test	
Dry Density	1.37 g / cm3
Saturated Density	1.86 g / cm3
e	0.94
Dr	0.25
B Value	1.00
Peak Strength	
Maximum Shear Strength	38.65 kPa
Effective Stress	25.90 kPa
Residual Strength	
Steady State Shear Strength	7.16 kPa
High Speed Steady State	6.16 kPa
Effective Stress	-0.85 kPa
Vane Speed	
Slow Testing	105 deg/min
Fast Testing	1062.6 deg/min

IC-U-100a

Consolidation Pressure	94 kPa

Start of Test	
Dry Density	1.34 g / cm3
Saturated Density	1.83 g / cm3
e	0.99
Dr	0.11
After Consolidation	
Dry Density	1.36 g / cm3
Saturated Density	1.85 g / cm3
e	0.96
Dr	0.20
After Test	
Dry Density	1.36 g / cm3
Saturated Density	1.85 g / cm3
e	0.96
Dr	0.20
B Value	0.88
Peak Strength	
Maximum Shear Strength	97.48 kPa
Effective Stress	73.43 kPa
Residual Strength	
Steady State Shear Strength	6.06 kPa
High Speed Steady State	3.66 kPa
Effective Stress	9.30 kPa
Vane Speed	
Slow Testing	81 deg/min
Fast Testing	1005 deg/min

IC-U-150a

Consolidation Pressure 148 kPa

Start of Test	
Dry Density	1.35 g / cm3
Saturated Density	1.84 g / cm3
e	0.97
Dr	0.17
After Consolidation	
Dry Density	1.37 g / cm3
Saturated Density	1.86 g / cm3
e	0.94
Dr	0.24
After Test	
Dry Density	1.37 g / cm3
Saturated Density	1.86 g / cm3
e	0.94
Dr	0.24
B Value	0.92
Peak Strength	
Maximum Shear Strength	125.44 kPa
Effective Stress	102.01 kPa
Residual Strength	
Steady State Shear Strength	13.26 kPa
High Speed Steady State	12.56 kPa
Effective Stress	14.00 kPa
Vane Speed	
Slow Testing	60 deg/min
Fast Testing	1062.6 deg/min

IC-U-50b

Consolidation Pressure 47 kPa

Start of Test	
Dry Density	1.39 g / cm3
Saturated Density	1.87 g / cm3
e	0.91
Dr	0.32
After Consolidation	
Dry Density	1.44 g / cm3
Saturated Density	1.90 g / cm3
e	0.85
Dr	0.50
After Test	
Dry Density	1.44 g / cm3
Saturated Density	1.90 g / cm3
e	0.85
Dr	0.50
B Value	0.99
Peak Strength	
Maximum Shear Strength	66.82 kPa
Effective Stress	37.17 kPa
Residual Strength	
Steady State Shear Strength	8.16 kPa
High Speed Steady State	6.56 kPa
Effective Stress	-0.25 kPa
Vane Speed	
Slow Testing	90.6 deg/min
Fast Testing	1062.6 deg/min

IC-U-100b

Consolidation Pressure	99 kPa

Start of Test	
Dry Density	1.39 g / cm3
Saturated Density	1.87 g / cm3
e	0.91
Dr	0.33
After Consolidation	
Dry Density	1.41 g / cm3
Saturated Density	1.88 g / cm3
e	0.89
Dr	0.40
After Test	
Dry Density	1.41 g / cm3
Saturated Density	1.88 g / cm3
e	0.89
Dr	0.40
B Value	1.00
Peak Strength	
Maximum Shear Strength	80.28 kPa
Effective Stress	68.18 kPa
Residual Strength	
Steady State Shear Strength	10.36 kPa
High Speed Steady State	8.26 kPa
Effective Stress	7.45 kPa
Vane Speed	
Slow Testing	84 deg/min
Fast Testing	1062.6 deg/min

IC-U-150b

Consolidation Pressure	153 kPa

Start of Test	
Dry Density	1.40 g / cm3
Saturated Density	1.87 g / cm3
e	0.91
Dr	0.34
After Consolidation	
Dry Density	1.41 g / cm3
Saturated Density	1.88 g / cm3
e	0.88
Dr	0.40
After Test	
Dry Density	1.41 g / cm3
Saturated Density	1.88 g / cm3
e	0.88
Dr	0.40
B Value	0.99
Peak Strength	
Maximum Shear Strength	143.99 kPa
Effective Stress	118.58 kPa
Residual Strength	
Steady State Shear Strength	18.66 kPa
High Speed Steady State	16.56 kPa
Effective Stress	23.67 kPa
Vane Speed	
Slow Testing	60 deg/min
Fast Testing	1062.6 deg/min

IC-U-200b

Consolidation Pressure	203 kPa

Start of Test	
Dry Density	1.39 g / cm3
Saturated Density	1.87 g / cm3
e	0.92
Dr	0.30
After Consolidation	
Dry Density	1.41 g / cm3
Saturated Density	1.88 g / cm3
e	0.89
Dr	0.38
After Test	
Dry Density	1.41 g / cm3
Saturated Density	1.88 g / cm3
e	0.89
Dr	0.38
B Value	0.97
Peak Strength	
Maximum Shear Strength	158.60 kPa
Effective Stress	149.84 kPa
Residual Strength	
Steady State Shear Strength	31.96 kPa
High Speed Steady State	26.96 kPa
Effective Stress	43.44 kPa
Vane Speed	
Slow Testing	60 deg/min
Fast Testing	1062.6 deg/min

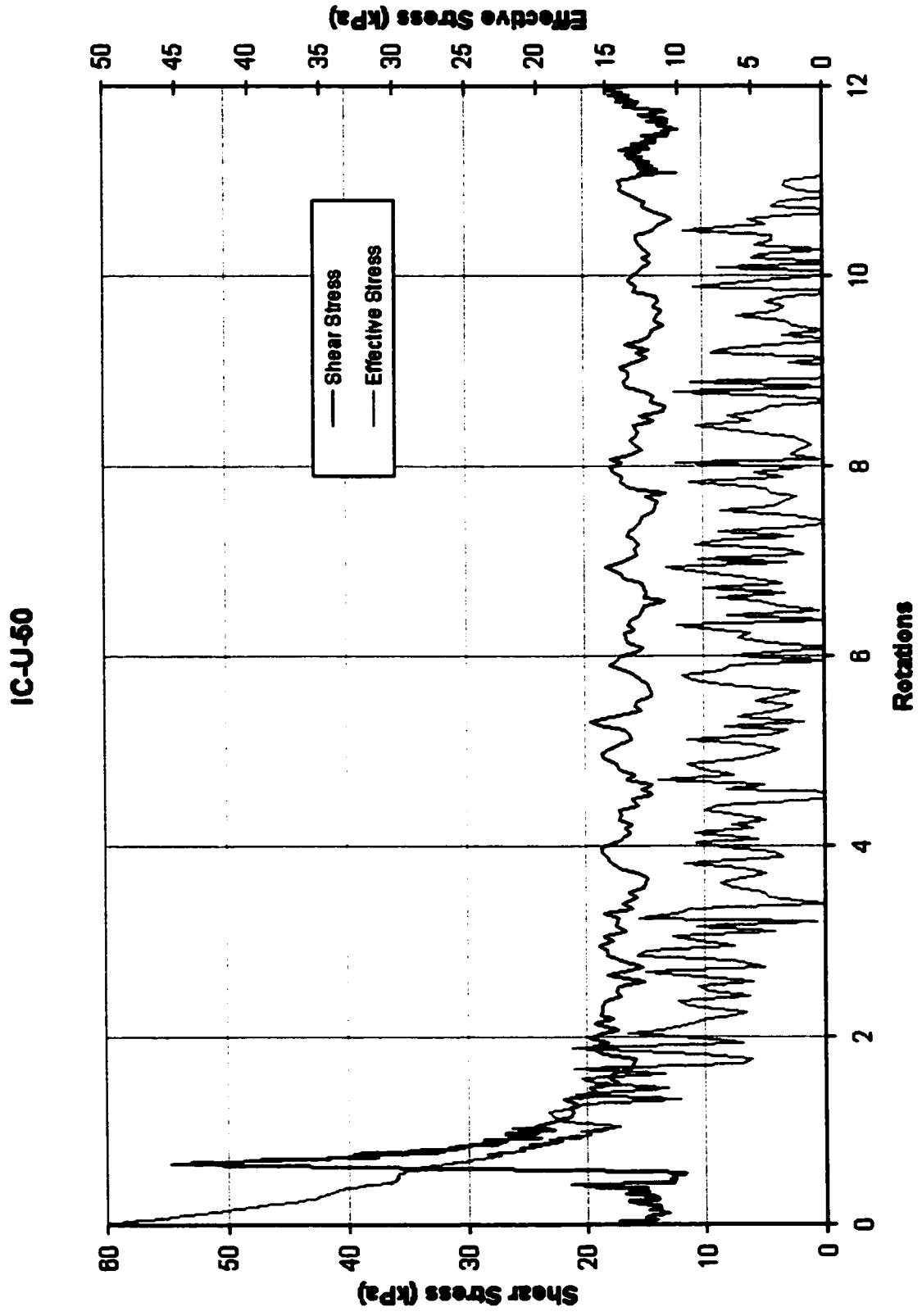
IC-U-60
Shear Stress (kPa)
Effective Stress (kPa)
Rotations
Shear Stress
Effective Stress
0
10
20
30
40
50
60
0
5
10
15
20
25
30
35
40
45
50
0
2
4
8
10
12

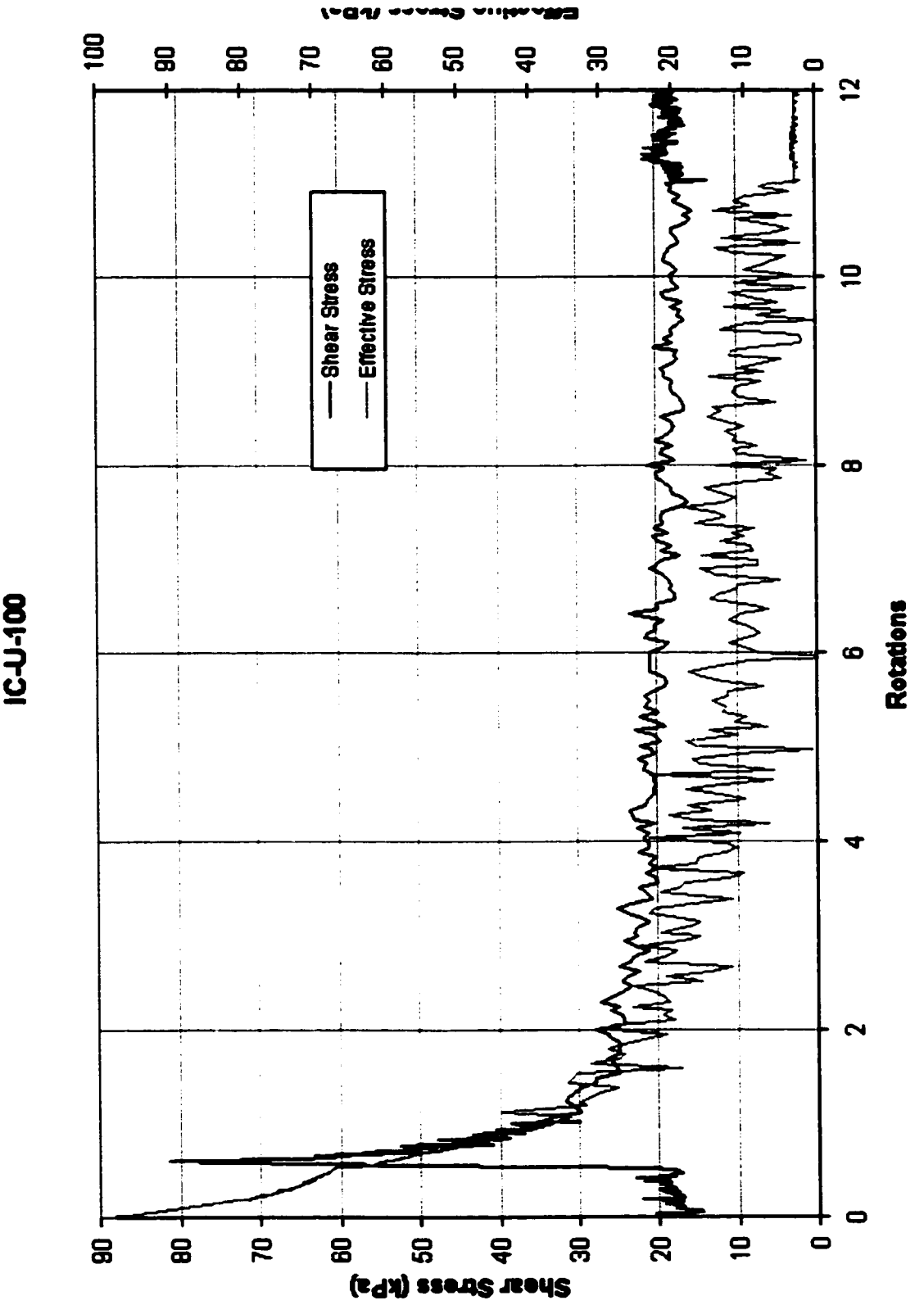
IC-U-100
Shear Stress (kPa)
Rotations
Shear Stress
Effective Stress
0
10
20
30
40
50
60
70
80
90
100
0
2
4
6
8
10
12

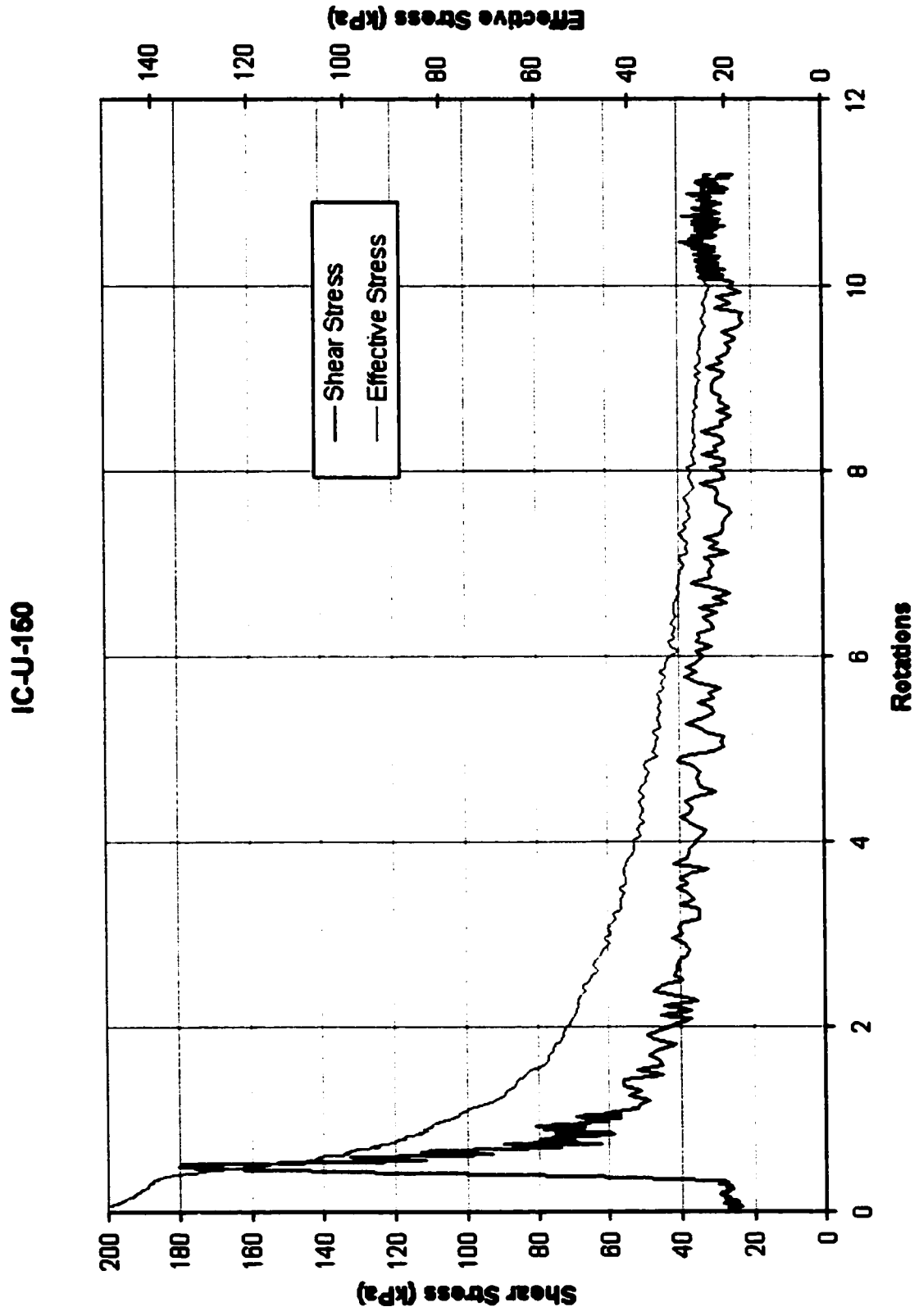
IC-U-160
Shear Stress (kPa)
Effective Stress (kPa)
Rotations
Shear Stress
Effective Stress
0
20
40
60
80
100
120
140
160
180
200
0
2
4
6
8
10
12

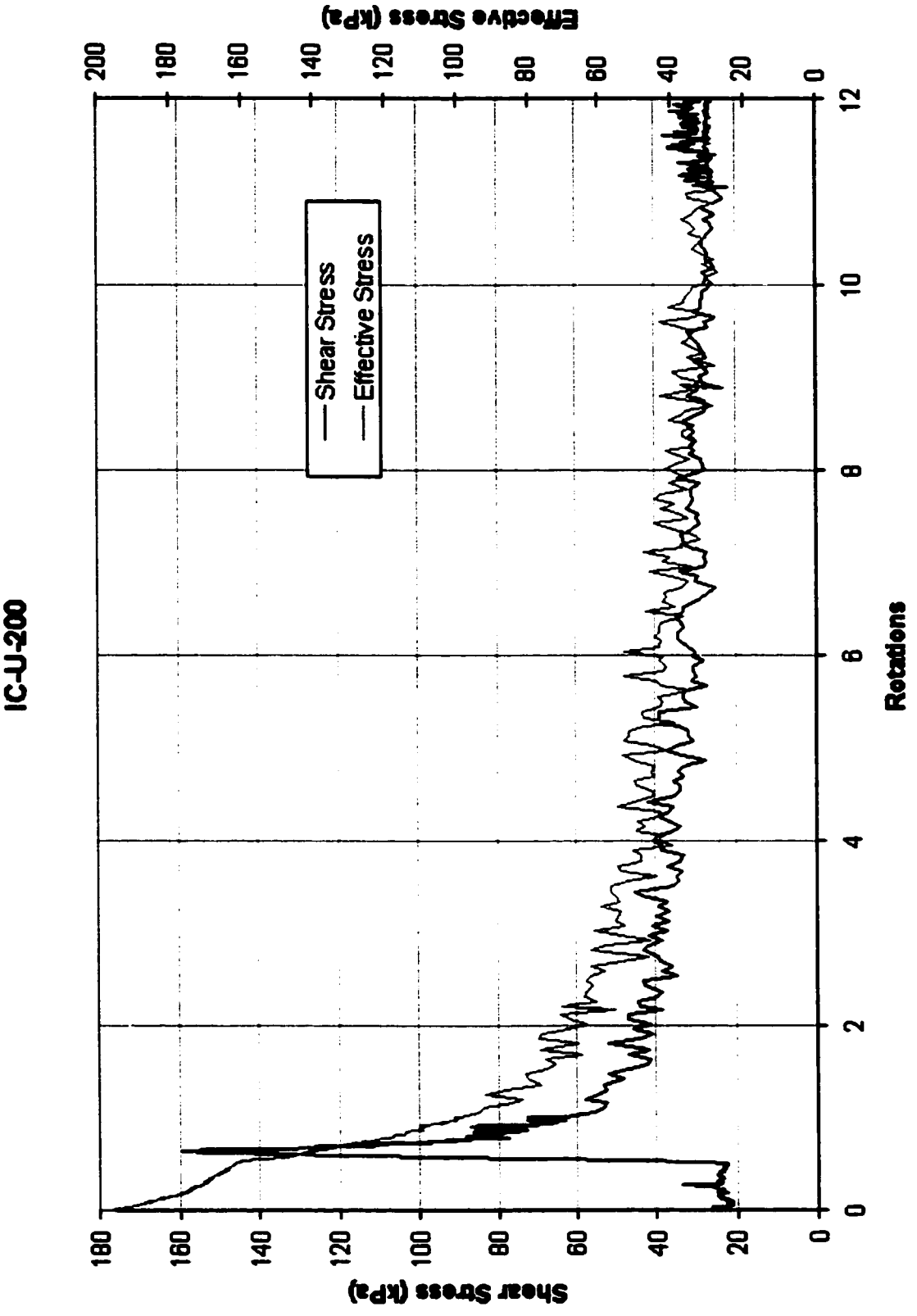
IC-U-200
Shear Stress (kPa)
Effective Stress (kPa)
Rotations
Shear Stress
Effective Stress
0
20
40
60
80
100
120
140
160
180
200
0
2
4
6
8
10
12

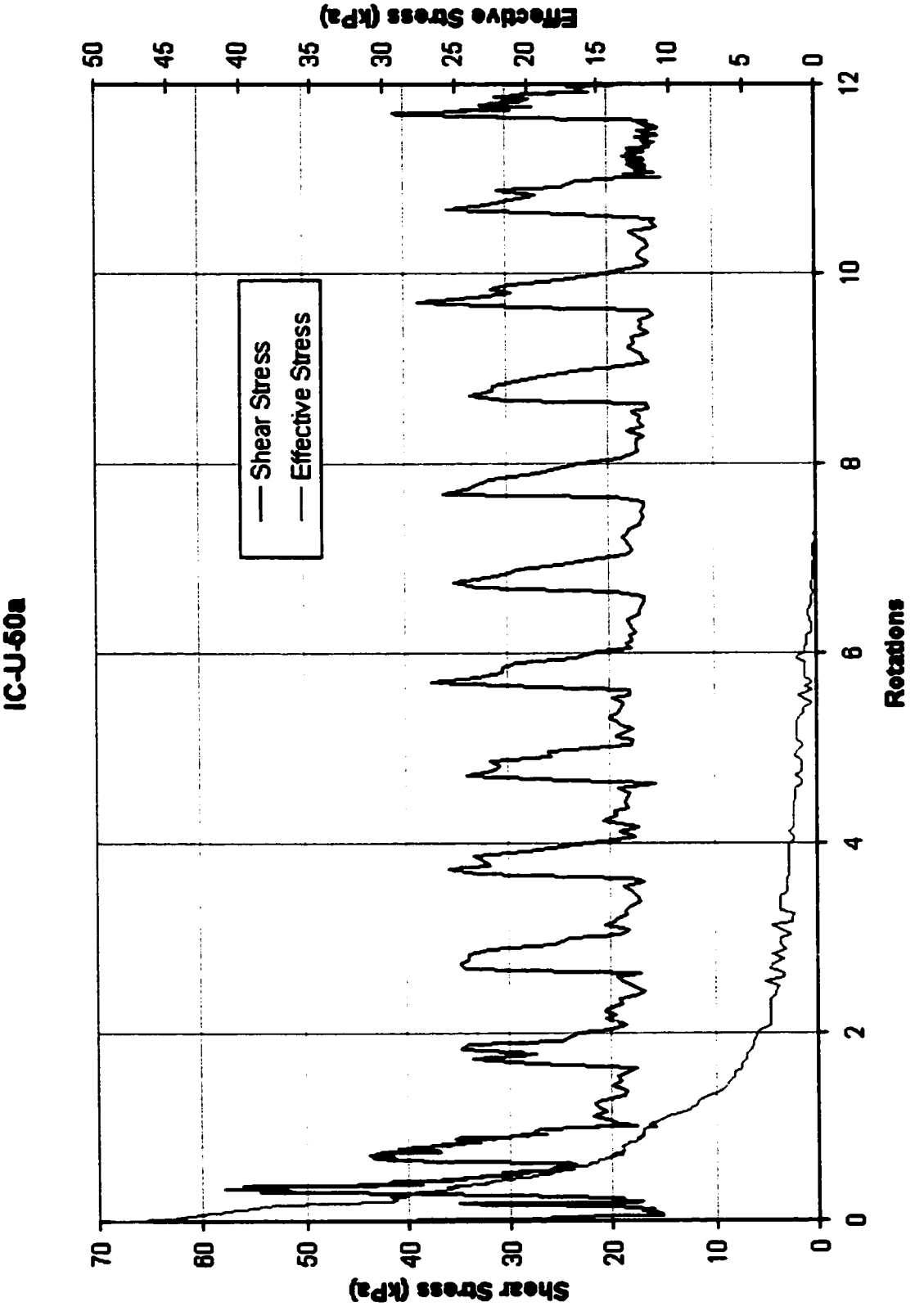
IC-U-50a
Shear Stress (kPa)
Effective Stress (kPa)
Rotations
Shear Stress
Effective Stress
0
10
20
30
40
50
60
70
0
5
10
15
20
25
30
35
40
45
50
0
2
4
6
8
10
12

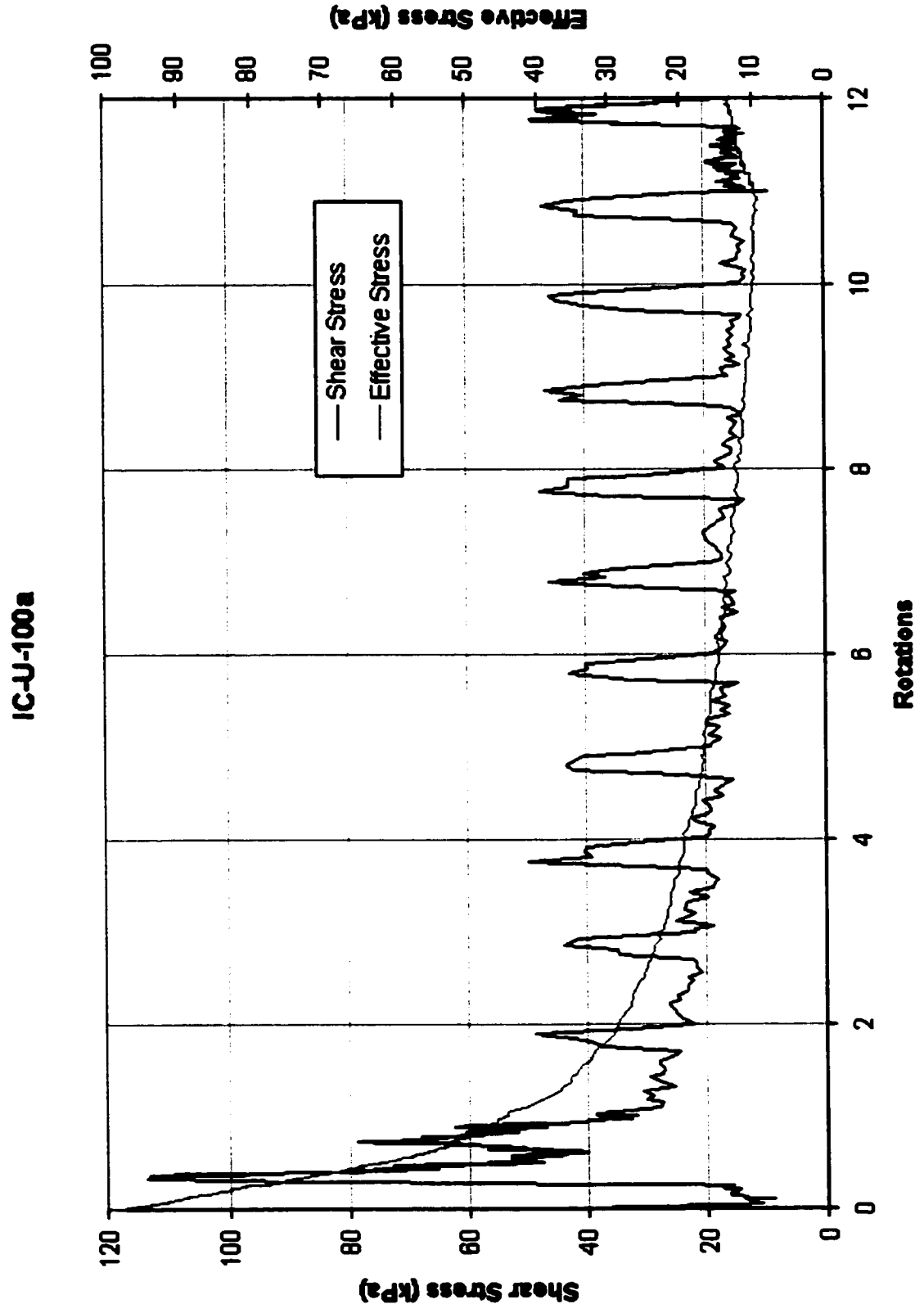
IC-U-100a
Shear Stress (kPa)
Effective Stress (kPa)
Rotations
Shear Stress
Effective Stress
0
20
40
60
80
100
120
0
10
20
30
40
50
60
70
80
90
100
0
2
4
6
8
10
12

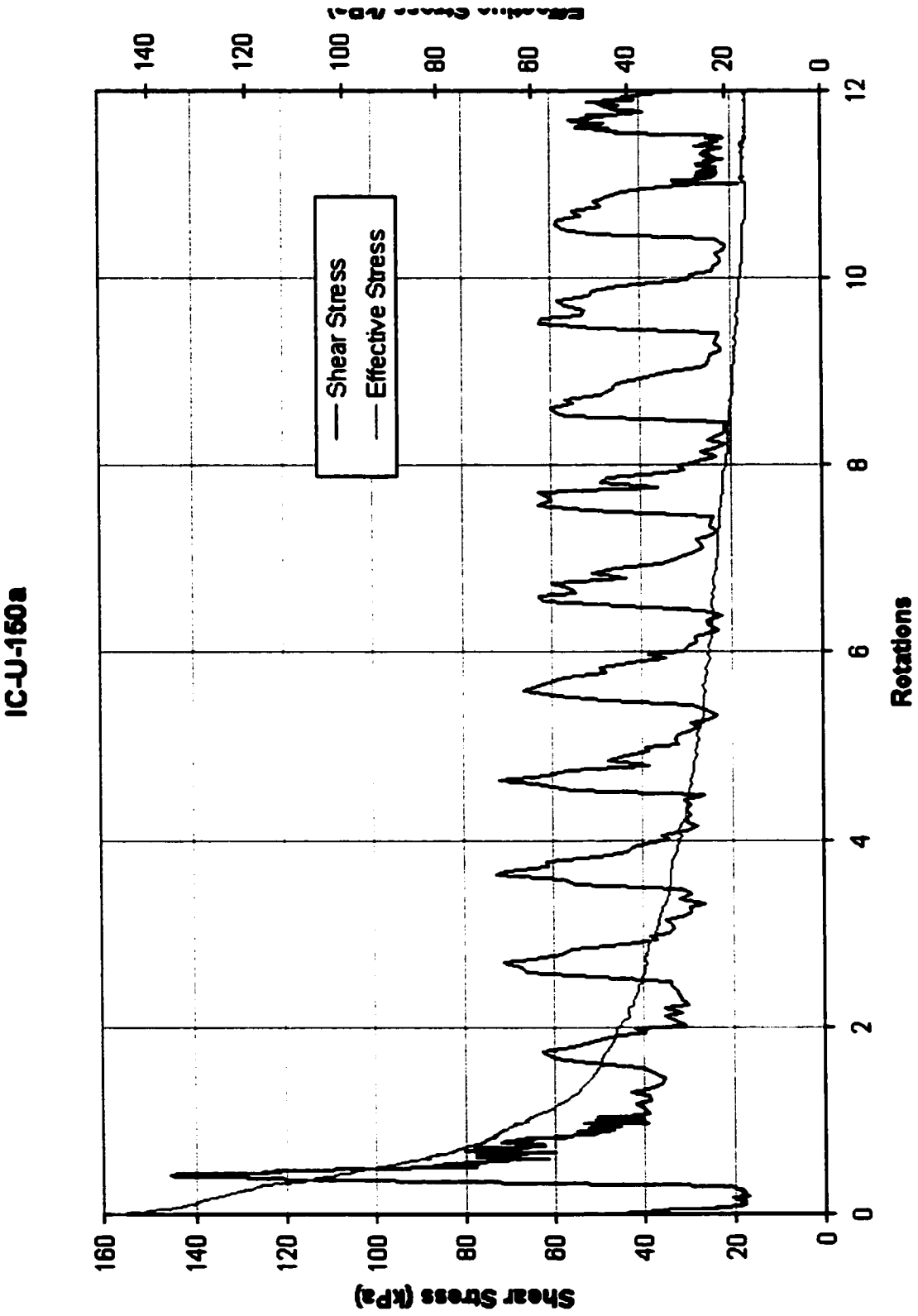
IC-U-150a
Shear Stress (kPa)
Rotations
Shear Stress
Effective Stress
0
20
40
60
80
100
120
140
160
0
2
4
6
8
10
12

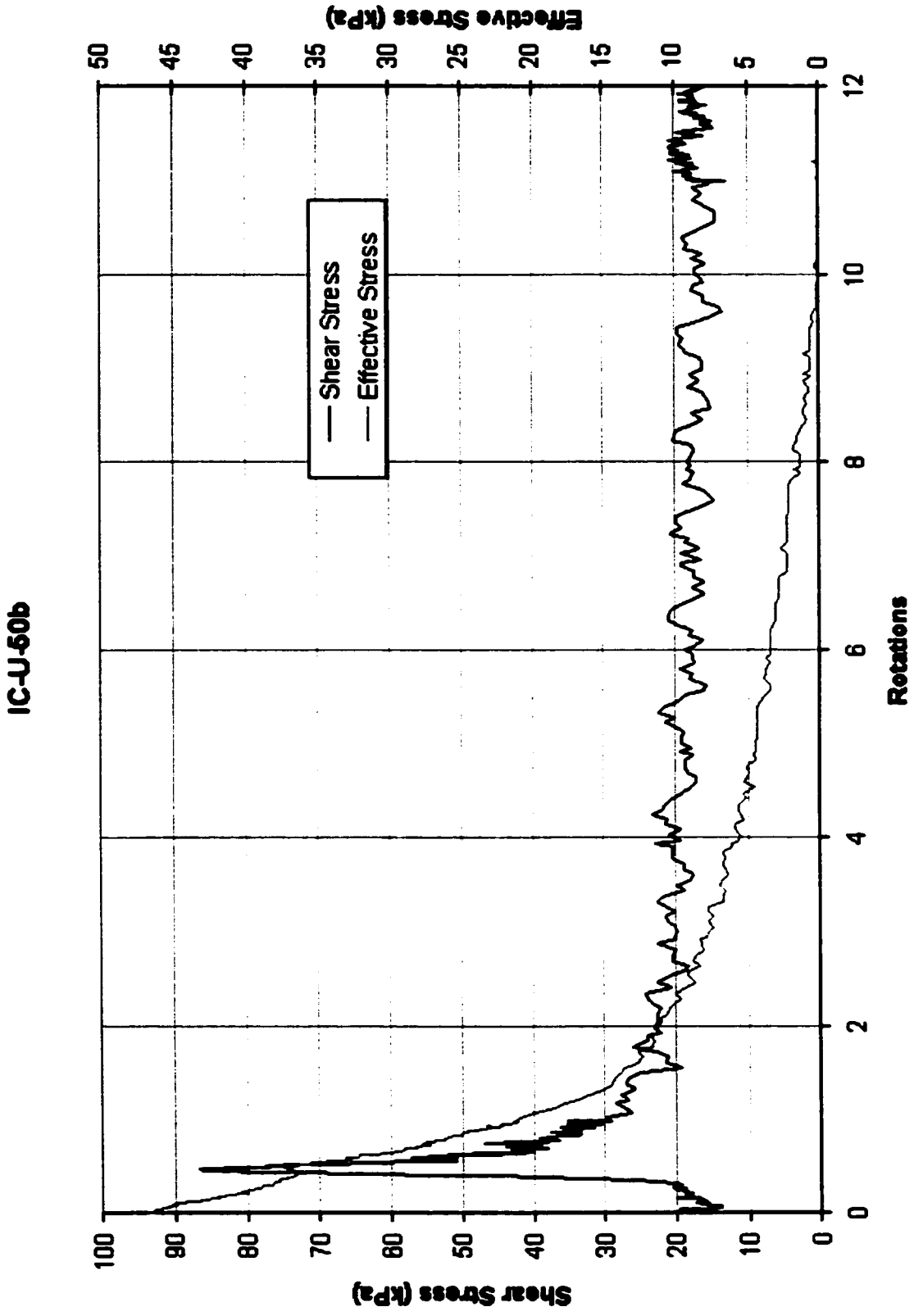
IC-U-60b
Shear Stress (kPa)
Effective Stress (kPa)
Rotations
Shear Stress
Effective Stress
0
10
20
30
40
50
60
70
80
90
100
0
5
10
15
20
25
30
35
40
45
50
0
2
4
6
8
10
12

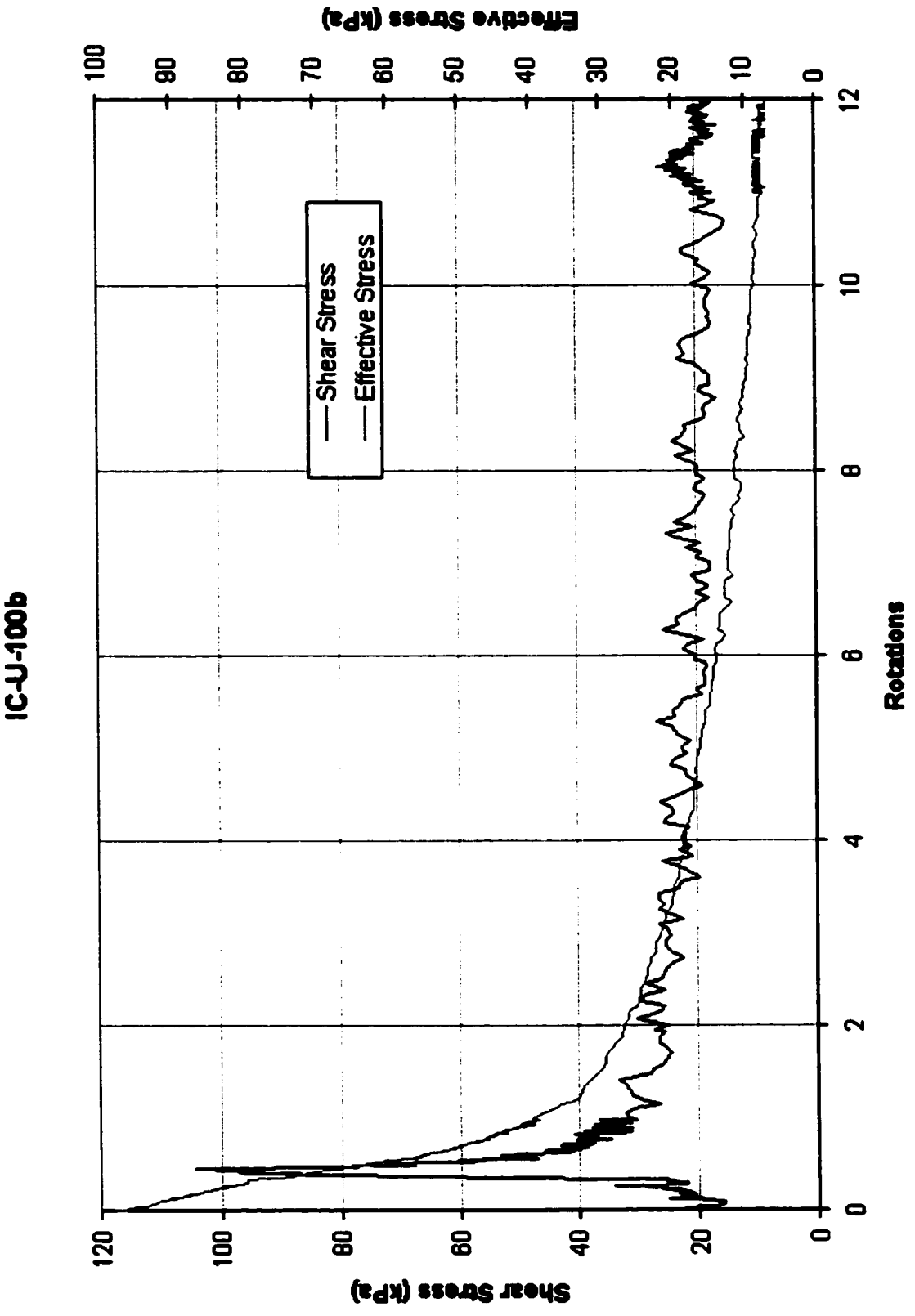
IC-U-100b
Shear Stress (kPa)
Effective Stress (kPa)
Rotations
Shear Stress
Effective Stress
0
20
40
60
80
100
120
0
10
20
30
40
50
60
70
80
90
100
0
2
4
6
8
10
12

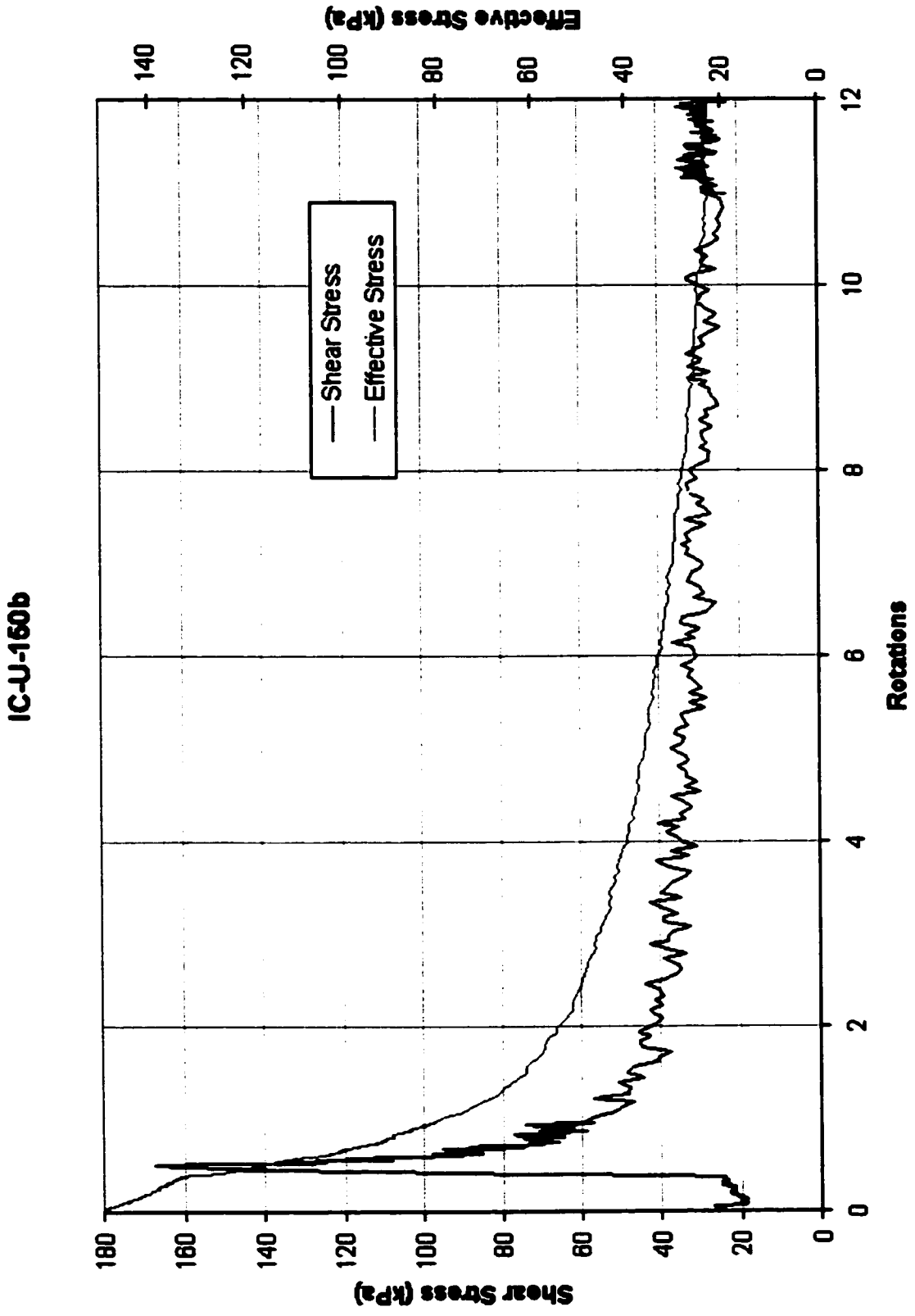
IC-U-150b
Shear Stress (kPa)
Effective Stress (kPa)
Rotations
Shear Stress
Effective Stress
0
20
40
60
80
100
120
140
160
180
0
2
4
6
8
10
12

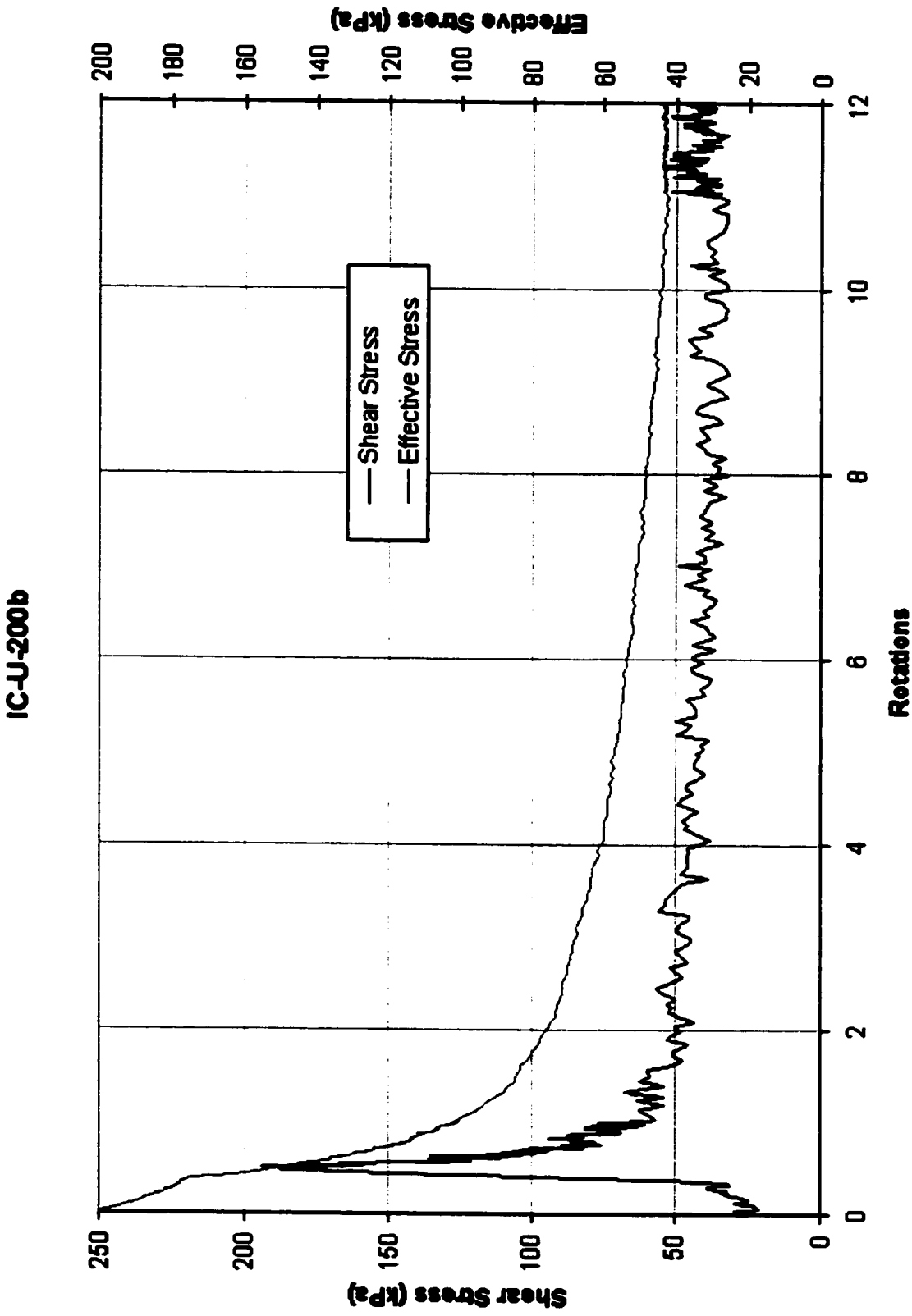
IC-U-200b
Shear Stress (kPa)
Effective Stress (kPa)
Rotations
Shear Stress
Effective Stress
0
50
100
150
200
250
0
20
40
60
80
100
120
140
160
180
200
0
2
4
6
8
10
12

Appendix 6: AC-D Triaxial Vane Tests

AC-D-100-70

Consolidation Pressure - Cell	99 kPa
Consolidation Pressure - Ram	78 kPa
Testing Pressure - Ram	71 kPa

Start of Test	
Dry Density	1.39 g / cm3
Saturated Density	1.87 g / cm3
e	0.91
Dr	0.32
After Consolidation	
Dry Density	1.46 g / cm3
Saturated Density	1.91 g / cm3
e	0.83
Dr	0.55
After Test	
Dry Density	1.48 g / cm3
Saturated Density	1.92 g / cm3
e	0.80
Dr	0.61
B Value	0.99
Peak Strength	
Maximum Shear Strength	92.98 kPa
Effective Stress	98.91 kPa
Residual Strength	
Steady State Shear Strength	69.96 kPa
High Speed Steady State	56.46 kPa
Effective Stress	98.91 kPa
Vane Speed	
Slow Testing	60 deg/min
Fast Testing	1062.6 deg/min

AC-D-100-88

Consolidation Pressure - Cell	103 kPa
Consolidation Pressure - Ram	94 kPa
Testing Pressure - Ram	88 kPa

Start of Test	
Dry Density	1.39 g / cm3
Saturated Density	1.87 g / cm3
e	0.91
Dr	0.33
After Consolidation	
Dry Density	1.41 g / cm3
Saturated Density	1.88 g / cm3
e	0.89
Dr	0.39
After Test	
Dry Density	1.43 g / cm3
Saturated Density	1.89 g / cm3
e	0.87
Dr	0.44
B Value	1.00
Peak Strength	
Maximum Shear Strength	134.59 kPa
Effective Stress	103.43 kPa
Residual Strength	
Steady State Shear Strength	82.36 kPa
High Speed Steady State	64.66 kPa
Effective Stress	103.43 kPa
Vane Speed	
Slow Testing	60 deg/min
Fast Testing	1062.6 deg/min

AC-D-100-116

Consolidation Pressure - Cell	106 kPa
Consolidation Pressure - Ram	125 kPa
Testing Pressure - Ram	116 kPa

Start of Test	
Dry Density	1.36 g / cm3
Saturated Density	1.85 g / cm3
e	0.96
Dr	0.21
After Consolidation	
Dry Density	1.38 g / cm3
Saturated Density	1.86 g / cm3
e	0.93
Dr	0.28
After Test	
Dry Density	1.39 g / cm3
Saturated Density	1.87 g / cm3
e	0.91
Dr	0.33
B Value	1.00
Peak Strength	
Maximum Shear Strength	156.75 kPa
Effective Stress	106.31 kPa
Residual Strength	
Steady State Shear Strength	87.26 kPa
High Speed Steady State	69.36 kPa
Effective Stress	106.31 kPa
Vane Speed	
Slow Testing	75.6 deg/min
Fast Testing	1062.6 deg/min

AC-D-100-172

Consolidation Pressure - Cell	105 kPa
Consolidation Pressure - Ram	188 kPa
Testing Pressure - Ram	173 kPa

Start of Test	
Dry Density	1.36 g / cm3
Saturated Density	1.85 g / cm3
e	0.96
Dr	0.19
After Consolidation	
Dry Density	1.38 g / cm3
Saturated Density	1.86 g / cm3
e	0.94
Dr	0.27
After Test	
Dry Density	1.39 g / cm3
Saturated Density	1.87 g / cm3
e	0.91
Dr	0.33
B Value	0.97
Peak Strength	
Maximum Shear Strength	135.59 kPa
Effective Stress	104.94 kPa
Residual Strength	
Steady State Shear Strength	97.76 kPa
High Speed Steady State	79.56 kPa
Effective Stress	104.94 kPa
Vane Speed	
Slow Testing	81 deg/min
Fast Testing	1062.6 deg/min

AC-D-100-201

Consolidation Pressure - Cell	101 kPa
Consolidation Pressure - Ram	224 kPa
Testing Pressure - Ram	202 kPa

Start of Test	
Dry Density	1.36 g / cm3
Saturated Density	1.85 g / cm3
e	0.96
Dr	0.20
After Consolidation	
Dry Density	1.40 g / cm3
Saturated Density	1.87 g / cm3
e	0.91
Dr	0.34
After Test	
Dry Density	1.41 g / cm3
Saturated Density	1.88 g / cm3
e	0.89
Dr	0.39
B Value	0.97
Peak Strength	
Maximum Shear Strength	120.89 kPa
Effective Stress	100.56 kPa
Residual Strength	
Steady State Shear Strength	106.56 kPa
High Speed Steady State	90.76 kPa
Effective Stress	100.56 kPa
Vane Speed	
Slow Testing	81 deg/min
Fast Testing	1062.6 deg/min

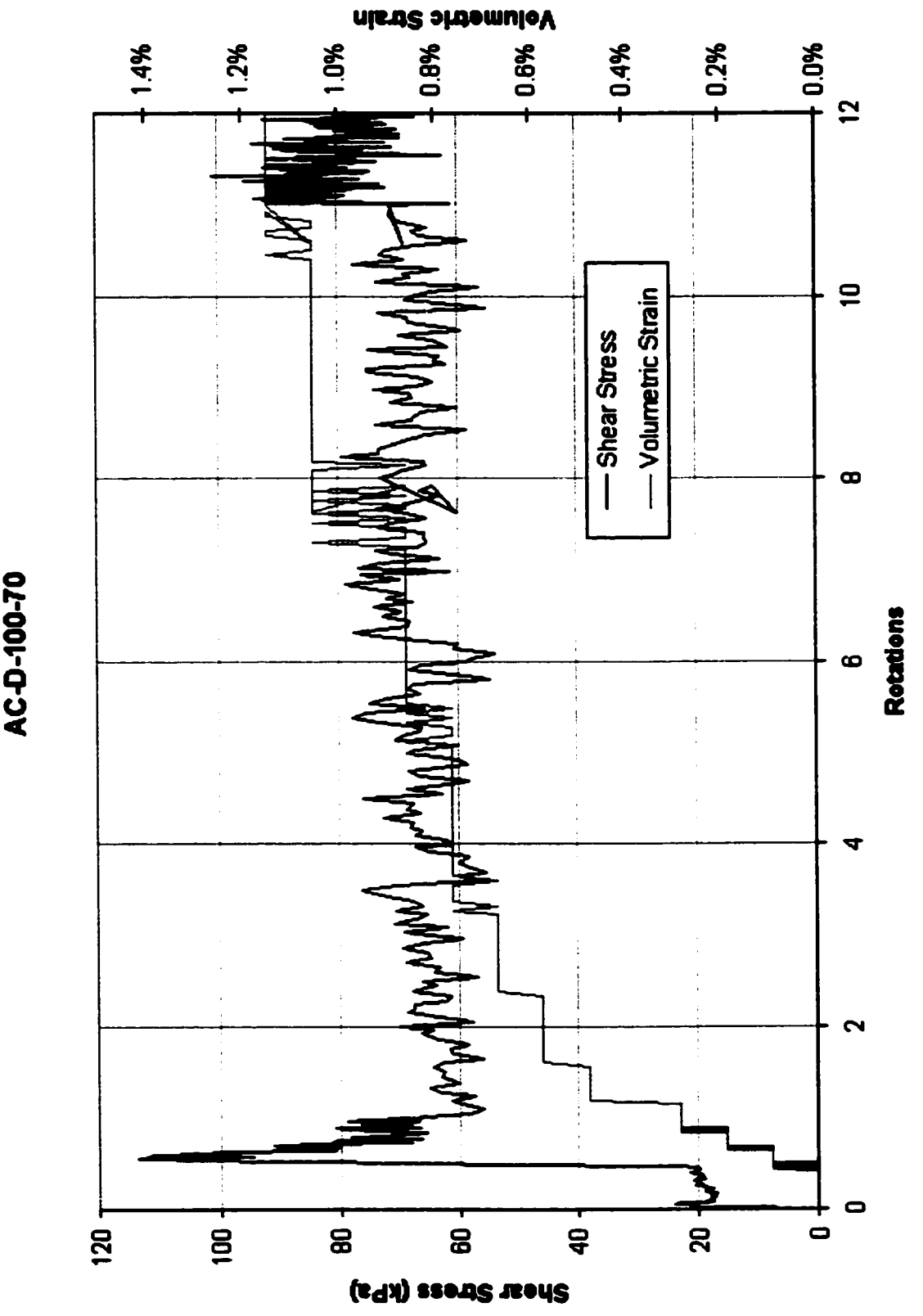
AC-D-100-70
Shear Stress (kPa)
Volumetric Strain
Rotations
Shear Stress
Volumetric Strain
0
20
40
60
80
100
120
0.0%
0.2%
0.4%
0.6%
0.8%
1.0%
1.2%
1.4%
0
2
4
6
8
10
12

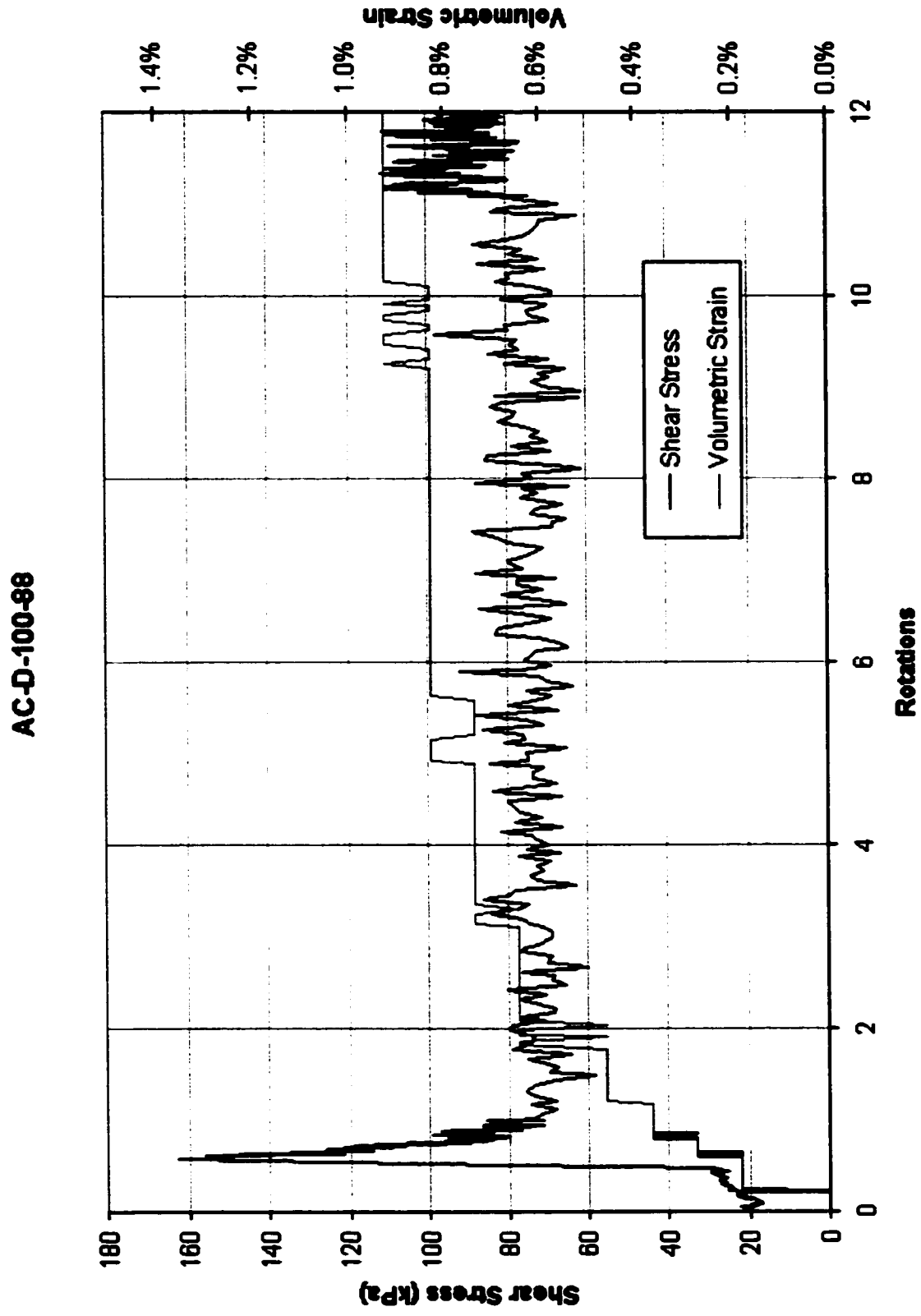
AC-D-100-98
Shear Stress (kPa)
Volumetric Strain
Rotations
Shear Stress
Volumetric Strain
0
20
40
60
80
100
120
140
160
180
0.0%
0.2%
0.4%
0.6%
0.8%
1.0%
1.2%
1.4%
0
2
4
6
8
10
12

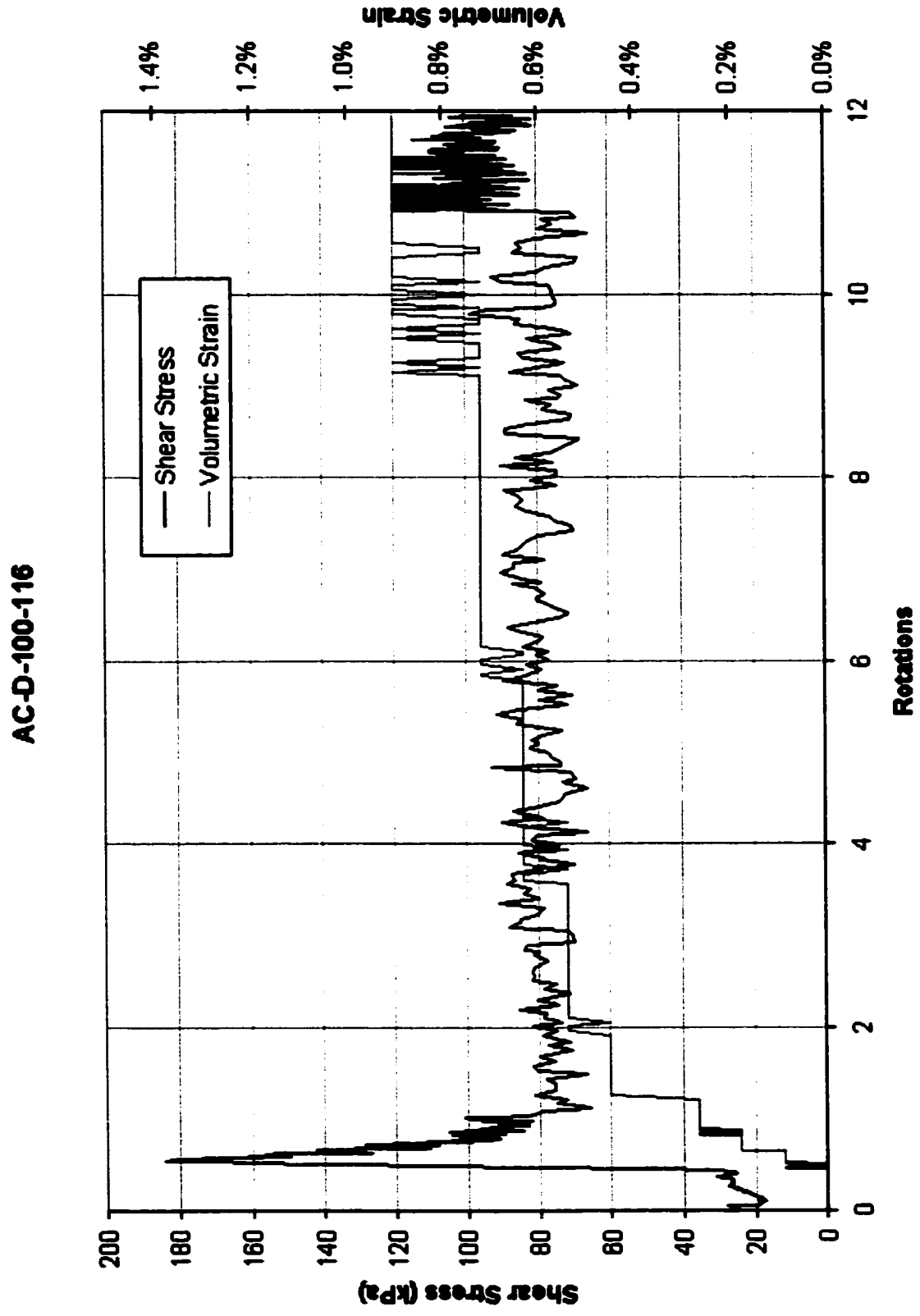
AC-D-100-116
Shear Stress
Volumetric Strain
Shear Stress (kPa)
Volumetric Strain
Rotations
0
20
40
60
80
100
120
140
160
180
200
0.0%
0.2%
0.4%
0.6%
0.8%
1.0%
1.2%
1.4%
0
2
4
6
8
10
12

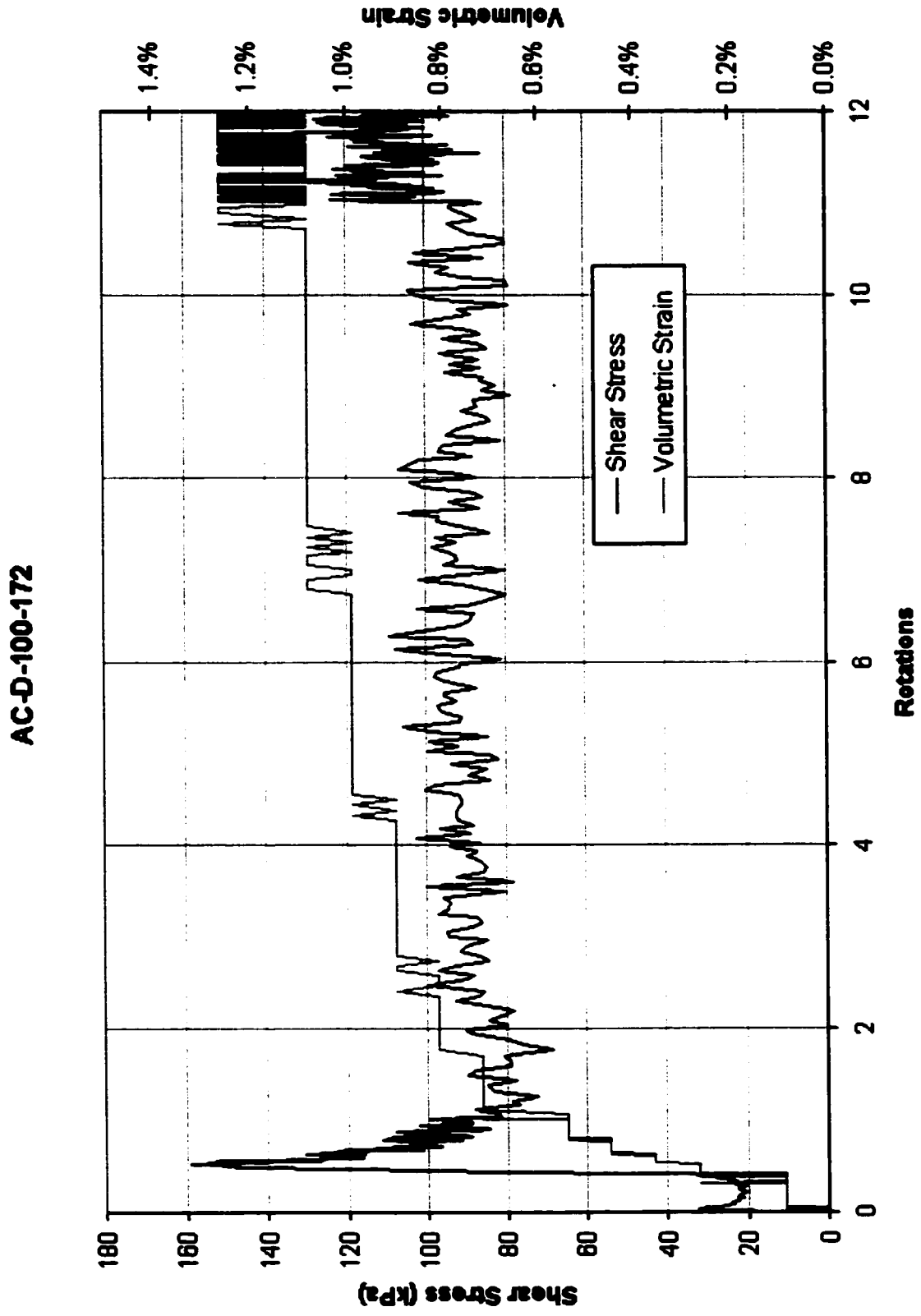
AC-D-100-172
Shear Stress (kPa)
Volumetric Strain
Rotations
Shear Stress
Volumetric Strain
0
20
40
60
80
100
120
140
160
180
0.0%
0.2%
0.4%
0.6%
0.8%
1.0%
1.2%
1.4%
0
2
4
6
8
10
12

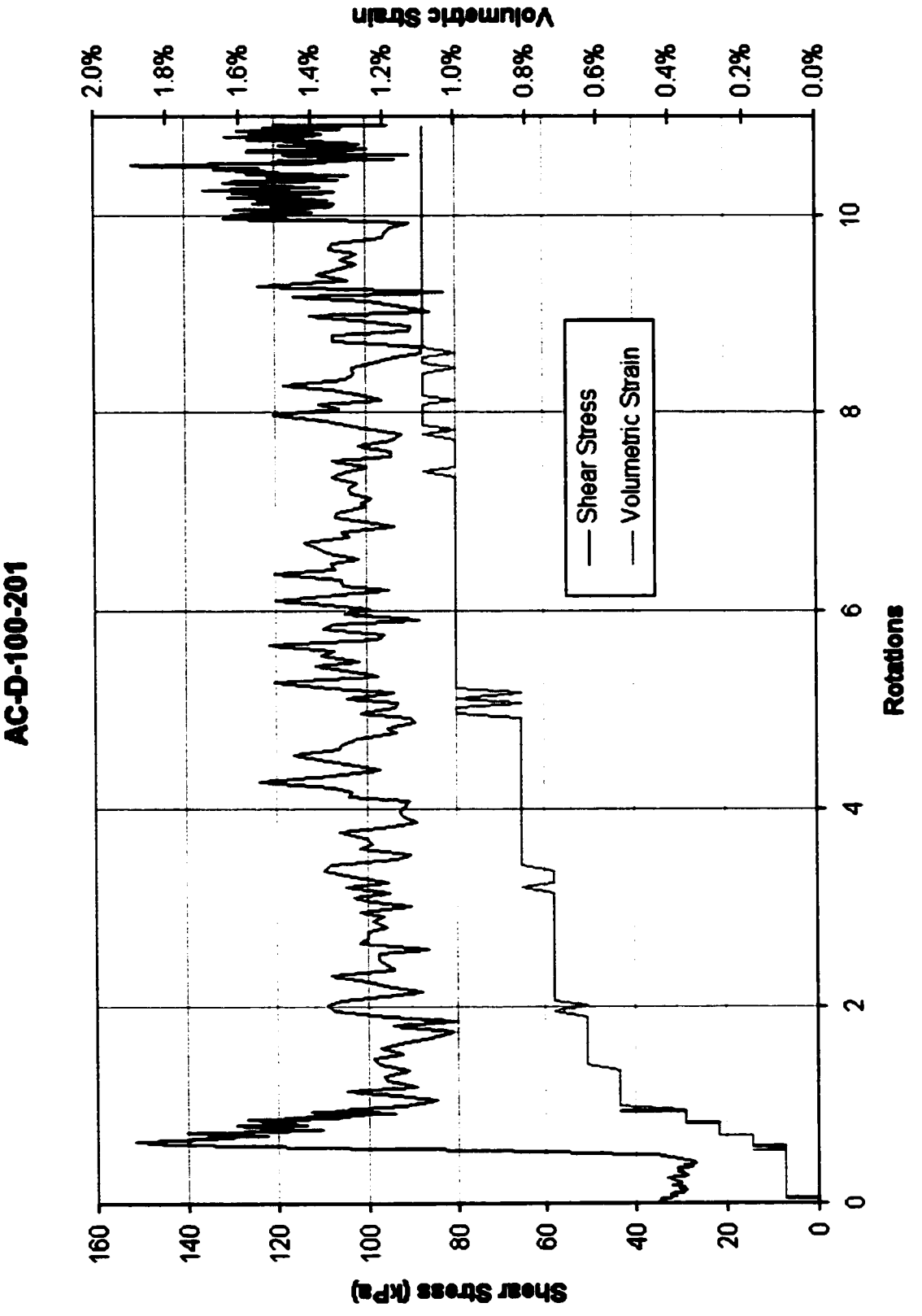
AC-D-100-201
Shear Stress (kPa)
Volumetric Strain
Rotations
Shear Stress
Volumetric Strain
0
20
40
60
80
100
120
140
160
0.0%
0.2%
0.4%
0.6%
0.8%
1.0%
1.2%
1.4%
1.6%
1.8%
2.0%
0
2
4
6
8
10